ABSTRACT

GAMMA RAY SPECTROSCOPIC STUDIES OF STATES IN NEUTRON-DEFICIENT Pb and Tl ISOTOPES

By

Raymond Edwin Doebler

In an effort to obtain more information on the energy level systematics in the neutron-deficient lead and thallium isotopes, γ-ray spectroscopic studies have been made on the following isotopes: Pb^{204m}, Pb^{203m}, Pb^{202m}, Pb^{201}, Pb^{100}, and Pb^{199}. A search was also made for an isomeric state in Pb^{200}.

These studies were conducted largely with Ge(Li) detectors in singles, in coincidence and anticoincidence arrangements with NaI(Tl) detectors, and in two-dimensional, Ge(Li)-Ge(Li), multiparameter systems.

Using a single-crystal Ge(Li) conversion coefficient spectrometer, *K*-conversion coefficients for the 899.2-keV *E*2 and the 911.7-keV *E*5 transitions in Pb^{204m} were measured. In the study of the 6.1-s isomer, Pb^{203m}, a 5.1-keV *M*2 transition was found to compete with the 825.2-keV *M*4 isomeric transition. After correcting for this branching decay, the *M*4 transition probability was found to be consistent with those of the other *M*4 transitions in the lead region. Six new γ transitions have been assigned to the decay of Pb^{202m} and a new level has been proposed at 1550-keV in Tl^{202}, populated by

electron-capture from the isomeric state. After an intensive search, an upper limit of ≈1 s was placed on any possible isomeric state in Pb^{200}.

Low-spin states in Tl^{200} have been studied via the decay of 21.5-h Pb^{200}. Nineteen γ transitions have been assigned to this decay and all have been placed in a consistent level scheme. States in Tl^{200} populated in the decay of Pb^{200} lie at 0, 147.63, 257.19, 289.24, 289.92, 450.56, 525.54, and 605.44 keV.

A total of 72 γ transitions have been observed in the decay of 9.4-h Pb^{201}. Excited states in Tl^{201} accommodating 65 of these transitions have been placed at 331.15, 692.41, 1098.46, 1134.81, 1157.41, 1238.82, 1277.09, 1290.05, 1330.38, 1401.21, 1420.00, 1445.85, 1479.87, 1550.5, 1617.45, 1639.47, 1672.00, 1712.5, and 1755.31 keV.

Eighty-nine of the 117 γ transitions assigned to the decay of 90-min Pb^{199} have been placed in a decay scheme with levels at 0, 366.90, 720.26, 1120.90, 1241.67, 1482.25, 1502.00, 1528.2, 1554.10, 1632.00, 1658.47, 1695.25, 1725.4, 1749.6, 1768.5, 1891.0, 1898.1, 1930.4, 1959.45, 1977.8, 2031.5, 2159.0, 2206.7, 2226.5, 2237.3, 2367.3, 2433.5, 2547.4, and 2643.2 keV.

Unique spin and parity assignments have been made for many of the states observed in these studies, with limits placed on most of the remaining ones. Spin and parity assignments were based on measured conversion coefficients, log *ft* values, and relative photon intensities.

The structures of the states in odd-odd Tl^{200} are discussed in

terms of the coupling of possible single-particle states in adjacent odd-A nuclei. The systematics of the odd-A Tl nuclei, including Tl^{201} and Tl^{199}, are discussed in terms of single-particle shell model states coupled to core states of the corresponding Pb nuclei.

GAMMA RAY SPECTROSCOPIC STUDIES OF STATES IN NEUTRON-DEFICIENT Pb AND Tl ISOTOPES

By

Raymond Edwin Doebler

A THESIS

Submitted to
Michigan State University
in partial fulfillment of the requirements
for the degree of

DOCTOR OF PHILOSOPHY

Department of Chemistry

1970

ACKNOWLEDGMENTS

I wish to thank Dr. Wm. C. McHarris for suggesting this region of study. His patience, encouragement, and readily available help during the experimental work and preparation of this thesis are greately appreciated.

Dr. W. H. Kelly of the Physics Department has provided many valuable suggestions and discussions during this project and his help is gratefully acknowledged.

Dr. H. G. Blosser, Mr. H. Hilbert, and Dr. W. P. Johnson assisted with the operation of the Michigan State University Sector-Focused Cyclotron, which was used to prepare most of the radioactive sources for these investigations.

Many of the energy and intensity standards used in this study were produced by neutron irradiation in the M.S.U. Triga reactor under the supervision of Dr. B. Wilkinson, Department of Chemical Engineering.

Dr. D. B. Beery, Mr. J. Black, Mr. W. B. Chaffee, Dr. J. B. Cross, Dr. R. E. Eppley, Mr. G. C. Geisler, Mr. R. Goles, Mr. K. Kosanke, and Mr. R. Todd all deserve special mention, for without their advice and "extra hands," most of the experiments described in this thesis could not have been done.

Miss T. Arnette, Mr. and Mrs. W. Merrit, and the cyclotron computer staff aided greatly in the data acquisition and evaluation

through their programming of the XDS Sigma-7 computer.

I wish to thank the Department of Physics for their friendly cooperation and financial support during this work.

Mrs. P. Warstler helped in the typing of this thesis and took care of many details connected with its final preparation.

The National Science Foundation, U. S. Atomic Energy Commission, and Michigan State University have provided the financial assistance which made this study possible.

I am grateful to my parents for their continued interest and support throughout the many years of this study.

Finally, I wish to thank my wife, Kathleen, who spent the short period of our engagement typing this thesis.

TABLE OF CONTENTS

Chapter Page

Chapter Page

LIST OF TABLES

Table

Page

LIST OF FIGURES

Figure

Page

Figure

Page

Figure

Page

Figure

Page

CHAPTER I

INTRODUCTION

Immediately after the formulation of the nuclear shell theory by Mayer [Ma49] and Jensen [Je49] in 1949, nuclei in the region of double shell closures became of tremendous theoretical interest. The nucleus ${}_{82}Pb_{126}^{208}$ is one of these "doubly-magic" nuclei, with closed shells of 126 neutrons and 82 protons. This nucleus is particularly stable in its ground state configuration, its first excited level lying at 2.62 MeV. The great stability of Pb^{208} suggests that one could treat those nuclei differing by only a few nucleons from this double-closed shell by the independent particle model. The nuclei ${}_{82}Pb_{125}^{207}$, ${}_{82}Pb_{127}^{209}$, ${}_{81}Tl_{126}^{207}$, and ${}_{83}Bi_{126}^{209}$, all of which have the "hard" core of Pb^{208} with one hole or one additional nucleon, should therefore exhibit a sequence of low-lying energy states in particularly good agreement with single-particle levels of the independent-particle shell model. Of these four nuclei, Pb^{207} is the best known, and the correspondence between the experimentally established levels and those predicted by the shell model is very striking. The states in Pb^{207} at low to moderate energies should consist of single neutron holes, and from simple shell-model predictions, one would expect these states to be, in increasing energy, $p_{1/2}$, $f_{5/2}$, $p_{3/2}$, $i_{13/2}$, $f_{7/2}$, and $h_{9/2}$. This is exactly the order found experimentally.

The next step was to use the experimentally determined single-

neutron levels of Pb^{207} as a basis for calculating levels in other, more neutron-deficient Pb isotopes. These attempts have been most successful in the description of Pb^{206} which is two neutrons removed from the N=126 closed neutron shell. However, instead of getting into a discussion of these calculations here, we would recommend an excellent review of these calculations, as well as the experimental results up to 1964 by Hyde [Hy64]. The important point here is that, even for this seemingly ideal case, two of the levels observed in Pb^{206} from the ε decay of Bi^{206} could not be accounted for by the shell model calculations and had to be characterized as collective in nature. As we get to the more neutron-deficient isotopes, collective effects play an increasingly more important role in the low-lying states, and in the very neutron deficient Pb isotopes we might even expect to find such species as "closed-shell" (82 protons) deformed nuclei by virtue of the distorting powers of the $i_{13/2}$ neutron states.

The shell model calculations become more complicated as we get to even more neutron-deficient isotopes of Pb; however, the situation becomes even more complex for the theoretician because of the lack of good experimental data for these isotopes. In the 1950's much work was done on these decay schemes. This work was done using conversion electron spectroscopy and NaI(Tl) γ-ray spectroscopy. However, because of the extreme complexity of these decay schemes and the limitations of the available tools, this work was only partially successful and much work had to be left unfinished. With the advent of Ge(Li) detectors, it has become possible to examine

the γ-ray spectra of these isotopes in more detail and from this additional information to construct more complete decay schemes. The techniques of γ-ray spectroscopy used in the present study are described in Chapter II.

After selecting this general region of the nuclidic chart for our study, we felt that before anyone attempted to determine the full decay schemes of the lighter Bi isotopes, preliminary studies on the decay of the isomeric states of the corresponding Pb isotopes would be very useful, as the decay of the isomeric states populates only a limited number of states. These states could then serve as the basic framework on which to build the full Bi decay schemes. The isomeric states in the Pb isotopes are due to the presence of low-lying single particle $i_{13/2}$ states. This is true of the even mass as well as the odd-mass isomers. Originally, we proposed to study only the isomeric states of Pb from Pb^{204m} to Pb^{196m}. Of these, odd-mass isomers from Pb^{203m} to Pb^{197m} and the even mass isomers, Pb^{204m} and Pb^{202m} had been observed in the earlier studies. We were therefore primarily interested in searching for the even-mass isomers Pb^{200m}, Pb^{198m}, and Pb^{196m}. Early in our search for Pb^{200m} we were sidetracked into a study of the decays of the neutron-deficient Pb isotopes to levels in the Tl daughters. However, we did complete studies on several of the Pb isomeric states and these results of our studies are given in Chapter III.

Our interest in the decay of Pb^{200} was stimulated by several factors. First, we were making a large amount of this isotopes in our attempts to find Pb^{200m} and as no γ-ray studies of this decay

using Ge(Li) detectors had been published, we felt that such a study might aid in tying up the loose ends in this decay scheme. Second, Tl^{200} and the other odd-odd thallium isotopes are in one of the most favorable regions for explaining properties of non-deformed odd-odd systems, for the single-particle states in many of the neighboring odd-mass nuclei are reasonably well characterized. The results of our study of the ε decay of Pb^{200} are given in Chapter IV along with a discussionsof the structure of the states in Tl^{200} in terms of the coupling of single-particle states in the adjacent odd-*A* nuclei.

In Chapter V and VI we present the results of our studies of the ε/β^+ decays of Pb^{201} and Pb^{199} to states in their odd-mass Tl daughters. Because ${}_{81}Tl_{120}^{201}$ and ${}_{81}Tl_{118}^{199}$ are only one proton removed from the Z=82 closed shell and have an even number of neutrons not too far removed from the N=126 neutron closed shell, most of their low-lying states should be successfully described by the single-particle shell model. The proton single-particle states available in this region are $s_{1/2}$, $d_{3/2}$, $d_{5/2}$, $h_{11/2}$, and $g_{7/1}$. Of these, only the $s_{1/2}$, $d_{3/2}$, and $d_{5/2}$ states lie low enough in energy to be fairly "pure" single particle states. The systematics of this series are especially interesting, as the neutron-deficient odd-*A* Tl isotopes provide one of the few series where we can observe the effects of successively plucking out pairs of neutrons on fairly "pure" single particle proton states.

Most of the isotopes used in the studies described in this thesis were produced by the bombardment of the appropriate targets

with proton or He^3 beams from the Michigan State University Variable-Energy Sector-Focused Cyclotron. The maximum beam energies readily available were 50 MeV for protons and 70 MeV for He^3. Table I-1 contains a list of the principal reactions and their associated "*Q*"-values, which were of interest to us in these studies. The Bi isotopes were produced principally for use as "cows" from which the Pb isomeric and ground states could be "milked". We also made use of the Michigan State University "Triga" Reactor facility to produce many of the γ-ray energy and intensity standards listed in Chapter II.

Table I-1

Q Values for Reactions Used to Produce Pb Isomers

Reaction	*Q* values (MeV) [a]	Reaction	*Q* values (MeV) [a]
$Pb^{206}(p,3n)Bi^{204}$	-20.0	$Tl^{203}(He^3,2n)Bi^{204}$	- 6.3
$Pb^{206}(p,4n)Bi^{203}$	-27.0	$Tl^{203}(He^3,3n)Bi^{203}$	-13.3
$Pb^{206}(p,5n)Bi^{202}$	-36.2	$Tl^{203}(He^3,4n)Bi^{202}$	-22.5
$Pb^{206}(p,6n)Bi^{201}$	-43.8	$Tl^{203}(He^3,5n)Bi^{201}$	-30.1
		$Tl^{203}(He^3,6n)Bi^{200}$	-39.6
$Tl^{205}(p,2n)Pb^{204m}$	- 9.7	$Tl^{203}(He^3,7n)Bi^{199}$	-47.2
$Tl^{205}(p,3n)Pb^{203m}$	-16.7	$Tl^{203}(He^3,8n)Bi^{198}$	-57.1
$Tl^{205}(p,4n)Pb^{202m}$	-25.2		
$Tl^{205}(p,5n)Pb^{201m}$	-32.3	$Hg^{200}(He^3,2n)Pb^{201m}$	- 6.0
$Tl^{205}(p,6n)Pb^{200}$	-40.0	$Hg^{200}(He^3,3n)Pb^{200}$	-12.7
		$Hg^{200}(He^3,4n)Pb^{199m}$	-22.0
$Tl^{203}(p,n)Pb^{203m}$	- 2.4	$Hg^{200}(He^3,5n)Pb^{198}$	-29.2
$Tl^{203}(p,2n)Pb^{202m}$	-10.9	$Hg^{200}(He^3,6n)Pb^{197m}$	-39.1
$Tl^{203}(p,3n)Pb^{201m}$	-18.1	$Hg^{200}(He^3,7n)Pb^{196}$	-46.7
$Tl^{203}(p,4n)Pb^{200}$	-24.7		
$Tl^{203}(p,5n)Pb^{199m}$	-34.1		
$Tl^{203}(p,6n)Pb^{198}$	-41.2		

[a] *Q* values based on "experimental" masses listed in reference [My65].

CHAPTER II

EXPERIMENTAL METHODS AND DATA ANALYSIS

The construction of the decay schemes described in this thesis required a great variety of experimental apparatus and techniques. In this chapter we have attempted to explain the purpose of each type of experiment and to describe, in a general way, the apparatus used. We have deliberately avoided a detailed listing of the electronics used in these experiments, as these are constantly being improved, making any such listing obsolete within a few years.

2.1. γ-Ray Singles Spectrometer

The first experiment generally performed in the elucidation of a decay scheme by γ-ray spectroscopy is a singles experiment. This experiment is used to determine the energies and relative intensities of the γ-rays given off in the decay of a radioactive isotope. Most of the singles experiments described in this thesis were performed using Ge(Li) detectors, although for very low energy (5-60 keV) γ-rays we made use of a Si(Li) detector.

A complete Ge(Li) or Si(Li) spectrometer system consists of a Ge(Li) detector biased with a regulated high-voltage supply and connected to a charge sensitive field effect transistor (FET) preamplifier whose output goes to a linear amplifier. The linear amplifier output goes on to an analog to digital converter (ADC) which is connected with some type of memory or storage unit that has an associated readout system. During the 4-year course of this work, there have been many refinements in all of these components. Our "best" system 4 years ago contained a Ge(Li) detector with a photopeak efficiency of 0.42% (relative to a 3×3-in. NaI(Tl) detector) and a resolution of >4.0 keV-FWHM for the 1332-keV γ from Co^{60}. This was connected with a 1024 channel analyzer. Our present "best" system possesses a 3.6% efficient Ge(Li) detector with a resolution of 2.0-keV FWHM connected with an 8192 channel ADC interfaced with an XDS Sigma-7 computer. A definition of "best" system is hard to define as it depends on the purpose of a particular experiment, but generally we would like a detector with the best resolution and the highest

efficiency connected to an ADC with enough channels to display the entire spectrum at a reasonable gain.

2.2. Ge(Li)-NaI(Tl) Coincidence Spectrometer

Having determined the energies and relative intensities of the γ-rays belonging to a particular isotope from the singles experiments, one would then like to know something about the coincidence relationships between these γ-rays. This includes determining which γ-rays are not in coincidence with any others (anticoincidence experiment), which are in coincidence with any other γ-ray (integral or any coincidence experiment), and for those γ-rays found to be involved in a coincidence we would like to know with which γ-rays they are in coincidence (gated coincidence experiment). In addition to these standard coincidence experiments with NaI(Tl) detectors, we have also used other more specialized experiments such as the anti-Compton and triple coincidence [511 keV-511 keV-any] experiments described below.

2.2.1. Anticoincidence and Anti-Compton Spectrometers

For the anticoincidence experiments performed in these studies, we used 0.42% or 2.5% efficient Ge(Li) detectors in conjunction with an 8×8-in. NaI(Tl) split annulus detector and a 3×3-in. NaI(Tl) detector. Figure II-1 shows the general setup for this experiment. The source is placed inside the annulus with a Ge(Li) detector in one end and the 3×3-in. NaI(Tl) detector blocking the other end. The signals from the NaI(Tl) detectors go through cathode followers to correct for impedance mismatching and then to linear amplifiers. The amplified signals then go to timing single-channel analyzers (TSCA) to obtain a logic signal for the coincidence unit or the AND/OR gate. The TSCA's are also used

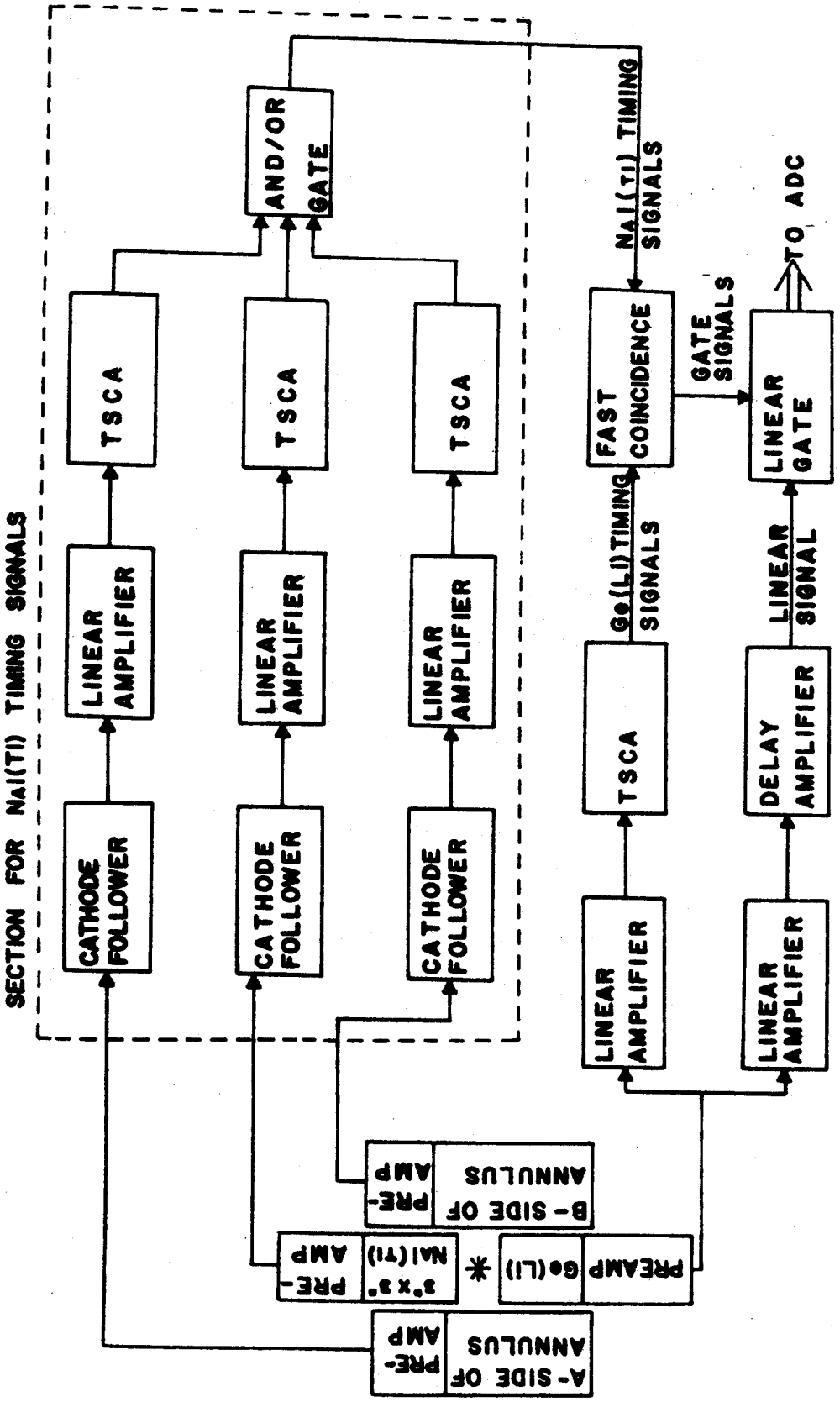

Figure II-1. Schematic illustration of the anticoincidence apparatus. This same apparatus is used for the integral, anti-Compton, and triple coincidence experiments after the elimination of the 3×3-in. NaI(Tl) detector [Ep70].

to discriminate against the x-rays. Signals from the Ge(Li) detector go through two linear amplifiers, one for timing purposes and one for obtaining the spectrum signal. The timing pulses from the AND/OR gate (NaI(Tl) side) and the Ge(Li) TSCA were fed into a fast coincidence unit with the resolving time, 2τ, generally set for 100 ns. The output from the fast coincidence unit was then used to operate a linear gate in the anticoincidence mode. In this mode of operation, the gate remains open, allowing the Ge(Li) signals to be recorded, until a coincidence is detected between any of the NaI(Tl) detectors and the Ge(Li) detector, when it closes to reject the Ge(Li) spectrum signal. This means that γ-rays detected by the Ge(Li) detector and involved in a cascade will be rejected when one of the NaI(Tl) detectors also picks up a member of the cascade. This results in a reduction in the intensities of cascade transitions in the final spectrum, or alternately, ground-state transitions fed directly by electron capture (ε) decay will be enhanced in an anticoincidence experiment. We should add a warning here, however, concerning this interpretation of all peaks enhanced in an anticoincidence experiment, for γ-transitions feeding a long-lived state ($>2\tau$) will also be enhanced as well as transitions from such states going directly to the ground state.

In addition to reducing the intensity of cascade transitions, the Compton background is also greatly reduced in the anticoincidence experiment, for any γ-ray scattered in the Ge(Li) detector has a good chance of being picked up by one of the NaI(Tl) detectors. With a slight modification of the anticoincidence apparatus, we can obtain

a "singles" spectrum with a greatly reduced Compton background. The arrangement of the detectors in this anti-Compton experiment is given in Figure II-2 and compared with that used in the anticoincidence and integral coincidence experiments. In the anti-Compton experiment, we replace the 3×3-in. NaI(Tl) detector with a graded Pb collimator, and place the source inside the collimator so that it is shielded from the NaI(Tl) annulus. In this configuration only γ-rays Compton scattered by the Ge(Li) detector will be picked up by the annulus. But whenever this happens the gate will be closed and the Compton event picked up by the Ge(Li) detector will be rejected. It is also helpful in reducing the Compton background if the source is collimated toward the center of the Ge(Li) detector, as γ-rays scattered in the center of the detector are more likely to be picked up by the rest of the crystal than those scattered near the edges of the detector. Such an anti-Compton experiment was performed with excellent results in our study of Pb^{201} (Figure V-5). In this experiment the Compton background was reduced enough to reveal several new transitions.

2.2.2. Integral, Gated, and Triple Coincidence Spectrometers

The apparatus shown in Figure II-1 can also be modified for obtaining integral, gated, and triple coincidence spectra. In the integral coincidence experiment the TSCA's associated with the NaI(Tl) detectors are set to accept all γ-ray energies above the x-ray, and the linear gate is used in the normal mode, that is, closed until opened by a signal from the fast coincidence unit. Therefore, the spectrum one obtains should ideally contain only those γ-rays involved in a cascade within the resolving time of the fast coincidence unit, usually

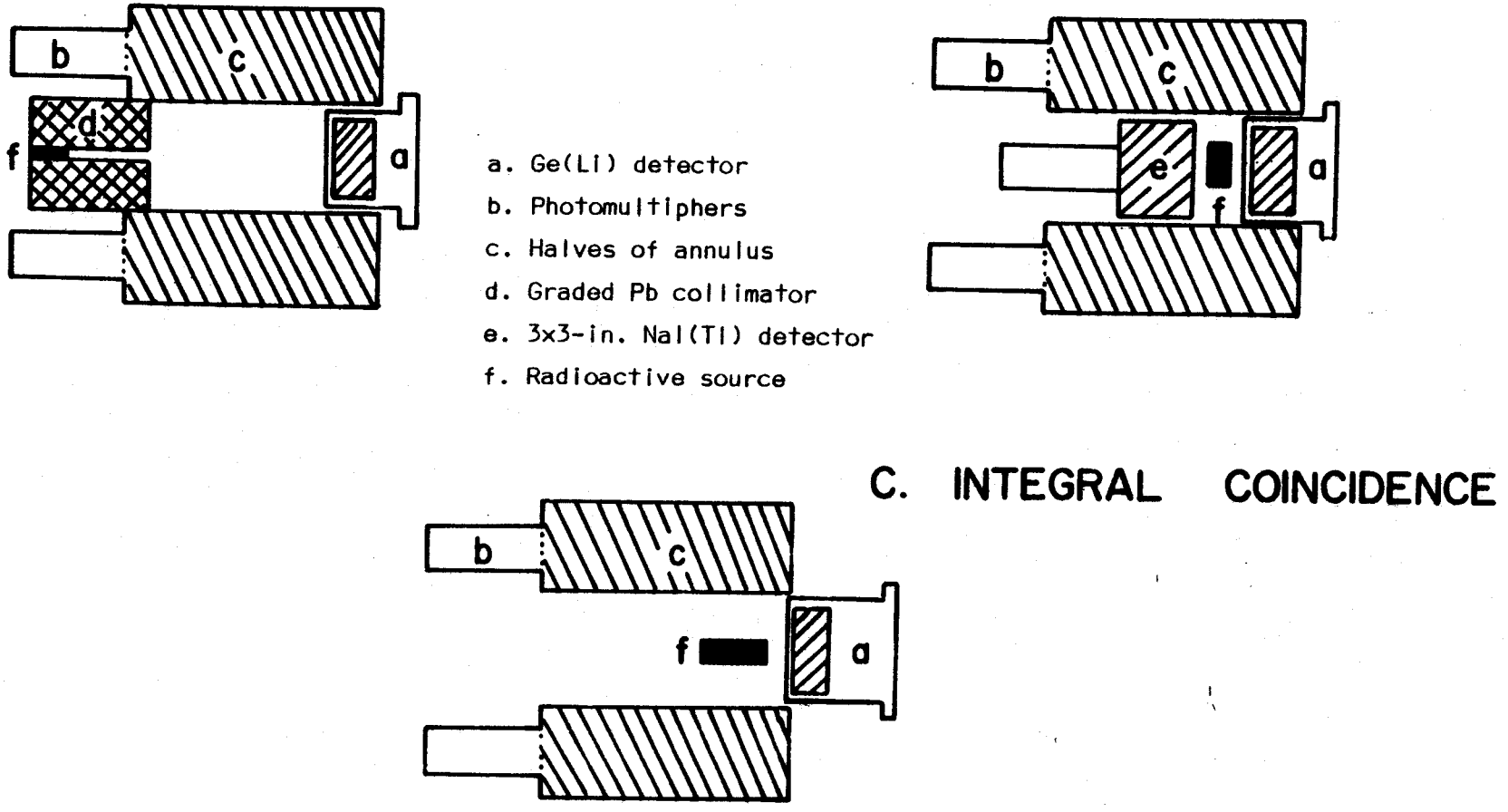

Figure II-2. Schematic illustrations of source and detector arrangements used in Anti-Compton, anticoincidence, and integral coincidence experiments.

50-100 ns.

The orientation of the detectors used in this experiment is shown in Figure II-2. We have moved the Ge(Li) detector outside the annulus and removed the 3×3-in. NaI(Tl) detector in order to reduce the Compton background. A typical integral coincidence experiment using the 8×8-in. NaI(Tl) annulus and the 0.42% detector is shown in Figure IV-4.

The setup for the gated coincidence experiment is exactly the same as that for the integral coincidence experiment; however, in this case we set an energy window with the TSCA's so that only those γ-rays falling within this window will cause the TSCA's to output a pulse to the fast coincidence unit. The resulting spectrum will then contain only those γ-rays in coincidence with this energy window, in which one normally chooses to include a γ-ray peak of interest. We used such a Ge(Li)-NaI(Tl) gated coincidence spectrometer in our integral studies of Pb^{200}. However, the resolution of the NaI(Tl) detectors were about 10%, for the 1332-keV γ-ray of Co^{60}, and this poor resolution made the interpretation of gated coincidence spectra very difficult, as each gate contained several γ-rays. Therefore, after the 2-d Ge(Li)-Ge(Li) megachannel coincidence spectrometer was developed we abandoned the NaI(Tl) detectors for obtaining gated coincidence spectra.

As we mentioned in Section 2.1.1., the 8×8-in. NaI(Tl) detector is a split annulus, having two optically-isolated halves. This allows us to perform triple-coincidence experiments, with the two sides of the annulus being used as the gates and a Ge(Li)

detector again used to obtain the coincidence spectrum. Such a triple-coincidence setup was used in our study of Pb^{201} in an attempt to obtain the relative β^+-feedings to the various levels. The triple-coincidence [511 keV-511 keV-any] experiment used the apparatus shown in Figure II-1 with the following modifications: The 3×3-in. NaI(Tl) detector and its associated electronics is removed, the AND/OR gate is replaced with another fast-coincidence unit, and the two TSCA's associated with the split annulus are set to accept only γ-rays in the 511-keV region. The orientation of source and detectors used for determining relative β^+-feedings is the same as that used in the integral coincidence experiment, Figure II-2.

2.3. Two-Dimensional γ-γ Coincidence Spectrometer

In the elucidation of a nuclear decay scheme, coincidence experiments (integral, anti, and gated) are generally the most time consuming. At the beginning of the studies described in this thesis all γ-γ coincidence experiments employed one Ge(Li) detector in coincidence with one or more NaI(Tl) detectors as described in the last section, and each experiment required the use of the detectors, associated electronics, and a multichannel analyzer. In addition, for shorter-lived isotopes we required the repeated use of the cyclotron to make the sources. This did not present a real problem as far as the anticoincidence and integral coincidence experiments were concerned, as these were generally performed only once (successfully) on a given isotope; however, for a moderately complicated decay scheme one is required to set many gates, and these consumed the largest amount of time and effort in elucidating a decay scheme. We were rescued from this drudgery by the introduction of a program called EVENT, written by D. Bayer to run under the JANUS time sharing monitor of the Sigma-7 computer.

Figure II-3 shows in flowsheet form the apparatus used in a typical two-dimensional coincidence experiment. When two photons are detected in coincidence, the linear gates are opened, allowing the output from detector 1 to go to the x-ADC while the output of detector 2 goes to the y-ADC. With the x- and y-ADC's operating in the synchronous mode, the signals going into the two ADC's must arrive within 1 μsec of each other in order to be recorded as a coincidence event. The 8192-channel ADC's are interfaced to the Cyclotron Laboratory's Sigma-7

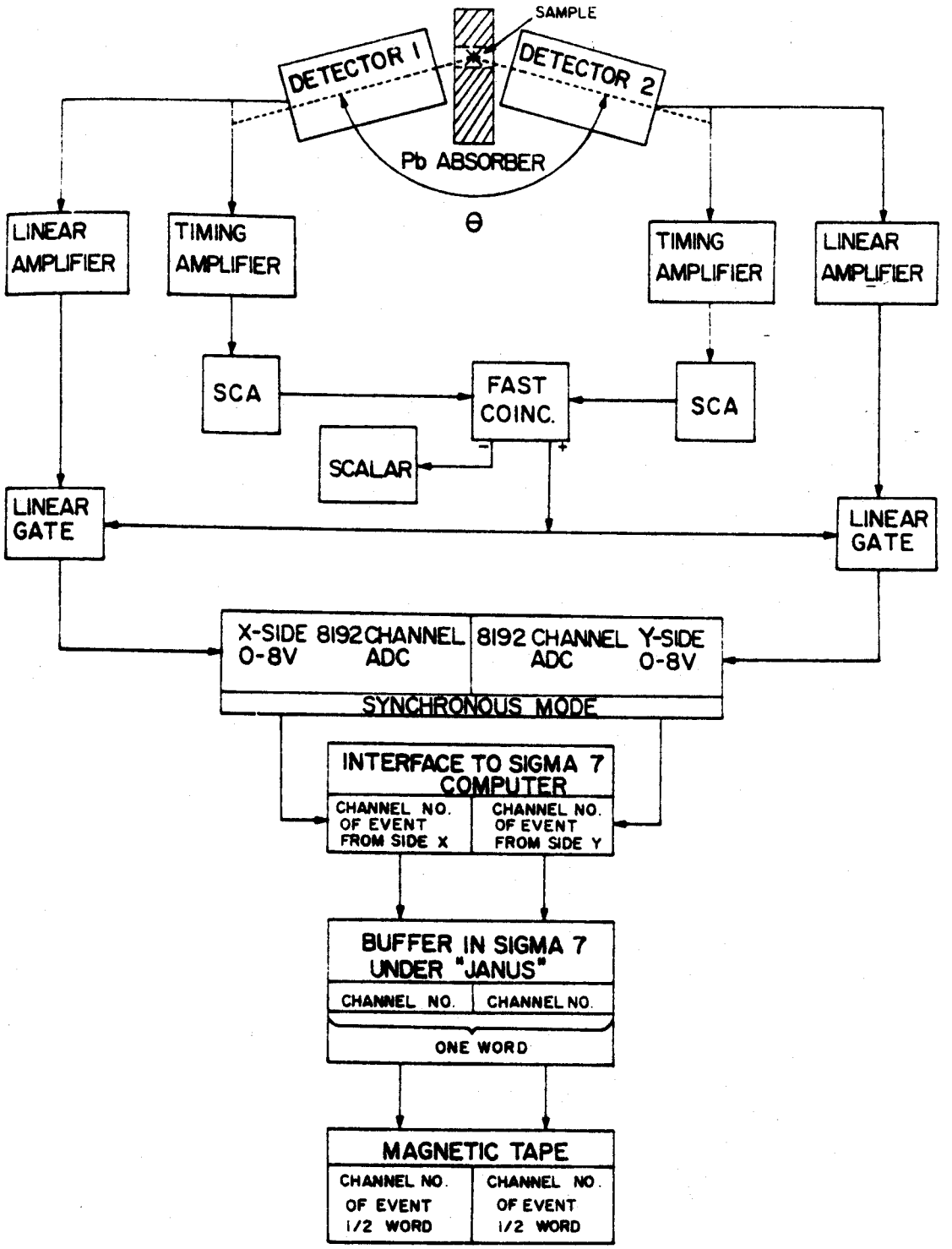

Figure II-3. Block diagram of the apparatus used to collect two-dimensional "megachannel" γ-γ coincidence spectra, using the Sigma-7 computer.

computer, and the program EVENT reads the data from both ADC's through a multipurpose interface. The events are then stored in a dedicated buffer in the computer until the buffer fills, whereupon the contents of the buffer are written on magnetic tape. The two coincident γ-rays are recorded by channel number in one word of memory in the computer and on the magnetic tape. Since the events are written to tape, this system cannot be used for count rates greater than ~2000 coincidence events per second.

The data on the magnetic tape are later recovered off-line using another program, event recovery [EVENT]. This program reads each event off the tape and separates the x and y addresses. It will then use up to 10 digital gates per pass of the tape to define coincidence spectra. Each gate can be either an "integral coincidence", that is, an open gate, or a selected gate of a few channels' width containing a peak of interest. The gates can be set on either the x or y address and background subtraction can be performed. The resulting one-dimensional coincidence spectra are then punched on cards for later plotting and data analysis.

The first experiments with this 2-d megachannel coincidence system made use of the 0.42% Ge(Li) detector and a 3×3-in. NaI(Tl) detector. However, we soon abandoned this arrangement in favor of one using two Ge(Li) detectors. During our study of Pb^{200} decay we performed the first successful Ge(Li)-Ge(Li) 2-d coincidence experiment at M.S.U. For this first experiment we used the 0.42% and 0.67% detectors. As the work described in this thesis progressed,

the detectors used in the 2-d experiments became larger, with the final system used in the elucidation of the Pb^{201} and Pb^{199} decay schemes having detectors with efficiencies of 2.5% and 3.6%.

Besides the obvious advantage of having to do only one experiment to obtain all the gated coincidence spectra, this system has the additional advantage of presenting all the results at the same gain for easy interpretation and allowing one to perform a linearly interpretated background subtraction of the adjacent background. The two integral coincidence spectra one obtains from this experiment may also make an integral coincidence run using a NaI(Tl) detector unnecessary. We have also used this system for resolving doublets that differ only slightly in energy and cannot be detected by peak broadening. This is done by gating on peaks that feed only different members of the multiplet and looking for a shift in the centroid of the multiplet. A discussion of how this technique was used in our study of Pb^{200} and Pb^{201} is given in Sections 4.3.2 and 5.3.5.d., respectively.

2.4. Determination of Photopeak Efficiency Curves

The photopeak efficiencies of Ge(Li) detectors are not constant with energy but generally decrease with increasing γ-ray energy. The exact behavior of this decrease is dependent on many factors, such as: The total active volume of the crystal, the ratio of depth to width of the active region, and the source to detector distance. Therefore, in order to obtain the relative intensities of the γ-rays emitted from a source, we must have available a photopeak efficiency curve for the particular detector and geometry used.

Efficiency curves for the detectors used in the present studies were determined by using a set of γ-ray sources, each of which emitted two or more γ-rays whose relative intensities were well-known. These sources were chosen to cover the widest energy range possible, and yet with each source overlapping, at least at one point, with another. This allowed us to bootstrap our efficiency curves to higher and lower energies. A list of the γ-ray relative intensity standards used to obtain the efficiency curves is given in Table II-1.

Previous to our work on the efficiency curves, the data were fit to a straight line on a log-log scale. However, we noticed a systematic deviation of our data from a straight line which suggested a 3rd order fit of the form, $\log(\text{efficiency}) = A + B\log E + C(\log E)^2 + D(\log E)^3$, where A, B, C, and D are empirical constants and E is the energy in keV. A computer program for fitting the efficiency data to this equation was written by G. Giesler. Actually, this program divides the curves into two sections, calculating one curve for

Table II-1

γ-Ray Relative Intensity Standards

Isotope	Photon Energy (keV)	Relative Intensity	Ref.
Cs^{137}	32.1	6.85	a
	36.5	1.54	a
	661.6	100	a
Tb^{160}	46	116	a
	52	28.8	a
	86.8	100	a
	(197)	(46.7)	a
Hg^{203}	72	11.9	a
	82	3.44	a
	279.2	100	a
Hf^{180m}	93.3	16.8	a
	215.3	80.6	a
	332.5	94.8	a
	444	83.0	a
	501	14.2	a
Lu^{177m}	105.3	100	b
	113.0	184	b
	128.5	131	b
	153.3	144	b
	204.1	117	b
	208.3	512	b
	228.4	310	b
	(233.8)	(≈48)	c
	281.8	118	b
	(283.4)	(≈5)	c
	327.7	152	b
	378.5	240	b
	(385.0)	(≈25)	c
	413.6	135	b
	418.5	172	b
	466.0	20	b
Ag^{110m}	446.8	3.5	d
	657.7	100	d
	706.7	17.2	d
	763.9	24.0	d
	818.0	7.8	d
	884.7	79.6	d
	937.5	36.5	d
	1384.2	27.7	d
	1475.7	4.5	d
	1504.9	14.8	
	1562.2	1.33	d
Co^{56}	846.8	100	e
	1037.9	14.3	e
	1175.1	2.30	e
	1238.3	67.6	e
	1360.2	4.34	e
	1771.4	15.8	e
	2015.4	3.10	e
	2034.9	7.95	e
	2598.6	16.8	e
	3010.2	1.01	e
	3202.3	3.03	e
	3253.6	7.39	e
	3273.3	1.76	e
	3451.6	0.875	e
	3547.9	0.178	e
Y^{88}	898.0	93	a
	1836.1	99	a
Co^{60}	1173.2	100	a
	1332.5	100	a
Na^{24}	1368.5	100	a
	2753.9	100	a

[a] C.M. Lederer, J.M. Hollander and I. Perlman, Table of Isotopes, J. Wiley and Sons, New York 1967, 6th Ed.

Table II-1 (cont'd)

[b] F.M. Bernthal, Ph.D. Thesis, University of California, Berkeley, 1969; UCRL-18651 (1969).

[c] A.J. Haverfield, F.M. Bernthal, and J.M. Hollander, Nucl. Phys. A94, 337 (1967).

[d] S.M. Brahmavar, J.H. Hamilton, A.V. Ramayys, E.E.F. Zganjar, and C.E. Bemis, Jr., Nucl. Phys. A125, 217 (1969).

[e] R.A. Meyer, Lawrence Radiation Laboratory, Livermore, private communication.

energies above 400 keV and one for energies from 100 to 400 keV. It then normalizes the two curves so they are continuous.

The efficiency curve for the 2.5% detector at 2 in. is shown in Figure II-4. As we mentioned earlier, the photopeak efficiency generally goes down with increasing energy however, it also falls off very rapidly below 100 keV because of absorption in both the aluminum can surrounding the detector and in the "dead" layer of the Ge crystal. Because of the difficulty in fitting the data below 100 keV to the rest of the efficiency curve, these points were not included in the calculated efficiency curve used in the MOIRAE E(I) program [Be67]. The intensities of γ-rays or x-rays in this energy region were calculated by hand, directly from efficiency curves such as the one shown in Figure II-4.

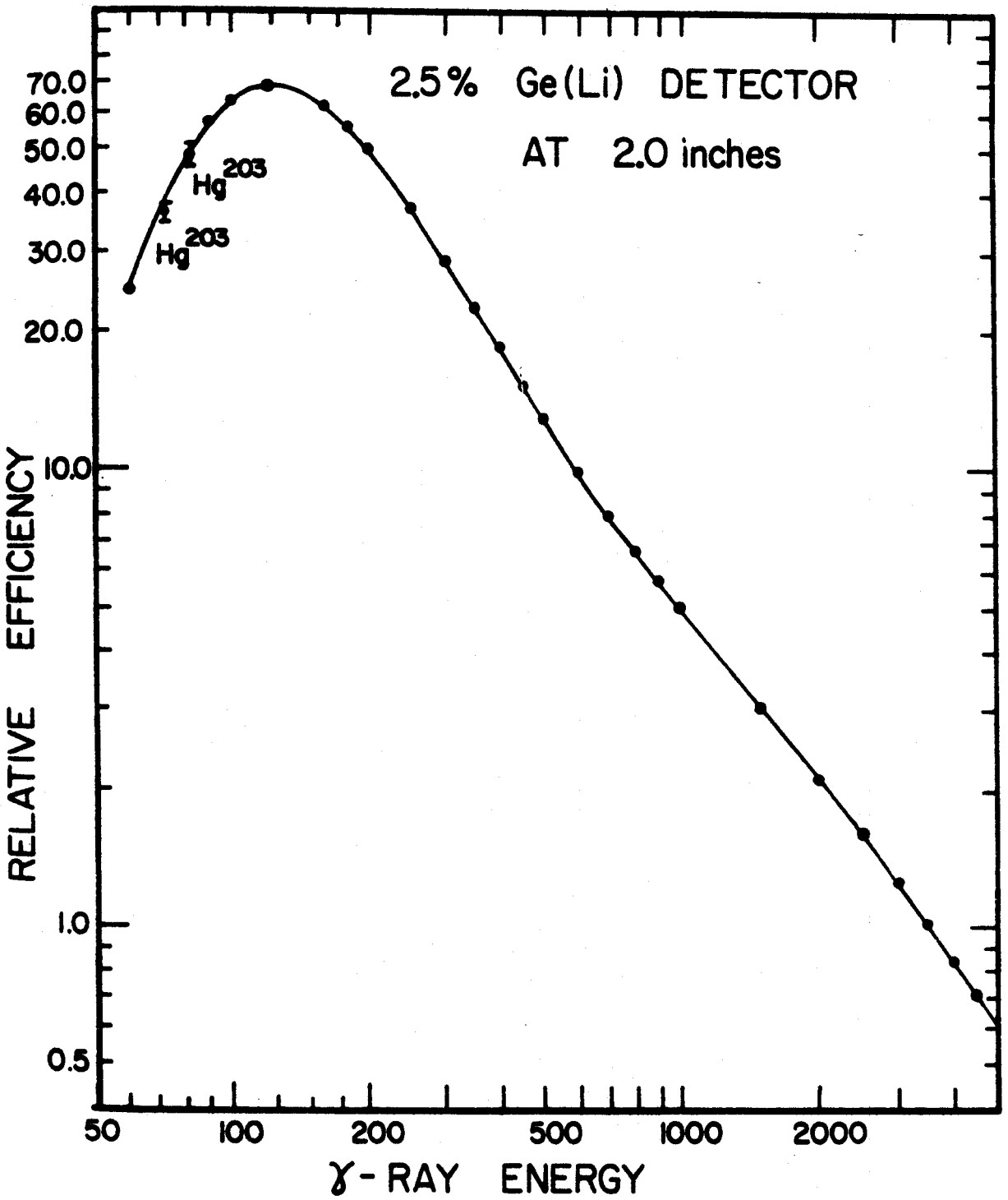

Figure II-4. Relative photopeak efficiency curve for the 2.5% detector determined using the sources listed in Table II-1 placed at 2 inches from the front fact of the detector.

2.5. Calibration of γ-Ray Standards

With the development of high resolution Ge(Li) detectors, it has become possible to measure γ-ray energies with a precision of better than 100 eV. This does not present any significant problem for energy determinations in the range from 100 to 1000 keV, for a great number of energy standards are available in this range, which are known precisely to tens of eV. However, the γ-ray energies greater than 1 MeV, there are significantly fewer γ-ray standards with this precision. We decided, therefore, to remeasure the energies of some common standards listed in the 1967 edition of the Table of Isotopes [Le67] in the region 1000 to 2000 keV.

The Ge(Li) detectors used in these measurements had resolutions of 2.1 and 2.3 keV for the 1332-keV peak of Co^{60} and efficiencies of 3.6% and 2.5%, respectively. The spectra were taken with both a Northern Scientific 4096-channel ADC interfaced with the PDP-9 computer and a Northern Scientific 8192-channel ADC interfaced to the XDS Sigma-7 computer. Energy determinations were made by counting the "unknown" simultaneously with several of the standards listed in Table II-2. The centroid channels were determined using the "MOIRAE" spectrum analysis program. From the centroid channels of the standards a least-squares quadratic calibration curve was calculated and the energies of the "unknown" γ-rays computed from this curve. Although we did not determine the linearity of our detector systems, the quadratic calibration curve was found to compensate for any non-linearity over the range of channels used. Because the

Table II-2

γ-Ray Calibration Standards

Isotope	Energy (keV)	Reference
Tl^{208}(ThC")	583.14±0.02	*a*
Cs^{137}	661.61±0.04	Average of *a* and *b*
Mn^{54}	834.83±0.04	Average of *b*, *c*, *d*, and *e*
Y^{88}	898.03±0.04	Average of *b*, *c*, *e*, and *f*
Co^{60}	1173.23±0.04	*a*
Na^{22}	1274.55±0.04	Average of *c*, *e*, *f*, and *g*
Co^{60}	1332.50±0.03	*b*
Na^{24}	1368.53±0.04	*a*
Y^{88}	1836.13±0.04	Average of *a*, *c*, *e*, *f*, and *g*
Tl^{208}(ThC")	2614.47±0.10	*a*
Na^{24}	2754.08±0.08	Average of *a* and *b*
Co^{56}	846.78±0.06	Average of *b*, *h*, and *i*
	1037.89±0.07	Average of *b*, *h*, and *i*
	1238.30±0.05	Average of *b*, *h*, and *i*
	1360.25±0.05	Average of *b*, *h*, and *i*
	1771.43±0.05	Average of *b*, *h*, and *i*
	2015.37±0.06	Average of *b*, *h*, and *i*
	2034.93±0.06	Average of *b*, *h*, and *i*
	2598.58±0.06	Average of *b*, *h*, and *i*
	3253.63±0.06	Average of *b*, *h*, and *i*

[a] G. Murray, R.L. Graham, and G.S. Geiger, Nucl. Phys. 63, 353 (1965).

[b] R. Gunnink, R.A. Meyer, J.B. Niday, and R.P. Anderson, Nucl. Instr. Methods 65, 26 (1968).

[c] W.W. Black and R.L. Heath, Nucl. Phys. A90, 650 (1967).

[d] H.H. Williams, E.K. Warburton, K.W. Jones, and J.W. Olness, Phys. Rev. 144, 801 (1966).

[e] A.V. Ramayya, J.H. Hamilton, S.M. Brahmavar, and J.J. Pinajian, Phys. Lett. 24B, 49 (1967).

Table II-2 (cont'd)

[f] J. Legrand, J.P. Boulanger and J.P. Brethon, Nucl. Phys. A107, 177 (1968).

[g] D.H. White and D.J. Groves, Nucl. Phys. A91, 453 (1967).

[h] M.E. Phelps, D.G. Sarantites, and W.G. Winn, Nucl. Phys. to be published.

[i] R.A. Meyer and D. Camp, Private communication, Lawrence Radiation Laboratory, Livermore, Calif. (1970).

non-linearity for most ADC's is most severe for the highest and lowest channels, we avoided the first and last 500 channels in these energy determinations.

Table II-3 contains the results of our measurements on Zn^{65}, Sc^{46}, Bi^{207}, and selected γ-rays from Ag^{110m}, Ta^{182}, and Ga^{66}. We have compared these with other recent measurements as noted in the table. Although we have not completed the energy calibration of Ga^{66}, the few γ-ray energies we have measured are in better agreement with those of Phelps, Sarantities, and Winn [Ph70] than with the unpublished results of Meyer and Camp [Me70]. This is worth mentioning here as the unpublished energies reported by Meyer and Camp for Co^{56} were found to be in excellent agreement with the other standards listed in Table II-2, when these were run as internal standards. However, when we ran the Co^{56} as an internal standard with the Ga^{66}, the resulting energies for Ga^{66} do not agree within experimental errors with those reported by Meyer and Camp. The energies of the 2751.99 and 3229.08-keV γ-rays from Ga^{66} were determined using the pair-peak method, that is, we determined the energy of the double-escape peaks using internal standards as described above and added 1022.01 keV to obtain the full-energy γ-rays.

Table II-3

Results of γ-Ray Energy Calibrations

Isotope	Energies (keV) Previous Standard Energies		Present Work
	Table of Isotopes[a]	J.B. Marion[b]	
Sc^{46}	889.18±0.10	889.14±0.15	889.28±0.06
	1120.41±0.10	1120.29±0.25	1120.58±0.06
Zn^{65}	1115.44±0.10	1115.40±0.12	1115.57±0.06
Bi^{207}	1063.58±0.06	1063.44±0.09	1063.64±0.06
	1769.71±0.13	1769.71±0.13	1770.22±0.08
Ta^{182}	1121.28±0.12		1121.31±0.05
	1189.03±0.20		1189.06±0.05
	1221.42±0.10		1221.42±0.05
	Brahmavar et al.[c]	Legrand et al.[d]	
Ag^{110m}	884.67±0.04	884.66±0.04	884.68±0.04
	937.48±0.04	937.46±0.06	937.48±0.04
	1384.22±0.04	1384.35±0.06	1384.26±0.05
	1475.73±0.04	1475.81±0.08	1475.76±0.07
	1504.90±0.08	1505.11±0.14	1505.01±0.07
	1562.22±0.06	1562.37±0.12	1562.35±0.08
	Phelps et al.[e]	Meyer and Camp[f]	
Ga^{66}	833.46±0.04	833.65±0.08	833.52±0.06
	1039.24±0.05	1039.35±0.08	1039.20±0.06
	2189.85±0.06	2190.24±0.15	2189.73±0.08
	2422.75±0.06	2422.51±0.15	2422.60±0.08
	2751.92±0.06	2752.27±0.10	2751.99±0.08(D)
	3229.16±0.06	3229.37±0.20	3229.08±0.15(D)

[a] C.M. Lederer, J.M. Hollander and I. Perlman, Table of Isotopes, John Wiley and Sons, New York 1967, 6th Ed.

[b] J.B. Marion, Nucl. Data, A4, 301 (1968).

[c] S.M. Brahmavar, J.H. Hamilton, A.V. Ramayya, E.F.F. Zganjar, C.E. Bemis, Jr., Nucl. Phys. A125, 217 (1969).

Table II-3 (cont'd)

[d] J. Legrand and J.P. Boulanger, Compt. Rend. 265, 697 (1967).

[e] M.E. Phelps, D.G. Sarantites, and W.G. Winn, Nucl. Phys. to be published.

[f] R.A. Meyer and D. Camp, private communication, Lawrence Radiation Laboratory, Livermore, Calif.

2.6. Data Analysis

Along with the rapid increase in data acquisition capabilities, we have been fortunate to have seen a similar rapid development in the data analysis routines available to us. The standard program for analyzing data at the beginning of these studies was the MIKIMAUS program written by G. Berzins [Be67]. This program calculated the centroids and intensities of photon peaks specified by control cards read into the computer along with the data deck. For each peak a control card was required, specifying the channel numbers of the low and high background intervals, as well as specifying the peak interval. The essential features of this program were later incorporated into the MOIRAE program using a live display scope with sense switches interfaced with the Sigma-7 computer. The scope is used to display the spectrum or a portion of the spectrum to be analyzed, the fitted background, and the difference between the background and the raw data. A marker displayed on the scope and controlled by a sense switch is used to specify the high and low background intervals used for fitting the background as well as specifying the peak interval. The background can be fitted to an nth-degree (up to $n = 9$) polynomial at the discretion of the operator. The great value of this program is that one can try different background intervals and different order fits until he is satisfied with the shape of the background under the peak. After subtraction of the background from the specified peak interval, the centroid is calculated using either the full width of the peak or only the upper two-thirds of the peak, again, at the discretion

of the operator. The centroid and the net area within the peak interval can then be outputted to a line printer and card punch. The punched cards obtained from MOIRAE are then used with another program, MOIRAE E(I) [Be67], to obtain the energies and intensities of the peaks. The centroids of known peaks are used to define a quadratic calibration curve from which the energies of the other peaks are calculated. The intensities are calculated using the areas from the MOIRAE cards and internal efficiency curves for the detector.

The most recent addition to our data analysis routines is SAMPO, a computer program developed by J. Routti [Ro69]. This program, after subtracting the quadratic background, fits the experimental peaks, to a Gaussian function having exponential tails using internal shape parameters or shape parameters calculated from singlet peaks chosen from the spectrum being analyzed. This program outputs the area and centroids of all the statistically significant peaks via the line printer. Although this routine is very useful for stripping multiplets, it was not used for general spectrum analysis in these studies because we had no control over the background which was fitted by a quadratic curve, and in many cases made for a poor fit. A more detailed discussion of the SAMPO and MOIRAE programs is given in theses by J. Cross [Cr70] and R. Eppley [Ep70].

CHAPTER III

THE DECAY SCHEMES OF SOME NEUTRON-DEFICIENT Pb ISOMERS

All the odd-mass Pb isotopes known below $N = 126$ have long-lived metastable states based on the $i_{13/2}$ neutron state. The three even-even isotopes Pb^{206}, Pb^{204}, and Pb^{202}, also have reported isomeric states, here 7- or 9- states resulting from coupling the $i_{13/2}$ neutron hole to other holes. In this chapter we report on our investigations of several of these isomers as well as our search for an isomeric state in Pb^{200}.

3.1. The Decay Scheme of Pb^{204m}

3.1.1. Introduction

The decay scheme of 66.9 m Pb^{204m} has been the object of many previous studies starting with Sunyar in 1950 [Su50]. An excellent summary of this previous work is given in reference [Hy64] and will not be repeated here. As the previous work on this decay scheme relied on conversion electron and NaI(Tl) γ-ray detectors, we felt that by using Ge(Li) detectors we might be able to observe some new transitions in this decay. However, in our brief examination of Pb^{204m} several years ago, we failed to detect any new transitions, and the decay scheme remains essentially the same as that proposed by Fritsch [Fr56] in 1956 and shown in Figure III-9. This decay scheme is also consistent with the results of J. Cross in his study of Bi^{204} decay [Cr70]. However, Cross proposed several states in Pb^{204} that lie below the 2185.4-keV isomeric state and could possibly be populated in the decay of Pb^{204m}. With this in mind, a re-examination of the Pb^{204m} decay scheme with the larger Ge(Li) detectors now available may reveal some of these transitions and help to establish more definite spin and parity assignments for these levels.

Although we were unable to detect any new γ-rays in our study, we did make direct measurements of the K-conversion coefficients for the 899.2-keV $E2$ and the 911.7-keV $E5$ transitions in Pb^{204m} using a unique single-crystal Ge(Li) conversion coefficient spectrometer [Gr69].

3.1.2. The Ge(Li) Conversion-Coefficient Spectrometer

The Ge(Li) detector used in this experiment was manufactured at the M.S.U. Cyclotron Laboratory by C. Maggiore. It is a planar drift device with a drift depth of ≈7 mm and an active volume of ≈0.4 cm. It was mounted in a conventional dipstick cryostat with a window of 0.25 mil Havar foil. The orientation of the detector and source is indicated in Figure III-1. The detector has a resolution of 1.8-keV FWHM for the 661.6-keV γ-ray of Cs^{137}.

The relative efficiencies for both γ-rays and conversion electrons were found to depend sensitively on source shape and position. To insure uniform reproducibility, the sources were vaporized through 3-mm diameter masks onto 0.25-mil Pt foil backings. These were mounted on Al rings which fit into the slot shown in Figure III-1. The efficiency of the detector was calibrated by using the standards listed in Table III-1, whose conversion coefficients had been determined precisely. An efficiency curve was also obtained using theoretical conversion coefficients from the table of R. S. Hager and E. C. Seltzer [Ha68]. The intensities of the electron peaks were determined by first taking a spectrum of both electrons and γ-rays, as shown for Cs^{137} in Figure III-2a. Then an Al absorber was placed between the source and the detector to stop the electrons, and a spectrum was taken which contained only the γ-rays, as shown in Figure III-2b. By overlapping the spectra and subtracting, the conversion electron intensities were easily obtained.

The efficiency curve for the present detector, obtained by

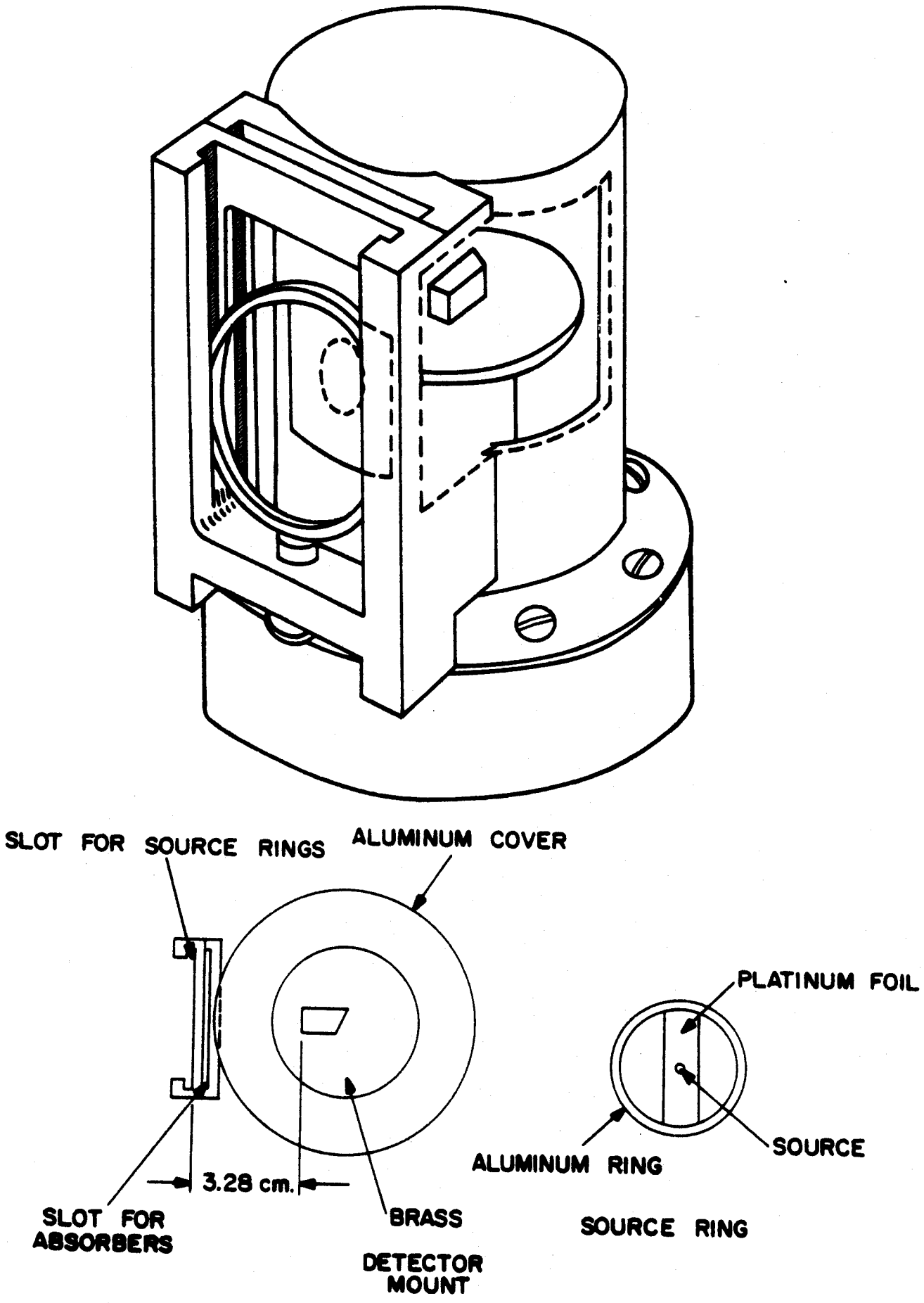

Figure III-1. The Ge(Li) conversion-coefficient spectrometer showing the orientation of the crystal and the source mount.

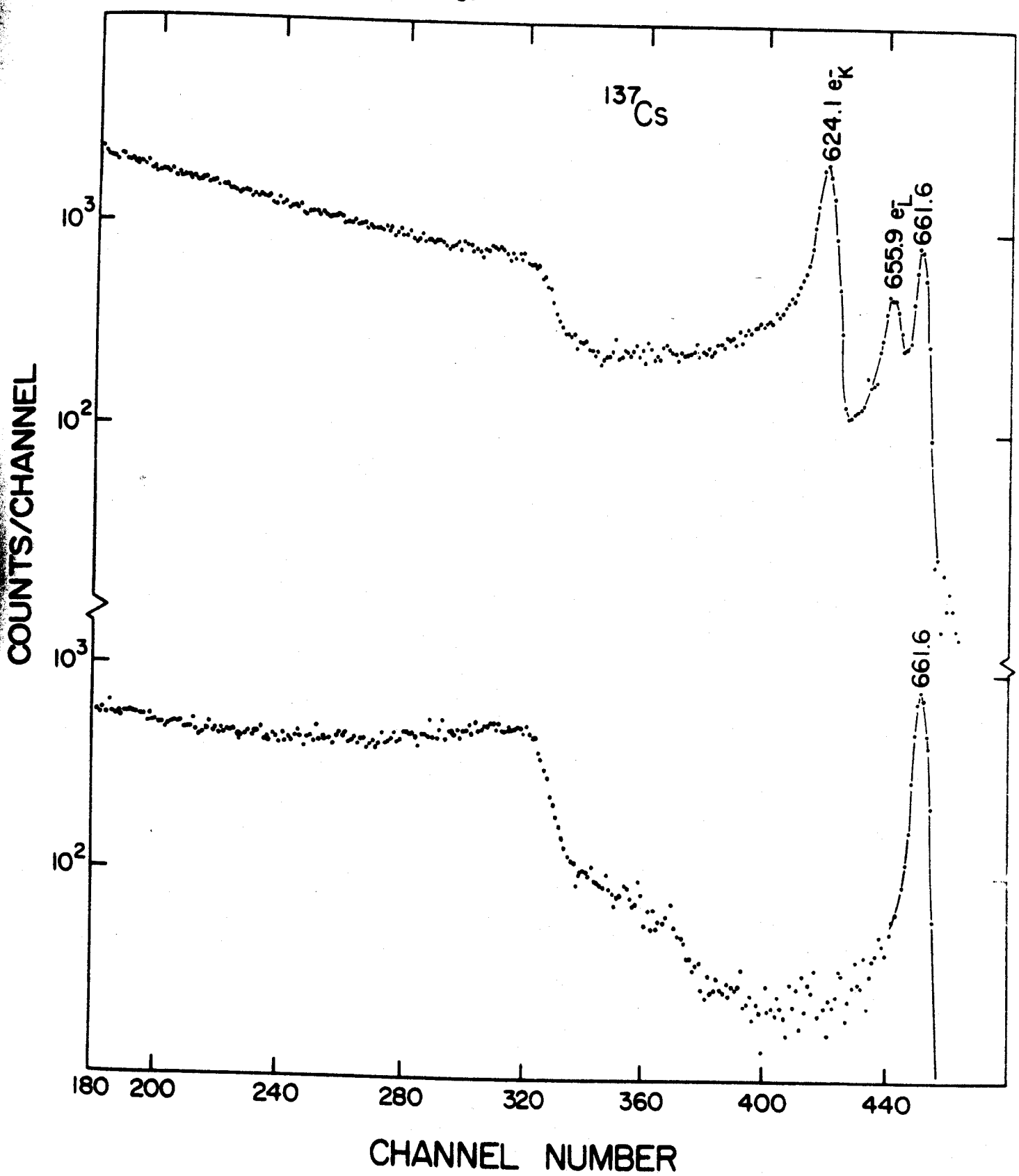

Figure III-2. Top: Cs^{137} spectrum showing the 661.6-keV γ-ray and its K and L conversion electrons. Bottom: Cs^{137} spectrum taken with an Al absorber between the source and the detector to block the electrons. By subtracting the bottom spectrum from the top one a clean electron spectrum can be obtained.

R. Todd is shown in Figure III-3. It takes the form of the relative efficiencies for γ-rays and electrons, i.e.,

$$C = \frac{D(\gamma)}{D(e-)} ,$$

vs. the γ-ray energy, $E\gamma$. To obtain the conversion coefficienct of a transition, one merely obtains an experimental intensity ratio for the γ-rays and electrons and multiplies this by the corresponding ordinate from Figure III-4, i.e.,

$$\alpha = C \frac{A_{e-}}{A_{\gamma}} .$$

Because the efficiency for electrons varies very slowly, the above efficiency curve is very nearly the same as the efficiency curve for γ-rays alone. The latter curve is presented in Figure III-3 with an offset scale for comparison.

3.1.3. Source Preparation

The sources used for our conversion coefficient measurements were made by bombarding separated isotope Pb^{206}(97.2%) with 30 MeV protons from the M.S.U. cyclotron to induce the reaction $Pb^{206}(p,3n)Bi^{204}$. The Bi^{204} has a half-life of 11.2-h, decaying by electron capture to states in Pb^{204} with ≈13% of the decays populating the isomeric level. The Bi^{204} activity was chemically separated from the Pb target (Appendix A), taken up in 6*M* HCl, and loaded onto a heated 1.5 mm diameter by 5 cm long Dowex 1×8 200-mesh anion-exchange column. The Bi^{204} activity stays on the resin, while the Pb^{204m} activity can be eluted with 0.3*M* HCl. The Pb^{204m} activy was allowed to build up

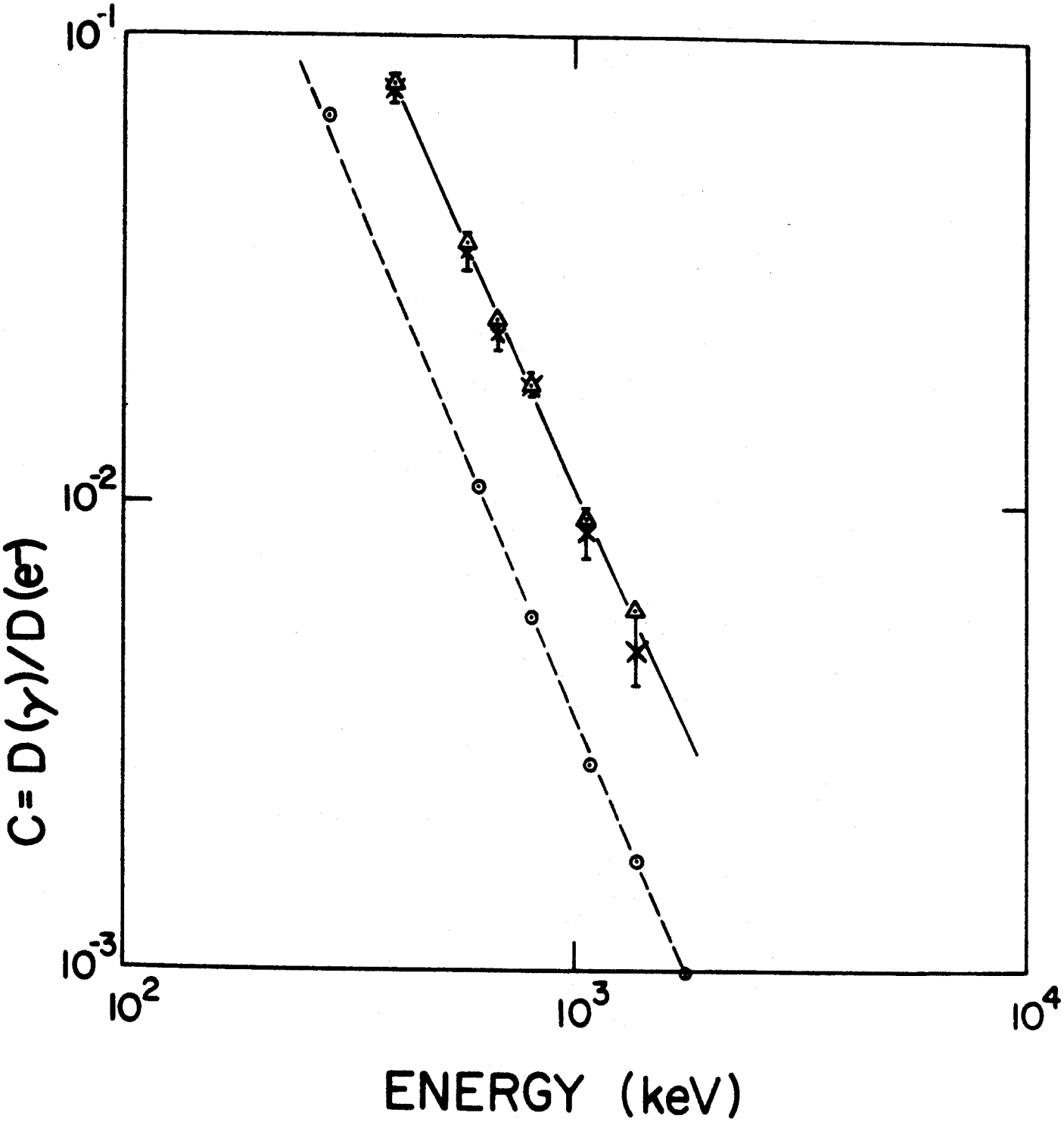

Figure III-3. Efficiency curves. The solid curve represents the composite γ-ray-electron efficiencies. Triangles are calculated from theoretical conversion coefficients, x's from experimental ones. The dashed curve shows a (displaced) γ-ray efficiency curve.

in the column for 1 hour before being eluted. The few drops of activity obtained were then vaporized through 3-mm diamter masks onto 0.25 mil Pt foil backings. As the Bi^{204} has an 11.2 h half-life, we were able to obtain many sources from one bombardment in this manner.

3.1.4. Experimental Results

Figure III-4 shows two spectra of Pb^{204m} taken with the Ge(Li) conversion coefficient spectrometer. The upper spectrum shows both the γ-rays and conversion electrons, while the lower spectrum was taken with an Al absorber placed between the source and detector. The areas of the 899.2- and 911.7-keV γ-ray peaks and conversion electron peaks were obtained by hand stripping these from the upper spectrum. Using the efficiency curve shown in Figure III-3, we calculated the K-conversion coefficients of the 899.2-keV $E2$ and the 911.7-keV $E5$ transitions. Our measured values are given in Table III-2, where they are compared with the theoretical values of Hager and Seltzer [Ha68]. We also included the K/L ratio for the $E5$ transition, however, we couldn't extract a reliable K/L ratio for the $E2$ because of the complexity of this portion of the spectrum.

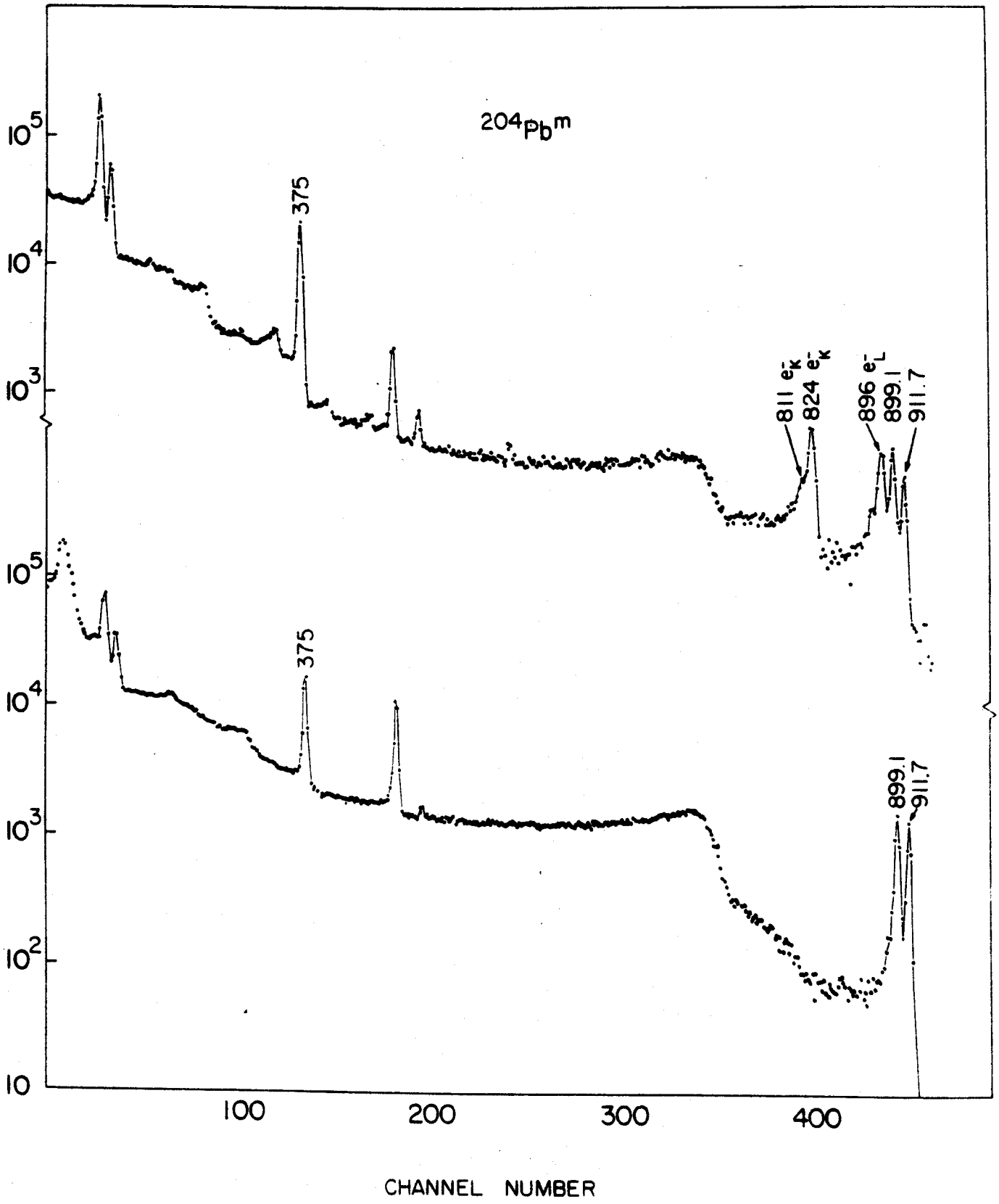

Figure III-4. Pb^{204m} spectra obtained with the Ge(Li) conversion-coefficient spectrometer. Only the Pb^{204m} transitions are labelled. Top: Spectrum showing both γ-rays and electrons. Bottom: Spectrum taken through an Al absorber to remove the electrons.

Table III-1

Conversion Coefficient Calibration Standards

Nuclide	γ-energy	Multi-polarity	α_K experimental	Ref.	α_K theoretical[a]
Sn^{113}	391.7	*M4*	$4.38\pm0.08\times10^{-1}$	b	$4.48\ 10^{-1}$
Cs^{134}	795.8	*E2*	$2.46\pm0.30\times10^{-3}$	c	$2.58\ 10^{-3}$
Cs^{134}	1365	*E2*	$6.8\ \pm0.5\ \times10^{-4}$	c	$8.19\ 10^{-4}$
Cs^{137}	661.595	*M4*	$8.94\pm0.10\times10^{-2}$	d	$9.28\ 10^{-2}$
Bi^{207}	569.6	*E2*	$1.56\pm0.07\times10^{-2}$	e	$1.59\ 10^{-2}$
Bi^{207}	1064	*M4*	$9.0\ \pm0.9\ \times10^{-2}$	e	$9.70\ 10^{-2}$

Table III-2

Pb^{204m} Conversion Data

Transition energy (keV)	MMulti-polarity	α_K experimental	α_K theoretical	*K/L* experimental	*K/L* theoretical[a]
899.1	*E2*	0.0072±0.0022	0.0065	---	---
912.0	*E5*	0.0545±0.0045	0.046	1.66±0.25	1.73

[a] R.S. Hager and E.C. Seltzer, Nuclear Data A4 (1968) 1.

[b] J.H. Hamilton, cited in C.M. Lederer, J.M. Hollander, and I. Perlman, Table of Isotopes, (J. Wiley and Sons, New York, 1967) 6th Ed.

[c] R.A. Brown and G.T. Ewan, Nucl. Phys. 68 (1965) 325; W. Van Wyngaarden and R.D. Conner, Can. J. Phys. 42 (1964) 42.

[d] J.S. Merritt and J.G.V. Taylor, Anal. Chem. 37 (1965) 351.

[e] K. Siegbahn, Nucl. Phys. A93 (1967) 63.

3.2. Pb^{203m} Decay and $M4$ Transition Probabilities

3.2.1. Introduction

Among electromagnetic transitions, the reduced transition probabilities of $M4$ transitions appear to be remarkably regular and consistent with the predictions of single-particle estimates. This can perhaps be explained partly by the fact that collective nuclear deformations are not likely to contribute appreciably to a magnetic hexadecapole field. Also, most known $M4$ transitions are isomeric transitions just below major closed shells and involve the high-spin states depressed by spin-orbit coupling from the next higher, opposite parity oscillator shells. Consequently, it is difficult for these transitions to be enhanced by suitable admixtures in the single-particle states. When one encounters an $M4$ reduced transition probability that is abnormally large, one is thus tempted to look for an experimental explanation. Such was the situation with Pb^{203m}.

The decay of the 6.1 sec isomer Pb^{203m} has been the subject of a number of investigations [St60] [Pr61] using conversion electron and NaI(Tl) spectrometers. These studies found only a single transition of about 825 keV, which was assigned an $M4$ multipolarity on the basis of conversion coefficient ratios and the mean lifetime of the γ-transition. The transition was assumed to go from a 13/2+ state to a 5/2- ground state, similar to those in the other odd-mass isomers of Pb. Because the $M4$ reduced transition probability was abnormally large, Stockendal [St60] suggested the possibility of an additional 5-keV transition from the isomeric state to a state at

820 keV, which is populated in the electron capture decay of Bi^{203}. Relatively little was known about the decay of Bi^{203} when this study was undertaken, both because of its complexity and because of the difficulty of preparing Bi^{203} free from Bi^{204}, which has the same half-life. Nevertheless, some progress had been made, and various investigators reported the spin and parity of the 820-keV state as 7/2- [No58] or 9/2- [St60]. If the level were 9/2-, the 5-keV transition would be an $M2$ and could possibly partially de-excite the 825-keV 13/2+ level along with the 825-keV $M4$ transition. In this study we observed such a branching decay.

Because a 5-keV transition would be highly converted and very difficult to observe directly, the easiest approach is to look for the 820-keV transition that would follow the 5-keV transition. Thus, the presence or absence of an 820-keV transition in the decay of Pb^{203m} would imply the presence or absence of the 5-keV transition. After this work was completed, J. Cross [Cr70] made a study of Bi^{203} decay and may have observed this 5-keV transition directly using a thin-window Si(Li) detector.

3.2.2. Experimental Method and Results

Separated isotope Pb^{206} in the form of $Pb(NO_3)_2$ was bombarded with 40-MeV protons from the Michigan State University Sector-Focused Cyclotron to produce Bi^{203}($t_{1/2}$=12 h) through the reaction $Pb^{206}(p,4n)Bi^{203}$. The Bi^{203} activity was separated chemically from the Pb target (Appendix A), taken up in 6M HCl and loaded onto a heated 1.5 mm diameter ×5 cm long Dowex 1×8 200-mesh anion-exchange

column. Pb^{203m} was eluted with 0.3M HCl, at the rate of two drops every 6 sec for a 2-h period. Each drop was immediately transferred to a 7 cm^3 Ge(Li) γ-ray detector. The resolution of our system was 2.7 keV FWHM for the 825.2-keV γ-ray from Pb^{203m}, and this could easily resolve the 820.1 and 825.2-keV γ-rays from Bi^{203} decay and could hopefully allow us to detect any 820.1-keV γ-ray from Pb^{203m}.

The spectrum in the region of interest of the Bi^{203} activity (which unavoidably contained some Bi^{204} with the same 12-h $t_{1/2}$) before being placed on the anion-exchange column is shown in Figure III-5a. The spectrum of the Pb^{203m} after separation, shown in Figure III-5b, clearly shows a peak at 820.1 keV. The areas of the two peaks obtained after stripping and correcting for the detector efficiency yield relative γ-ray intensities of 10.6±1.0% and 89.4±1.0% for the 820.1 and 825.2 keV γ-rays, respectively. Using the theoretical conversion coefficients of Sliv and Band [Sl65] for the K and L shells and those of Rose [Ro58] for the M shell to correct for internal conversion, the 13/2+ state is found to decay 8% by the 5.1-keV transition and 92% by the 825.2-keV $M4$ transition. Our proposed decay scheme for Pb^{203m} is shown in Figure III-6. The previous uncertainty in the assignment for the 820.1-keV state can be removed. The 5.1-keV transition is an $M2$, making the state 9/2-.

To check the possibility that some of the Bi^{203} might have been eluted from the anion-exchange column along with the Pb^{203m} and thereby have caused the 820.1-keV peak, the drops of eluted activity were saved and counted after the Pb^{203m} had died away. No Bi^{203} activity was found in these drops.

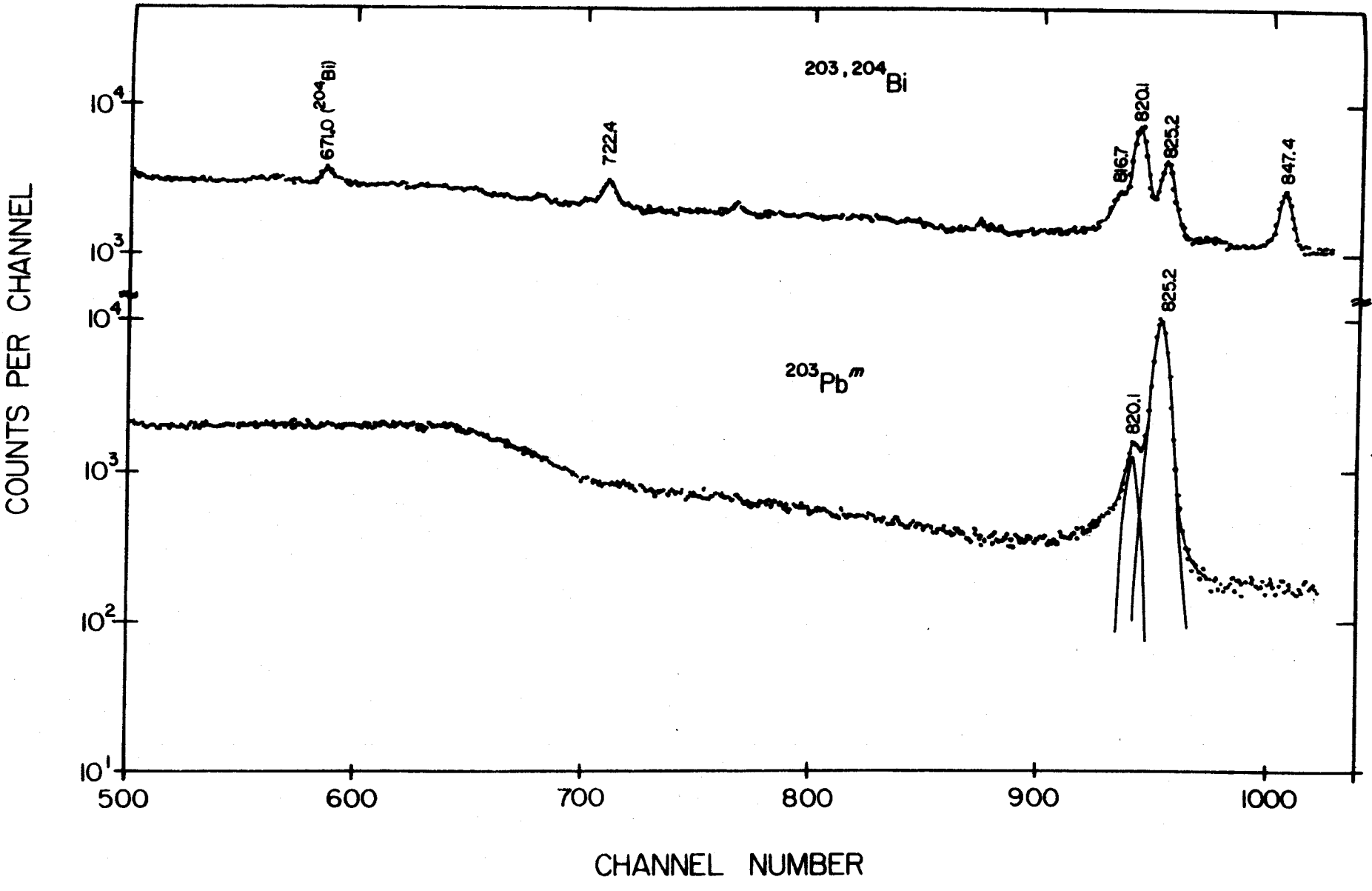

Figure III-5. The γ-ray spectrum of: a) Bi^{203} (unavoidably containing some Bi^{204}, which has the same half-life): b) Pb^{203m} after chemical separation from its Bi^{203} parent.

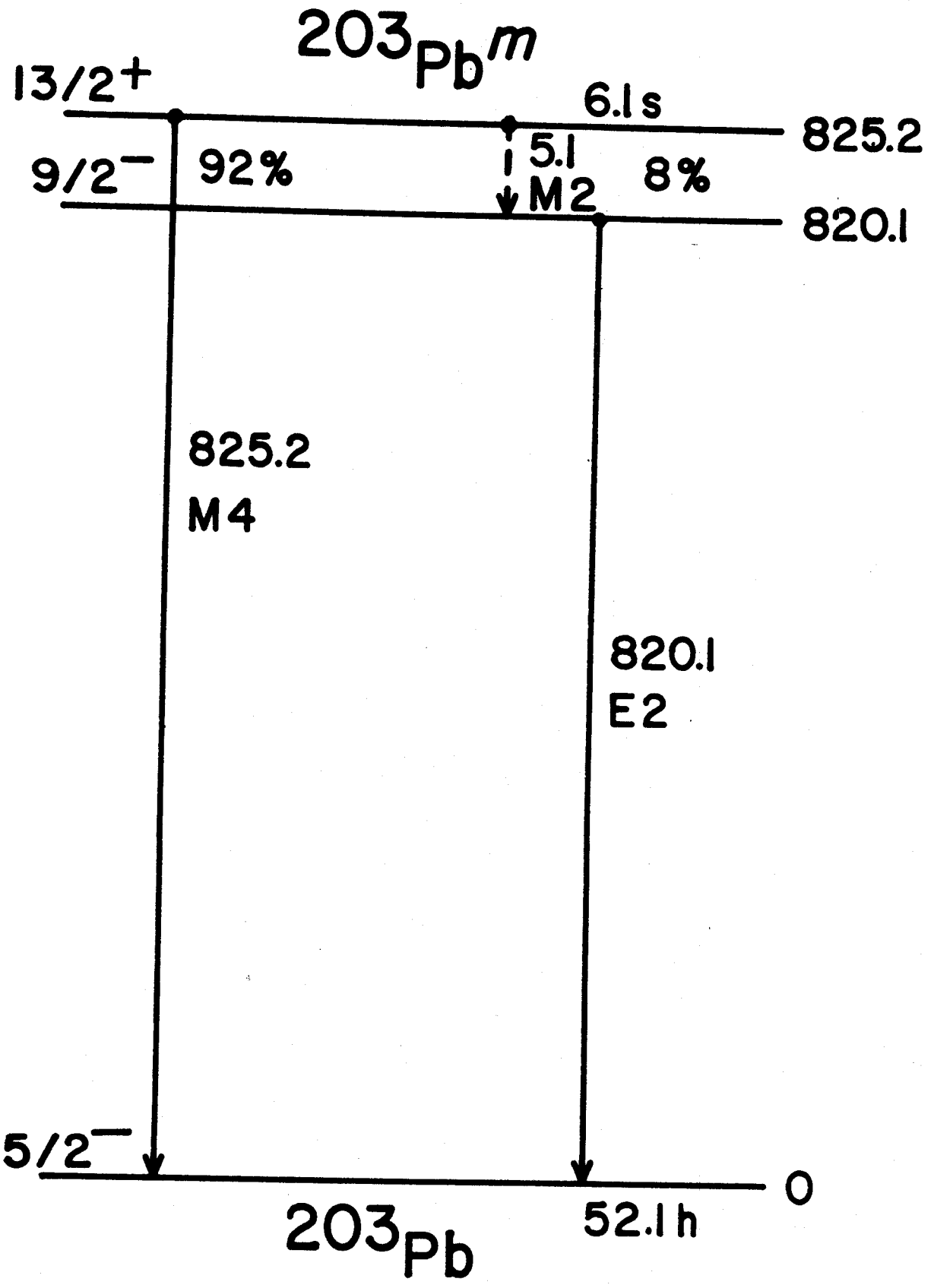

Figure III-6. The decay scheme of Pb^{203m} as determined from the present study.

Stockendal and his co-workers [St60] [St55] calculated the squares of the radial matrix elements for the $i_{13/2} \rightarrow f_{5/2}$ $M4$ γ-transitions in the odd-mass Pb isomers, using Mɒszkowski's approximations [Mo53]. They found the $|M|^2$ value for the transition in Pb^{203m} to be 15% larger than the average of the others. Their later values [St60] are listed in Table III-3, along with those that we calculated in the same manner, using the most recent partial half-life values for all the $M4$ γ-transitions [Hy64]. The $|M|^2$ value for the Pb^{203m} transition now fits nicely in line with the others, indicating that this transition behaves regularly, as one would expect for $M4$ transitions.

Table III-3

Radial Matric Elements for *M*4 γ-transitions in Odd-mass Pb Isotopes

$\|M\|^2$	*A*	197	199	201	203	205	207
Stockendal[a]		3.8±0.5	3.8±0.2	3.5±0.2	4.3±0.1		3.7±0.1
Present calc.[a]		3.6±0.4	3.7±0.2	3.5±0.2	3.8±0.2	(18±2)[b]	3.6±0.1

[a] We have used our own experimental data for the Pb^{203m} calculation and the most recent half-life values tabulated in ref. [Hy64] for the other calculations.

[b] The value of $|M|^2$ for Pb^{205m} is inexplicably large, perhaps because of the presence of two unresolved 1014-keV transitions, and is included only for the sake of completeness. See ref. [St60].

3.3. The Decay of Pb^{202m}

3.3.1. Introduction

The 3.62 h isomeric state in Pb^{202} was first reported by Maeder, Wapstra, Nijgh, and Ornstein [Ma54] in 1954. They produced Pb^{202m} in the bombardment of a Tl target with 25-MeV deuterons. This study and later studies by Bergkvist and co-workers [Be55], McDonell and co-workers [Mc57], and Johansson [Jo59] have resulted in the decay scheme as shown in Figure III-7 with the exception of those transitions marked with a crossed-dotted line and the 1552-keV level which were, tentatively, added in the present work. Although the decay scheme of Pb^{202m} is similar to that of Pb^{204m}, the isomeric level being 9- in both cases, it does differ from Pb^{204m} in that some de-excitation by ε decay to Tl^{202} is observed.

3.3.2. Source Preparation

In our initial examination of this decay in 1967, we tried to measure the conversion coefficients of some transitions in the decay of Pb^{202m} using the conversion coefficient spectrometer described in Section 3.2. The sources were made by bombarding natural Tl foils with 17-MeV protons to induce the reaction $Tl^{203}(p,2n)Pb^{202}$. Our attempts to measure the conversion coefficients required carrier-free sources. These were made using the chemistry described in Appendix D and vaporizing the carrier-free Pb^{202m} onto 1 mil Al backings as described in Section 3.1.2. The γ-ray singles measurements were done on sources made from both natural Tl foils and enriched Tl^{203} (70%) targets bombarded with 17-MeV protons. In this case we used the $PbSO_4$ precipitation procedure described in

Figure III-7. Decay scheme of Pb^{202m}. The transitions marked with the crossed-dotted lines were added in the present study. The transition intensities given here are γ-ray intensities only. The intensity of the 129.09-keV transition may seem improbable, however, as this is an $E4$ transition, it is very highly converted.

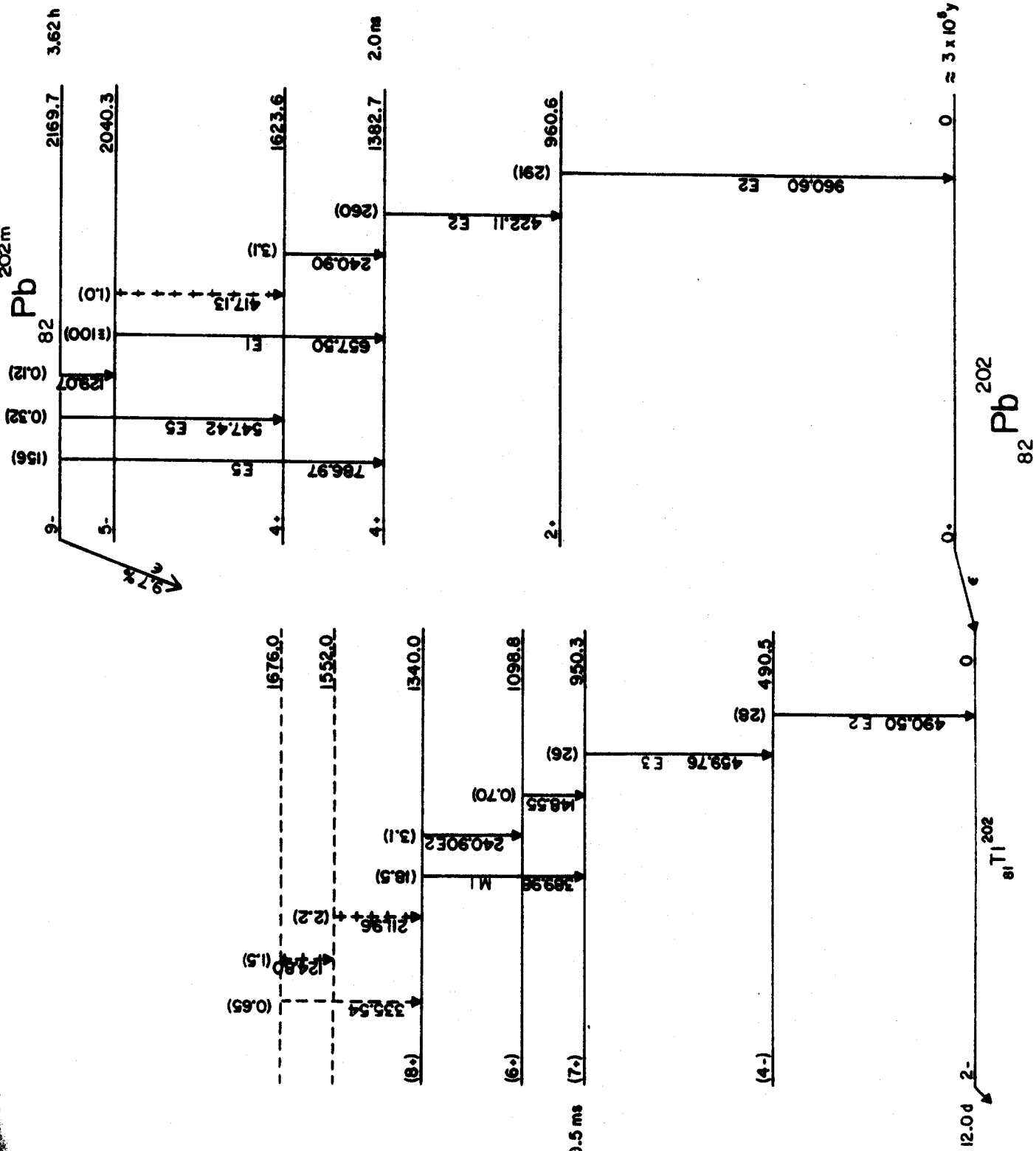
$^{82}Pb^{202m}$
3.62 h
2.0 ms
2169.7
2040.3
1623.6
1382.7
960.6
0
≈ 3 x 10⁵ y
9-
5-
4+
4+
2+
0+
(156)
(0.32)
(0.12)
(≥100)
(1.0)
(3.1)
(260)
(291)
786.97 E3
547.42 E3
429.07
657.50 E1
417.13
240.90
422.11 E2
960.60 E2
ε
$^{81}Tl^{202}$
12.0 d
2-
0
490.5
(28)
490.50 E2
459.76 E3
(26)
950.3
0.5 ms
(7+)
M1 48.55
(0.70)
1098.8
(9+)
389.96
(18.5)
240.90E2
(3.1)
1340.0
(8+)
211.96
(2.2)
1552.0
124.80
(1.5)
1676.0
375.54
(0.65)
(4-)

Appendix B to separate the Pb^{202m} from the Tl targets. We have also recently prepared Pb^{202m} from the decay of 1.6 h Bi^{202} using a combination of the ion-exchange procedure described in Section 3.1.3. (Appendix C) and the precipitation procedure described in Appendix B.

3.3.3. Experimental Results and Discussion

The initial examination of this isomer in 1967 revealed no new information on the decay scheme, as the detectors used were very small and the spectra obtained using the conversion-coefficient spectrometer were almost impossible to interpret, as the broad conversion-electron peaks overlapped many of the γ-ray peaks. We, therefore, abandoned our investigation of this decay scheme until several months ago, when we found that several of the γ-rays from Pb^{202m} decay overlapped with γ-rays from the decay of Pb^{201} (Chapter V), and we needed accurate γ-ray intensities for Pb^{202m} in order to subtract these from the intensities in the Pb^{201} spectra. Much to our surprise, in this brief examination we found several new γ-rays which seemed to have a ≈3 to 4 h half-life. Figure III-8 shows a typical spectrum obtained in this experiment using the 2.5% efficient detector. Table III-4 contains a list of the γ-rays found in this examination along with their relative intensities in the singles experiments. The 124.80-, 211.96-, 417.13-, 601.92-, 954.43-, and 1002.78-keV γ-rays were previously unreported. Although we have yet to perform coincidence experiments on this isomer, we have been able to make some speculations on the placement of certain of these γ-rays. These γ-rays are shown in the decay scheme, Figure III-7 as the crossed-dotted lines. Work on this isomer is continuing with both γ-γ and γ-x-ray two-dimensional experiments planned. The γ-x-ray coincidence experiment is

designed to allow us to assign the transitions either to the internal transition de-excitation or to the ε decay branch to Tl^{202}.

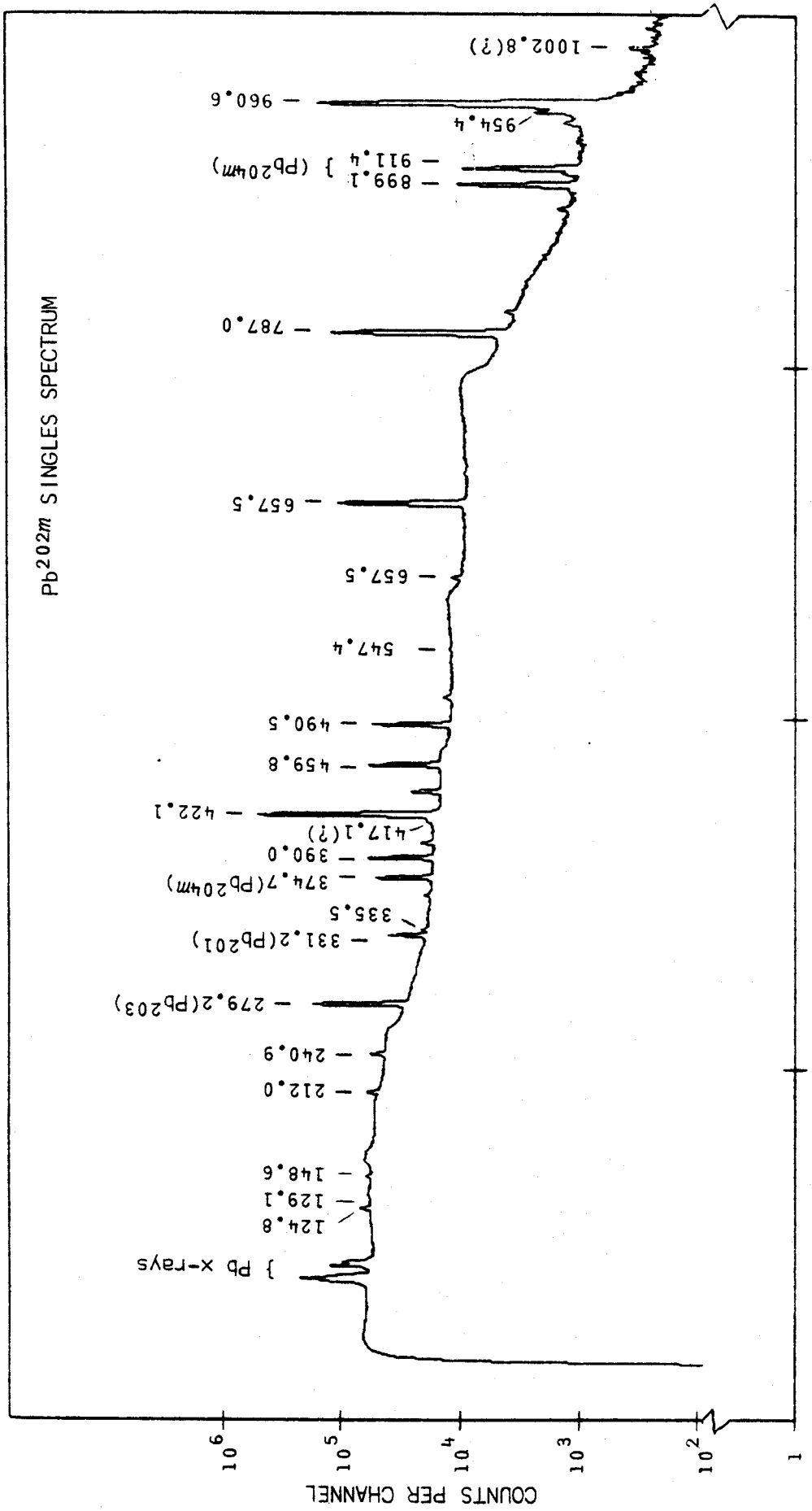

Figure III-8. A singles γ-ray spectrum of Pb^{202m} recorded by a 2.5% efficient Ge(Li) detector. The source used to obtain the spectrum was prepared by the $(p,2n)$ reaction on enriched Tl^{203}(70%).

Table III-4

Energies and relative intensities of γ-rays from the decay of Pb^{202m}

Measured energies (keV)	Relative intensity in singles
124.80±0.08	1.5
129.07±0.15	0.12
148.55±0.08	0.70
211.96±0.08	2.2
240.90±0.08	3.1
335.54±0.15	0.65
389.98±0.07	18.5
417.13±0.20 (?)	1.0
422.11±0.07	260
459.76±0.07	26
490.50±0.07	28
547.42±0.25	0.32
601.92±0.08	1.8
657.50±0.07	≡100
786.97±0.07	156
954.43±0.25	3.6
960.60±0.07	291
1002.78±0.15 (?)	0.29

3.4. Search for an Isomeric State in Pb^{200}

All of the odd-mass Pb isotopes known below $N = 126$ have long-lived isomeric states based on the $i_{13/2}$ neutron state. The three even-even isotopes, Pb^{206}, Pb^{204}, and Pb^{202}, also have isomeric states, here 7- or 9- states resulting from coupling the $i_{13/2}$ neutron hole to other holes. Since the $i_{13/2}$ neutron hole decreases in energy with decreasing mass number, we hoped to be able to find a similar isomer in Pb^{200}.

Figure III-9 shows the basic aspects of the even-mass lead isomers. From the apparent systematic behavior of these isomers we expected to find an isomeric state in Pb^{200} at about 2150 keV. This isomeric state has been the object of previous investigations [Hy64], with no positive results. Bergkvist, et al., [Be55] set an upper limit of one hour on the half-life of Pb^{200m}.

We began our search for Pb^{200m} late in 1967. Our first attempts involved bombarding Tl^{203} with protons to induce the reaction $Tl^{203}(p,4n)Pb^{200m}$. This type of reaction has been used to produce the other isomers in good yield. Bombardments were made at proton energies of 31, 36, and 40 MeV. Four 1024-channel Ge(Li) γ-ray spectra containing the results of numerous bombardments were obtained at each energy, each source being counted consecutively for periods ranging from 5 sec to 15 min. For the very short counting periods we made use of a fast pneumatic target system (rabbit) to bring the target from the beam to the counting system in less than 3 sec. [Ko69]. These experiments failed to produce any evidence of a new isomer, and

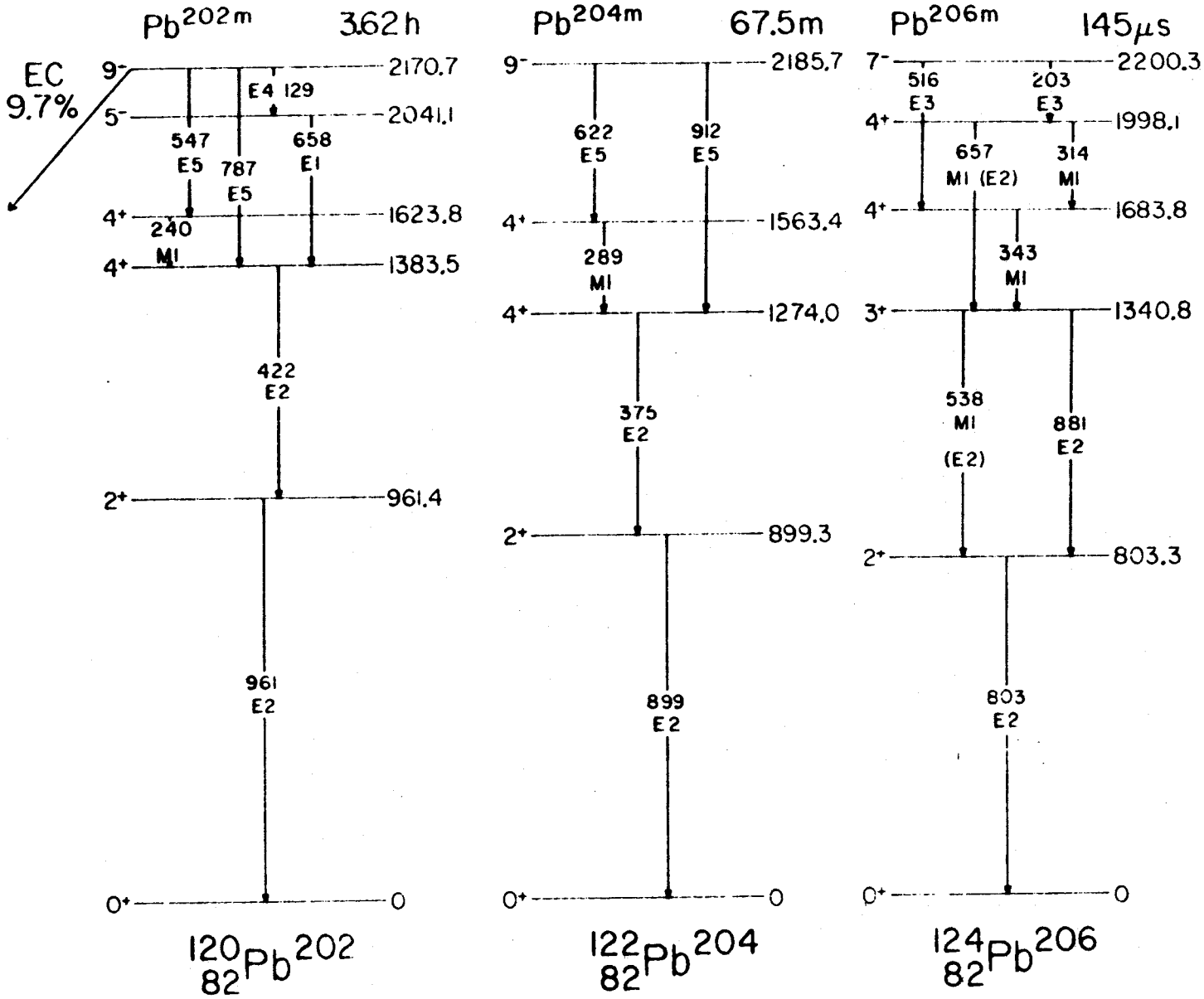

Figure III-9 Systematics and decay schemes of the known even-even Pb isomeric states.

we set an upper limit of about 1 sec on the half-life of any new activity.

We next attempted to populate an isomeric state in Pb from the decay of Bi^{200}. This procedure was similar to that used successfully in our study of 6.1-second Pb^{203m} (Section 3.2). 35-minute Bi^{200} has an estimated electron capture decay energy of 6.5 MeV and a ground state spin of 7 and should therefore populate high spin states in Pb^{200}. Bi^{200} was produced by bombarding separated isotope Tl^{203} (70%) with a 50-MeV He^3 beam to induce the reaction $Tl^{203}(He^3,6n)Bi^{200}$. The Bi^{200} was chemically separated from the Tl target (Appendix C) and loaded onto an anion-exchange column. The Pb^{200} activity was eluted with 0.3*M* HCl periodically and counted using the 0.42% efficient Ge(Li) detector. The rate of elution was varied for several different runs, the fastest rate being several drops every 5 seconds. However, we failed to detect any evidence of an isomeric state in Pb^{200} longer than ≈1 second in these experiments.

With the recent development of a helium thermalizer and jet transport system for nuclear recoils at the M.S.U. Cyclotron Laboratory [Ko69], we should be able to extend our search for Pb^{200m} into the millisecond range. Delayed coincidence experiments, similar to those used to measure the 4-msec half-life of Pb^{205m} [Be60], would be another method for reaching into the millisecond range. However, our failure to find an isomeric state with a half-life longer than ≈1 second indicates that a high spin state, such as the 7- state in Pb^{206m}, falls below the 9- state, destroying any possibility for a long-lived isomeric state.

CHAPTER IV

THE ELECTRON CAPTURE DECAY OF Pb^{200}

4.1. Introduction

In this chapter we present the results of our investigation of the electron capture decay of 21.5-h Pb^{200} to states in the odd-odd nucleus $_{81}Tl^{200}_{119}$. This isotope and the other odd-odd isotopes of thallium are in one of the most favorable regions for explaining properties of non-deformed odd-odd systems, for the single particle states in many of the neighboring odd-mass nuclei are reasonably well characterized.

The first published study of the decay of Pb^{200} was by Bergkvist and his co-workers [Be55] in 1955. They bombarded natural Tl with protons and investigated the conversion electrons in the energy region 10-1600 keV with a double-focusing β spectrometer. They measured the half-life of Pb^{200} to be 21.5±0.4 h and assigned 10 transitions to its decay. In 1956, Gerholm [Ge56] proposed a decay scheme consisting of four excited levels at 148.0, 257.3, 289.5, and 525 keV; these were placed on the basis of electron-electron coincidence experiments. Åström, Johansson, and Bergström [As57] next measured the relative conversion-electron intensities more precisely and also measured the half-life of the 148-keV state to be 8 nsec. (The half-life of this state was later determined to be 7.1±0.15 nsec by Johansson, Alväger, and Zuk. [Jo59]). They characterized the 148.0-keV transition to the ground state as a

"pure" $E2$ transition, which allowed them to make an assignment of $I\pi$ = 0- for the 148-keV state. (The Tl^{200} ground state had been assigned 2- on the basis of its decay properties [He57] to Hg^{200}, where the spin of 2 had been established previously by atomic spectra and atomic beams methods [Hu61].

The latest work on the decay of Pb^{200} was carried out by Wirhed and Herrlander [Wi62] in 1962, who studied the conversion lines with flat-field permanent magnet β spectrometers having energy resolutions as good as 0.1%. They also performed some electron-electron coincidence experiments. Conversion lines corresponding to 15 transitions in Tl^{200} were found, and multipolarities were assigned for 10 of these on the basis of conversion-coefficient ratios. These workers devised a decay scheme including excited levels at 147.61, 257.15, 289.11, 289.92, 450.5, 525.6, and 605.3 keV. They also made several tentative spin and parity assignments for these levels.

Thus, although a reasonable amount of information on the decay of Pb^{200} had been obtained and assembled, many uncertainties remained. These included the log ft's, several multipolarities, and spin and parity assignments for several states. One of the more fascinating problems concerned the verification of two closely spaced levels at 289.1 and 289.9 keV proposed by Wirhed and Herrlander [Wi62] but not reported by previous workers. In addition, as no γ-ray studies of Pb^{200} decay had been published, we felt that γ-ray spectroscopy using Ge(Li) detectors might allow us to find new transitions. This was a large order to fill, especially for the small, poor resolution detectors used in the initial experiments, for

we were competing with β spectrometers in an energy region (<1 MeV) where the resolution of these devices are better than 1 keV and internal conversion intensities are highest. The fact that we observed any new transitions at all in this worked-over isotope is convincing proof of the ability of the Ge(Li) detectors to compete successfully with β spectrometers in this energy region.

4.2. Source Preparation

4.2.1. Introduction

Since the decay of Pb^{200} had been the subject of many previous investigations, it was obvious that if we were to observe any new γ transitions from this decay we would need sources free from contaminating activities. This was especially critical in the case of Pb^{200} because all the γ-rays belonging to this decay are lower in energy than 605 keV and the underlying Compton distributions from contaminant γ-rays tended to hide very weak peaks. Therefore, a great deal of time and effort was spent trying to make impurity-free sources.

4.2.2. $Tl^{203}(p,4n)Pb^{200}$

Our first attempts to make Pb^{200} consisted of bombarding natural Tl foils (29.5% Tl^{203} 70.5% Tl^{205}) with 34-MeV protons from the Michigan State University Cyclotron to induce the $Tl^{203}(p,4n)$ Pb^{200} reaction. Bombarding times varied from 1-5 hours depending on the beam current. This energy was chosen because it is just below the threshold for producing Pb^{199}. However, we still produced in significant amounts all the possible Pb isotopes from (p,xn) reactions on Tl^{203} and Tl^{205}, where $4 \geq x \geq 1$. γ-rays from the following isotopes were found in the freshly bombarded sources: Pb^{204m}(67 min), Pb^{203} (52h), Pb^{202m}(3.6h), and Pb^{201}(9.4h). Because of the short half-lives of Pb^{204m} and Pb^{202m} as compared to the 21-h Pb^{200}, it was an easy matter virtually to eliminate these by aging the sources for 2 or 3 days. During this 2 or 3 day aging the 9.4-h Pb^{201} was also reduced to an acceptable level, although several of its more intense γ-rays

could still be detected. However, γ-rays from the 52-h Pb^{203} contaminant were greatly enhanced and became the dominant activity. The Pb^{203} was a problem not because of the number of γ-rays emitted in its decay, since there are only three (279, 401, and 680 keV), but because they contribute very significantly to the Compton background in the energy region of interest and thereby tended to obscure the weaker peaks from the decay of Pb^{200}. As the Pb^{203} was produced mainly by the $(p,3n)$ reaction on Tl^{205}, we decided to raise the bombarding energy to 37 MeV in order to maximize the $(p,4n)$ reactions on both Tl^{203} and Tl^{205}. For Tl^{203} this would enhance the production of 3.6-h Pb^{202m} at the expense of Pb^{203}. Although we did go slightly over the threshold for the production of Pb^{199}, this did not present a problem because the half-life of this isotope is only 1.5-h, and after 2 or 3 days any remaining Pb^{199} activity was not detectable. However, simply aging the sources did not eliminate our problems of source purity, for although we could eliminate the Pb parents, some of the daughter Tl isotopes are also γ-ray emitters. These included 7.4-h Tl^{199}, 73-h Tl^{201}, and 12-d Tl^{202}. This would have been an easy matter to correct if these were the only Tl contaminants, for we could simply have performed a single chemical separation at the end of the aging period without fear of any more Tl activities growing in. As you might have guessed we were not so blessed, and indeed the daughter of Pb^{200}, Tl^{200}, is unstable with a half-life of 26-h. This would not have been a significant problem if the Tl^{200} decay produced only a few γ-rays; but such was not the case and the Table of Isotopes [Le67] reports

61 γ-rays associated with this decay (actually, we observed several additional unreported γ-rays in just a cursory look at this decay). Because the Tl^{200} was constantly building up in our sources from the decay of Pb^{200}, it was necessary to perform a chemical separation periodically to get rid of it. The time between separations was generally one hour, but time periods up to 3-h were sometimes used. The chemical separation used is given in Appendix B.

While the $(p,4n)$ reaction on natural Tl was used for many experiments in the early days of this study, it still suffered from the presence of a large amount of Pb^{203} impurity. Although we were stuck with this method of production for a long time, two new methods of producing Pb^{200} were opened to us after the M.S.U. Cyclotron began accelerating He^3 beams on a routine basis.

4.2.3. $Tl^{203}(He^3,6n)\ Bi^{200} \xrightarrow{\xi} Pb^{200}$

The first of these made use of a 58-MeV (70-MeV degraded with 20 mil of aluminum) He^3 beam to induce the $Tl^{203}(He^3,6n)\ Bi^{200}$ reaction on natural or enriched (70%Tl^{203}, 30%Tl^{205}) Tl targets. The Bi^{200} has a half-life of about 37 minutes and decays by electron capture to Pb^{200}. As in the case of the (p,xn) reactions, there are many competing reactions in the (He^3,xn) case also. In this case we produced the following Bi isotopes: Bi^{205}(15.3-d), Bi^{204}(11.2-h), Bi^{203}(11.8-h), Bi^{202}(1.6-h), and Bi^{201}(1.8-h). If we had simply let the Tl target age for 2 or 3 days we would have ended up with essentially the same ratio of lead isotopes as in the direct approach using protons. However, if we examine the half-lives of the Bi isotopes we see that the Bi^{200} has

a shorter half-life than any of the others produced by this reaction, and most important, it is much shorter than that of Bi^{203} (11.8-h). Our reasoning was that if we could separate the Pb isotopes from the Bi isotopes within a short time after the end of the bombardment, say 1 or 2 hours, most of the Bi^{200} would have decayed to Pb^{200}, while very little of the other Bi isotopes, especially Bi^{203}, would have decayed to their Pb daughters. This was accomplished using essentially the same ion-exchange method described in our search for Pb^{200m} (section 3.4). In our search for Pb^{200m} we did occasionally use enriched Tl^{203} targets and as a by-product of these experiments we obtained a few sources of Pb^{200} to use in this study.

Although this method produced the purest sources used during this study, a great deal of effort was required to obtain sources of the required strength.

4.2.4. $Hg^{202}(He^3,5n)\ Pb^{200}$

The second method of producing Pb^{200} using He^3 beams turned out to be the most satisfactory from the standpoint of both ease of preparation and reducing the Pb^{203} contaminant. This method made use of a 50-MeV (70-MeV degraded with 32 mil aluminum) He^3 beam to induce the $Hg^{202}(He^3,5n)\ Pb^{200}$ reaction on natural Hg. At first glance this seems like a very messy way of making any Pb isotope because of the many stable Hg isotopes. The stable isotopes of Hg are listed in Table IV-1 along with their per cent abundances. Looking over these stable Hg isotopes it is apparent however, that the only isotope of Hg that could give rise to any significant amount of Pb^{203} from a He^3

Table IV-1

Stable Isotopes of Hg and % Abundances

Isotope	Naturally occurring abundance [a]
Hg^{196}	0.146%
Hg^{198}	10.02 %
Hg^{199}	16.84 %
Hg^{200}	23.13 %
Hg^{201}	13.22 %
Hg^{202}	29.80 %
Hg^{204}	6.85 %

[a] As compiled in the Chart of Nuclides by the Knolls Atomic Power Laboratory, Ninth Edition (1966).

beam of 50-MeV is Hg^{204}. Fortunately this has a relative abundance of only 6.85% compared to 29.8% for Hg^{202} from which most of the Pb^{200} was produced. Actually, a significant amount of Pb^{200} also resulted from the reactions $Hg^{201}(He^3,4n)Pb^{200}$ and $Hg^{200}(He^3,3n)Pb^{200}$. This gave us a favorable ratio of >7:1 for the amount of Pb^{200} produced to that of Pb^{203}. The remaining stable Hg isotopes produce Pb isotopes with mass numbers below 200. However, these were not a problem since they all have half-lives of less than 2.5 hours and the sources were aged for several days before counting. HgO was found to be the most satisfactory form of mercury for these bombardments. The same chemistry used to separate Pb^{200} from the Tl targets (Appendix B) was used to separate the Pb^{200} from the HgO targets, the only change being the addition of Tl^{+++} in place of Hg^{++} as the hold-back carrier. Most of our final experiments, including the singles spectrum shown in Figure IV-1 used sources prepared in this way.

Even after performing the chemical separations, we did observe some contaminant peaks that we could not assign to any of the known Pb or Tl isotopes. However, these were shown not to originate from Pb^{200} decay because of their differing relative intensities throughout the many singles spectra taken at different times and with different sources.

4.3. Experimental Results

4.3.1. γ-ray Singles Spectra

Energies and intensities of the Pb^{200} γ-rays were determined using two five-sided trapezoidal Ge(Li) detectors having photopeak efficiencies at 1.332 keV of 0.42% and 2.5%. Typical resolutions were 3.0 and 2.3 keV FWHM at the same energy. Both detector systems used room-temperature FET preamplifiers, low noise *RC* linear amplifiers with pole-zero compensation and near-Gaussian shaping, and 1024- to 4096-channel analyzers or ADC's coupled to the PDP-9 or Sigma-7 computer.

The energies of the prominent γ-rays were measured by counting the Pb^{200} sources simultaneously with the energy standards listed in Table IV-2. The energies of most of the weaker Pb^{200} γ-rays were then determined by using the energies of the prominent Pb^{200} γ-rays as secondary standards. The centroids and intensities of the photopeaks were determined using the live-display computer program MOIRAE [Moir].

Figure IV-1 shows a γ-ray spectrum obtained in 7-h with the 2.5% detector. In this figure only those γ-rays assigned to the decay of Pb^{200} are labeled. Nineteen γ transitions were so assigned, having the energies and intensities listed in Table IV-3. Of these, the 155.29-, 139.39-, 348.23-, 377.92-, and 525.54-keV transitions had not been reported in the earlier studies.

The energies of the 142.28-, 147.63-, and 348.23-keV γ's were determined by stripping these peaks by hand and then calculating the centroids. The 348.23-keV γ had to be stripped from an unresolved triplet that contained two contaminant peaks. Because even our best

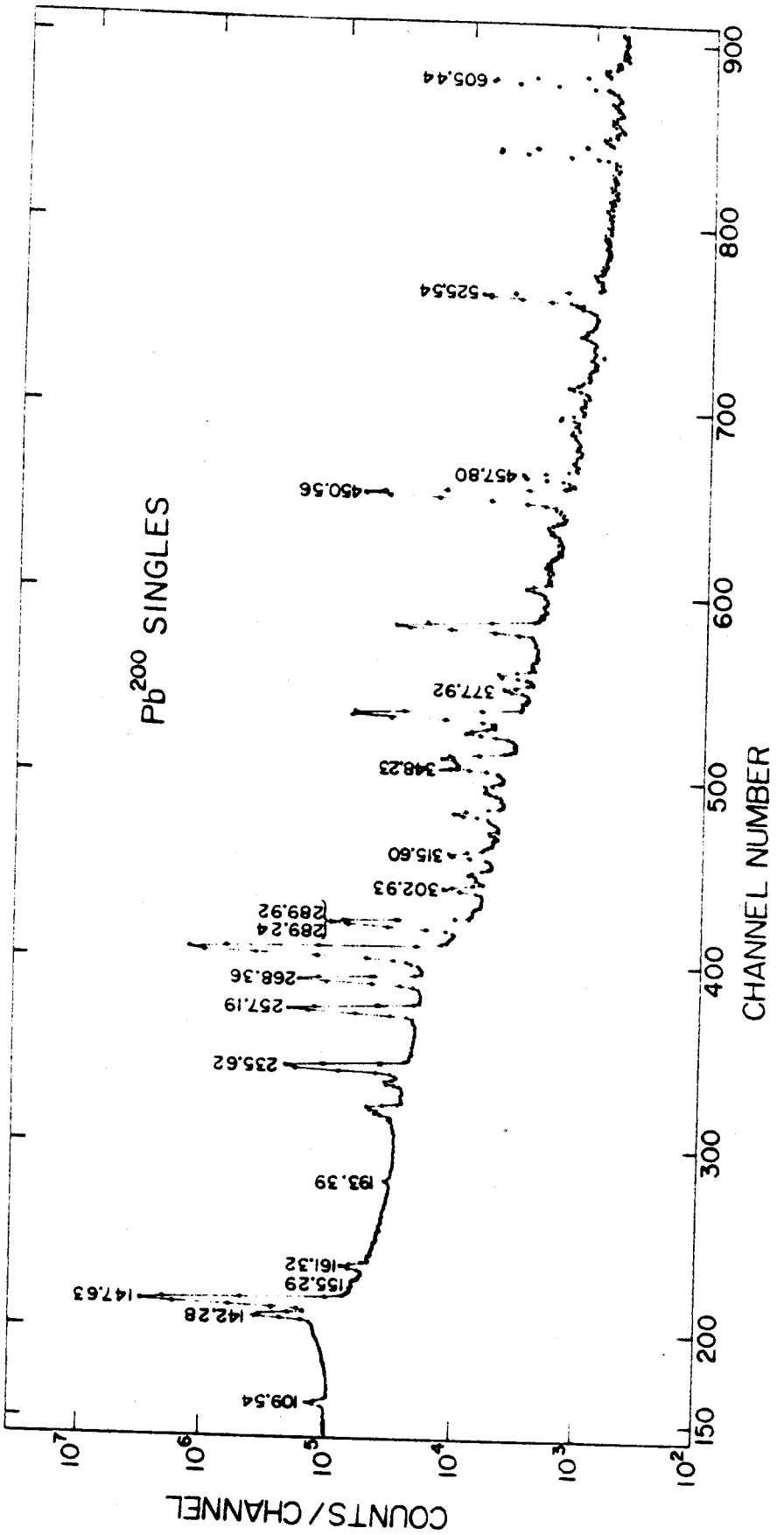

Figure IV-1. γ-ray singles spectrum of Pb^{200} obtained in 7 h with a 2.5% efficient Ge(Li) detector. Only those peaks belonging to the decay of Pb^{200} are labeled.

Table IV-2

γ-Rays Used as Energy Standards

Nuclide	γ-Ray energy (keV)	Reference
Am^{241}	59.543±0.015	a
Co^{57}	121.97 ±0.05	b
	136.33 ±0.04	b
Ce^{139}	165.84 ±0.03	c
Pb^{203}	279.17 ±0.02	b
Ta^{182}	100.104±0.002	d
	152.435±0.003	d
	156.387±0.003	d
	179.393±0.004	d
	222.109±0.005	d
	229.322±0.008	d
	264.072±0.009	d
Au^{198}	411.795±0.009	e
Bi^{207}	569.63 ±0.08	b
Cs^{137}	661.595±0.076	f

[a] T. Yamazaki and J. M. Hollander, Nucl. Phys. 84, 505 (1966).

[b] J. B. Marion, Gamma-Ray Calibration Standards, Univ. of Maryland Technical Report 653 (1957)

[c] J. S. Geiger, R. T. Graham, I. Bergström, and F. Brown, Nucl. Phys. 68. 352 (1965).

[d] Average of: U. Gruber, R. Koch, B. P. Maier, and O.W.B. Schult, Z. Naturforsch. 20a, 929 (1965) and E. J. Seppi, H. Henrikson, F. Boehm, and J.W.M. Dumond, Nucl. Instr. Methods 16, 17 (1962).

[e] G. Murray, R. T. Graham, and J. S. Geiger, Nucl. Phys. 45, 177 (1963).

[f] J. S. Geiger, R. T. Graham, and F. Brown, Can. J. Phys. 40, 1258 (1962).

Table IV-3

Energies and Relative Intensities of γ Rays

from the Decay of Pb^{200}

Measured energies (keV)	Relative intensities		
	Singles	Integral γ-γ coincidence	Anticoincidence
K x-rays	3156 ± 350	-	-
109.54±0.04	14.5 ±2.0	370	12
142.28±0.03[a]	95.1 ±5.0[a]	4900	55
147.63±0.03[a]	1133 ± 30[a]	21,500	1020
155.29±0.10	1.4 ±0.5	-	-
161.32±0.04	9.1 ±1.0	650	6.6
193.39±0.10	1.0 ±0.4	-	-
235.62±0.04	129 ±4.0	7000	81
257.19±0.03	134 ±4.0	5100	100
268.36±0.03	119 ±5.0	6000	80
289.24±0.15[a]	32 ± 10[a]	1950	70
289.92±0.10[a]	51.6 ± 10[a]		
302.93±0.05	5.0 ±1.0	125	3.5
315.60±0.08	6.7 ±1.0	260	4.5
348.23±0.08[a]	4.8 ±1.5[a]	130	-
377.92±0.05	0.8 ±0.3	9.7	-
450.56±0.05	≡100	≡100	≡100
457.80±0.07	3.5 ±0.6	24	2.3
525.54±0.06	12.6 ±1.0	-	12
605.44±0.06	16.9 ±1.2	23	19

[a]Be sure to read the text for comments on how these energies and intensities were obtained.

detector could not resolve the doublet consisting of the 289.24- and 289.92-keV γ's well enough to allow us to strip these peaks, the energies for these transitions given in Table IV-3 were obtained from sum and difference relationships among the other transitions. The intensities were determined on the basis of the relative contributions necessary to reproduce the energy of the doublet, "289.66-keV". Evidence for the doublet nature of the 289.7-keV peak will be given in Section 4.3.2.

The uncertainties in the energies listed in Table IV-3 are based on the uncertainties in the energy standards, the heights of the peaks above backgrounds, and the reproducibilities of the calculated energies from many different spectra. The relative intensities listed are averaged from spectra obtained with both detectors. Their uncertainties are based on the reproducibilities of the intensities and the uncertainties in our experimentally-determined efficiency curves for the detectors.

The *K* x-ray intensity for Pb^{200} listed in Table IV-3 was obtained in the following manner. A Pb^{200} source was aged until the 9.4-h Pb^{201} was only a minor contaminant, thereby avoiding a correction for its x-rays. This left Pb^{203} and Tl^{200} as the only major contributors to the total x-ray intensity. Since spectra of Pb^{203} and Tl^{200} could be obtained relatively free from contaminants, it was an easy matter to determine how much each of these contributed to the total x-ray intensity in the Pb^{200} spectrum. After subtracting out their contributions, the remaining *K* x-ray intensity belonged essentially to Pb^{200}. The three spectra taken to obtain this x-ray intensity are shown in Figure IV-2.

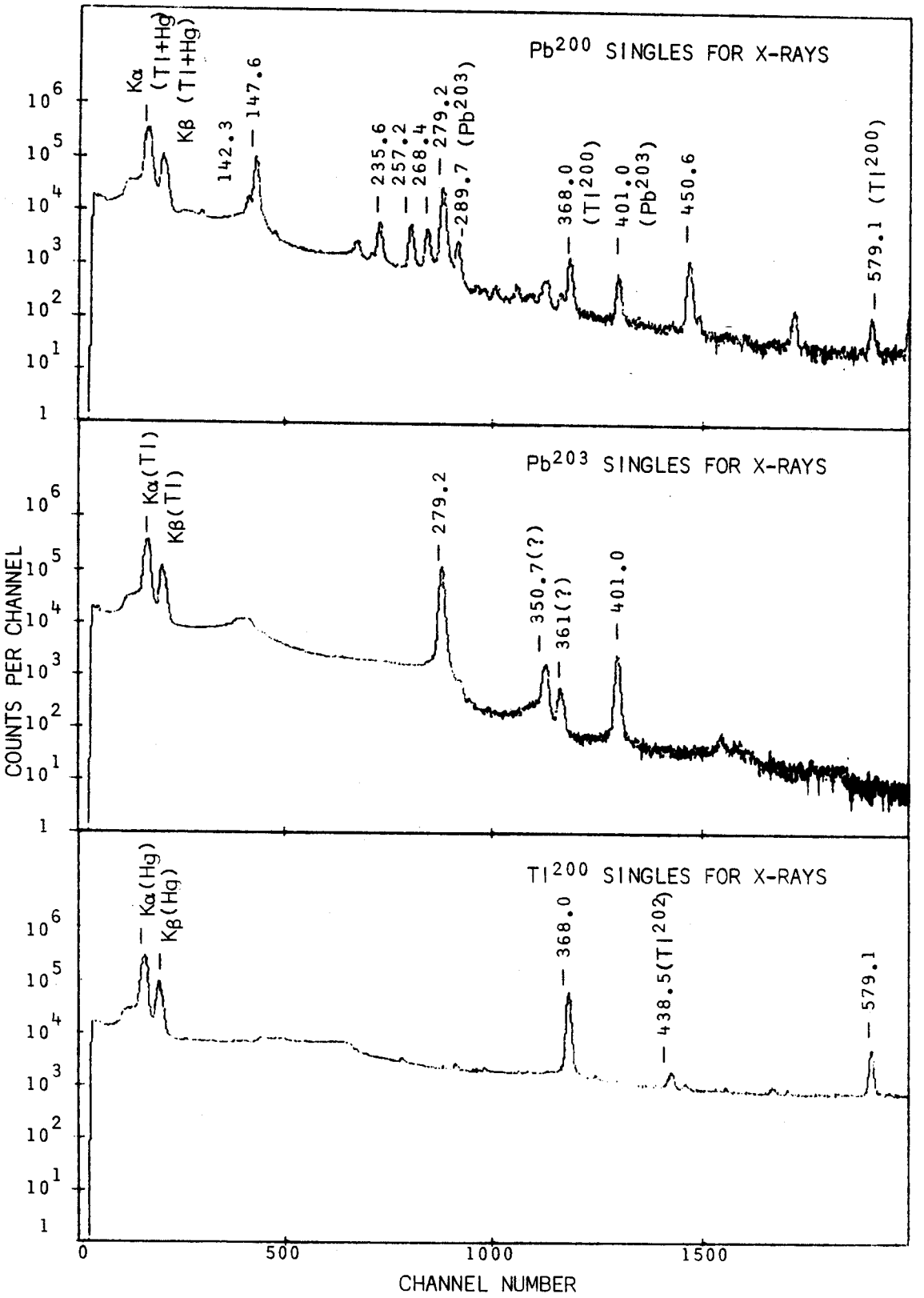

Figure IV-2. Low energy γ-ray spectra of Pb^{200}, Pb^{203}, and Tl^{200} taken with 0.42% efficient Ge(Li) detector and used to obtain the *K* x-ray intensity for Pb^{200} decay.

4.3.2. Coincidence Spectra

In order to determine which γ-rays appear in cascades and which are primarily ε-fed ground-state transitions, we used the 0.42%-efficient Ge(Li) detector in an anticoincidence experiment with an 8×8-in. NaI(Tl) split annulus and a 3×3-in. NaI(Tl) detector [Au67] The Pb^{200} source was placed on top of the Ge(Li) detector and this inserted into the other end. The single-channel analyzers associated with each of the NaI(Tl) detectors were set to accept all γ-rays above 90-keV to eliminate the Tl *K* x-rays. A resolving time (2τ) of ≈100 nsec was used to obtain the spectrum shown in Figure IV-3. The relative intensities from the anticoincidence experiment are listed in Table IV-3. The 147.63-, 450.56-, 525.54-, and 605.44-keV peaks are obviously greatly enhanced in the anticoincidence spectrum relative to their singles intensities. The 257.19- and 289.7-keV (289.24- and 289.92-keV doublet) peaks are also enhanced with respect to some peaks, such as the one at 235.62-keV.

To complement the anticoincidence experiment and determine which γ-rays are involved in strong coincidences, we performed an integral coincidence experiment, using essentially the same set-up as for the anticoincidence experiment except the 3×3-in. NaI(Tl) detector was removed. The resulting spectrum is shown in Figure IV-4 and the relative intensities are included in Table IV-3. From the integral coincidence and anticoincidence experiments alone it is quite apparent that all of the Pb^{200} γ-rays are in relatively strong coincidences except for the 450.56-, 525.54-, and 605.44-keV γ's,

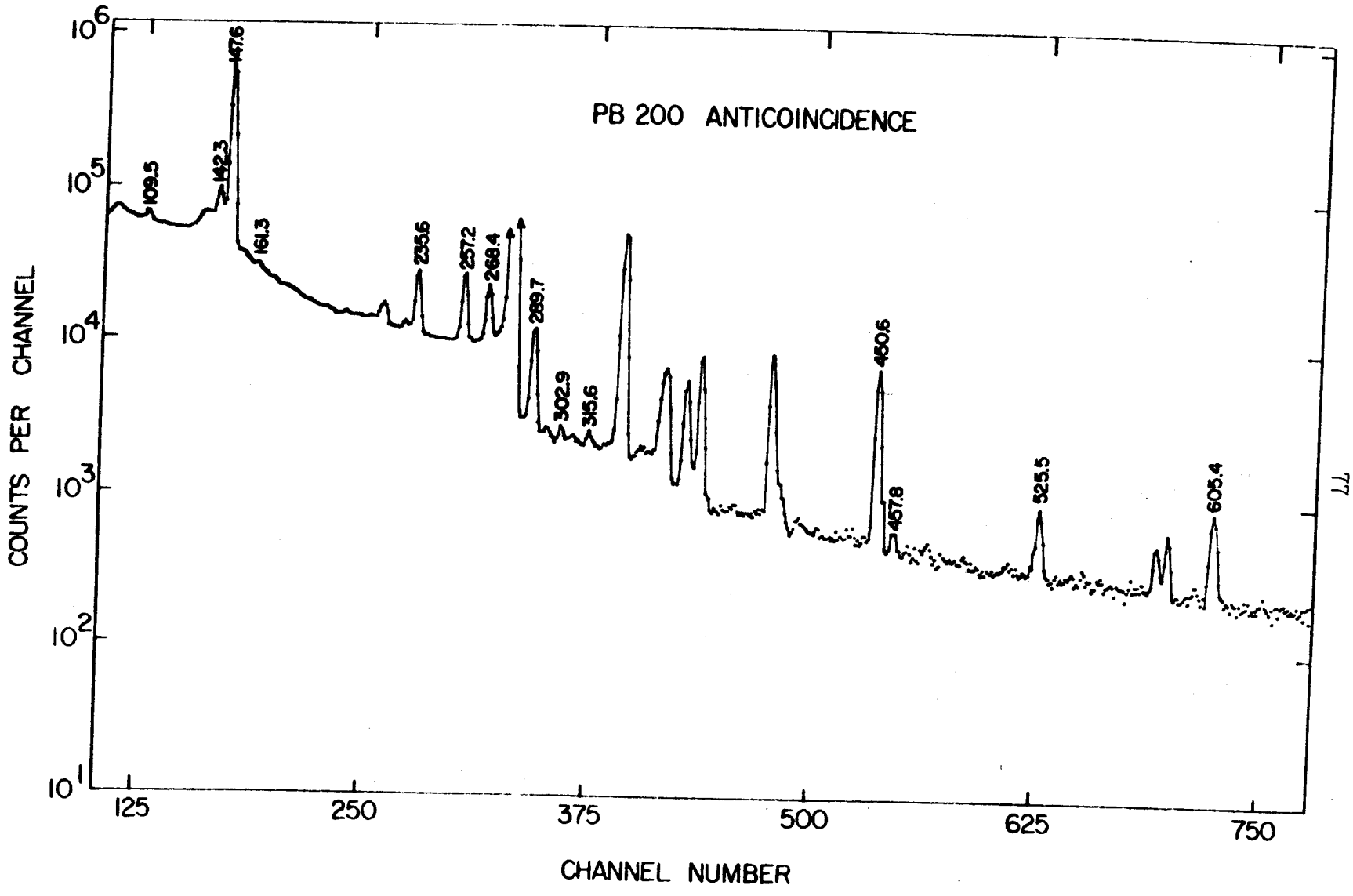

Figure IV-3. Anticoincidence spectrum of Pb^{200} γ rays. This spectrum was obtained with a 0.42% efficient Ge(Li) detector placed inside an 8x8-in. NaI(Tl) split annulus with a 3x3-in. NaI(Tl) detector blocking the other end. Only peaks belonging to Pb^{200} decay are labeled.

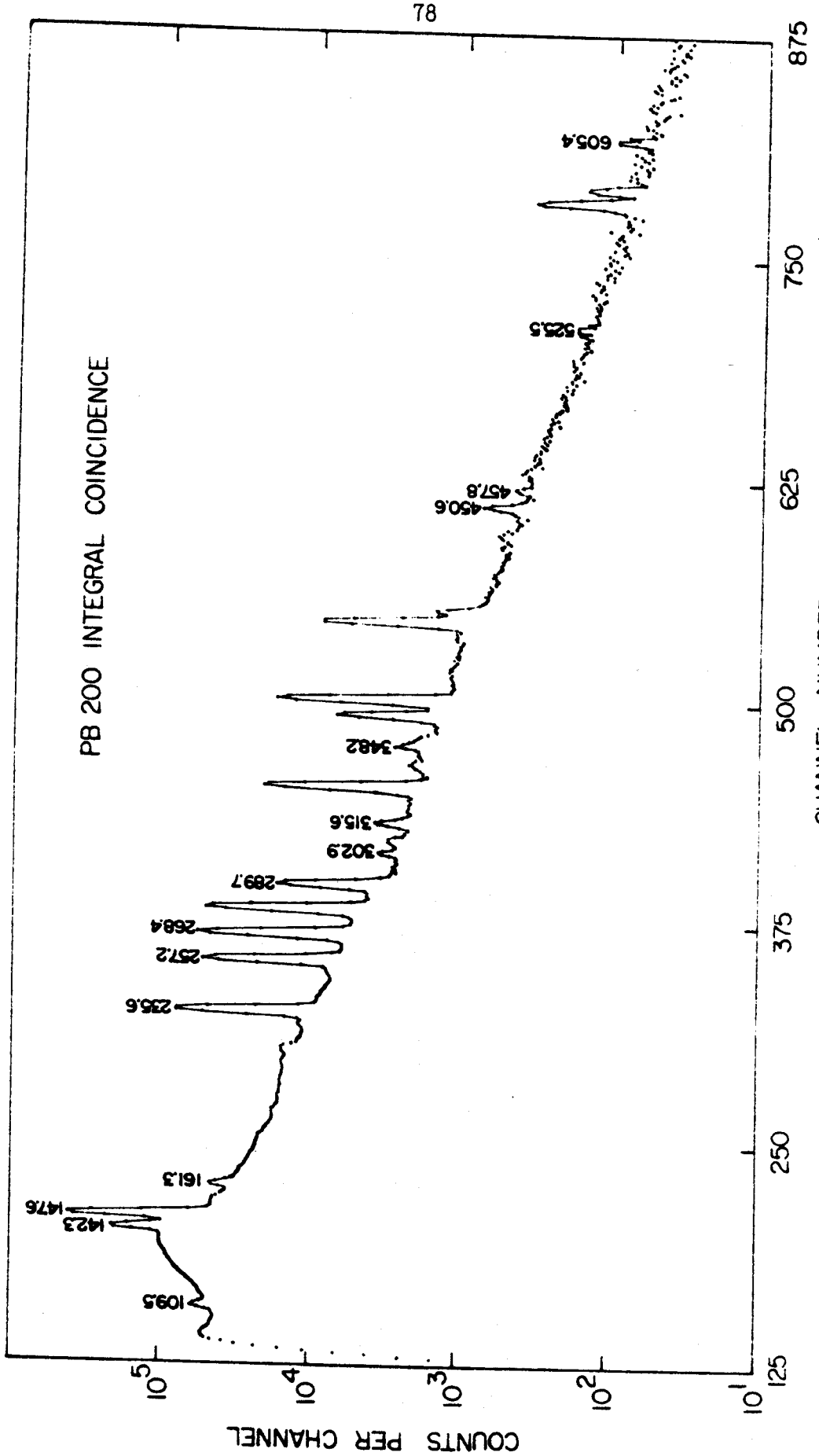

Figure IV-4. Integral coincidence spectrum of Pb^{200} γ rays. This spectrum was obtained by using a 0.42% efficient Ge(Li) detector in coincidence with an 8x8-in. NaI(Tl) split annulus. All γ-rays above the K x-rays were included in the gate.

which we can safely assume are primarily ε-fed ground-state transitions. We can also deduce that the 147.63-, 257.19-, and 289.24- and/or 289.92-keV γ's are partially ε-fed ground state transitions that are also fed by γ-rays from higher levels. These results are consistent with those of Wirhed and Herrlander [Wi62].

To aid in the placement of the remaining γ-rays in a consistent decay scheme we employed several two-dimensional "megachannel" γ-γ spectrometer systems. For a more complete description of this two-dimensional system and the recovery program see Section 2.3. The first system employed was a Ge(Li)-NaI(Tl) system using the 0.42% Ge(Li) detector in coincidence with a 3×3-in. NaI(Tl) detector. The results of this experiment however were very difficult to interpret because of the poor resolution of the NaI(Tl) detector. When another Ge(Li) detector of 0.67% efficiency became available we again tried the two-dimensional experiment, this time using both Ge(Li) detectors. This was the first successful two-dimensional Ge(Li)-Ge(Li) experiment performed at M.S.U. Although the data obtained from this experiment far surpassed any previous gated coincidence runs using a Ge(Li)-NaI(Tl) system, it did suffer from poor statistics because of the small efficiencies of the detectors. The experiment was therefore repeated for the final time when two larger volume (2% and 2.5%) Ge(Li) detectors became available. The two detectors were placed 90° to each other with a graded Pb absorber bisecting the 90° angle to prevent Compton scattering between the detectors. The Pb^{200} source was placed equidistant from the centers of both detectors and was replaced with a freshly

separated source every 3 hours. During a 24-h period we collected a total of about 500,000 events. The two integral coincidence spectra obtained with the 2.0% and 2.5% detectors are shown in Figure IV-5. A selection of the gated coincidence spectra used in the construction of the decay scheme of Pb^{200} are shown in Figure IV-6. A summary of the coincidence relationships obtained from these spectra is given in Table IV-4.

From these data we could confidently place all the observed transitions in a decay scheme, with the exception of the 155.29- and 193.39-keV γ's, for which we had only weak coincidence data. And even these two transitions could easily be placed in the decay scheme between well-defined existing levels by using sum and difference techniques. In addition to helping us place the transitions, the two-dimensional experiments aided in identifying peaks that were part of the unresolved multiplets. As mentioned before, the 348.23-keV γ is part of a triplet containing two long-lived contaminant peaks at 350.11 and 352.02-keV, as can be seen in Figure IV-1. We had failed to identify this peak as belonging to Pb^{200} decay until we looked at the results of the two-dimensional experiments and observed a single peak at 348-keV that appeared to be in strong coincidence with the 257.19-keV transition (Figure IV-6) and fit nicely into the decay scheme.

As mentioned in the introduction to this chapter, confirmation of the doublet nature of the 289.66-keV peak presented one of the most fascinating problems in this study. Our first attempts centered on detecting a broadening of this peak, using the 0.42% Ge(Li) detector

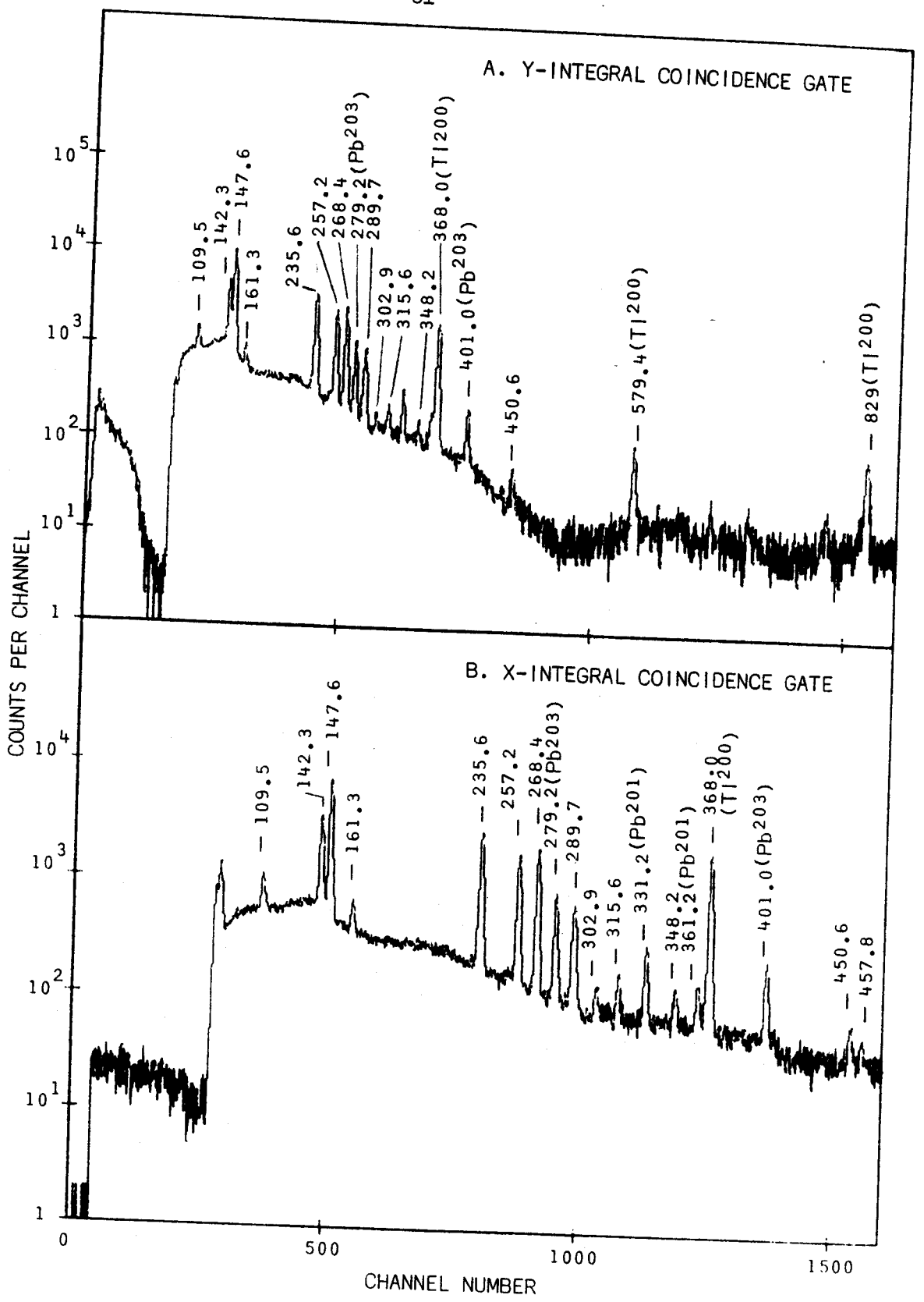

Figure IV-5. Integral coincidence spectra obtained with the 2.0% detector (Y-integral coincidence gate) and the 2.5% detector (X-integral coincidence gate) during the two-dimensional γ-γ coincidence experiment on Pb^{200}.

Figure IV-6. A selection of the gated coincidence spectra obtained from the two-dimensional γ-γ coincidence experiment on Pb^{200}. All gated spectra have had the background subtracted except where otherwise specified. All spectra were obtained by gating on the *Y*-side (2.0% detector) and displaying the *X*-side (2.5% detector) except where specified as *Y*-display. Spectra identified as high or low background resulted from gating on the background adjacent to the specified peak.

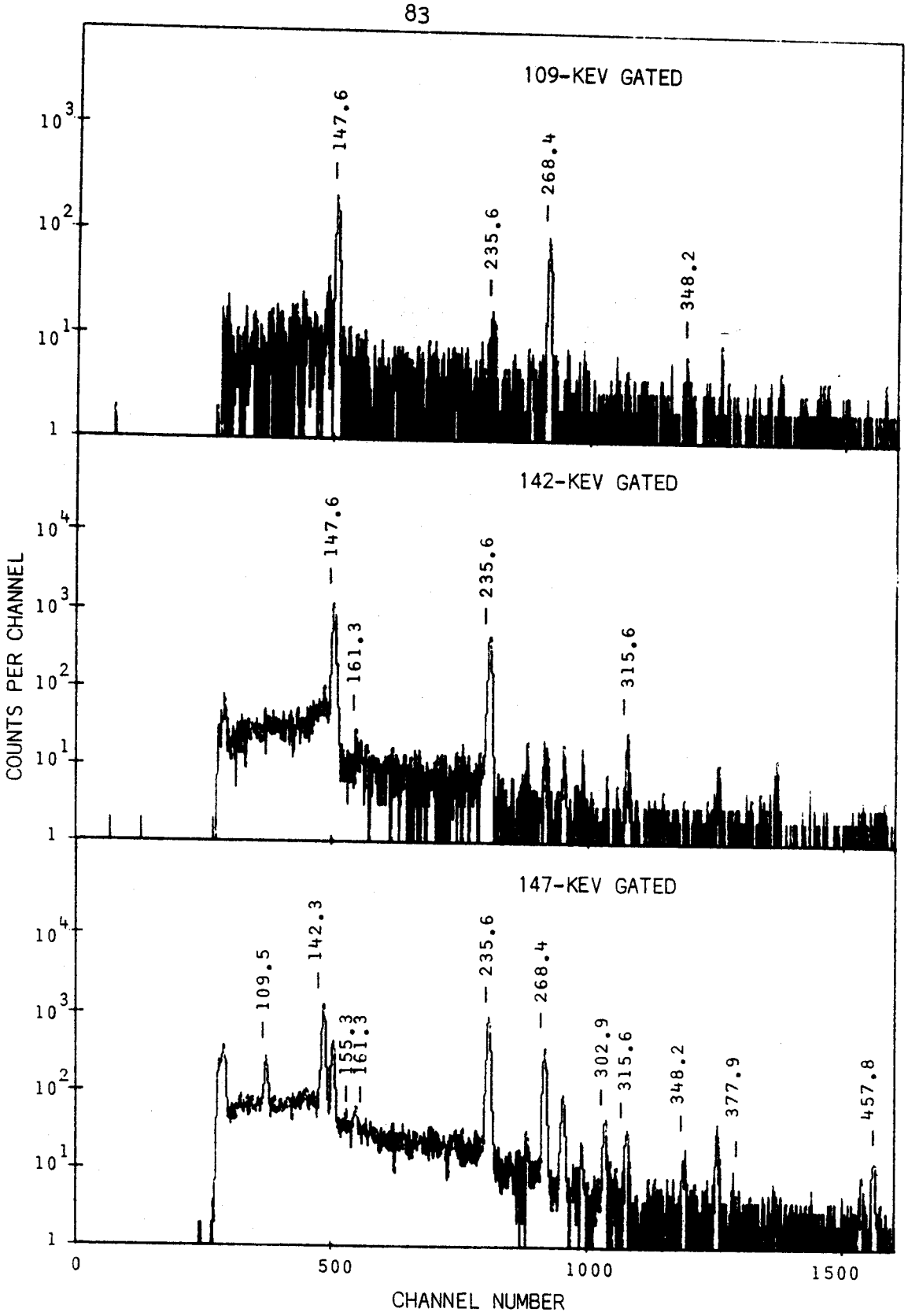

Figure IV-6 (cont'd)

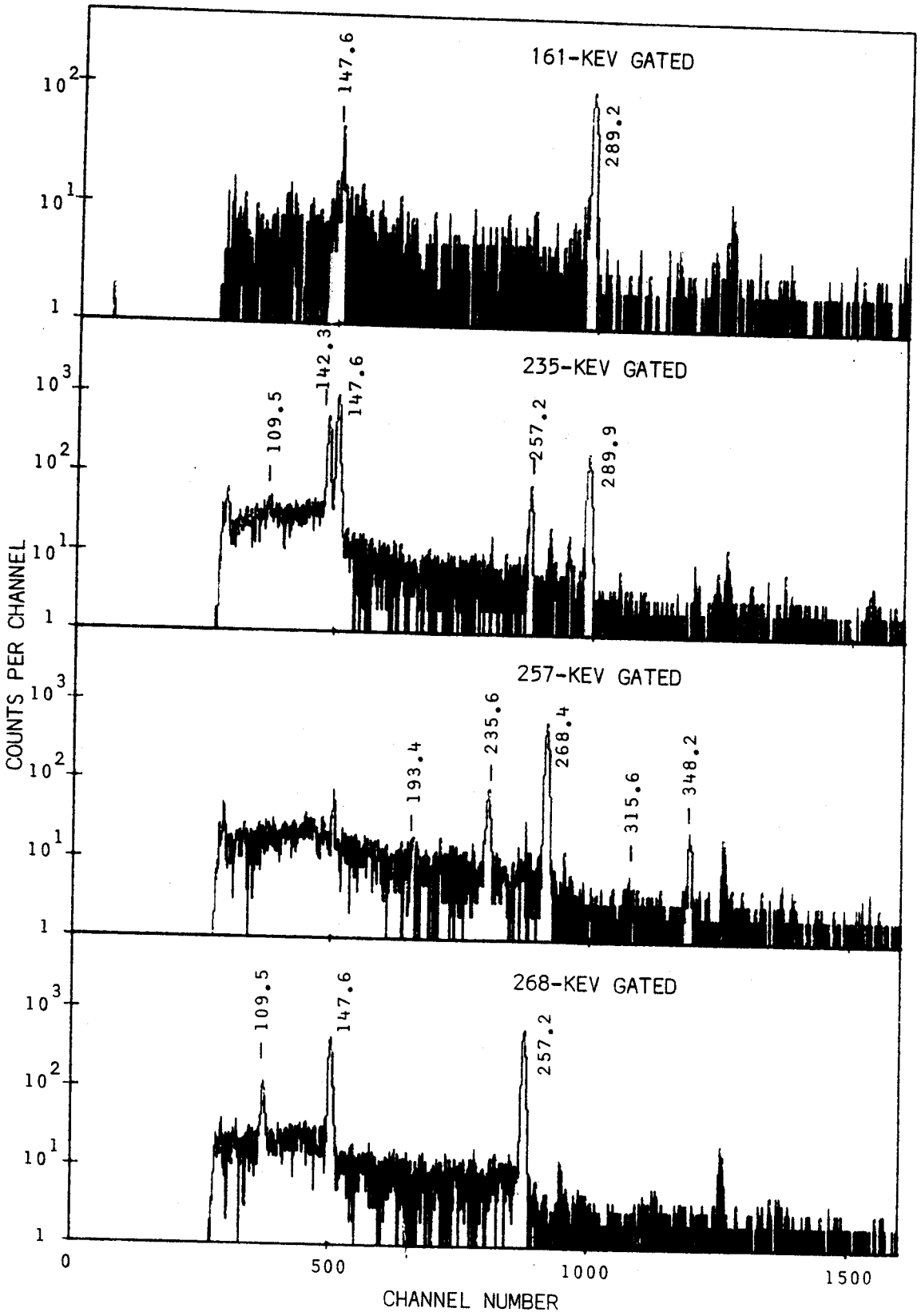

Figure IV-6 (cont'd)

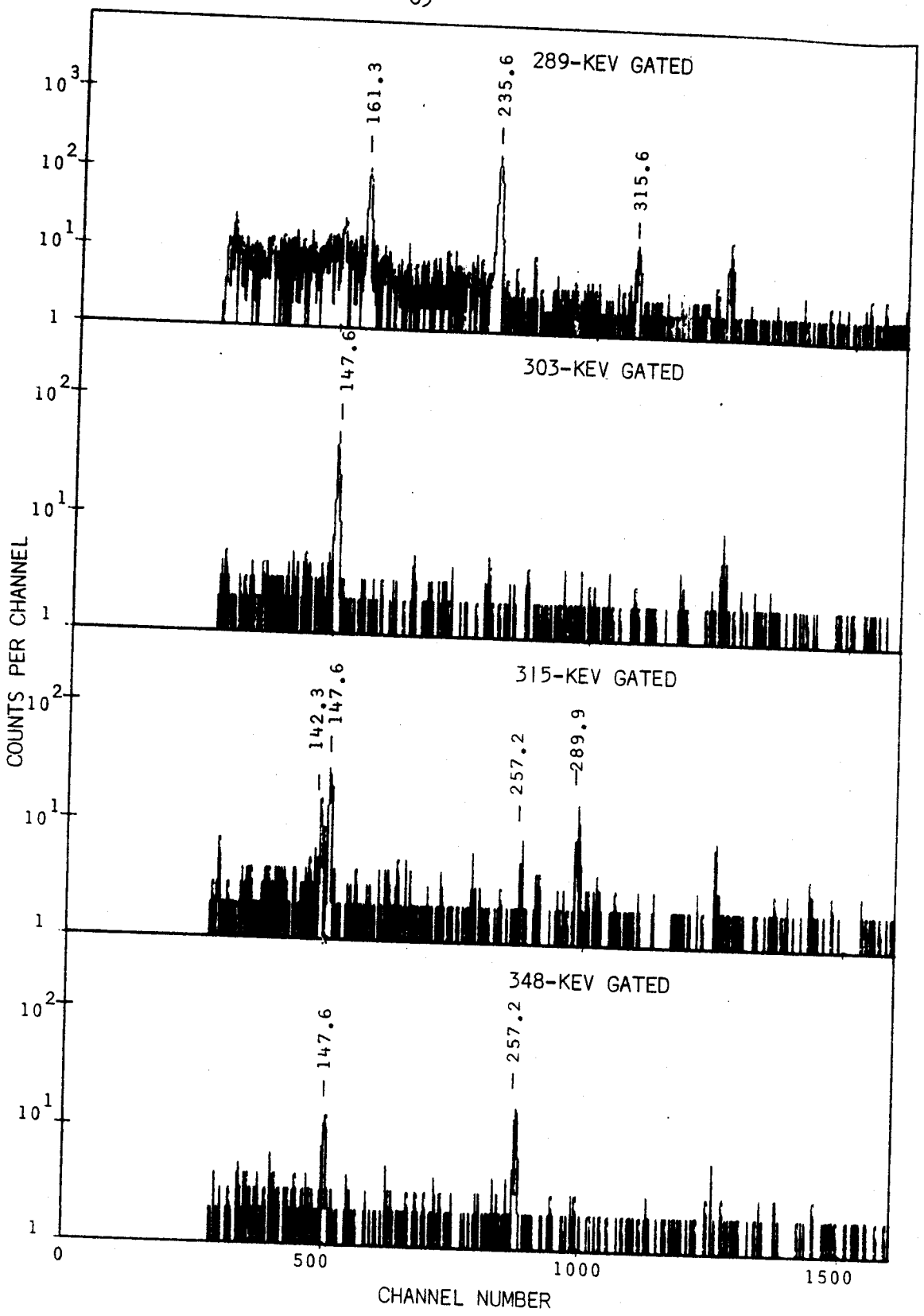

Figure IV-6 (cont'd)

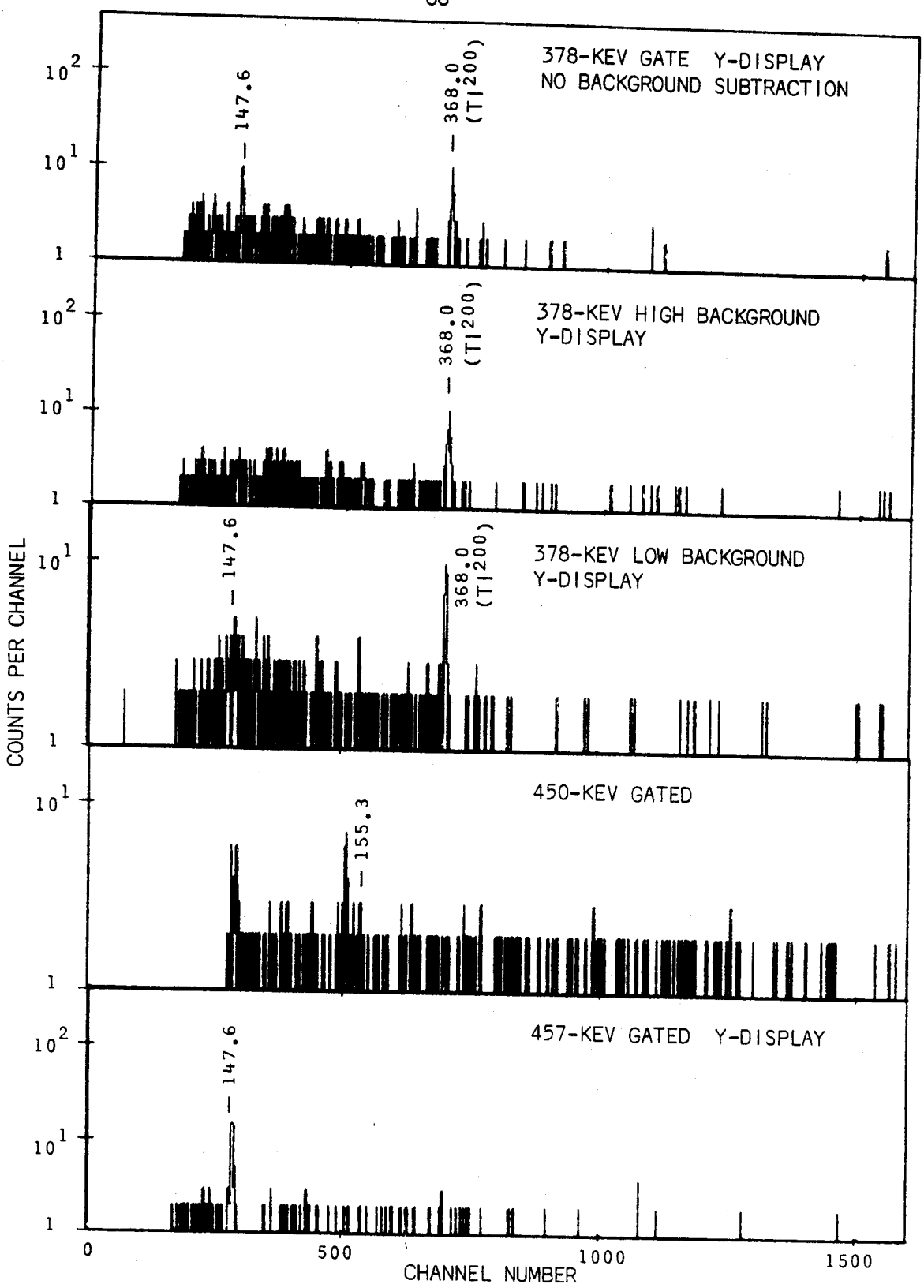

Figure IV-6 (cont'd)

Table IV-4

Results of γ-γ Coincidence Study Using 2-Dimensional Analysis

Gated Energy	Energies of γ rays in Coincidence with Gate		
	Strong	Weak	Very Weak
109.5	147,268	235, 348	-
142.3	147,235, 315	161	-
147.6	109,142,235, 268,303,315, 457	161,348,378	155
161.3	289.24	147	-
235.6	289.92,142, 147,257	109	-
257.2	268,348,235	193,315	155
268.4	109,147,257	-	-
289.2 / 289.9	161,235,315	-	-
302.9	147	-	-
315.6	142,147,289	257	-
348.2	147,257	-	-
377.9	-	147	-
450.5	-	-	155
457	147	-	-

with a resolution of 3.0 keV FWHM at 1332 keV. Using a gain of 0.21 keV per channel we expected to see a broadening of the peak by several channels. However, no such broadening was observed. From energy sums and differences however, it appeared that a 235.62-keV γ-ray populated a state at 289.92-keV while a 161.32-keV γ-ray populated a state at 289.24-keV. If this were indeed the case, we reasoned that if we could perform a gated coincidence experiment on the 161.32-keV γ and without changing the gain of the amplifiers perform a similar experiment gating on the 235.62-keV γ, we should observe a shift in the centroid of the 289.6-keV peak in the resulting spectra. In our first attempt at this approach we used a 3×3-in. NaI(Tl) detector to set the gates and the 0.42% detector to obtain the coincidence spectra. The result of this experiment was inconclusive as one might have expected, since the 161.3-keV γ-ray is not very intense and rides on top of a Compton distribution from the 235.6-keV γ-ray. However, with the development of the two-dimensional Ge(Li)-Ge(Li) spectrometer system, our interest in this approach was revived.

From the data obtained in the two-dimensional run we could easily perform gated coincidence experiments on the 161.3- and 235.6-keV peaks, and in addition perform a correction for the underlying Compton distribution. We carefully analyzed the resulting spectra, looking for a shift in the centroid of the 289.6-keV peak. This shift can be seen in Figure IV-7 thereby confirming the presence of two γ-rays. The energies obtained from this experiment were 289.22- and 289.79-keV, as compared with our adopted values of 289.24- and 289.92-keV obtained by sums and differences.

Figure IV-7. Results of the two-dimensional coincidence experiment used to confirm the doublet nature of the 289.6-keV peak. *A*. y-side integral coincidence spectrum used for the gates. *B*. x-side integral coincidence spectrum showing the region near the 289.6-keV peak on an expanded scale. *C*. x-side spectrum in coincidence with the 161.3-keV peak (background subtracted). *D*. x-side spectrum in coincidence with the 235.6-keV peak (background subtracted).

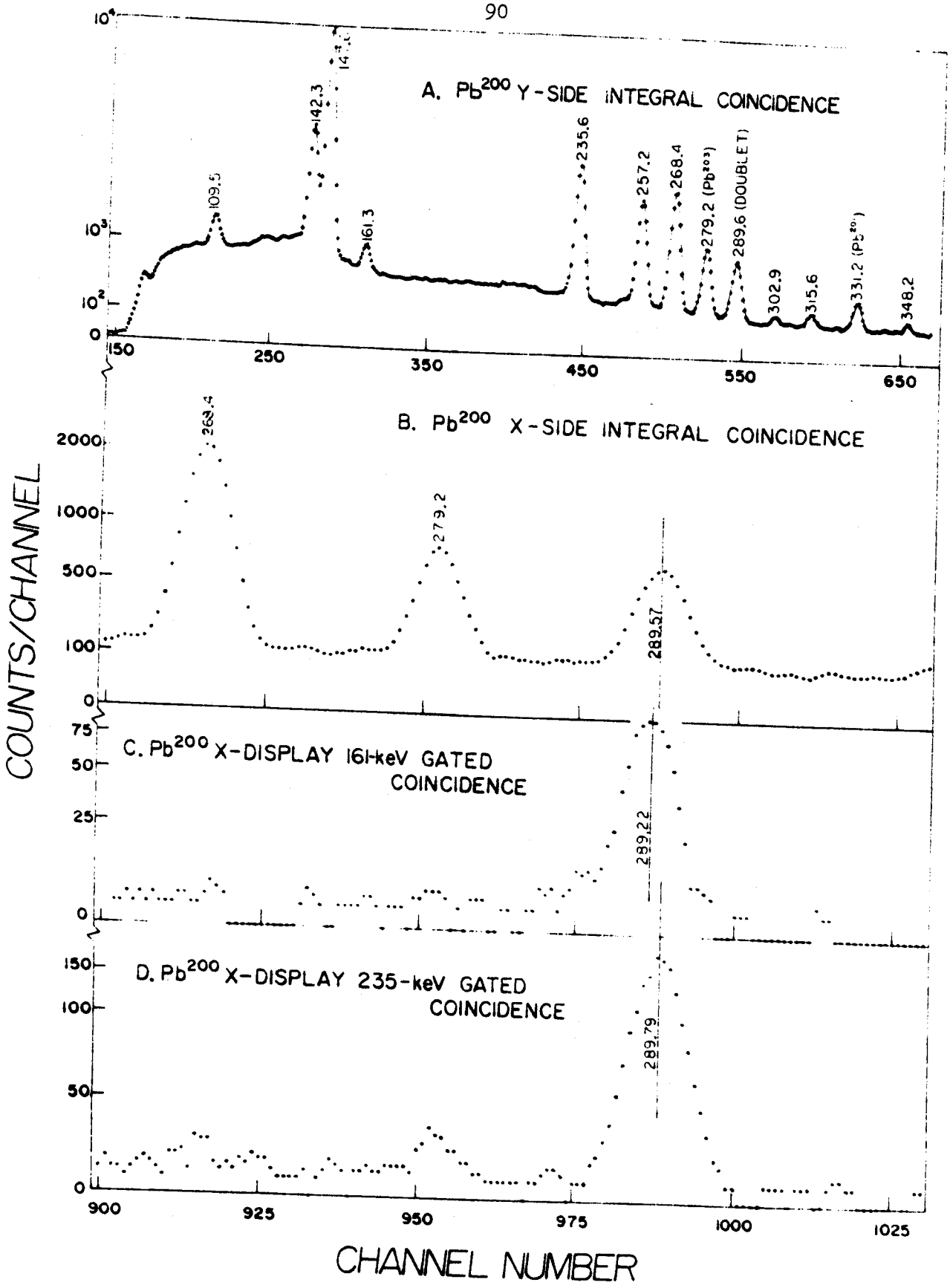
A. Pb200 Y-SIDE INTEGRAL COINCIDENCE
142.3
161.3
235.6
257.2
268.4
279.2 (Pb203)
289.6 (DOUBLET)
302.9
315.6
331.2 (Pb203)
348.2
B. Pb200 X-SIDE INTEGRAL COINCIDENCE
269.4
279.2
289.57
C. Pb200 X-DISPLAY 161-keV GATED COINCIDENCE
289.22
D. Pb200 X-DISPLAY 235-keV GATED COINCIDENCE
289.79
COUNTS/CHANNEL
CHANNEL NUMBER

Figure IV-7

4.3.3. Conversion Coefficients

Conversion coefficients for most of the transitions were determined using our photon intensities and the conversion-electron intensities of Wirhed and Herrlander [Wi62]. In order to normalize the two sets of data, we assumed that the 147.63-keV transition was a pure $E2$ transition [As57] and that the theoretical conversion coefficients of Hager and Seltzer [Ha68] were correct for this transition. Table IV-5 contains the transition data for PB^{200} along with the multipolarity assignments we propose for those transitions where both photon and electron intensities were available. The uncertainties in the experimental conversion coefficients represent the quoted uncertainties in both the photon [Table IV-3] and electron [Wi62] intensities as well as the uncertainty in the normalization factor. The normalization factor was taken as the average of those obtained using the K, $L_I(L_{II})$, and L_{III} conversion coefficients for the 147.63-keV transition. Figure IV-8 shows the theoretical K-conversion coefficients of Hager and Seltzer together with the experimental points. K-shell conversion coefficients were determined for all but the 155.29-, 193.39-, 348.23-, 377.92-, and 525.54-keV transitions, and L- and M-shell conversion coefficients were determined for many of the transitions. The multipolarity predictions all basically agree with those from the K/L and L-subshell ratios of Wirhed and Herrlander, although the latter are not very sensitive indicators.

As can be seen from Figure IV-8 and Table IV-5, all of the transitions are $M1$'s with the exception of the 147.63-keV $E2$ and the 257.19-keV transition, which is $\simeq$40% $M1$ and $\simeq$60% $E2$. These $M1$ transitions

Table IV-5

Transition Data for Pb^{200}

Energy (keV)	Photon intensity	Conversion-electron intensity[a]		Experimental conversion coefficient	Theoretical conversion coefficient[b]	Multipole order
109.54	14.5	K	22	5.2±0.9	5.7	$M1$
		L_I	4.2	1.1±0.2	0.93	$M1$
		L_{II}	0.42			
142.28	95.1	K	69	2.5±0.2	2.7	$M1$
		$L_I(L_{II})$	14.2	0.51±0.06	0.48	$M1$
		M_I	3.4	0.12±0.02	0.095	$M1$
147.63	1133	K	100	0.30±0.03	0.34	$E2$
		$L_I(L_{II})$	137	0.41±0.04	0.43	$E2$
		L_{III}	90	0.27±0.04	0.27	$E2$
		$M_{II}M_{III}$	63	0.19±0.04	0.19	$E2$
161.32	9.06	K	4.5	1.7±0.3	1.9	$M1$
235.62	129	K	26.7	0.70±0.05	0.65	$M1$
		$L_I(L_{II})$	4.6	0.12±0.01	0.11	$M1$
		M_I	1.35	0.036±0.004	0.023	$M1$
257.19	134	K	10.1	0.26±0.02	0.51	$M1$
					0.091	$E2$
		$L_I(L_{II})$	2.8	0.071±0.009	0.092	$M1$
					0.048	$E2$
		L_{III}	0.5	0.013±0.005	0.00063	$M1$
					0.019	$E2$
268.36	119	K	18.4	0.53±0.05	0.46	$M1$
		$L_I(L_{II})$	3.1	0.089±0.013	0.077	$M1$
		M_I	0.65	0.018±0.006	0.016	$M1$
289.24	32	K	3.7	0.39±0.13	0.37	$M1$
289.92	51.6	K	5.4	0.35±0.08	0.37	$M1$
302.93	5.03	K	0.70	0.47±0.12	0.32	$M1$
		$L_I(L_{II})$	0.12	0.081±0.026	0.057	$M1$

Table IV-5 (cont'd)

315.60	6.69	K	0.68	0.35±0.07	0.29	$M1$
		$L_I(L_{II})$	0.20	0.10±0.03	0.049	$M1$
450.56	100	K	4.4	0.15±0.02	0.11	$M1$
		$L_I(L_{II})$	0.76	0.026±0.003	0.019	$M1$
		M	0.16	0.0054±0.0008	0.0044	$M1$
457.80	3.49	K	0.40	0.39±0.08	0.11	$M1$
605.44	16.9	K	0.24	0.046±0.009	0.051	$M1$
		L	0.04	0.008±0.001	0.009	$M1$

[a] Ref. [Wi62]
[b] Ref. [Ha68]

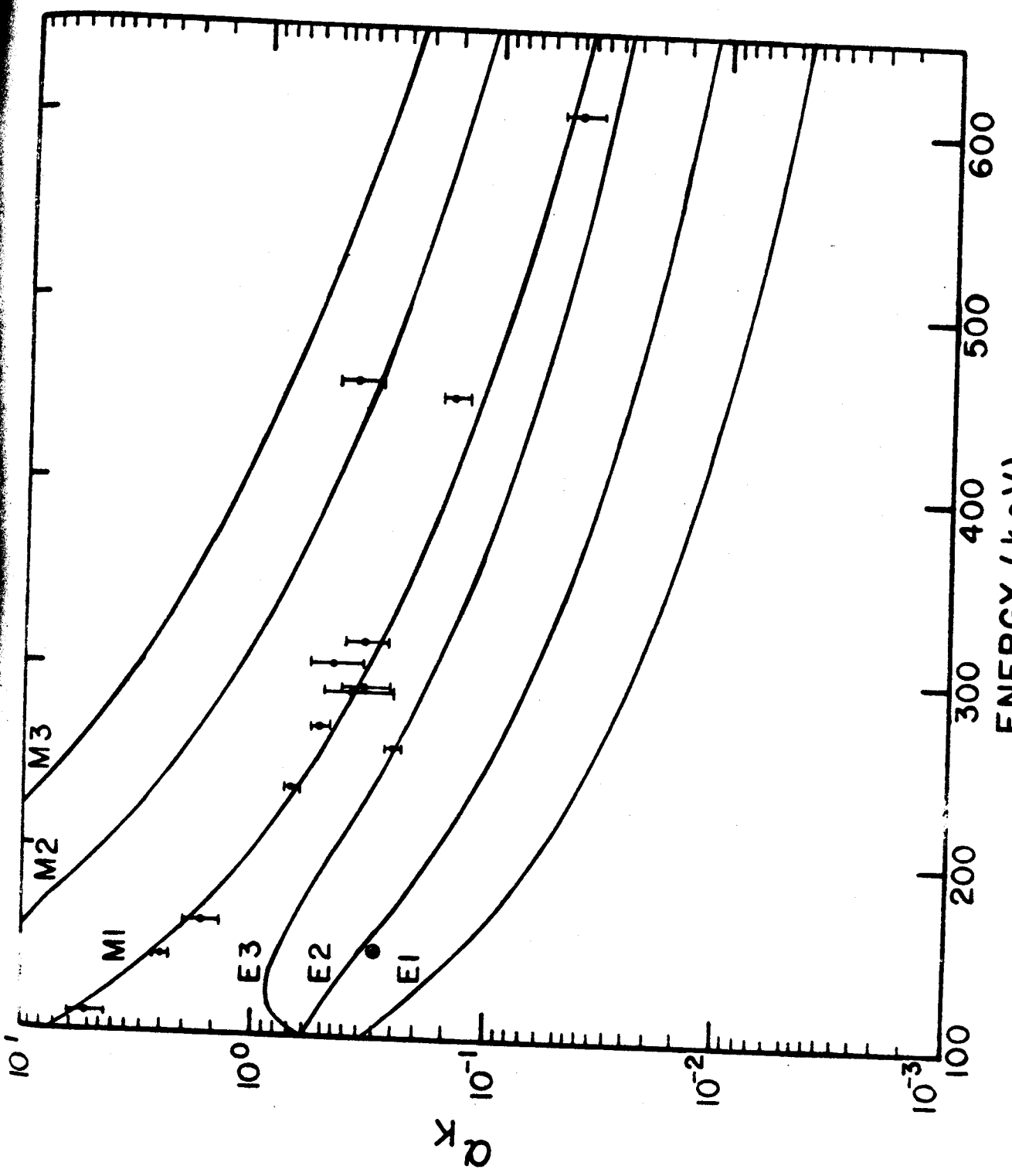

Figure IV-8. Experimental and theoretical K-shell conversion coefficients for transitions following the decay of Pb^{200}. The smooth curves were drawn to fit the theoretical values of Hager and Seltzer [Ha68].

all appear to have extremely little $E2$ admixing, which is somewhat surprising, considering the $E2$ enhancements that show up in some of the Pb isotopes much closer to the doubly closed shell. It would be helpful to have careful angular correlation experiments performed on this nucleus in order to improve the limits on $E2$ admixtures in the $M1$ transitions.

On the basis of the experimental α_K, the 457.80-keV transition would seem to be an $E2$; however, for reasons mentioned later we have assigned it as an $M1$.

4.4. Decay Scheme

Figure IV-9 shows the decay scheme we deduced from our experiments. Transition and excited-state energies are given in keV, with the adopted energies for the levels being weighted average based on our confidence in the respective cascade and crossover transitions. As mentioned in Section 4.3.1, the energies of the 289.24- and 289.92-keV levels are based on sum and difference relations. The Q_ε of ~939 keV was calculated from the "experimental" masses listed in the table of Myers and Swiatecki [My65]. We have included for the sake of completeness the levels in Tl^{200} populated by the decay [Di63] of 37-msec Tl^{200m}. It can be seen that there is little overlap in the two decay schemes, so we forego further discussion of the high-spin levels.

From the conversion coefficients in Table IV-5 and from the theoretical conversion coefficients of Hager and Seltzer where experimental values were not available, the total transition intensities, including conversion in higher shells, were calculated. These total transition intensities, in per cent of the total Pb^{200} disintegrations, are given in the decay scheme. The total intensity for the 32.7-keV transition was obtained from the conversion intensity measured by Wirhed and Herrlander [Wi62]. This was corrected for the γ-ray intensity by using the *L*-shell conversion coefficients for an *M*1 transition, which they assigned on the basis of its *L*-subshell ratios. From the measured *K* x-ray intensity, *K*-conversion intensities, and *K* fluorescent yield, 0.95, [Fi66] the total ε-feeding intensity to the ground state was

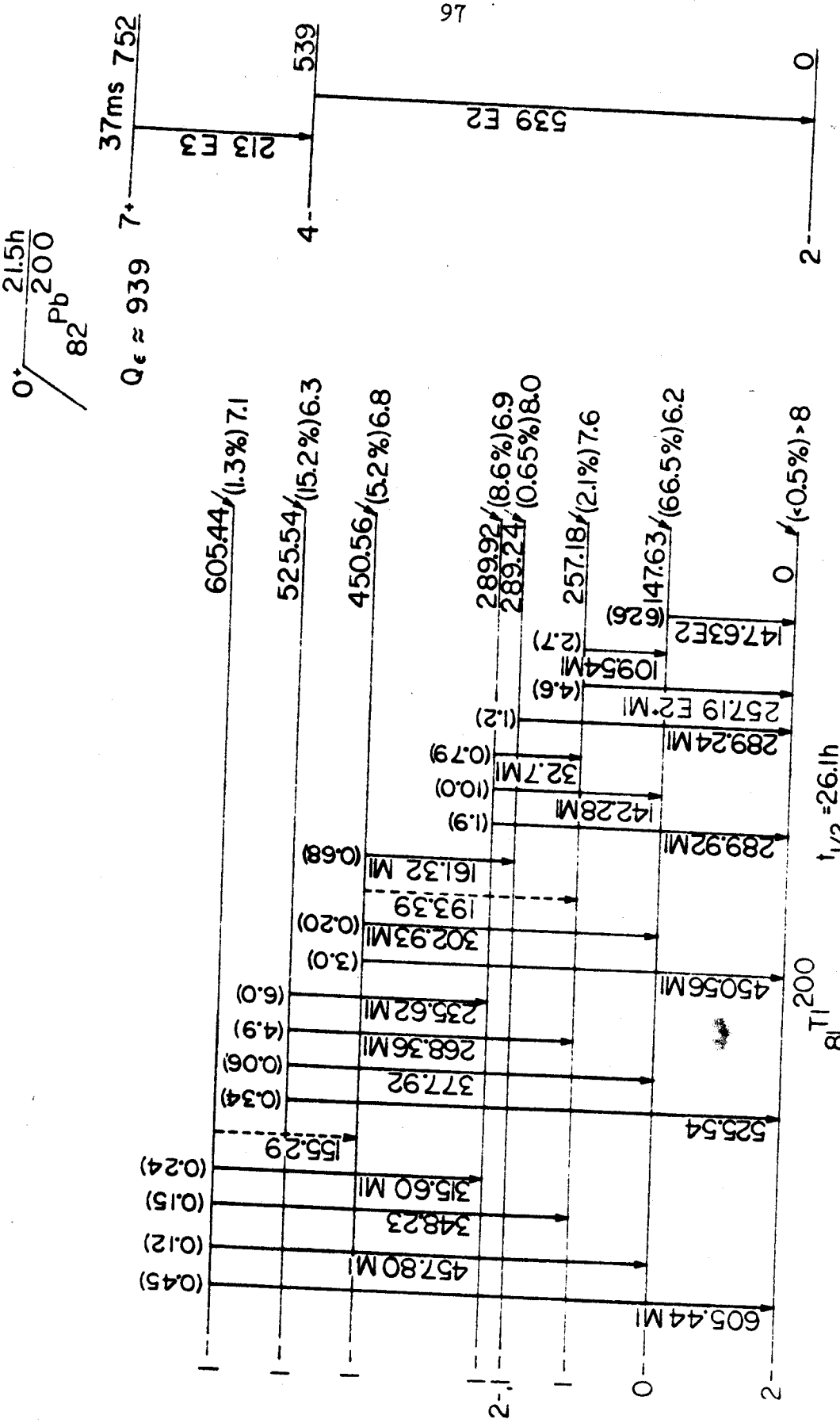

Figure IV-9. Decay scheme of Pb^{200}. The intensities of all (total) transitions are given in per cent of the Pb^{200} disintergrations. The per cent ε decay to each state and the log ft values for that state are listed to the right of the state. At the extreme right we show the states populated by the decay of Tl^{200m}; these higher-spin states were not populated by the decay of Pb^{200}.

determined to be less than 0.5%. This corresponds to a log ft > 8. The total ε-feeding intensities for decays to each state were then calculated assuming that there was no ground-state feeding. These intensities are given in the decay scheme to the right of the energy levels. Log ft values based on them appear in italics at the extreme right of the levels.

4.5. Spin and Parity Assignments

Ground state. Herrlander and Gerholm [He57] assigned $I\pi$ = 2- to the ground state of Tl^{200} on the basis of a Kurie analysis of the positron spectrum resulting from the decay of this state to the 0+ ground state of Hg^{200}. (The Tl^{200} ground state had a measured spin of 2 from atomic spectra and atomic beams experiments [Hu61]. Our upper limit of 0.5% on direct ε population to this state corresponds to a log *ft* > 8. This is in agreement with a predicted first-forbidden unique log *ft* ≈9 for such a 0+ → 2- transition.

147.63-keV state. The first excited state at 147.63-keV was previously assigned $I\pi$ = 0- by Åström, Johannson, and Bergström [As57] on the basis of the seemingly pure *E*2 nature of the 147.63-keV γ transition and the strong ε population of the state. Our work supports this 0- assignment, as the log *ft* of 6.2 lies in the range expected for a fairly rapid first-forbidden transition.

257.18-keV state. The log *ft* for ε decay to this state was found to be 7.6. This could indicate either an allowed or a first-forbidden transition, which would populate 1+ and 0+ or 1- and 0- states, respectively. From the definite *M*1 assignment for the 109.5-keV γ to the 147.63-keV 0- state, we can eliminate the 1+ and 0+ possibilities on the basis of parity and the 0- state on the basis of observing the photons. The 257.2-keV γ to the 2- ground state is a mixture of *M*1 and *E*2 multipolarities and also rules against the 1+, 0+, and 0- assignments. We can thus quite confidently assign $I\pi$ = 1- to the 257.18-keV state.

The four highest-lying states. The log *ft* values for these states range from 6.3 to 7.1, thus falling into the range of both allowed and first-forbidden (non-unique) transitions. This implies choices of 1+, 0+, 1-, and 0- for these states.

Based on the *M*1 nature of the 289.92-keV γ, we can narrow the choice to 1- for the 289.92-keV state. This is also supported by the *M*1 nature of the 142.28- and 32.7-keV transitions. By analogous arguments the 450.56-keV state can also be assigned 1-.

The *M*1 nature of the 268.36- and 235.62-keV transitions allows the assignment for the 525.54-keV state to be narrowed to 1- or 0-. As we were unable to determine the multipolarity of the 525.54-keV γ to the 2-ground state, we could not distinguish between the 1- or 0- choices from this; however, the fact that we observed photons at all in the 377.92-keV transition from the 525.54-keV state to the 147.63-keV 0- state strictly rules out the 0- possibility. Again we are left with a 1- assignment.

The 605.44-keV state can also be assigned 1- from the *M*1 nature of its ground-state γ transition, and this is consistent with the *M*1 nature of the 315.60-keV transition. The only inconsistency in this assignment arises from the 457.80-keV γ, which goes to the 0- state and has a measured α_K in the range expected for an *M*2 transition. If this γ-ray were indeed an *M*2, the 605.44-keV state would be 2+ and the ε decay would be second forbidden, obviously inconsistent with the log *ft* of 7.1 as well as with the multipolarities of the other γ-rays. Therefore, it appears that the measured α_K is in error, and the multipolarity of the 457.80-keV γ is undoubtedly *M*1 not *M*2.

289.24-keV state. The determined log *ft* of 8.0 for ε decay to this state is close enough to the range for a first-forbidden unique transition that we must include the possibility of a 2- assignment to those of 1+, 0+, 1-, and 0-. From the *M*1 multipolarity of the 289.24-keV γ to the ground state and also that of the 161.32-keV γ from the 450.56-keV 1- state, we can exclude the positive parity and 0- possiblities, leaving us with 1-or 2-. We prefer the 1- assignment slightly because of the log *ft* value but do not exclude the 2- possibility. We shall discuss the assignment for this state in the next section.

4.6. Shell-Model Assignments and Discussion

$^{200}_{81}Tl_{119}$ is an odd-odd nucleus one proton removed from the closed shell at $Z = 82$ and seven neutrons removed from the closed shell at $N = 126$. The simplest approach to such nuclei is to extend the odd-group model, as normally applied to odd-even and even-odd nuclei. In this model the properties of the nuclear states are assumed to be determined primarily by the odd group of particles. In extending it to odd-odd nuclei we assume that the wave functions for the states in the odd-odd nuclei are simple vector-coupled products of the wave functions of the two odd groups. If we assume that the residual p-n interactions are weak compared to spin-orbit forces [De61], we can use jj coupling, with its resulting simplications. With the assumption of jj coupling, a given proton and neutron configuration, $|\ell_p j_p \ell_n j_n>$, can take on all integral spins, $|j_p - j_n| \leq I \leq j_p + j_n$, where the nature of the residual p-n interaction will determine the ordering of these spins. The modified Nordheim coupling rules proposed by Brennan and Bernstein [Br60] can be useful in predicting the ordering of the spins resulting from a given configuration. Here j_p and j_n are the single-particle total angular momenta obtained from the adjacent odd-mass nuclei, while ℓ_p and ℓ_n (assumed to be pure) are the orbital angular momenta obtained from standard single-particle shell-model assignments. In order to keep our analysis as simple as possible, we have assumed that both odd groups are of the lowest possible seniority. Explicit calculations show that in many cases the admixtures of higher seniorities in the wave function of a given

low-lying nuclear state are quite small, [Oq59] so we are probably not going too far wrong here.

The question also arises concerning collective states and their effects on the odd-odd states, perhaps even core-coupled states. The positions of the first 2+ quadrupole vibrational state is known in three of the four nearest even-even nuclei: Pb^{202}, at 961.4-keV [Mc57]; Hg^{200}, at 368.0-keV [Sa65]; and Hg^{198}, at 411.80-keV [Mu63]. The energy range of states we are considering in Tl^{200} starts to overlap with these, but the effects of blocking in this odd-odd system should make the nucleus a little more rigid, if anything, with respect to vibrations. This appears to be borne out by the lack of significant *E*2 admixtures in most of the *M*1 transitions, so in our discussion we do not consider collective effects explicitly. It must be remembered, however, that we are discussing only a few low-spin states in a nucleus that must have a high level density even at low energies, so to obtain a more complete picture the effects of collective modes and configuration interactions will have to be included. As mentioned in Section 4.3.3, a more sensitive measurement of *E*2 admixtures, such as angular correlations, would be most welcome here.

In attempting to assign the shell-model configurations in this odd-odd nucleus, we assume that the low-lying states should result from combinations of the lowest configurations in the adjacent odd-proton and odd-neutron nuclei. The proton configurations contributing to the low-lying states were assumed to be the ground and first two excited states in the adjacent odd-mass Tl isotopes. The resulting spins of 1/2+, 3/2+, and 5/2+ are consistent with the shell-model

assignments, $s_{1/2}$, $d_{3/2}$, and $d_{5/2}$. The spacing of these states in the odd-mass Tl isotopes is shown in Figure IV-10. The last two protons of the Z = 82 closed shell should fill the $s_{1/2}$ orbit, so it is not surprising that the ground state for the odd-mass Tl isotopes is consistently 1/2+. The first two excited states in these isotopes then consist of the promotion of a proton from the filled $d_{3/2}$ or $d_{5/2}$ orbits to the $s_{1/2}$ hole.

For neutron members just below the N = 126 closed shell, the odd neutron can populate the $p_{1/2}$, $i_{13/2}$, $p_{3/2}$, or $f_{5/2}$ orbits in the ground or lowest excited states. Because of the large pairing energy of the $i_{13/2}$ orbit, it should be filled in preferentially by pairs and not by odd particles, which may account for the fact that no $i_{13/2}$ ground states have been observed. In order to obtain an idea of the ordering of the low-lying neutron configurations contributing to the states in Tl^{200}, we would like to examine the ground and lowest excited states in the odd-mass isotones with 119 neutrons. Of particular interest are the states in Pb^{201} and Hg^{199}. As can be seen from Figure IV-11, only the ground state is known in Pb^{201} (excluding the $i_{13/2}$ excited isomeric state). The $I\pi$ = 5/2- suggests an $f_{5/2}$ assignment as its primary component. We should be able to get some idea of the ordering of the excited states in Pb^{201}, however, by looking at some of the systematics of the better-known odd-mass Pb isotopes, as shown in Figure IV-12. From these systematics, it would appear that the neutron states (holes) of interest in order of increasing energy are $f_{5/2}$, $p_{3/2}$, and $p_{1/2}$. The quasiparticle calculations of Kisslinger and Sorenson [Ki60] for Pb^{201} agree with this ordering. However, as is apparent

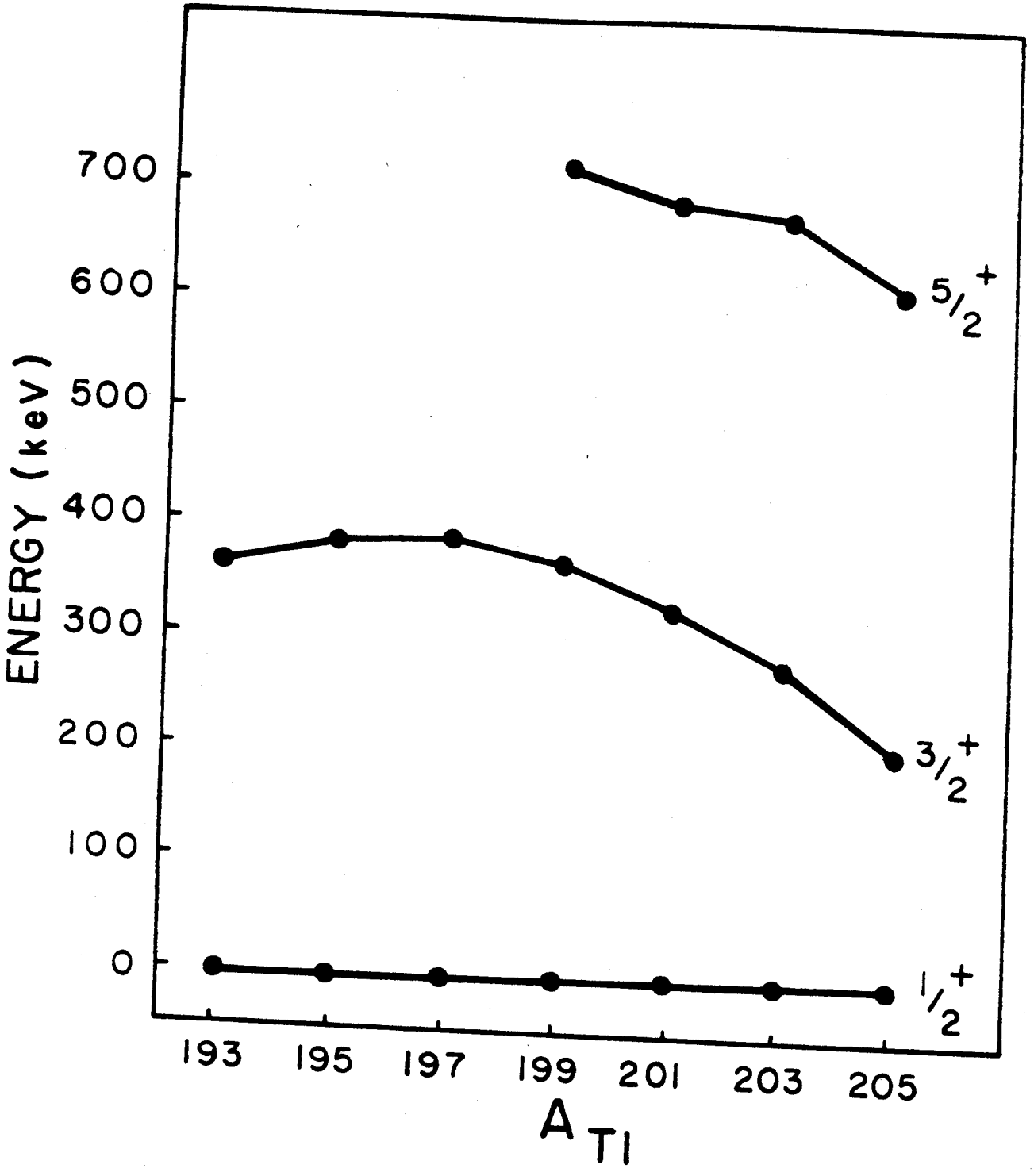

Figure IV-10. Systematics of the low-lying 1/2+, 3/2+, and 5/2+ states in odd-mass Tl isotopes. These should be relatively pure $s_{1/2}$, $d_{3/2}$, and $d_{5/2}$ shell-model states.

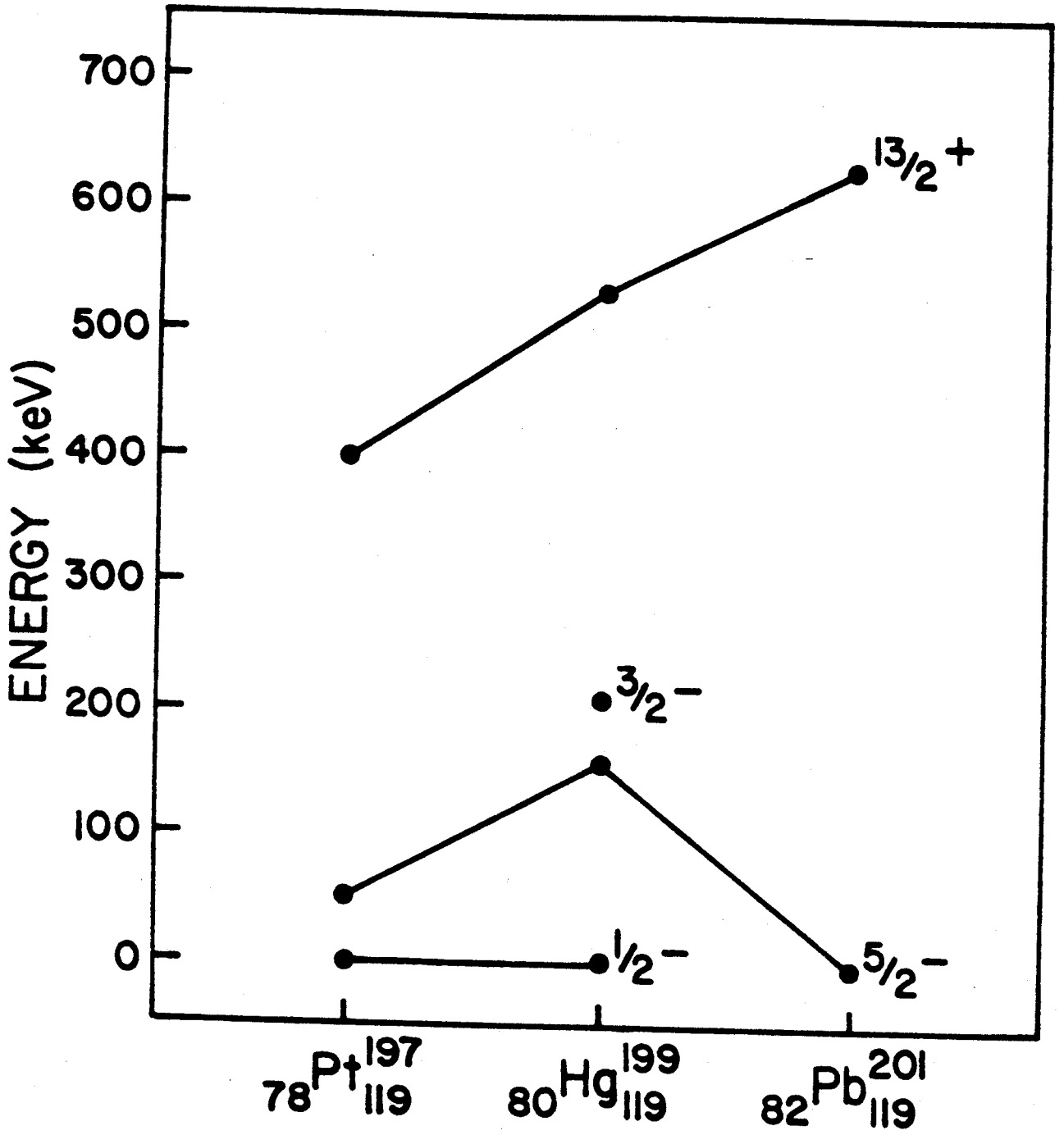

Figure IV-11. Systematics of low-lying states in odd-mass isotones having 119 neutrons. These correspond to relatively pure $p_{1/2}$, $f_{5/2}$, and $i_{13/2}$ shell-model states.

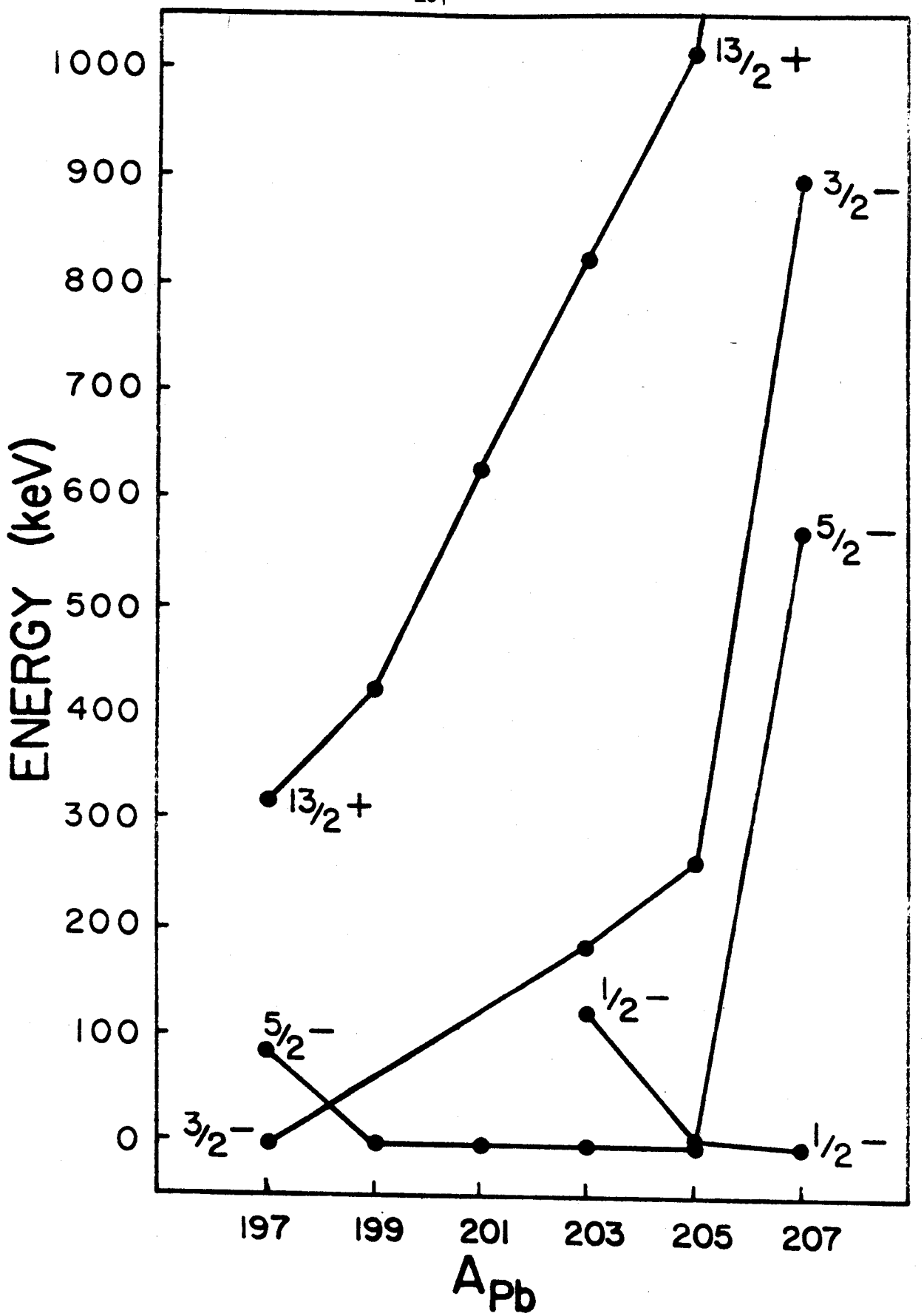

Figure IV-12. Systematics of the $f_{5/2}$, $p_{1/2}$, $p_{3/2}$, and $i_{13/2}$ states in the odd-mass neutron-deficient Pb isotopes.

from Figure IV-12, the spacing between the $f_{5/2}$ and $p_{3/2}$ state is probably small in Pb^{201}, as the two states have crossed between here and Pb^{197}, where the ground state is $p_{3/2}$. It is not altogether certain whether the ground state of Pb^{199} is $f_{5/2}$ or $p_{3/2}$. Again referring to Figure IV-11, we see that for Hg^{199} and Pt^{197} the ground state and first excited states are in the order 1/2- ($p_{1/2}$) and 5/2- ($f_{5/2}$), with the second excited state in Hg^{199} being 3/2- ($p_{3/2}$). These isotones therefore suggest an ordering of $p_{1/2}$, $f_{5/2}$, and $p_{3/2}$. It is obvious from this analysis that we cannot unambiguously assign an order to the single-neutron configurations contributing to the states in Tl^{200}. This will make the assignment of configurations more difficult.

Based on the proton states and the neutron states available, we can immediately make the prediction that all the low-lying, low-spin states in Tl^{200} should have negative parity. This is borne out without exception in the experimental states determined in our studies. (We do not include the $i_{13/2}$ state in the list of available states for the additional reason that it would lead only to higher-spin states, which are not populated in Pb^{200} ε decay.)

Table IV-6 contains a summary of all the possible spins resulting from p-n configurations using the $s_{1/2}$, $d_{3/2}$, and $d_{5/2}$ proton states and the $p_{5/2}$, $p_{3/2}$, and $f_{5/2}$ neutron states. We shall concern ourselves principally with the configurations giving rise to 0-, 1-, and 2- states, as these were the only states we observed populated in the ε decay of Pb^{200}.

Table IV-6

Possible Configurations for Producing Some Low-Lying Odd-Odd States in Tl^{200}

$I\pi$	(π,ν) Configurations
0-	$(s_{1/2}p_{1/2})$ $(d_{3/2}p_{3/2})$ $(d_{5/2}f_{5/2})$
1-	$(s_{1/2}p_{1/2})$ $(s_{1/2}p_{3/2})$ $(d_{3/2}f_{5/2})$ $(d_{3/2}p_{1/2})$ $(d_{3/2}p_{3/2})$ $(d_{5/2}p_{3/2})$ $(d_{5/2}f_{5/2})$
2-	$(s_{1/2}f_{5/2})$ $(s_{1/2}p_{3/2})$ $(d_{3/2}p_{1/2})$ $(d_{3/2}f_{5/2})$ $(d_{3/2}p_{3/2})$ $(d_{5/2}p_{1/2})$ $(d_{5/2}p_{3/2})$ $(d_{5/2}f_{5/2})$
3-	$(s_{1/2}f_{5/2})$ $(d_{3/2}f_{5/2})$ $(d_{3/2}p_{3/2})$ $(d_{5/2}f_{5/2})$ $(d_{5/2}p_{3/2})$ $(d_{5/2}p_{1/2})$
4-	$(d_{3/2}f_{5/2})$ $(d_{5/2}p_{3/2})$
5-	$(d_{5/2}f_{5/2})$

It has been suggested by Bergström and Andersson [Be57] that the 2- ground state of Tl^{200} has the configuration, $[(\pi s_{1/2})(\nu f_{5/2})_{2-}$. This could be consistent with our analysis above. The "strong" coupling rule of Nordheim [No50] predicts that the 2- state will lie lower than the 3- state for this configuration. However, DeShalit and Walecka [De61] have suggested a configuration of $[(\pi s_{1/2})(\nu p_{3/2})]_{2-}$ for this ground state. Because of the uncertainty in ordering of the neutron states in this region, this also could be consistent with our above analysis. The 2- state is also predicted to lie lower than a 1- state from this configuration according to Nordheim's "weak" rule and the modified rules of Brennan and Bernstein [Br60]. DeShalit and Walecka proposed their assignment on the basis of the systematics of the states populated by the decays of the isomeric states in the odd-odd Tl isotopes. As shown in Figure IV-13, the neutron-deficient odd-odd Tl nuclei have 2- ground and 0- first excited states. However, in Tl^{198} and Tl^{196} we see two closely spaced excited states with $I\pi$ = 2- and 3- separated by 23 and 34-keV, respectively. The *M*1 transitions between these states compete very favorably with the much more energetic *M*1 transition to the ground state, which prompted DeShalit and Walecka to assume that these states have the configurations, $[(\pi s_{1/2})(\nu f_{5/2})_{2-}$ and $[(\pi s_{1/2})(\nu f_{5/2})]_{3-}$. The 2- ground state of Tl^{200} must then be primarily one of the other possibilities listed in Table IV-6, of which $[(\pi s_{1/2})(\nu p_{3/2})]_{2-}$ seems to be the best choice. Since the *M*1 transition, $[(\pi s_{1/2})(\nu f_{5/2})]_{3-} \rightarrow [(\pi s_{1/2})(\nu p_{3/2})]_{2-}$, is ℓ-forbidden, whereas the *M*1 transition, $[(\pi s_{1/2})(\nu f_{5/2})]_{3-} \rightarrow [(\pi s_{1/2})(\nu f_{5/2})]_{2-}$ is not, this could explain the γ-branching ratio for the cases of Tl^{198} and Tl^{196}. Also, the

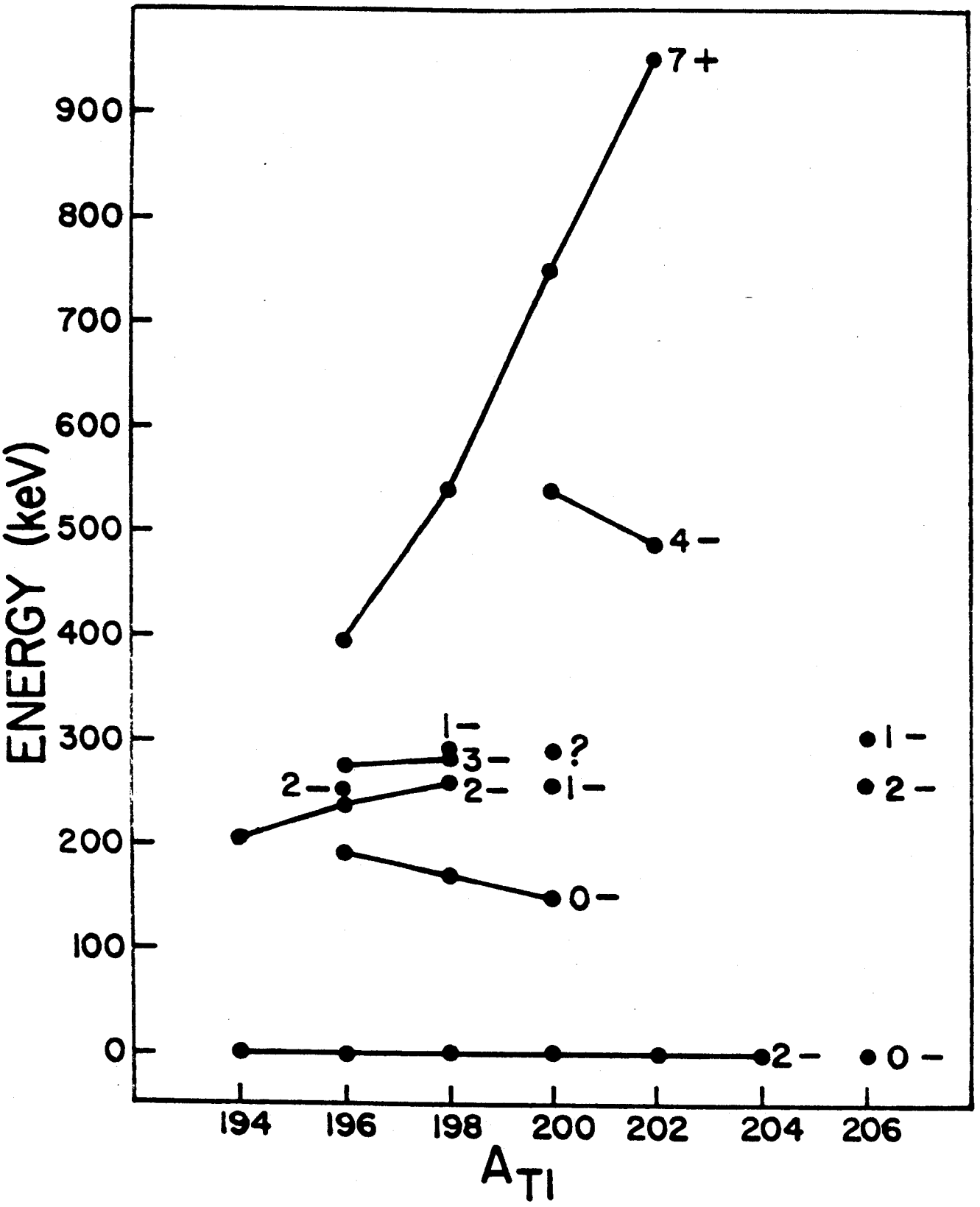

Figure IV-13. Systematics of some selected states in odd-odd Tl isotopes. The states connected by lines are assumed to be primarily the same configurations. The 289.24-keV state in Tl^{200} is marked by a ?, for we have been unable to decide between 1- and 2- for its assignment.

small splitting between the two states of the latter configuration is consistent with theoretical predictions, and many other examples of such doublets are presented in Ref. [De61]. However, the arguments are not conclusive for Tl^{200}, and, based on our present knowledge, we have to accept either possibility for the ground state.

Another potential source of information that might allow one to choose between the two above configurations for the primary component of the Tl^{200} ground state is the magnetic moment of this state. This has been deduced from atomic spectral studies, where it was found that $|\mu| < 0.15\mu_N$. Now, relatively little has been done with respect to characterizing the magnetic moments of odd-odd states in terms of simple shell-model states, e.g., determining the damping effects of the odd proton and odd neutron on each other, so one can use such predictions only very qualitatively. Nevertheless, according to our somewhat simplistic estimates, one might expect the effective magnetic moment for each of the two above configurations to be almost the same, lying somewhere in the vicinity of $+0.8\mu_N$, an odd-odd "Schmidt limit". One cannot use this as a basis for choosing between the configurations either.

From Table IV-6 we find that there are three possibilities for the 0- first excited state. Because the $s_{1/2}$ proton state lies much lower than the $d_{3/2}$ and $d_{5/2}$ states in this region, and the $f_{5/2}$, $p_{3/2}$, and $p_{3/2}$ neutron states are much closer together, we expect the lowest configurations to include the $s_{1/2}$ proton state. We therefore conclude that the $[(\pi s_{1/2})(\nu p_{1/2})]_{0-}$ configuration is the best choise

for the first excited state. This follows the "strong" Nordheim rule, which suggests that the 1- state from this configuration will lie higher in energy than the 0- state. Since all the states above the first excited state that are populated by Pb^{200} decay have 1- assignments, with the possible exception of the 289.24-keV state, we cannot unambiguously assign the $[(\pi s_{1/2})(\nu p_{1/2})]_{1-}$ configuration to any specific one of them. However, one would expect to observe a strong *M*1 transition between the $[(\pi s_{1/2})(\nu p_{1/2})]_{1-}$ and $[(\pi s_{1/2})(\nu p_{1/2})]_{0-}$ states, which eliminates the 289.24-, 450.56-, 525.55-, and 605.44-keV states as contenders. This leaves the 257.18- and 289.92-keV states as possibilities for the major portion of the $[(\pi s_{1/2})(\nu p_{1/2})_{1-}$ strength. This is consistent with the prediction of a small splitting between the states of this configuration [Br60, Ze58]. Based on the fact that the 142.28-keV *M*1 transition between the 289.92- and 147.63-keV states competes very favorably with the more energetic ground-state transition, we tend to favor the $[(\pi s_{1/2})(\nu p_{1/2})]_{1-}$ configuration for the 289.92-keV state. However, if the ground-state configuration were $[(\pi s_{1/2})(f_{5/2})]_{2-}$ and the 289.92-keV state configuration were $[(\pi s_{1/2})(\nu p_{3/2})]_{1-}$, one could easily explain the weakness of the ground-state transition by its being ℓ-forbidden.

From Table IV-6 we see that there are seven possible configurations that can result in low-lying 1- states populated by the decay of Pb^{200}. Experimentally we have found six, possibly seven, such states. Cnnsidering the small energy differences between these states, one would expect configuration mixing to play a very important role in this nucleus. Thus, one should take the foregoing arguments as an outline of

the procedures to be followed in such assignments. And, of course, further attempts here to assign specific configurations to specific states could well be even more foolhardy, for the mixing could easily obviate simple selection rules for, say, the γ transitions.

As mentioned in Section 4.5, we have not been able to assign an unambiguous spin to the 289.24-keV state on the basis of the experimental data. There is some support for the 2- assignment in the systematics of the states in the other odd-odd Tl isotopes. In the ε decays of Pb^{198} and Pb^{196}, 2- states are reported to be populated at 259.5 and 240.3-keV, respectively [Ju60], [Sv61]. A 2- state has also been tentatively observed at 205-keV in Tl^{194} [Ju59]. Thus, we might expect to find a 2- state at about 280-keV in Tl^{200}. One possible configuration for this state could be $[(\pi s_{1/2})(\nu f_{5/2})]_{2-}$, as suggested by DeShalit and Walecka for the 2- states in Tl^{198} and Tl^{196}. On the other hand, if the ground state were $[(\pi s_{1/2})(\nu f_{5/2})]_{2-}$ and not $[(\pi s_{1/2})(\nu p_{3/2})]_{2-}$, the 289.24-keV state might contain an appreciable fraction of the latter configuration. All other things being equal, one might expect the ground state of Pb^{200} to populate the latter configuration more strongly than the former, as the $s_{1/2}$ protons are expected to lie closest to the Fermi surface in Pb. However, this is a very weak argument, and, in fact, if one reasons in terms of the ε-decay probabilities, then a 1- assignment is slightly favored for the 289.24-keV state, as was discussed in Section 4.5.

Although we have included the states populated by (7+?) Tl^{200m} decay [Di63] in Figure IV-9 for the sake of completeness, we have purposely refrained from including them in our discussion. We

expect very little overlap of these states with the ones we have just discussed, and to include them would have resulted in undue complexity. However, we would like to emphasize that odd-odd nuclei do provide one of the most convenient natural probes for studying the p-n residual interaction, so a complete study of states in odd-odd Tl^{200} and the other odd-odd Tl isotopes would be most welcome. Now that high-resolution reaction-product spectrometers are coupled with moderate-energy, highest-resolution sector-focused cyclotrons, reactions such as (p,d) on Tl^{203} and Tl^{205} and (τ,t) on the even-even Hg isotopes could well be a very probitable study.

CHAPTER V

THE DECAY OF Pb^{201}

5-1. Introduction

In this chapter we present the results of our study of the states in Tl^{201} populated by the decay of 9.4-h Pb^{201}. Because $_{81}Tl^{201}_{120}$ is only one proton removed from the Z=82 closed shell and 6 neutrons removed from the N=126 closed shell, most of its low-lying states should be successfully described by the single-particle shell model. The systematics of this region are especially interesting as the neutron-deficient, odd-mass Tl isotopes provide one of the few series where we can observe the effects of successively plucking out pairs of neutrons on fairly pure single-particle states. Because of this and the similarity of the shell model assignments in Tl^{201} and Tl^{199} we have postponed a discussion of the systematics and shell model assignments in this region until we have presented the results of our study into the decay of Pb^{199} in Chapter VI.

The first published work on the decay of Pb^{201} was by Howland and co-workers [Ho46] in which they reported a half-life measurement of 5-h for an activity resulting from the reaction $Tl^{203}(d,4n)Pb^{201}$. Neuman and Perlman [Ne50] in 1950 reported an 8±2-h activity in Pb as a daughter of the 62-min and 2-h isomers of Bi^{201}.

Using a β-ray spectrometer of 3% resolution, Wapstra and co-workers [Wa54] in 1954 observed several conversion-electron lines from the decay of Pb^{201} to which they assigned γ-ray energies of 325 and 583 keV.

In 1955 Bergkvist and co-workers [Be55] published a more complete study of Pb^{201} decay using a β-spectrometer with a resolution of 0.2%. They found 15 γ transitions belonging to ≃9-h Pb^{201}. At about the same time T. Gerholm [Ge55] showed by $\bar{e}$-$\bar{e}$-coincidence measurements in a double lens spectrometer that the 330- and 361-keV γ-rays were in coincidence. Based on these measurements two excited states at 330 and 692 keV were proposed.

In 1960 J. Lindskog, E. Bashandy, and T. Gerholm reported a half-life for the first excited state in Tl^{201} at 330 keV of 0.07 nsec [Li60].

The decay scheme was extended considerably in 1961 by the work of Pettersson and co-workers [Pe61]. They performed gamma-gamma angular correlation and electron-gamma coincidence experiments on several of the stronger transitions. They also measured the *K*-conversion coefficients for the 330-, 361-, and 585-keV transitions. Based on their singles and coincidence results, they proposed a decay scheme of 9 excited states at 330, 692, 907, 1097, 1277, 1406, 1618, 1728, and 2012 keV. (Of these we have confirmed only the 330-, 692-, 1097-, and 1277-keV levels.)

The most recently published work on the decay of Pb^{201} was by Aasa and co-workers [Aa64] using an iron yoke double focusing β-spectrometer with resolutions as good as 0.17%. They assigned 32 transitions to the decay of Pb^{201} and proposed 10 excited levels at 331.22, 692.55, 753.2, 931.8, 1098.5, 1157.4, 1238.6, 1277.1, 1401.0, and 1479.7 keV. (We have confirmed all of these except for the 753.2- and 931.8-keV states.)

The only known observation of positron emission in the decay of Pb^{201} was made by Bergvist in 1957 and reported by Bergström and Andersson [Be57]. They merely stated that two positron components, whose energy difference is 0.35 MeV, had been observed. It was not known whether the positron emission goes to the ground and first excited states (ΔE=331 keV) or to the first and second excited states (ΔE=361 keV).

In addition to the levels in Tl^{201} excited by the decay of Pb^{201}, several workers have reported the direct excitation of an isomeric state in Tl^{201} of $I\pi = 9/2-$. The first report of this isomer came in 1964 by K. Brandi and co-workers [Br64] who used the photonuclear reaction $Tl^{203}(\gamma,2n)Tl^{201m}$ to excite it. They measured a half-life of 2.1 msec for this state and observed two γ-rays of 335±8 and 597±12 keV de-exciting it. They proposed a state at 927 keV based on these two γ-rays. The second report of this isomeric state appeared in 1965 by Gritsyna and Forster [Gr65] who excited the isomeric state directly by bombarding Hg isotopes with protons to produce the reactions $Hg^{201}(p,n)Tl^{201m}$ and $Hg^{204}(p,4n)Tl^{201m}$. They measured a half-life of 1.8±0.1 msec for a level at 907 keV de-excited by γ-rays of 225±10, 325±10, and 585±10 keV. The most recent observation of this isomeric state was reported by T. W. Conlon in 1967 [Co67]. They also used the proton bombardment of Hg to produce the isomer. They measured a half-life of 2.65±0.2 msec for the isomeric state and γ-ray energies of 330.6 and 583.3 keV, which placed the isomeric state at 912.9±0.5 keV.

It is apparent from this survey that a great deal of information had been accumulated on the decay of Pb^{201} and states in Tl^{201}.

However, if we examine the decay scheme which summarizes these data, Figure V-1, it is equally apparent that a great many gaps remained in the data. We felt that a γ-ray study of this isotope using Ge(Li) detectors would go a long way in filling these gaps, and indeed it has, although it has also raised many new questions. Where previously 32 γ-transitions between 10 states in Tl^{201} had been observed in the decay of 9.4-h Pb^{201}, we report here 72 γ-transitions between 20 states. We have also been able to assign multipolarities to 25 γ-transitions where previously only 3 γ-transitions had multipolarities assigned. We have also been able to make specific spin and parity assignments or at least put limits on these for all 20 levels.

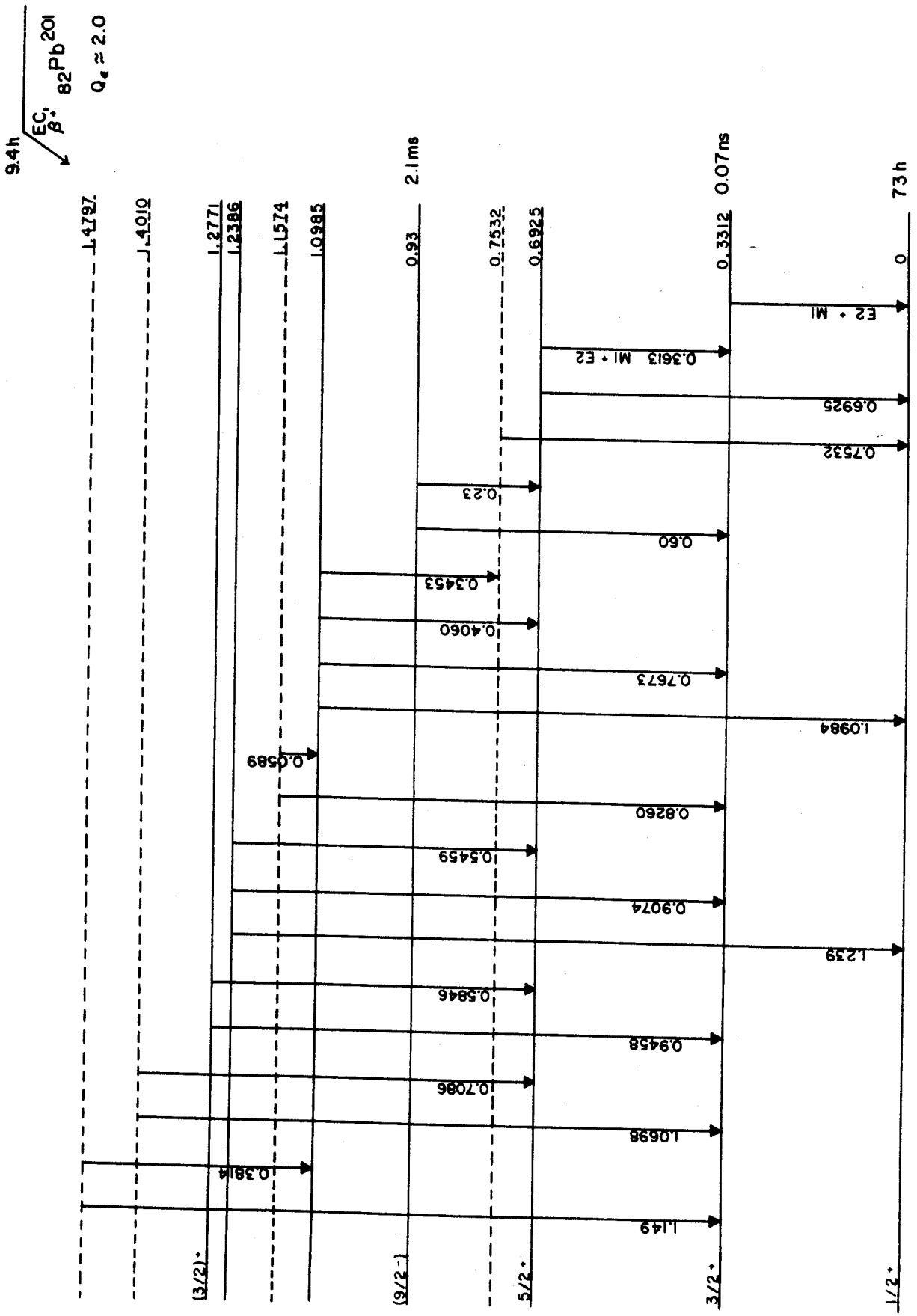

Figure V-1. The decay scheme of Pb^{201} as known before the present study. The energies of the transitions and states are given in MeV.

5.2. Source Preparation

5.2.1. $Tl^{203}(p,3n)Pb^{201}$

The Pb^{201} sources used in most of the experiments described in this chapter were produced using 27-MeV protons from the M.S.U. cyclotron to induce the $Tl^{203}(p,3n)Pb^{201}$ reaction on natural Tl foils (70.5% Tl^{205}, 29.5% Tl^{203}). The proton energy of 27 MeV was chosen to maximize the $(p,3n)$ reaction and yet not produce a measurable amount of Pb^{200}. Although the energy of 27 MeV is slightly above the calculated threshold of 24.7 MeV for producing Pb^{200} by the $(p,4n)$ reaction, we did not observe any Pb^{200} in our sources even after they were aged several days. However, we did produce several contaminating activities by the (p,n) and $(p,2n)$ reactions on Tl^{203} giving rise to 52-h Pb^{203} and 3.6-h Pb^{202m} respectively. We also produced 67 min Pb^{204m} and 52-h Pb^{203} activities from the $(p,2n)$ and $(p,3n)$ reactions on Tl^{205}. The 67 min Pb^{204m} presented no particular problem as we merely had to age the source for 12 hours after which it was virtually undetectable. The Pb^{202m} contaminant did present a slight problem as its half-life of 3.6-h was long enough that aging the source for only 12 or 18 hours did not reduce this activity to an undetectable level. However, this was not a particularly troublesome problem because of the small number of well-known γ-rays associated with this decay. The 52-h Pb^{203} was by far the most intense contaminant activity in these sources and actually accounted for more of the source activity than the Pb^{201}. This is easy to understand, for we produced the Pb^{203} from both Tl^{203} by the (p,n) reaction and Tl^{205} by the $(p,3n)$ reaction.

Of course the $(p,3n)$ reaction on Tl^{205} was by far the largest contributor, as Tl^{205} accounted for 70% of the target, and while 27 MeV protons maximized the production of Pb^{201} from Tl^{203}, they also maximized the production of Pb^{203} from Tl^{205}. The Pb^{203} activity was also enhanced with respect to the 9.4-h Pb^{201} by aging the sources. At the end of our experiments on Pb^{201} we did make one source using enriched Tl^{203}(70%) and the Pb^{203} activity was substantially reduced in this source.

As in the case of Pb^{200}, simply aging the sources did not eliminate the problem of source-purity, for the Tl daughters of Pb^{202m} and Pb^{201}, 12-d Tl^{202} and 73-h Tl^{201}, are also γ-ray emitters. Because of their long half-lives and the small number of well-known γ-rays emitted in their decay, these did not present any major problem. However, we did perform a chemical separation of the lead activity from the Tl target at the end of the 12-18-h aging period for all the sources used in this study. We also performed a separation every 3-5 hours on the sources to keep the Tl^{201} activity to a minimum. The chemical separation used is given as Appendix B. During most of the experiments, sources made from a given Tl target were used for only 5-12 hours of actual counting before being replaced by sources from another target bombarded 5-12 hours later. This was done in order to keep the ratio of Pb^{201} to Pb^{203} as high as possible while still allowing the sources to age for 12-18 hours.

5.2.2. $Tl^{203}(He^3,5n)Bi^{201} \xrightarrow{\varepsilon} Pb^{201}$

When the M.S.U. cyclotron began accelerating He^3 beams on a

routine basis we decided to investigate an alternate method of preparing Pb^{201} similar to that described in Section 4.2.3. for preparing Pb^{200}. In this case we bombarded natural Tl with a 48-MeV (70 MeV degraded with 40 mil aluminum) He^3 beam to induce the Tl^{203} $(He^3,5n)Bi^{201}$ reaction. Bi^{201} has a half-life of 1.8 h and decays by electron capture to Pb^{201}. Of course we also produced varying amounts of other Bi isotopes by the competing (He^3,Xn) reactions on both Tl^{203} and Tl^{205}, where $1 \leq X \leq 5$. The major radioactive Bi isotopes produced by these reactions were: 15-d Bi^{205}, 11.2-h Bi^{204}, 11.8-h Bi^{203}, and 1.6-h Bi^{202}. However, the half-lives of these Bi isotopes are all significantly longer than that of Bi^{201} except for Bi^{202}, which has a comparable half-life.

The Tl targets were bombarded for ~1 hour with a 2-μamp He^3 beam. The Pb activity was separated from the Bi activity and the Tl target by the ion exchange procedure described in Appendix C. In this case, however, we allowed the Pb activity to build up in the ion-exchange column for ~4 hours before washing it off. The sources were aged for ~12 hours and the Pb activity was separated from the Tl daughters by the precipitation procedure described in Appendix B. Although sources prepared in this manner did have a more favorable Pb^{201} to Pb^{203} ratio than those prepared by the proton bombardment of natural Tl, we did not use this preparation extensively because of the involved chemistry and the difficulty in making sources of the required strength.

5.3. Experimental Results

5.3.1. γ-ray Singles Spectra

Pb^{201} γ-ray energies and intensities were determined using two five-sided trapezoidal Ge(Li) detectors (0.42% and 2.5% efficient) and a true coaxial Ge(Li) detector (3.6% efficient) having resolutions of 3.0, 2.3, and 2.1 keV, respectively, for the 1332-keV γ of Co^{60}. All detector systems used room-temperature FET preamplifiers, low noise RC linear amplifiers with pole-zero compensation and near-Gaussian shaping. The data were recorded by a Nuclear Data Model 2200 4096 channel analyzer or by Norhtern Scientific 4096 and 8192 channel ADC's coupled to the Nuclear Chemistry group's PDP-9 computer and the M.S.U. Cyclotron Laboratory's Sigma-7 computer.

The energies of the prominent γ-rays were determined by counting the Pb^{201} sources simultaneously with the energy standards listed in Table V-1. The Tl^{201} and Pb^{203} were always present in our sources to some extent and were therefore very convenient to use as energy standards. The energies of the weaker Pb^{201} γ-rays were then determined by using the now well-known γ-rays from Pb^{201} as secondary standards. The centroids and peak areas were determined using the live-display computer program MOIRAE [Moir].

Figure V-2 shows a typical γ-ray singles spectrum taken with the 0.42% detector. The source for this experiment was prepared by the $(p,3n)$ reaction on natural Tl foils, and as was discussed in Section 5.2.1. the 279-keV γ-ray from the Pb^{203} contaminant is the most prominent peak in the spectrum. From the data obtained with the 0.42% detector we assigned 45 γ-rays to the decay of Pb^{201}. When the larger

Table V-1

γ-Rays Used as Energy Standards

Nuclide	γ-Ray energy (keV)	Reference
Tl^{201}	135.34 ±0.04	a
	167.43 ±0.07	a
Pb^{203}	279.19 ±0.008	b
Au^{198}	411.795±0.009	c
Ag^{110m}	446.77 ±0.04	d
	620.22 ±0.03	d
	657.72 ±0.03	d
	677.55 ±0.03	d
	686.80 ±0.03	d
	744.19 ±0.04	d
	763.88 ±0.04	d
	818.00 ±0.04	d
	884.67 ±0.04	d
	937.48 ±0.04	d
	1384.26 ±0.05	e
	1505.01 ±0.07	e
Bi^{207}	569.63 ±0.08	b
	1063.60 ±0.06	b
Mn^{54}	834.83 ±0.04	f
Y^{88}	898.03 ±0.04	f
	1836.13 ±0.04	f
Ta^{182}	1121.31 ±0.04	e
	1189.06 ±0.04	e
	1221.42 ±0.04	e
Co^{60}	1173.23 ±0.04	b
	1332.50 ±0.03	f

[a] C.J. Herrlander, R. Stockendal and R.K. Gupta, Ark. Phys. 17, 315 (1960).

[b] J.B. Marion, Nuclear Data A4, 301 (1968).

Table V-1 (cont'd)

[c] J.S. Geiger, R.T. Graham, I. Bergström, and F. Brown, Nucl. Phys. 68, 352 (1965).

[d] S.M. Brahmavar, J.H. Hamilton, and A.V. Ramayya, Nucl. Phys. A125, 217 (1969).

[e] R.E. Doebler, Nuclear Chemistry Annual Report, Michigan State University, COO-1779-13 (1969).

[f] Average of b and g.

[g] R. Gunnink, R.A. Meyer, J.B.Niday, and R.P. Anderson, Nucl. Instr. Methods 65, 26 (1968).

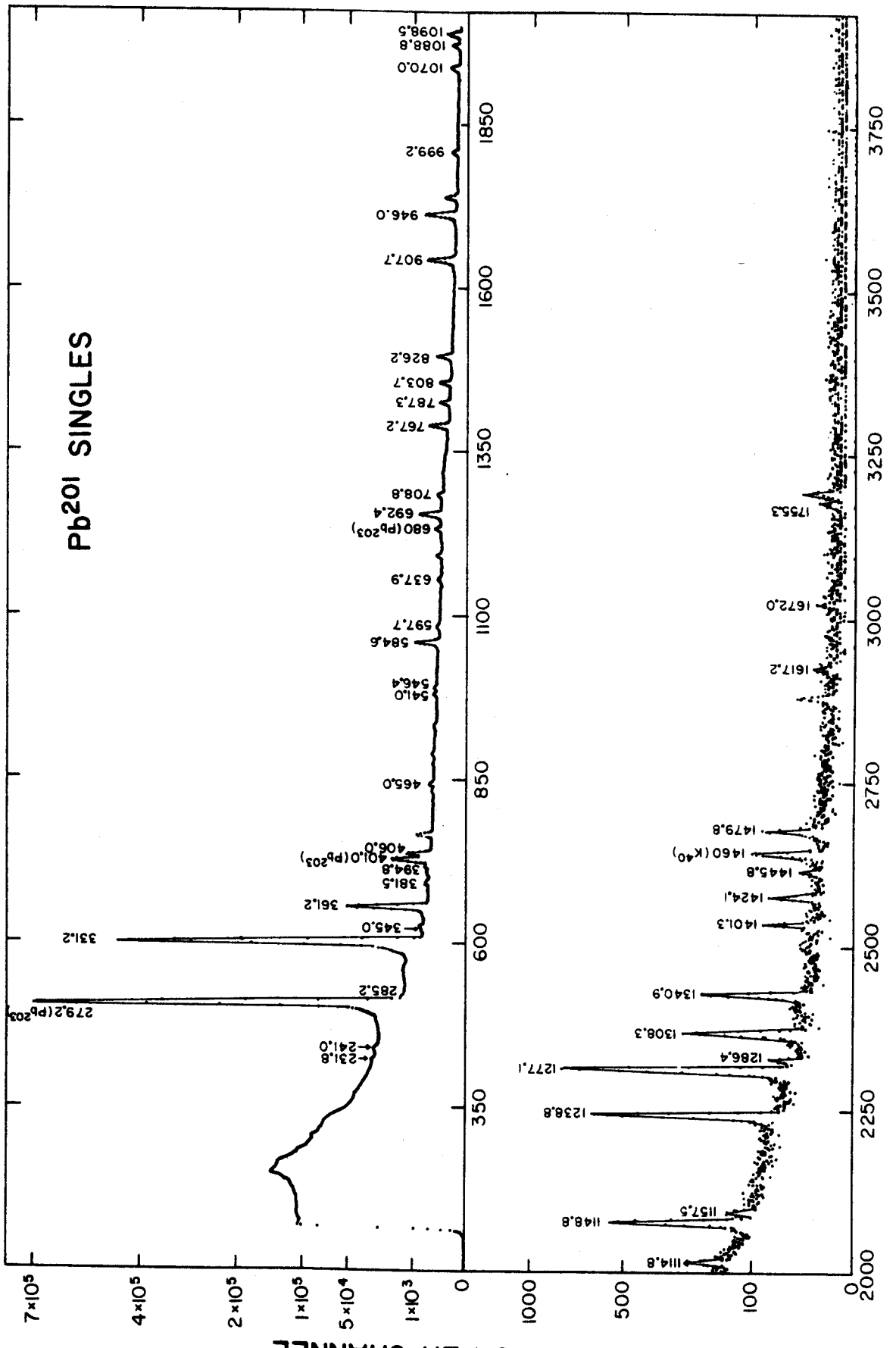

Figure V-2. Pb^{201} singles γ-ray spectrum taken with a 0.42% efficient Ge(Li) detector. The source used to obtain this spectrum was prepared by the $(p,3n)$ reaction on natural Tl.

volume Ge(Li) detectors became available we re-examined the decay and obtained the singles spectrum shown in Figure V-3. This was taken with the 3.6% detector during a 24-hour period using a source prepared by the $(p,3n)$ reaction on enriched Tl^{203}. From the many singles spectra obtained with the 2.5% and the 3.6% detectors we have been able to assign a total of 72 γ-transitions to the decay of Pb^{201}.

The energies and relative intensities of these 72 γ-transitions are listed in Table V-2. As noted in Table V-2, several of the γ-transitions have been corrected for underlying peaks from the decay of Pb^{202m}. The energies and intensities for the 945.96- and 946.78-keV doublet were obtained from the two-dimensional γ-γ coincidence experiment. The method used to obtain these will be described in Section 5.3.5.d. The uncertainties in the energies listed in Table V-2 are based on the uncertainties in the energy standards, the heights of the peaks above the underlying Compton background, and the reproducibilities of the calculated energies from many different spectra. Uncertainties in the relative γ intensities are based on their reproducibilities in many spectra and the uncertainties in the experimentally determined efficiency curves for the Ge(Li) detectors.

The K x-ray intensity for Pb^{201} listed in Table V-2 was obtained from the spectra of Pb^{201} and Pb^{203} shown in Figure V-4 in the following manner. A Pb^{201} source prepared from enriched Tl^{203} was allowed to age for ~15-h to reduce the Pb^{204m} and Pb^{202m} to an acceptable level. After this period the only major contaminant contributing to the total x-ray intensity was Pb^{203}. A Pb^{203} source was then made from

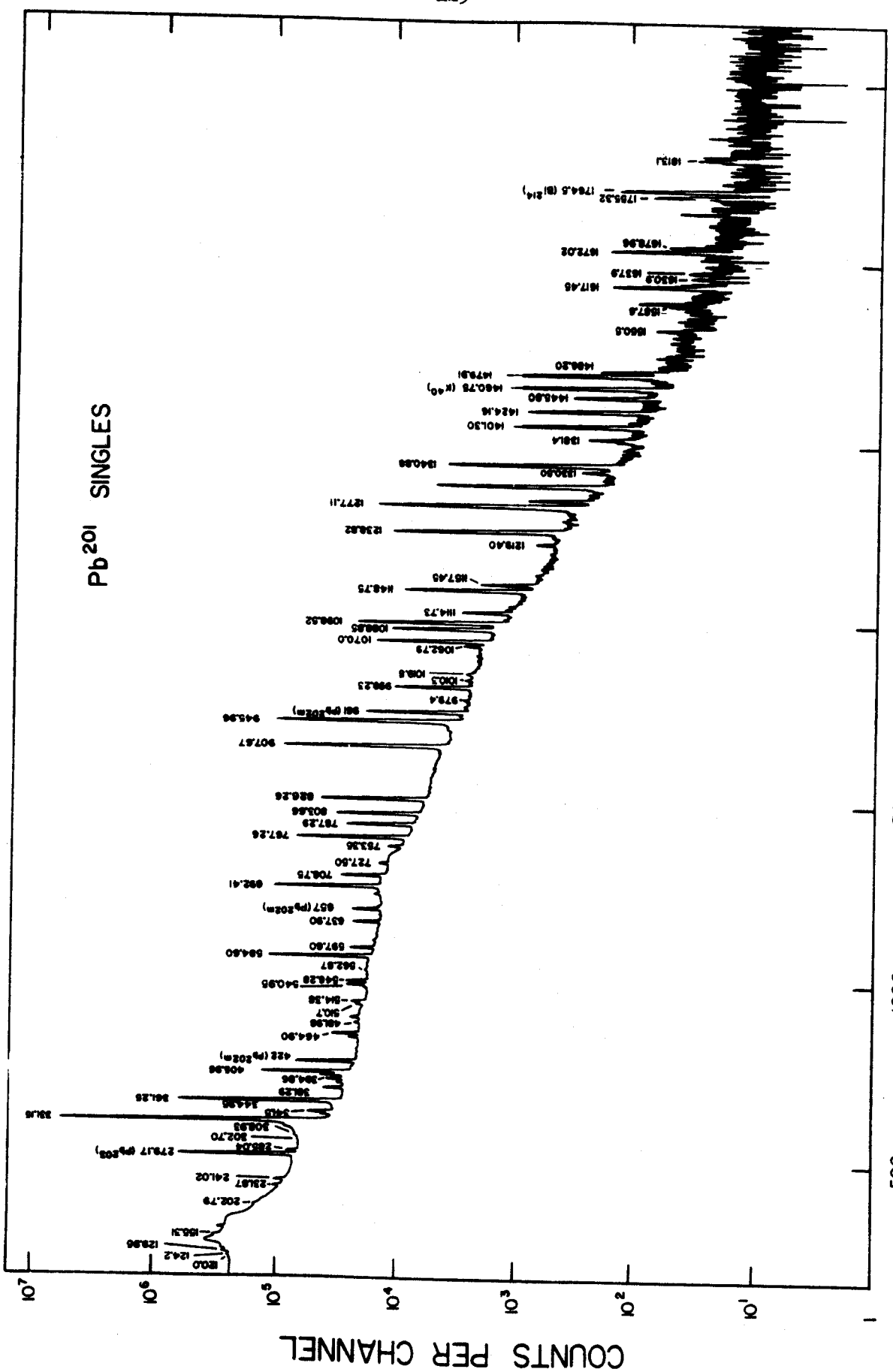

Figure V-3. A singles γ-ray spectrum recorded by a 3.6% efficient Ge(Li) detector during a 24-h period. The source used to obtain this spectrum was prepared by the $(\alpha,3n)$ reaction on enriched Tl^{203}(70%).

Table V-2

Energies and relative intensities of γ rays from the decay of Pb^{201}.

Measured energies (keV)	Relative intensities		
	Singles	Anticoincidence	Intergal γ-γ coincidence
K x-rays	4980 ±250	-	-
120.0 ±0.2	1.20± 0.3	-	30± 5
124.2 ±0.2	2.5 ± 0.5[a]	-	34± 5
129.95±0.1	6.4 ± 0.6[a]	-	114±12
155.31±0.1	8.2 ± 1.0	6.0± 1.0	179±15
202.79±0.1	4.0 ± 0.5	-	80±10
231.87±0.1	6.5 ± 0.8	1.6± 0.5	106±11
241.02±0.08	10.0 ± 1.0[a]	2.1± 0.5	139±14
285.04±0.07	10.3 ± 1.0	1.5± 1.0	166±17
302.70±0.4	0.65 ± 0.15	-	23± 5
308.93±0.15	2.3 ± 0.3	-	25± 5
322.42±0.15	4.4 ± 0.6	-	104±15
331.15±0.06	4550 ±250	2800 ±150	20,290±1000
341.51±0.08	6.8 ± 0.8	1.4± 0.6	85±10
344.95±0.07	18.3 ± 1.5	5.0± 1.0	269±20
361.25±0.06	560 ± 30	156 ±10	6730±400
381.29±0.08	12.9 ± 0.7	3.5± 0.5	183±15
394.86±0.09	10.8 ± 0.7	4.3± 1.0	213±20
405.96±0.07	120 ± 6	33 ± 5.0	1717±150
464.90±0.08	19.8 ± 1.0	5.4± 0.6	275±20
481.98±0.09	3.2 ± 0.6	-	53± 8
510.7 ±0.20	6 ± 1	1.3± 0.3	31± 5
514.38±0.09	9.1 ± 2.0	1.6± 0.2	119± 15
540.90±0.09	16.2 ± 1.0	4.5± 0.7	238± 25
546.28±0.09	16.5 ± 1.0	4.4± 0.5	231± 25
562.81±0.10	1.8 ± 0.4	-	-
584.60±0.08	211 ± 10	60.2± 3.0	2814± 200

Table V-2 (cont'd)

597.60±0.09	19.0 ± 1.0	4.4 ± 0.2	303± 25
637.90±0.09	21.7 ± 1.0	6.3 ± 0.3	295± 25
692.41±0.08	254 ± 12	182 ±10	1365± 80
708.75±0.09	46.2 ± 2	14.5 ± 0.6	636± 50
727.50±0.09	7.10± 0.7	2.3 ± 0.2	93± 10
753.35±0.09	8.75± 0.8	2.6 ± 0.2	105± 15
767.26±0.08	194 ± 10	75.5 ± 4.0	1685± 150
787.29±0.10	34 ± 4[a]	13 ± 3	468± 100[a]
803.66±0.07	90 ± 6	23.3 ± 1.0	1184± 80[a]
826.26±0.08	141 ± 7	54.9 ± 3.0	1240± 80
907.67±0.08	362 ± 20	157 ± 8.0	2766± 140
945.96±0.08[b]	424 ± 30[b]	205 ±10	3460± 170
946.78±0.4 [b]	28 ± 10[b]	-	-
979.4 ±0.3	1.1 ± 0.3	1.1± 0.4	21± 4
999.23±0.07	38.3 ± 2	17.0± 1.0	327± 30
1010.3 ±0.3	1.0 ± 0.2	-	6.8± 1.5
1019.8 ±0.3	1.4 ± 0.4	-	16± 5
1062.79±0.15	4.0 ± 0.5	2.2± 0.2	57± 6
1070.04±0.08	71.8 ± 4.0	35.5± 2.0	516± 40
1088.85±0.09	53.2 ± 3.0	24.9± 1.5	378± 30
1098.52±0.07	111 ± 6.0	108 ± 6.0	173± 10
1114.73±0.08	9.8 ± 0.6	4.42± 1.0	82± 10
1124.9 ±0.2	0.57± 0.1	-	-
1148.75±0.08	47.3 ± 2.5	24.1± 1.2	318± 20
1157.45±0.09	7.2 ± 0.4	8.64± 0.7	15± 3
1219.40±0.15	1.4 ± 0.1	0.80± 0.2	20± 3
1238.82±0.07	68.0 ± 4.0	71.9± 4.0	74± 5
1277.11±0.07	≡100	≡100	≡100
1286.3 ±0.2	3.75± 0.2	1.90±0.3	7.2
1308.32±0.08	32.6 ± 1.6	17.0 ±1.0	192± 15
1330.50±0.15	0.86± 0.15	0.46±0.1	-
1340.88±0.09	26.9 ± 1.5	13.0± 0.6	150± 10
1381.4 ±0.3	1.1 ± 0.2	-	16± 3

Table V-2 (cont'd)

1401.30±0.08	7.90 ± 0.4	7.90± 0.4	13±4
1424.16±0.09	5.75 ± 0.3	2.2 ± 0.3	30±6
1445.80±0.10	2.10 ± 0.1	2.5 ± 0.4	-
1479.91±0.10	10.4 ± 0.5	10.4 ± 0.6	9±3
1486.20±0.12	1.1 ± 0.1	-	-
1550.5 ±0.4	0.27 ± 0.04	-	-
1587.6 ±0.5	0.15 ± 0.05	-	-
1617.45±0.15	1.4 ± 0.1	1.6 ± 0.2	-
1630.9 ±0.6	0.14 ± 0.04	-	-
1639.1 ±0.5	0.20 ± 0.05	0.55± 0.10	-
1672.02±0.10	1.45 ± 0.10	1.60± 0.2	-
1678.96±0.13	0.24 ± 0.03	-	-
1755.32±0.10	0.65 ± 0.06	0.83± 0.2	-
1813.1 ±0.3	0.26 ± 0.05	-	-

[a] These intensities have been corrected for the underlying peaks from Pb^{202m} decay based on the γ intensities listed in Chapter III.

[b] These energies and intensities have been determined with the aid of the 2-d experiment. See text for an explanation of how this was done.

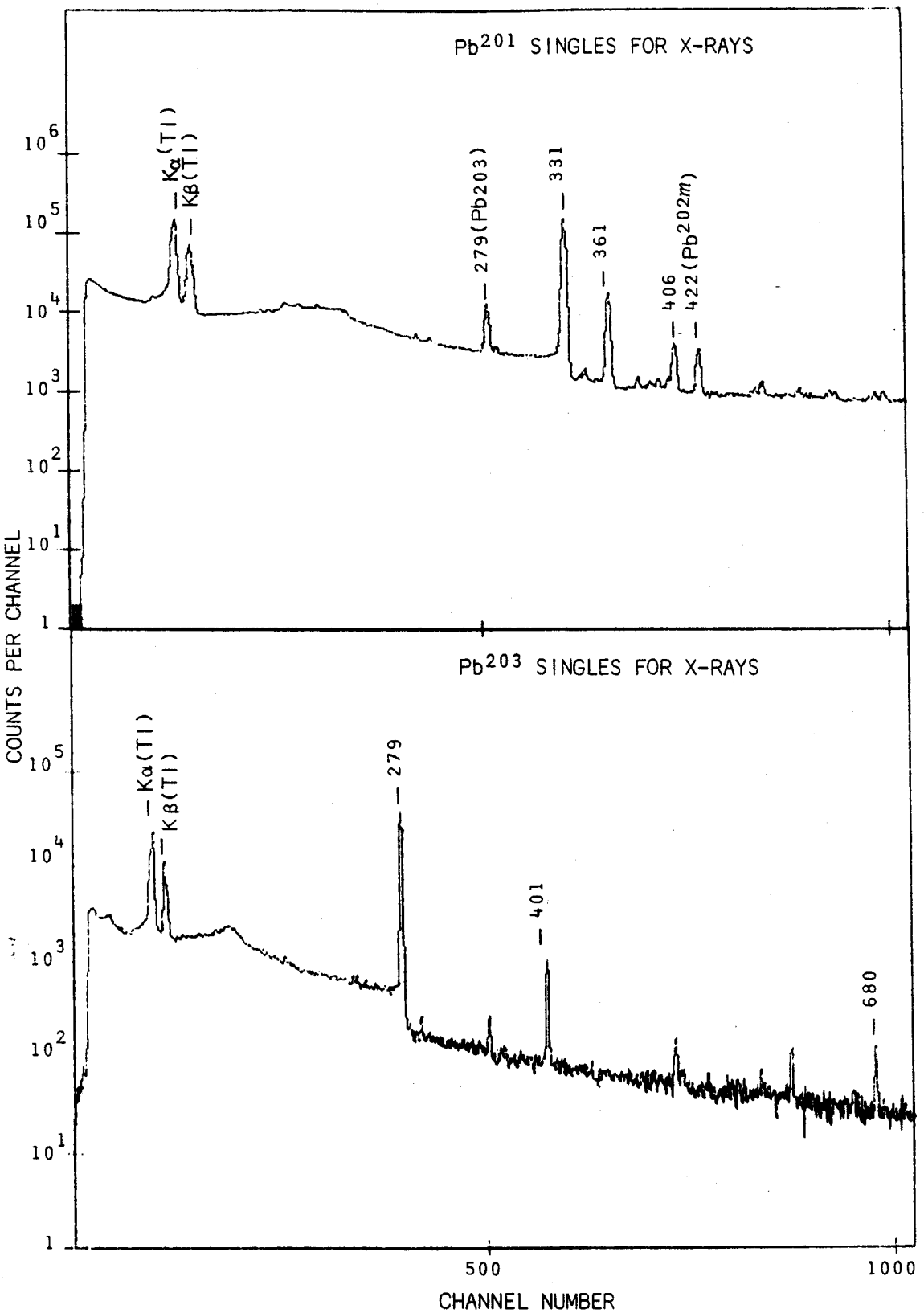

Figure V-4. Low energy γ-ray spectra of Pb^{201} and Pb^{203} taken with a 2.5% efficient Ge(Li) detector and used to obtain the *K* x-ray intensity for Pb^{201} decay.

enriched Tl^{203} by the $Tl^{203}(p,n)Pb^{203}$ reaction. This source was aged ≈24-h before the spectrum shown in Figure V-4 was recorded. It was then an easy matter to subtract out the Pb^{203} x-ray intensity from the Pb^{201} spectrum.

5.3.2. Anti-Compton Spectrum

The masking of γ-rays by the Compton distributions of higher energy γ-rays is one of the major limitations in detecting very weak γ-rays in a singles experiment using Ge(Li) detectors. This was an especially bad problem in the case of our early singles runs on Pb^{201}, for the Compton distribution of the 279-keV γ-transition from Pb^{203} was very large as can be seen in Figure V-2. Even in the singles experiment in which we used the enriched Tl^{203} the Compton distribution from the 331-keV peak of Pb^{201} itself contributed to a substantial Compton background as is evident in Figure V-3.

The conversion-electron spectra of Aasa and co-workers [Aa64] contained several peaks below 331 keV that were masked in our γ-ray singles experiments using natural Tl targets by this large Compton background. The only solution available to us at the time was to perform an anti-Compton experiment using the 8×8-in. NaI(Tl) annulus in coincidence with the 2.5% Ge(Li) detector. The general experimental setup for this experiment has been discussed in Section 2.2.1. The sources were made from natural Tl targets and counted for ≈30 h to obtain the anti-Compton spectrum shown in Figure V-5.

Although it may not show up very well in this figure, we were able to obtain intensities for several low energy γ-rays which

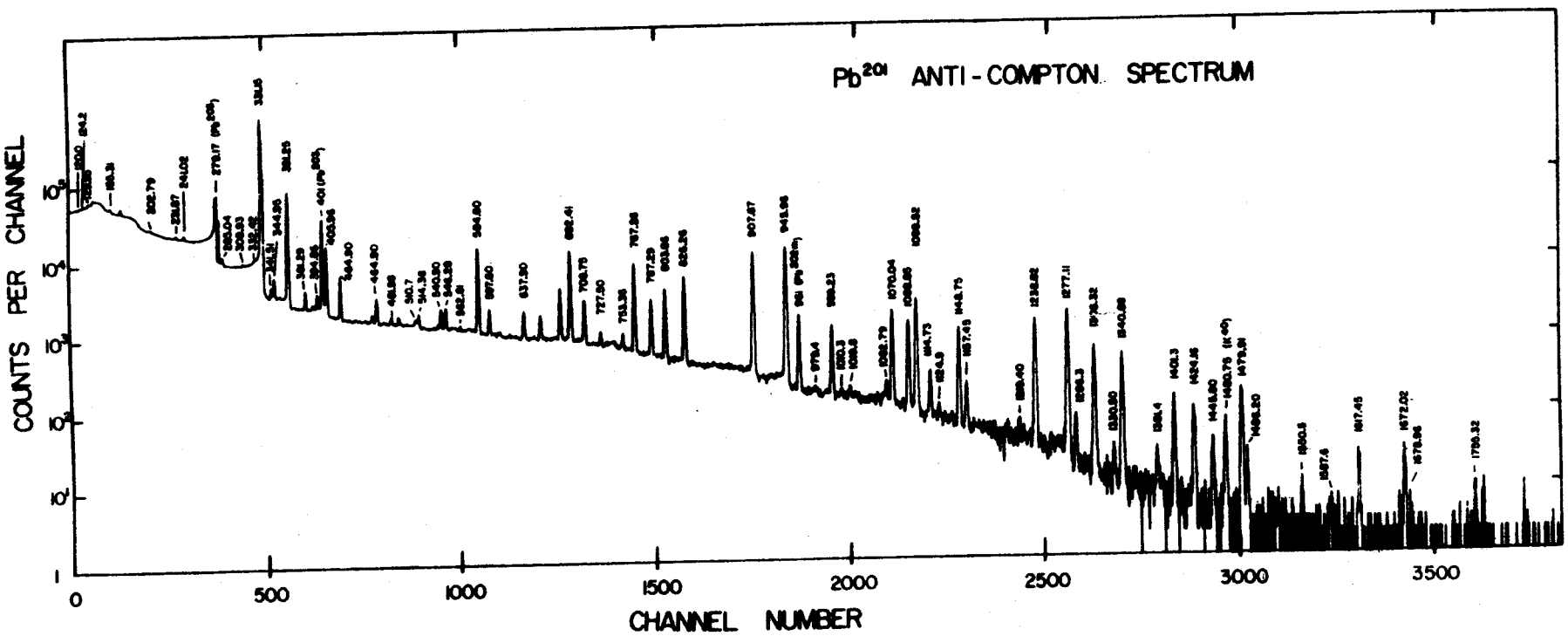

Figure V-5. Anti-Compton spectrum of Pb^{201} γ-rays using the 2.5% efficient Ge(Li) detector placed inside one end of an 8×8-in. NaI(Tl) annulus with a collimated source at the other end of the tunnel. Only peaks belonging to the decay of Pb^{201} are labeled except where otherwise indicated.

we could not even detect in our singles experiments using the natural Tl targets. Because of the reduced Pb^{203} in our last singles experiment using the enriched Tl^{203} targets, we also observed these weak, low-energy transitions in that experiment. The relative intensities obtained from a "true" anti-Compton experiment should be the same as those obtained in a singles experiment and, indeed, in this experiment the γ-ray relative intensities were essentially the same throughout the spectrum as those obtained in the singles experiments. Of course the Compton distribution was not only reduced below 331 keV, but throughout the whole spectrum, which made all the weaker peaks show up better, and we actually used the intensities from this experiment in arriving at the final relative intensities listed in Table V-2.

5.3.3. Anticoincidence Spectra

In order to determine which γ's are primarily ε-fed ground-state transitions, we used the 2.5% detector in an anticoincidence experiment with an 8×8-in. NaI(Tl) split annulus and a 3×3-in. NaI(Tl) detector as described in Section 2.3. A resolving time (2τ) of 100 nsec was used to obtain the spectrum shown in Figure V-6. The relative intensities obtained are listed in Table V-2. In order to compare the anticoincidence with the singles intensities and also the integral coincidence results, we have arbitrarily assigned a relative intensity of 100 to the 1277-keV transition in all three cases. This was chosen because it is a relatively strong transition and an essentially 100% ε-fed ground-state transition (a γ-transition depopulating a level which is

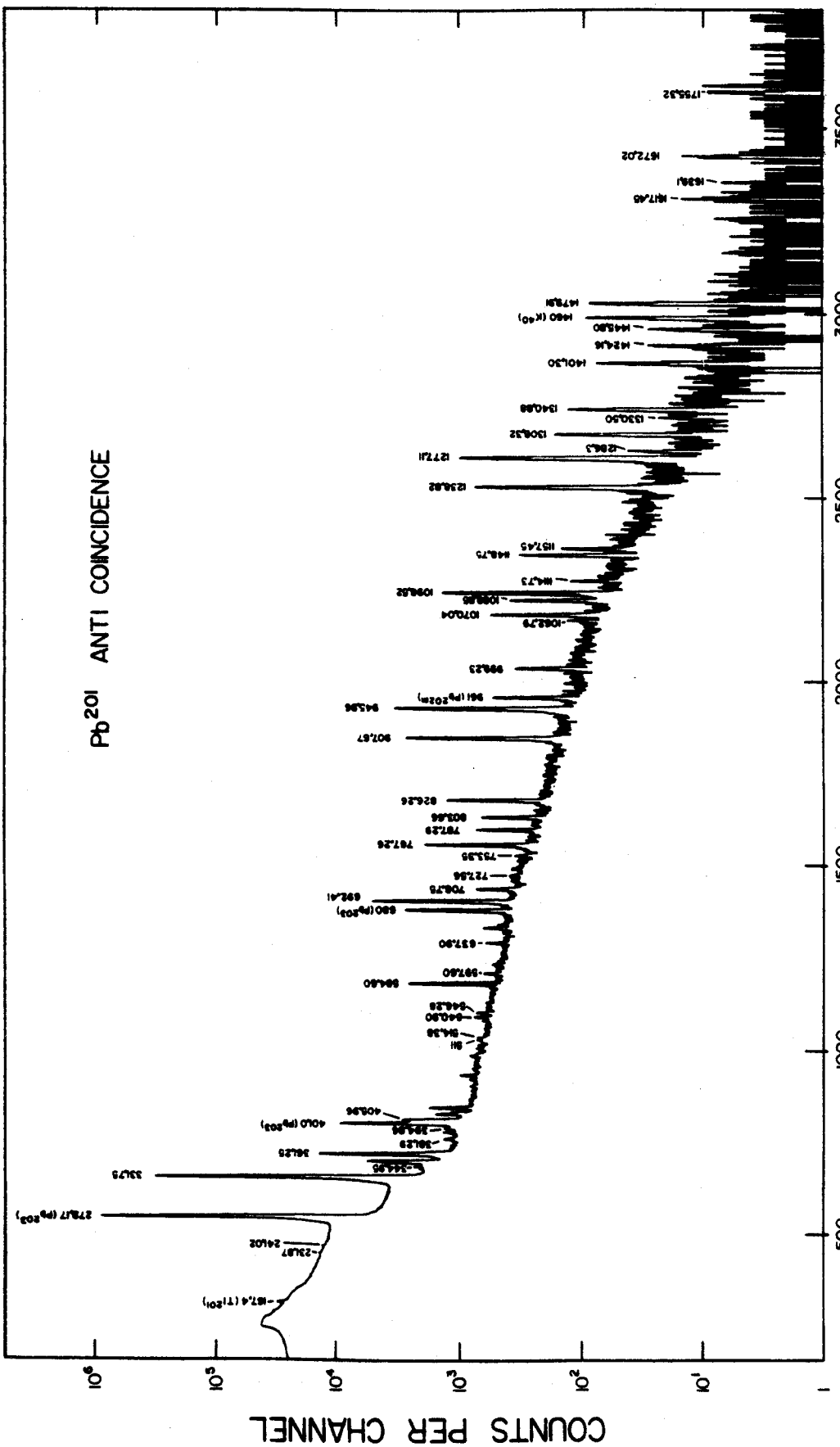

Figure V-6. Anticoincidence spectrum of Pb^{201} γ-rays using a 2.5% efficient Ge(Li) detector placed inside an 8×8-in. NaI(Tl) annulus with a 3×3-in. NaI(Tl) detector blocking the other end. Only peaks belonging to the decay of Pb^{201} are labeled except where otherwise indicated.

primarily fed directly by electron capture with little or no γ-feeding from higher levels). The argument may sound a little circular here, as we did not know the 1277-keV level was primarily ε-fed until after we analyzed the anticoincidence data, however, for the purpose of displaying the final results this met the above requirements.

Based on the results of this experiment it appears that the 1755.32-, 1672.02-, 1639.1-, 1617.45-, 1479.91-, 1445.80-, 1401.30-, 1277.11-, 1238.82-, 1157.45-, 1098.52-, and 979.4-keV transitions are all primarily ε-fed ground-state transitions. The 692.41- and 331.15-keV transitions are not reduced in intensity as much as most of the other transitions. This leads us to believe that these are ground-state transitions partially fed by other γ-rays from above.

5.3.4. Integral Coincidence Spectra

To complement the anticoincidence experiment we also performed an integral coincidence experiment. In our first attempt we used the 0.42% efficient detector in coincidence with the 8×8-in. NaI(Tl) annulus. However, because of the poor efficiency and resolution of this detector we did not observe many of the weaker transitions present in the singles and anticoincidence spectra. Instead of repeating this experiment with a larger Ge(Li) detector and the NaI(Tl) annulus, we used the integral coincidence spectrum recorded by the 2.5% detector in the 2-d γ–γ coincidence experiment discussed in the next section to obtain the intensities listed in Table V-2. This spectrum is shown in Figure V-7. The intensities obtained from the integral coincidence experiment using the 0.42% detector with the

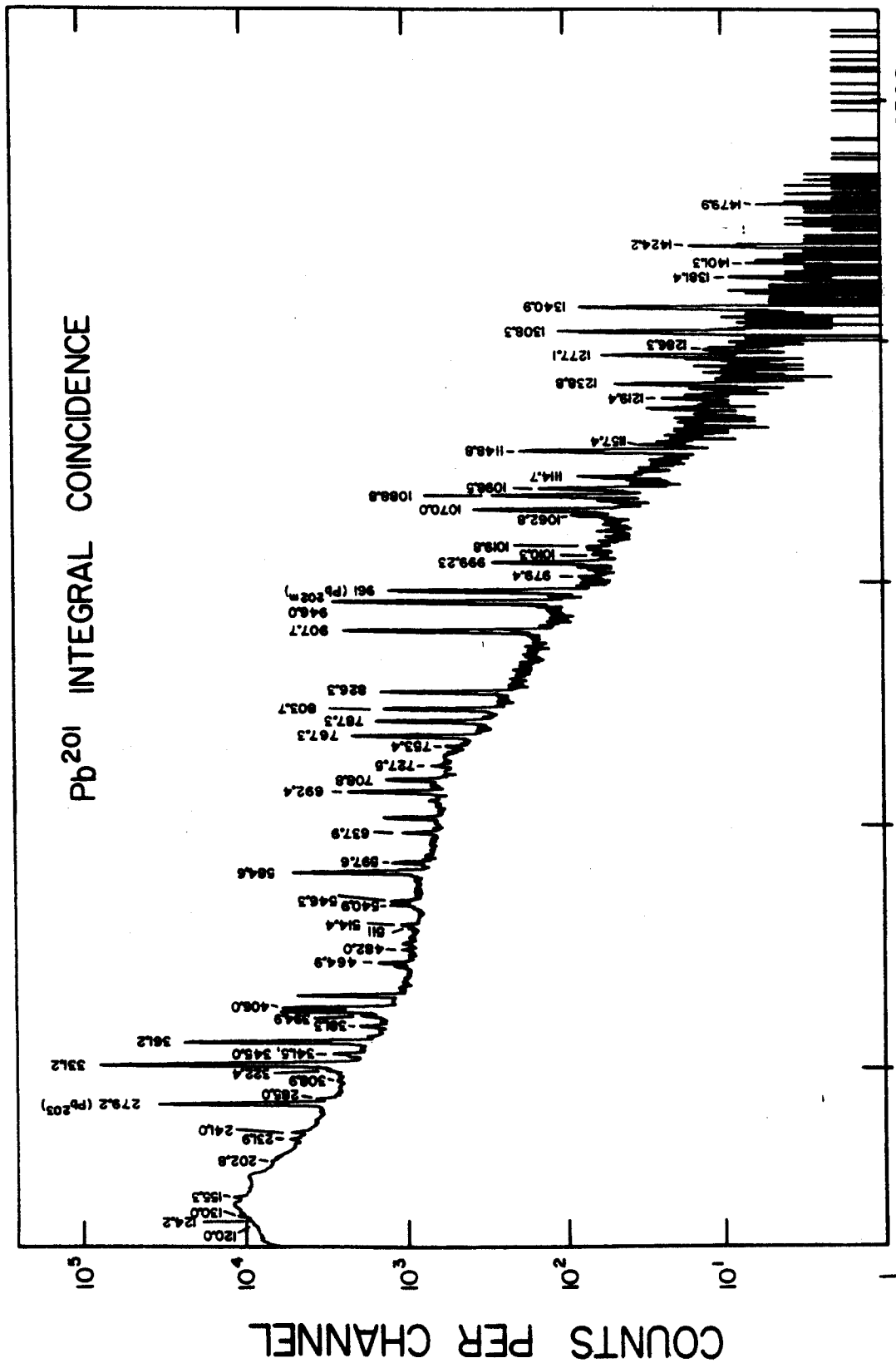

Figure V-7. Integral coincidence spectrum of Pb^{201} γ-rays. This spectrum was obtained by using a 2.5% efficient Ge(Li) detector in coincidence with a 3.6% efficient Ge(Li) detector. All γ-rays above the *K* x-rays were included in the gate.

NaI(Tl) annulus were consistent with the results from the 2-d integral coincidence spectrum for those peaks appearing in both spectra. These results were also consistent with those obtained in the anticoincidence experiment with one notable exception. In the integral coincidence experiment the 979.4-keV γ intensity is greatly enhanced over the singles intensity, which indicates that the 979.4-keV transition is not an ε-fed ground-state transitions as was indicated by the anticoincidence experiment. However, this is not particularly upsetting as this peak is very weak and its intensity was subject to much uncertainty in all runs.

From the results of the anticoincidence and integral coincidence experiments alone we were able to tentatively propose states at 331.1, 692.4, 1098.5, 1157.4, 1238.8, 1277.1, 1401.3, 1445.8, 1479.9, 1617.4, 1639.1, 1672.0, and 1755.3 keV.

5.3.5. 2-d γ-γ Coincidence Experiment

The 2-d γ-γ coincidence experiment using two Ge(Li) detectors was of invaluable help in constructing the Pb^{201} decay scheme, not only by establishing coincidence relationships, but also in determining the energies and intensities of the 945.96-, 946.78-keV doublet. The general experimental setup for this experiment has been discussed in Section 2.3. and will not be repeated here.

5.3.5.a. Integral Coincidence Spectra

Using the 3.6% detector in coincidence with the 2.5% detector we accumulated a total of 4,055,416 coincidence events in a 48-hour

period. The integral coincidence spectra obtained from this experiment are shown in Figure V-8. The y-side integral coincidence spectra were recorded by the 3.6% detector and the X-side by the 2.5% detector. In Figure V-8 we have shown two integral coincidence spectra for the y-side with different gains. This came about when we noticed after the first 30 hours of taking data that no peaks above 1000 keV appeared in the y-side integral coincidence spectrum, while several rather strong peaks appeared above this energy in the X-side spectrum. This phenomenon was traced to a missing 93 ohm terminator from the input to the y-side ADC. Somehow this caused the high energy pulses to be rejected by the y-ADC. During the last 18 hours of the experiment we used a terminator on this ADC to correct the problem. However, this caused the gain shift seen in Figure V-8. The X-side ADC was terminated during the entire 48-hour run and hence did not show a similar gain shift. The shift in the Y-side spectra presented a nuisance in recovering the data, since we were required to set different gates on the Y-side for the two series of tapes, but we could still sum the resulting X-side spectra to obtain the best statistics. In addition, we could not gate above 1000 keV on the y-side from data obtained in the first 30 hours.

5.3.5.b. Gated Coincidence Spectra

A selection of the gated coincidence spectra used in the construction of the decay scheme are shown in Figure V-9. A summary of the coincidence relationships obtained from this experiment is given in Table V-3. The actual number of gated coincidence spectra

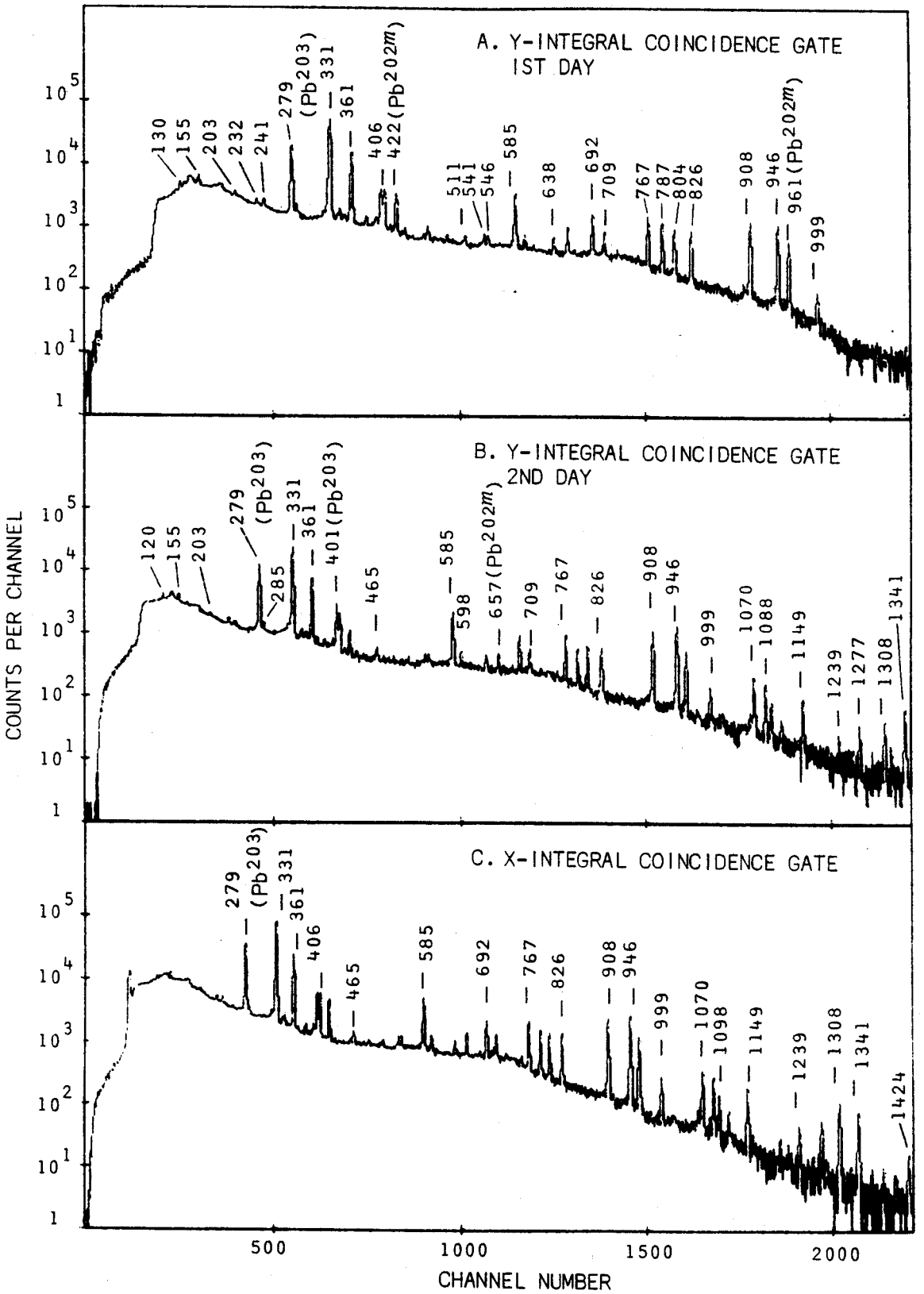

Figure V-8. Integral coincidence spectra taken during two-dimensional γ-γ coincidence experiment on Pb^{201}. *A. Y*-side spectrum taken during first day with a 3.6% Ge(Li) detector. *B. Y*-side spectrum taken during second day with 3.6% Ge(Li) detector. *C. X*-side spectrum taken during two-day run with 2.5% detector.

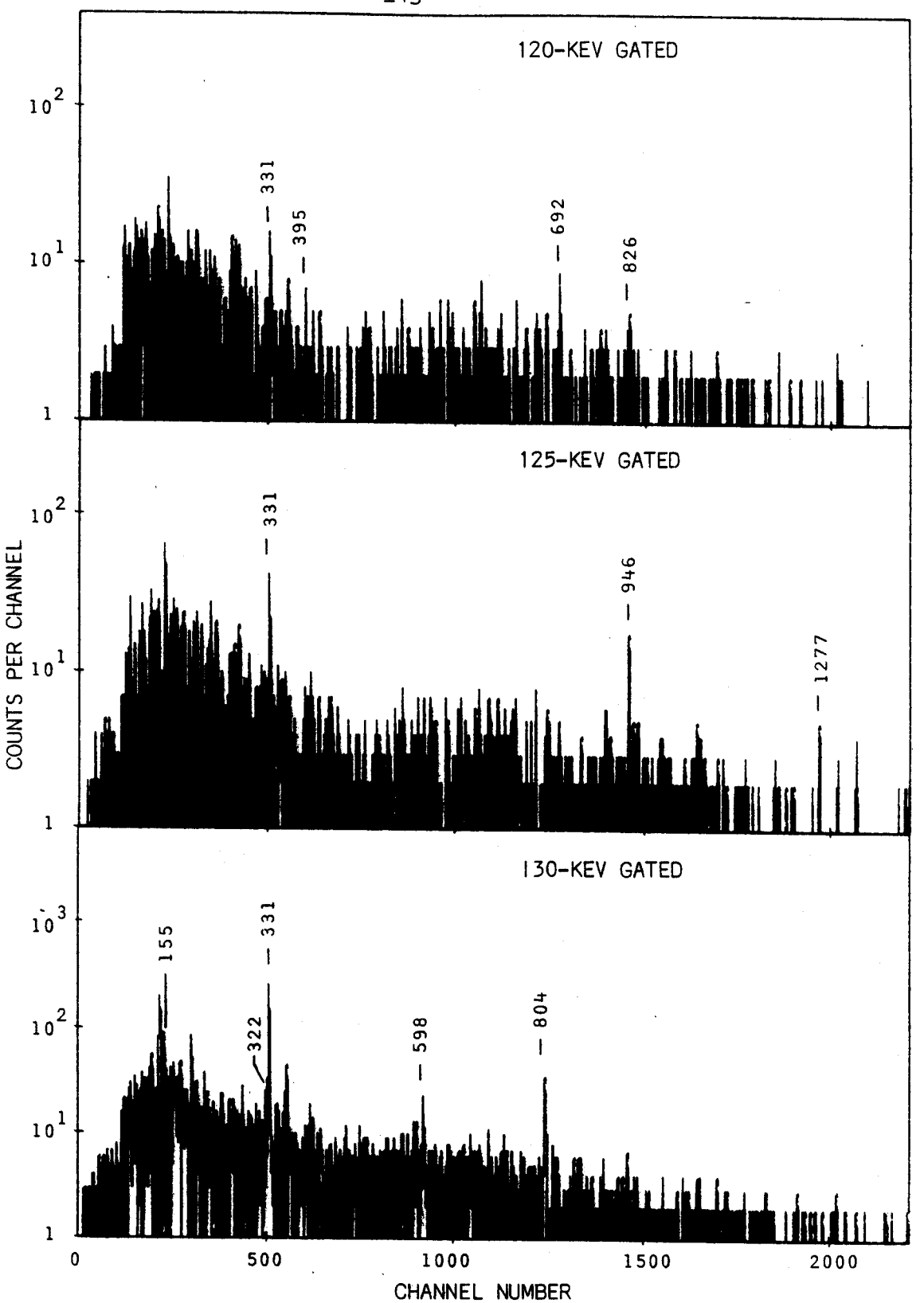

Figure V-9. A selection of the gated coincidence spectra obtained from the two-dimensional γ-γ coincidence experiment on Pb^{201}. All gated spectra have had the background subtracted except where otherwise specified. All spectra were obtained by gating on the *Y*-side(3.6% detector) and displaying the *X*-side (2.5% detector) except where specified as *Y*-display.

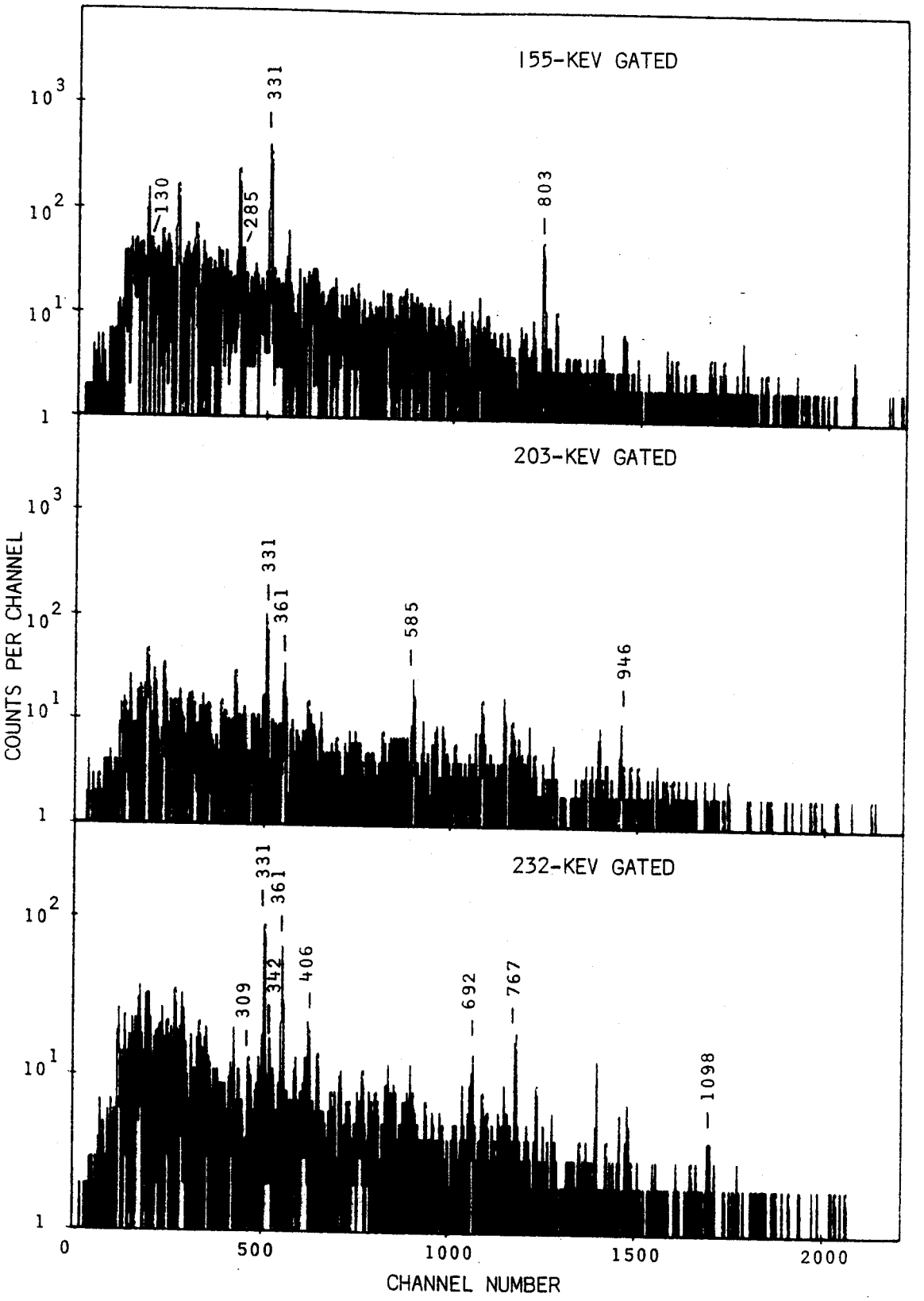

Figure V-9 (cont'd)

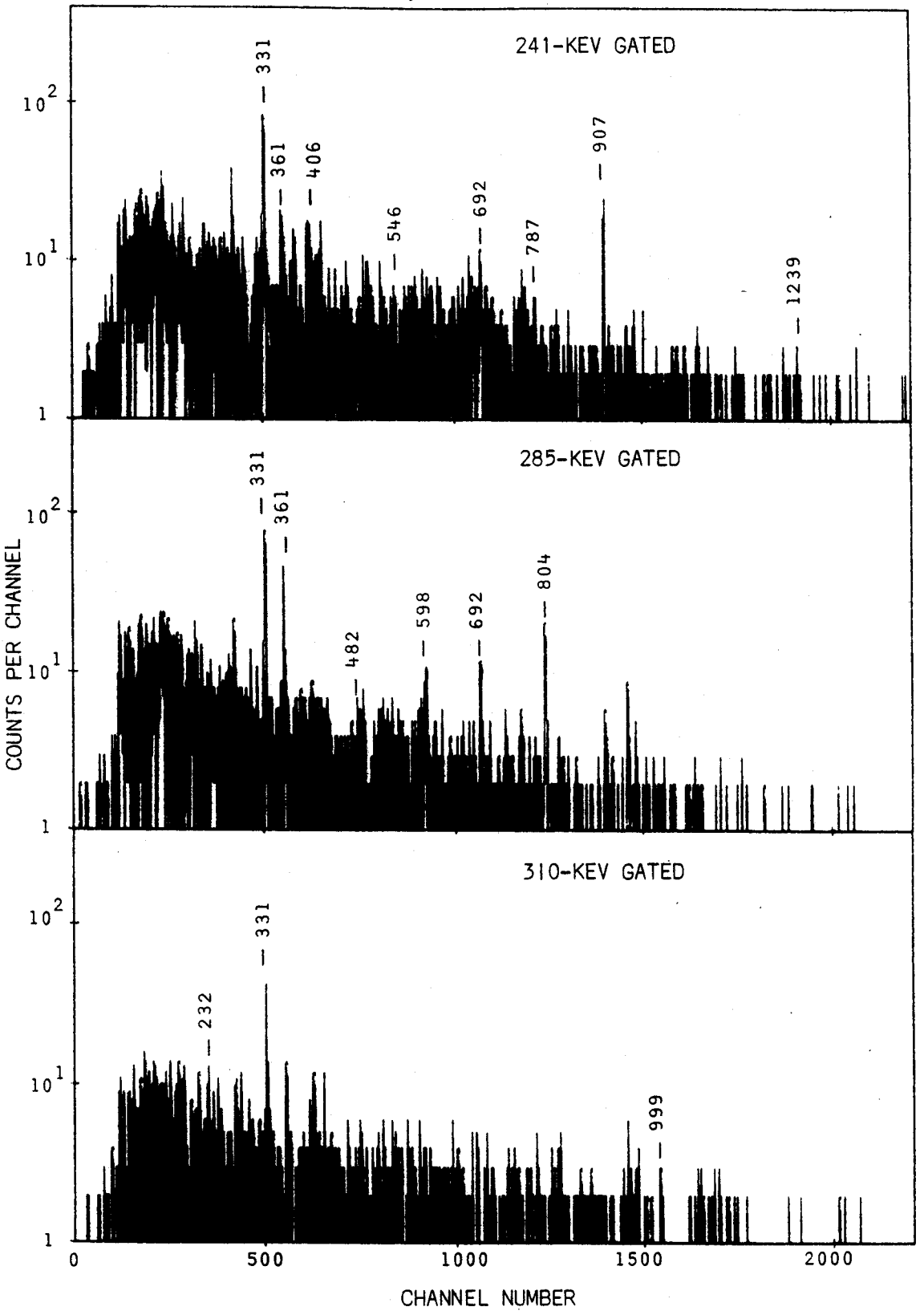

Figure V-9 (cont'd)

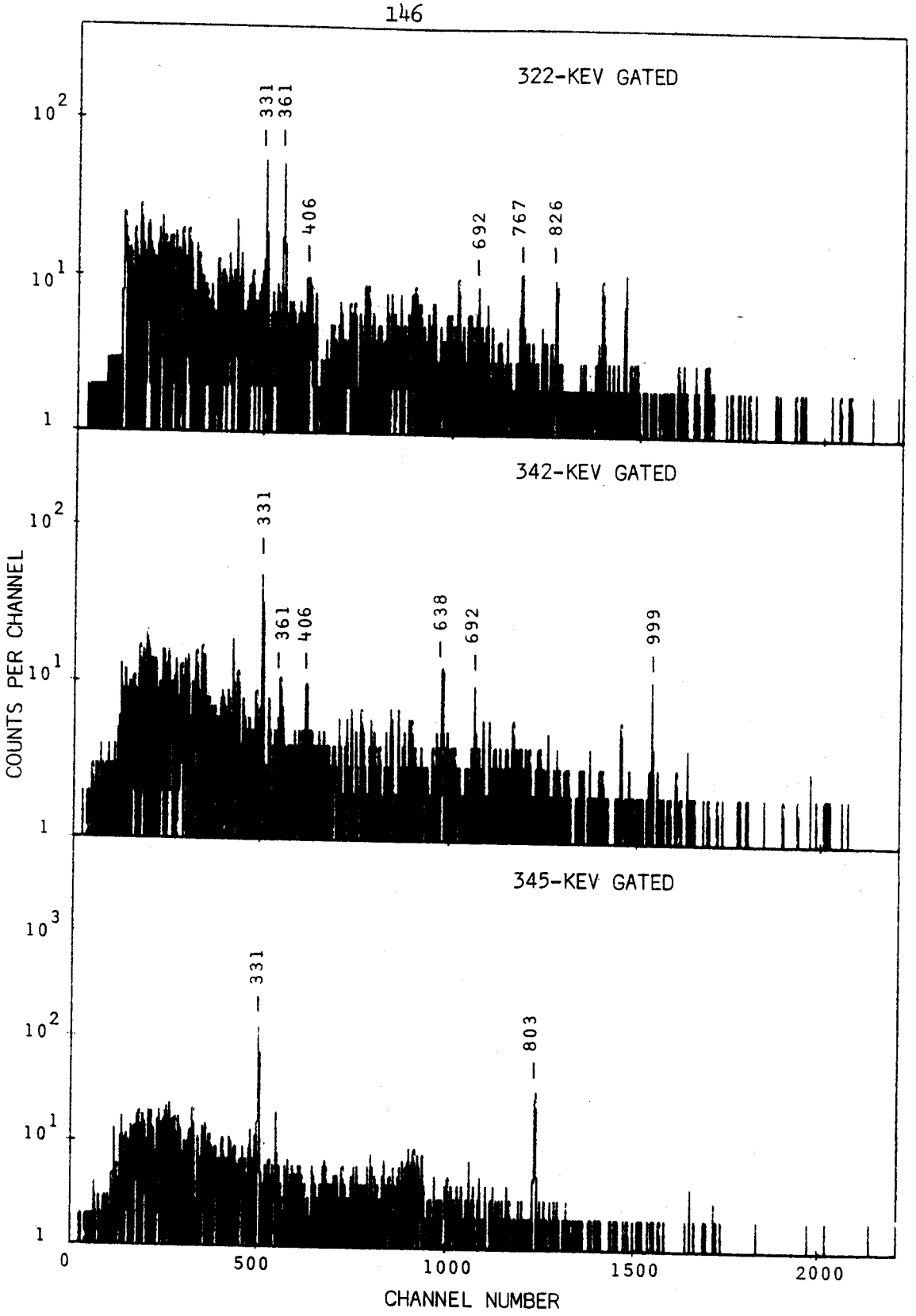

Figure V-9 (cont'd)

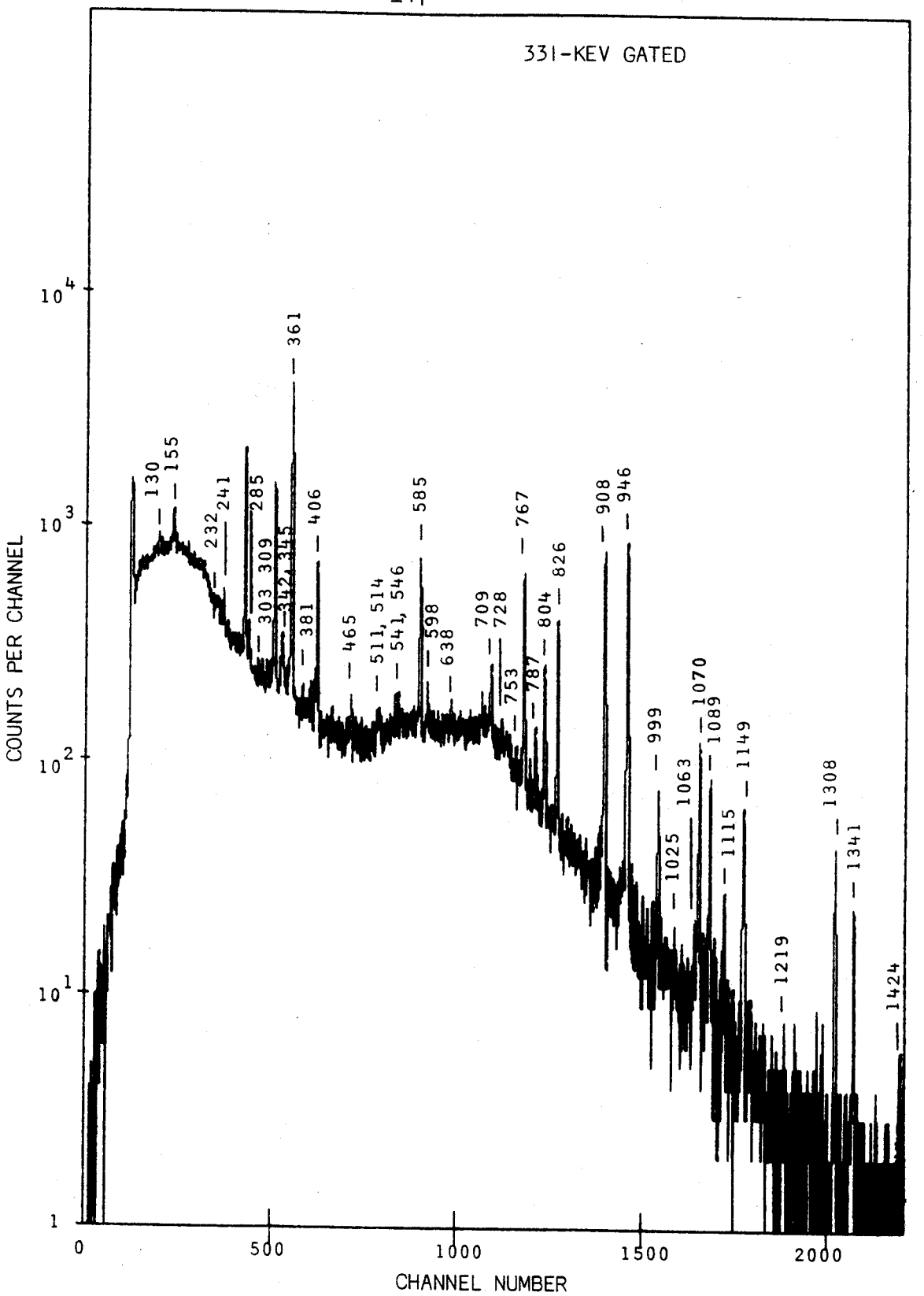

Figure V-9 (cont'd)

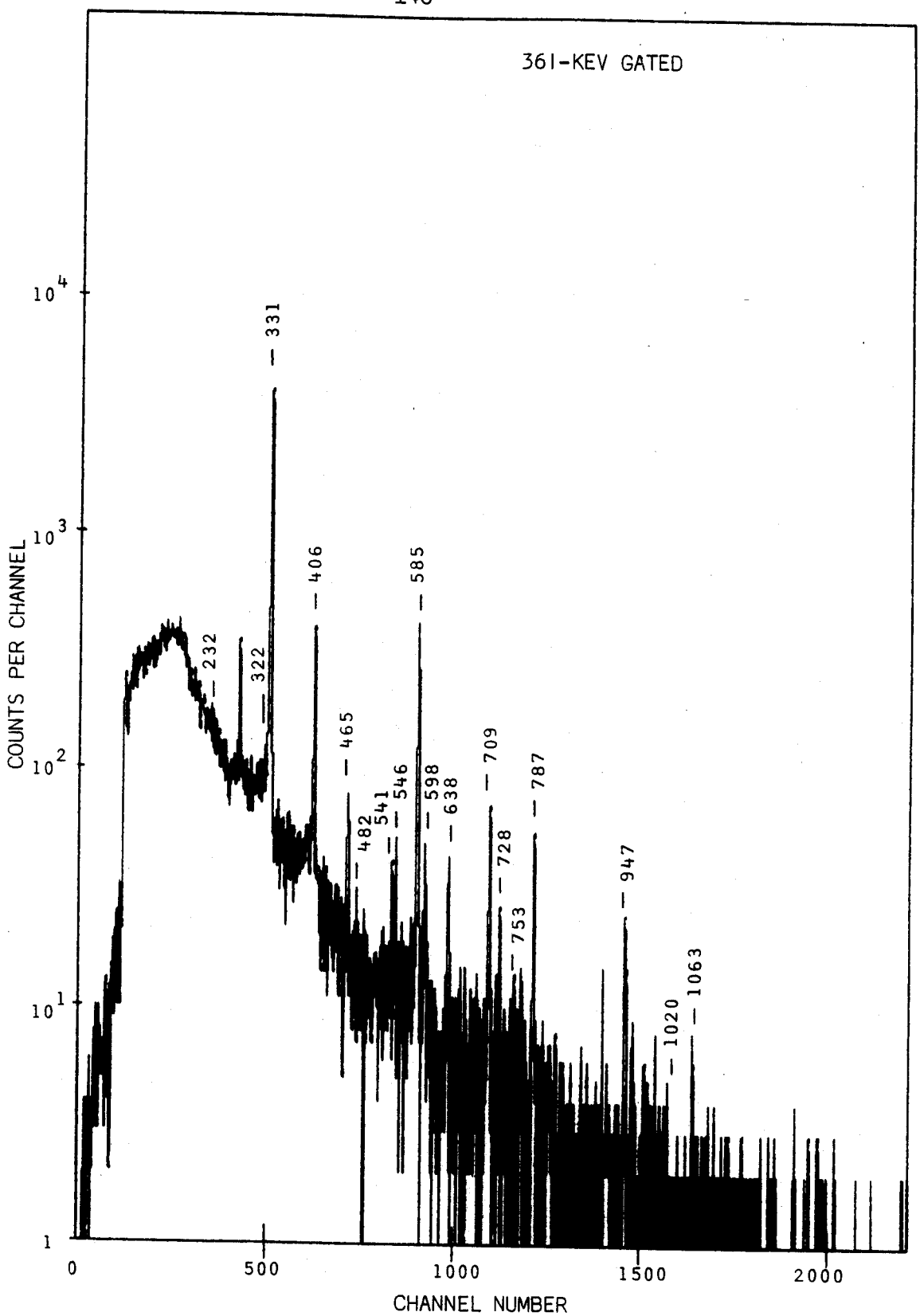

Figure V-9 (cont'd)

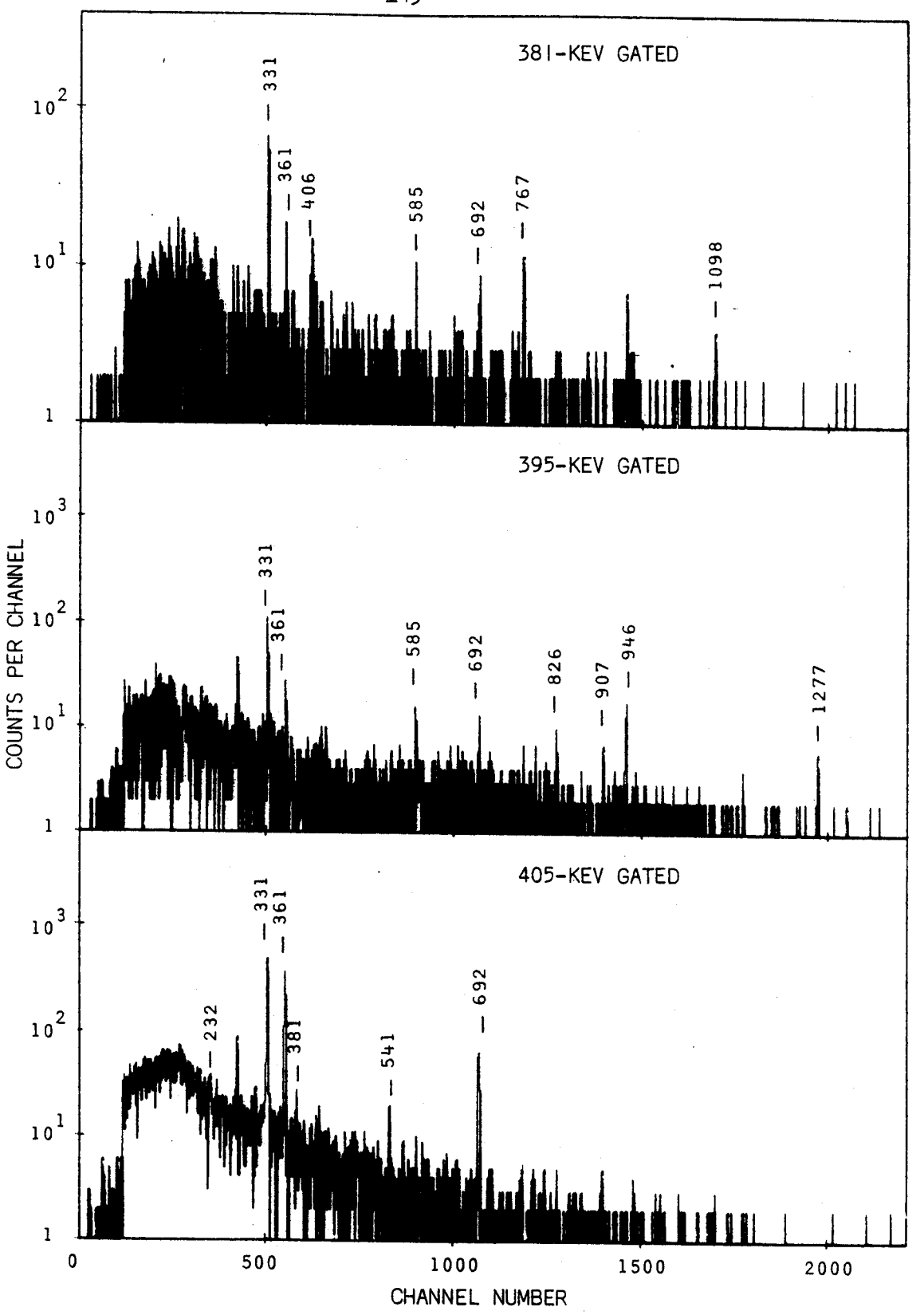

Figure V-9 (cont'd)

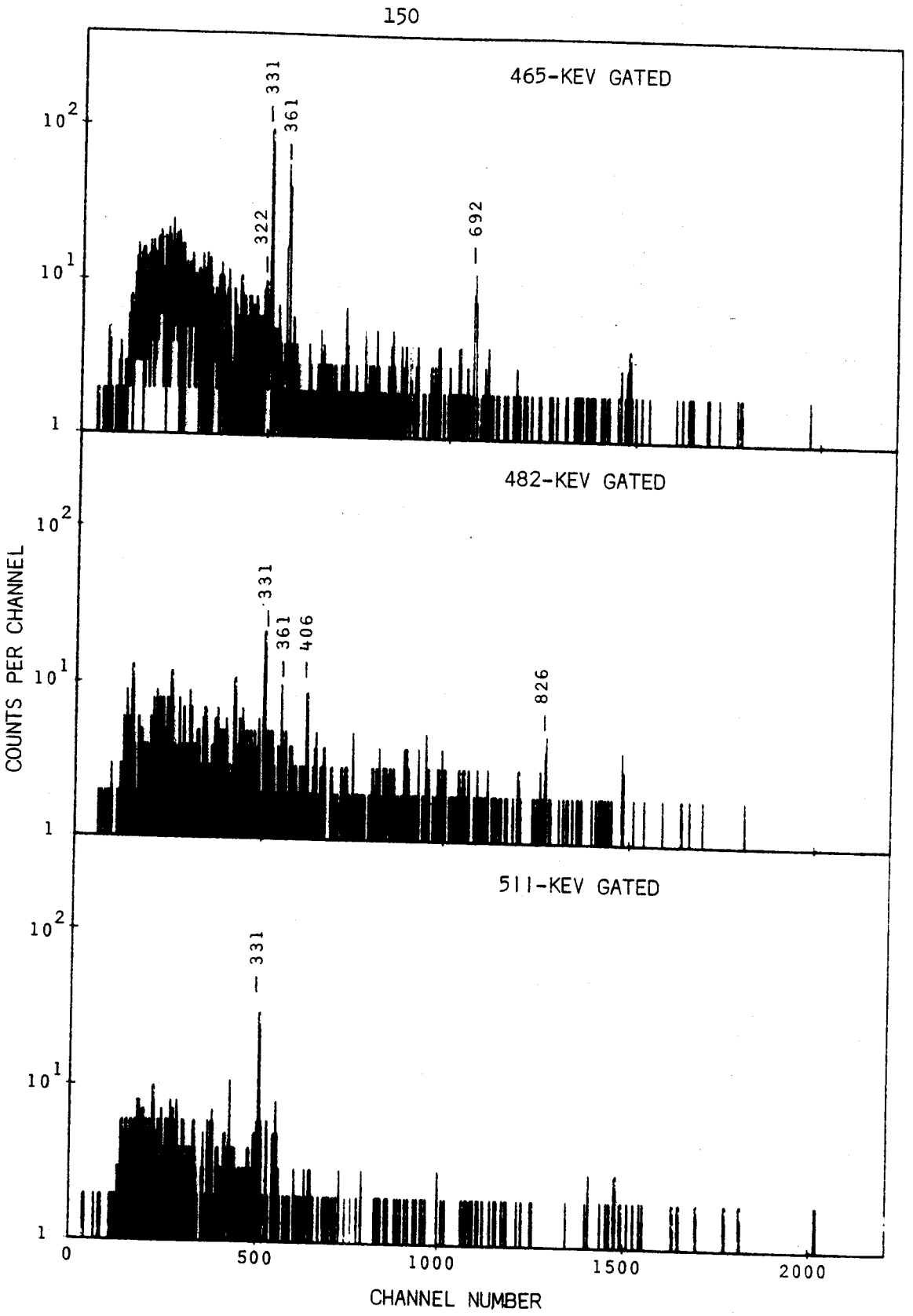

Figure V-9 (cont'd)

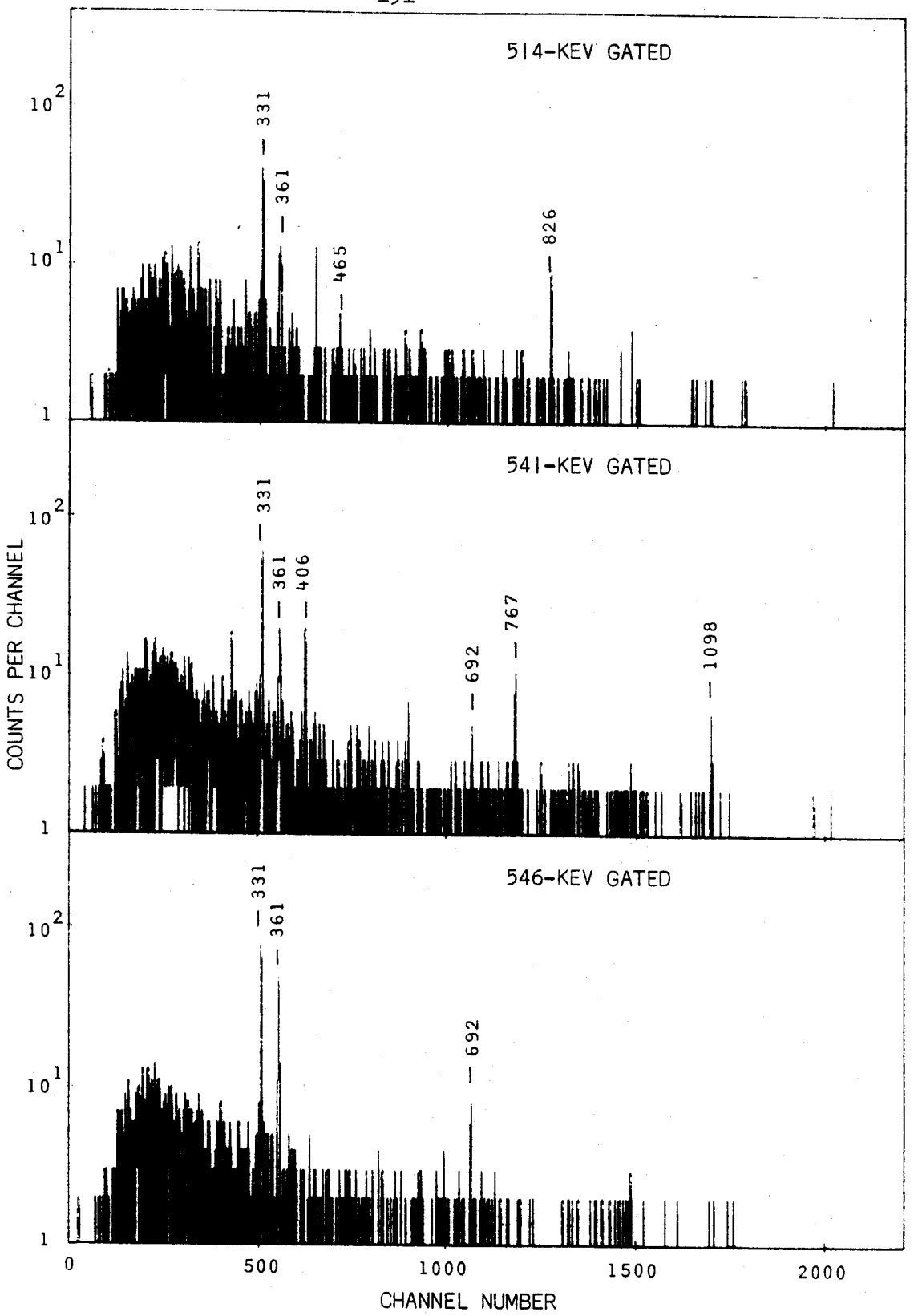

Figure V-9 (cont'd)

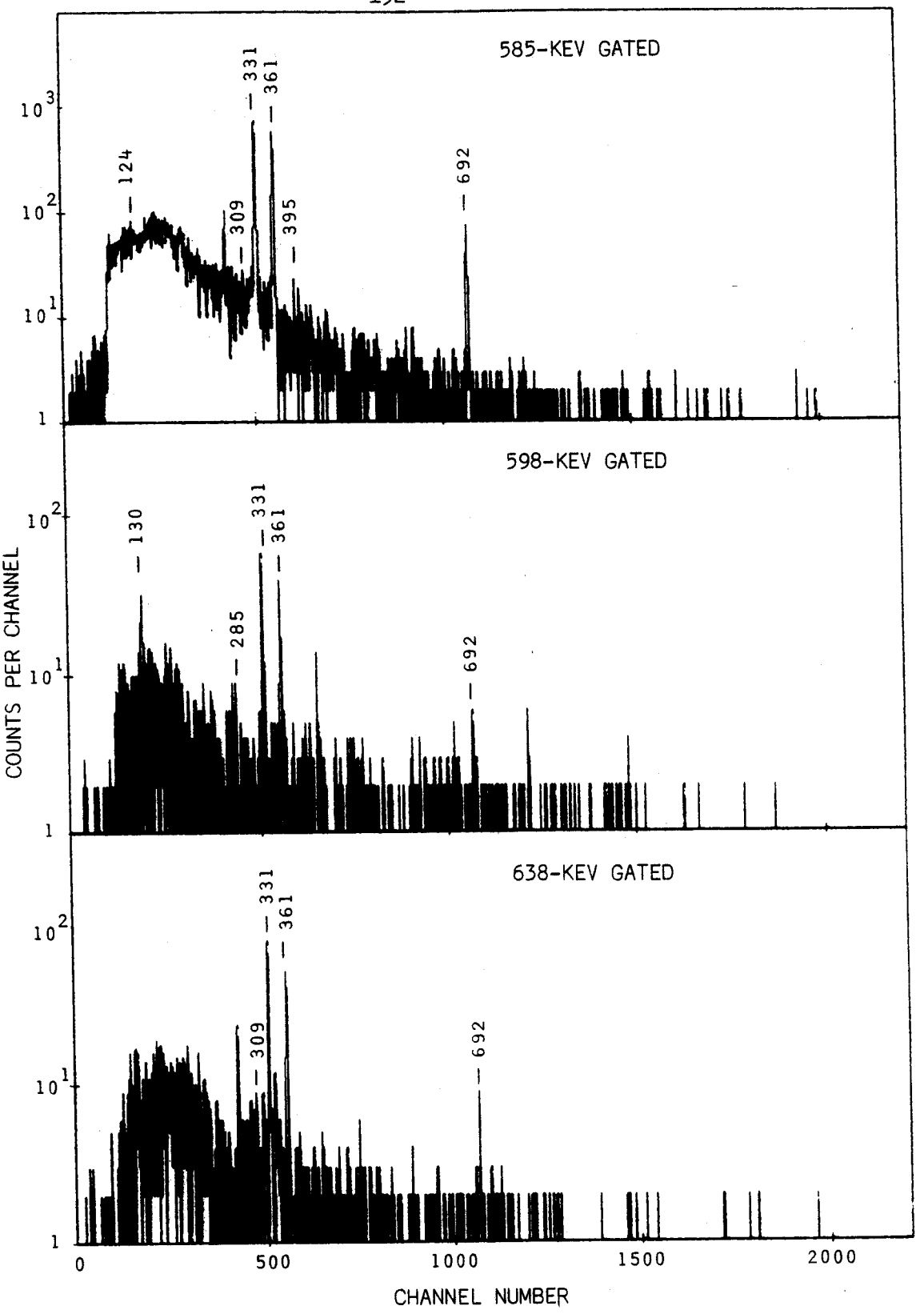

Figure V-9 (cont'd)

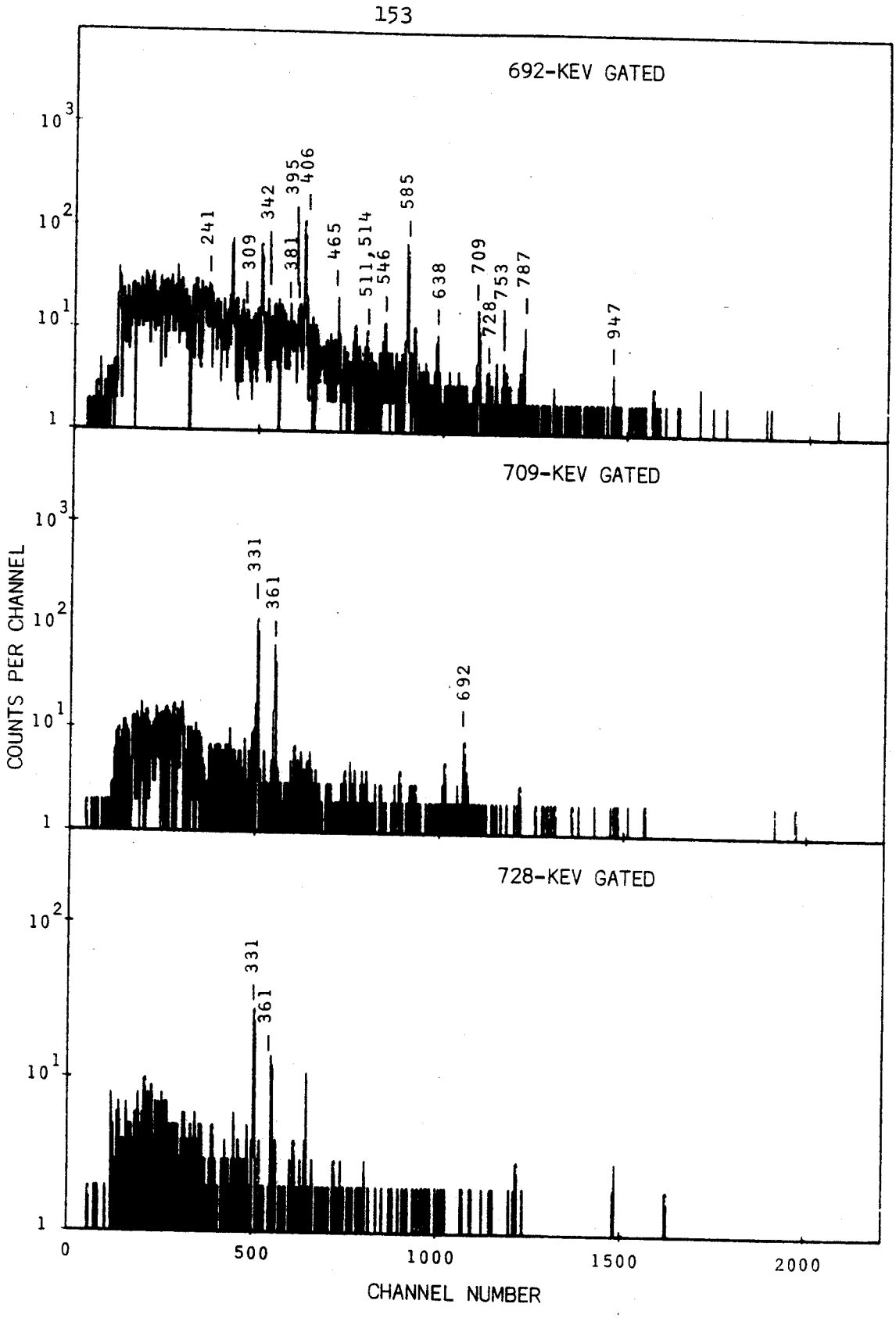

Figure V-9 (cont'd)

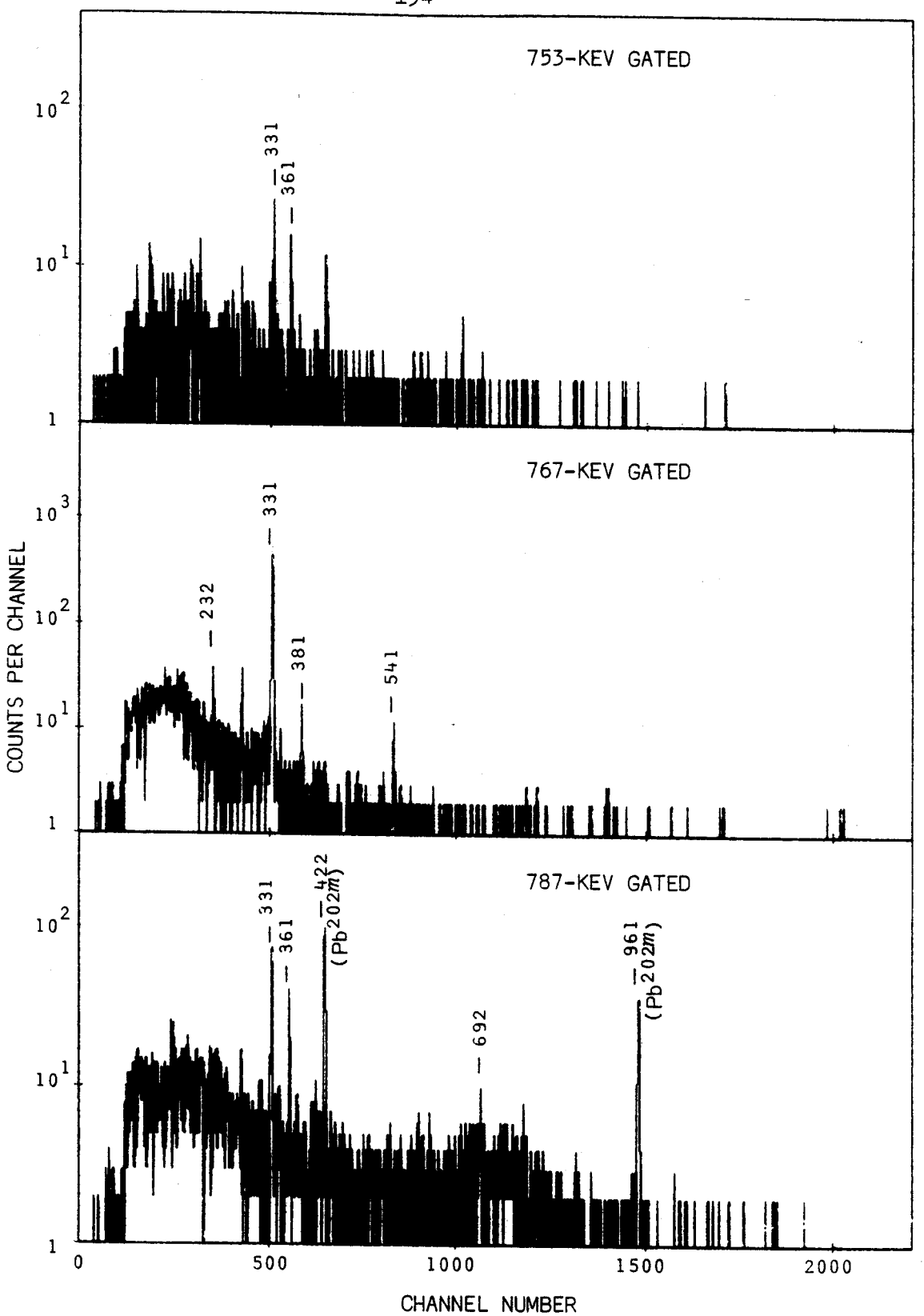

Figure V-9 (cont'd)

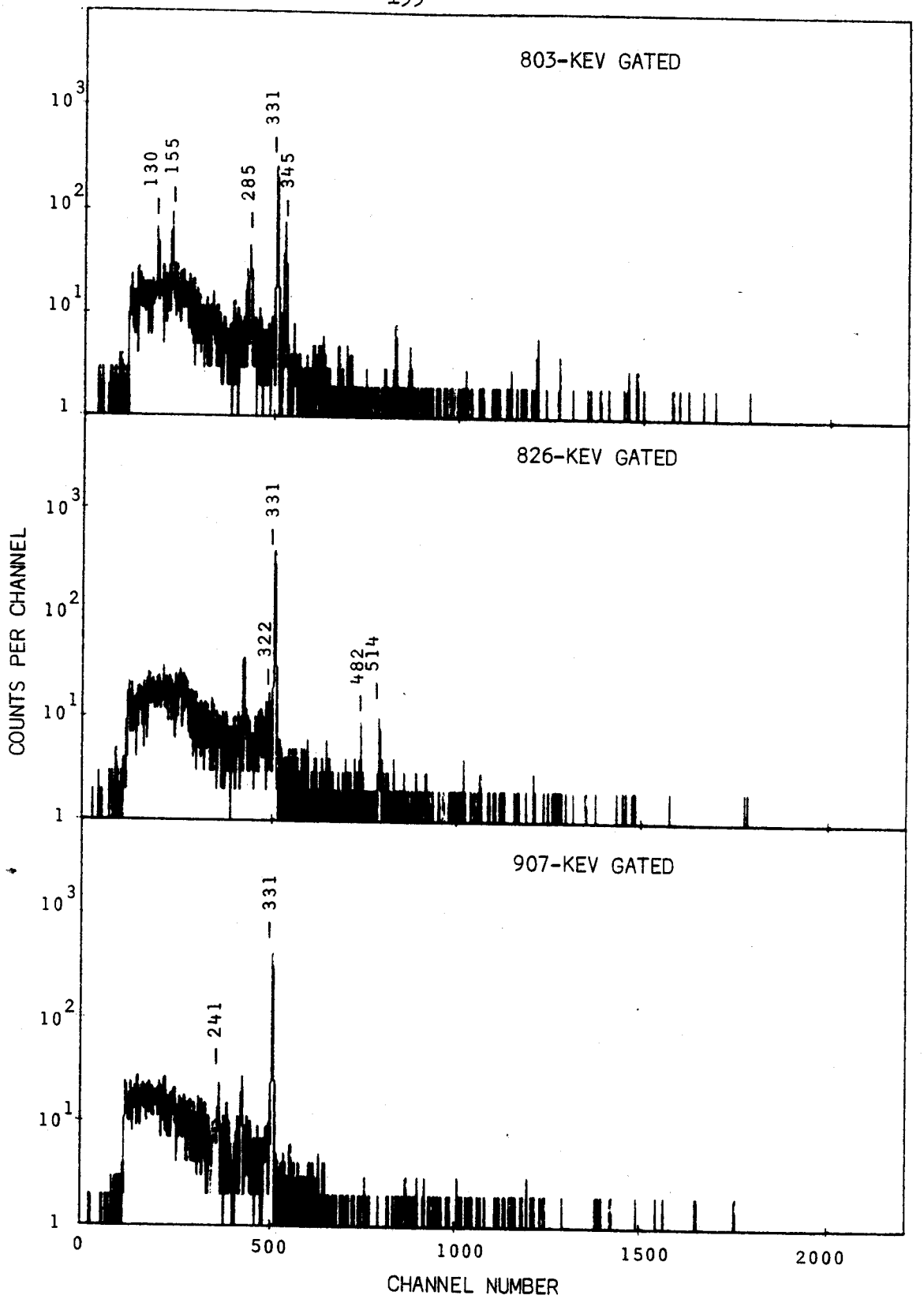

Figure V-9 (cont'd)

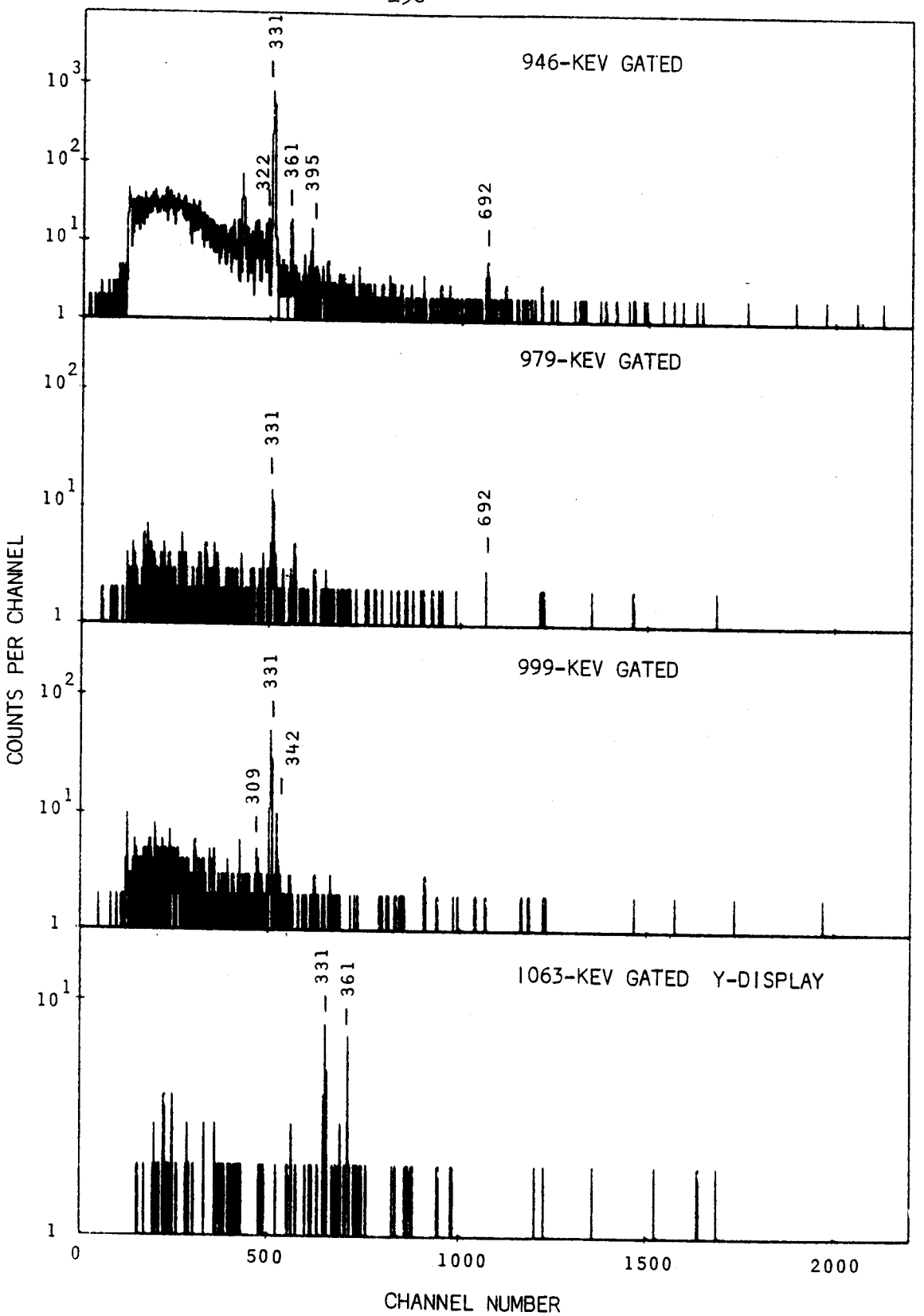

Figure V-9 (cont'd)

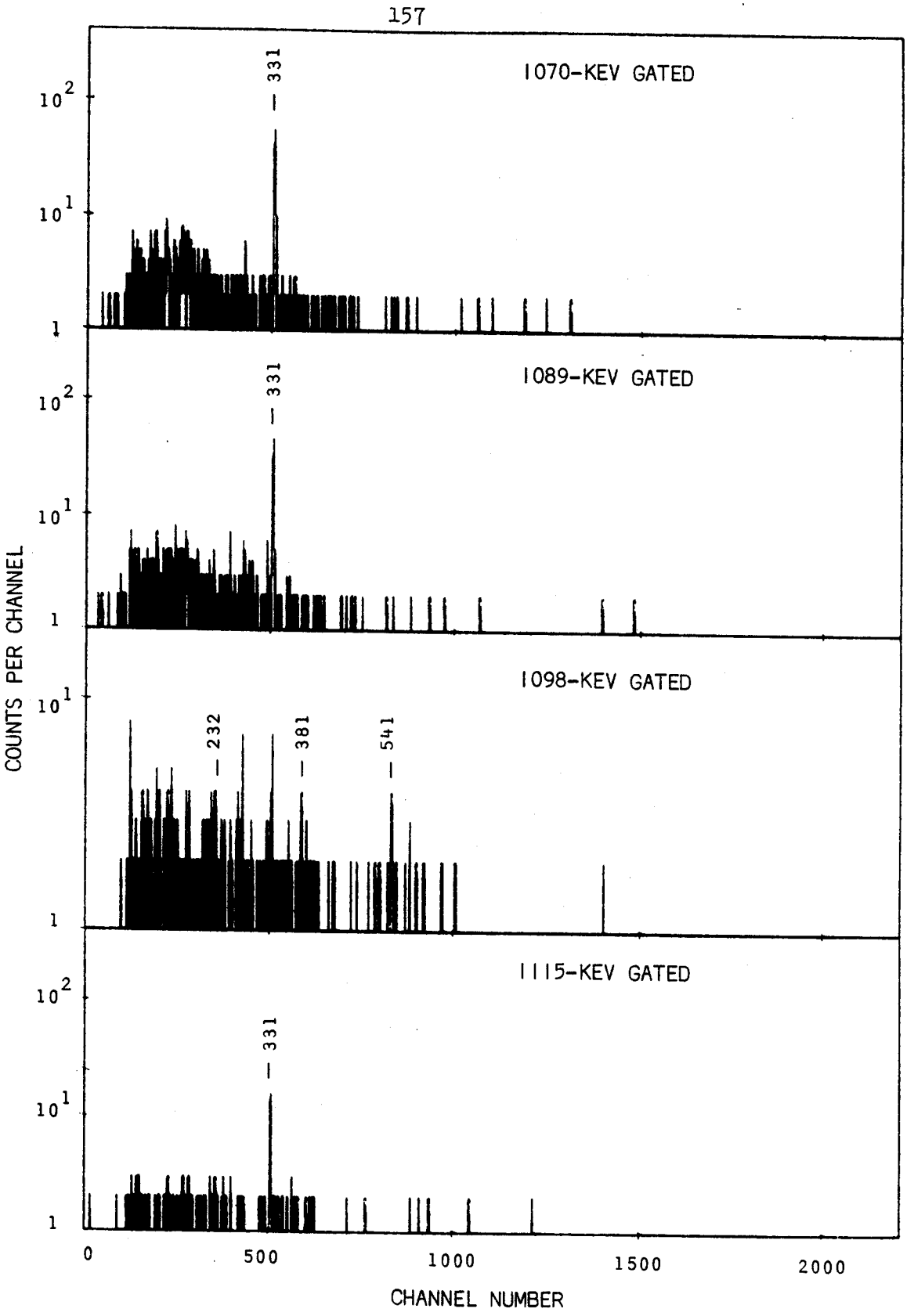

Figure V-9 (cont'd)

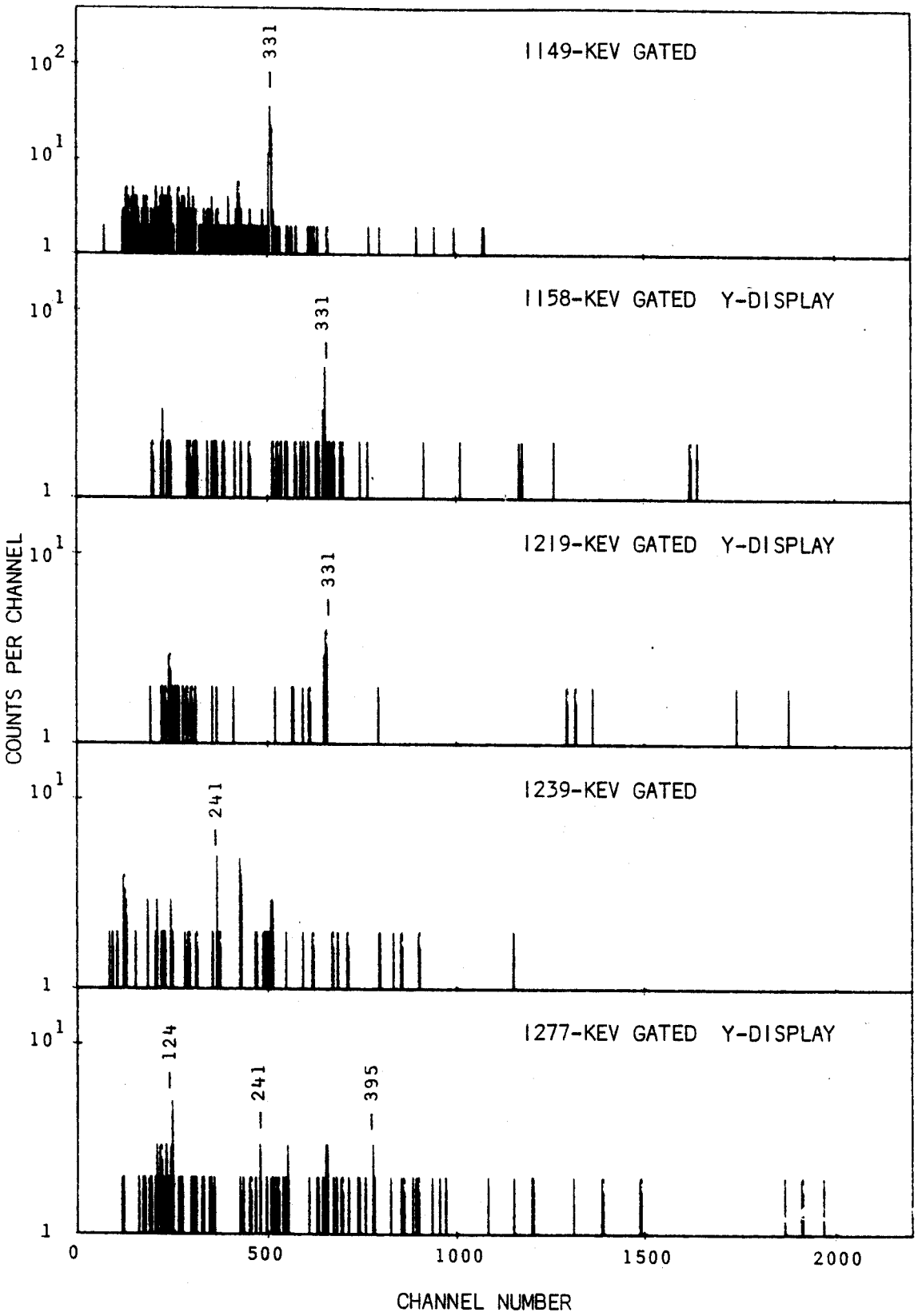

Figure V-9 (cont'd)

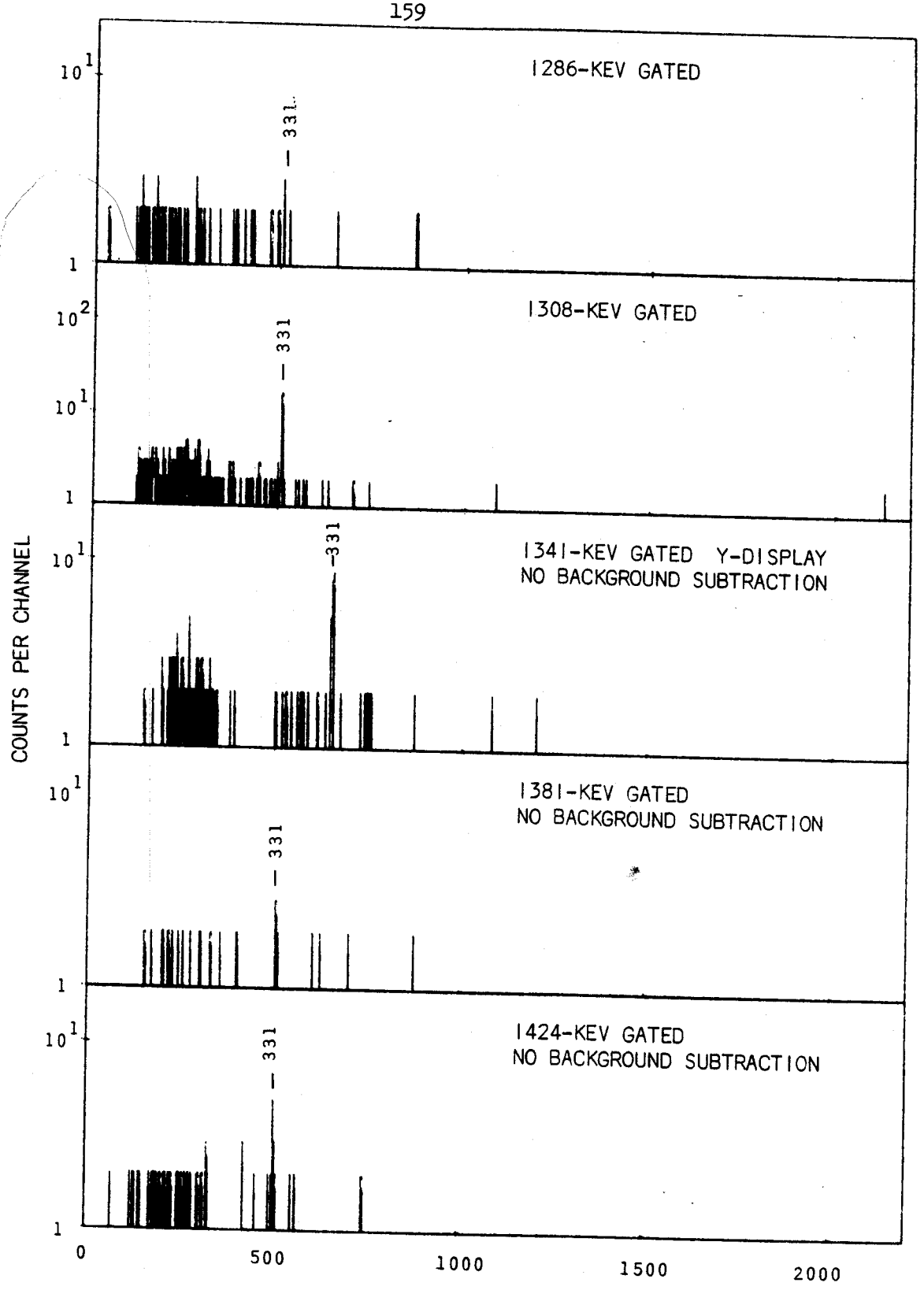

Figure V-9 (cont'd)

Table V-3

Results of γ-γ coincidence study using 2-dimensional analysis

Gated energy (keV)	Energies of γ-rays in coincidence with gate	
	Strong	Weak
120	826	331,395
124	1277,946,787	331
130	331,598,803,155	322
155	331,803,130	285
203	331,361,585,946	
232	331,361,692 767,1098,406	310,342
241	331,907	361,692,787, 406,1239,546
285	804,598,331	361,482,692
309	999	232,331
322	331,361,767,826	692,406
331	130,155,241,285,343, 345,361,381,395,406, 465,511,514,541,546, 585,598,638,709,767, 787,804,826,908,946,999, 1063,1070,1089,1115,1149, 1157,1219,1308,1341,1424	232,303,309, 316,322,728, 753,1025, 1083,120
342	638,999,331,361,405,692	
345	331,803	
361	331,322,406,465,541,546, 585,598,638,709,728,753, 787,946,1063	232,482,1020
381	331,361,692,406,767,1098	585
395	331,361,692,585,946,826, 1277	514,907
406	232,331,361,381,541,692	
465	331,361,692	322
482	331,361,406,826	

Table V-3 (cont'd)

511	331	
514	465,826,331,361	
541	331,361,406,767,1098,692	
546	331,361,692	
585	331,361,692,395	309,124
598	130,331,361,692	285,303
638	331,361,342,692	309
692	406,585,787,465,546,638, 709,395,381,309	728,753,511, 514,342,241
709	331,361,692	
728	331,361	
753	331,361	
767	331,381,232,541	
787	331,361,692	
804	331,155,130,285,345	
826	331,482,514,322	
908	331,241	
946	331,361,692,395	322
979		331,692
999	331,342,309	
1063	331,361	
1070	331	
1089	331	
1098	381,541	232
1115	331	
1149	331	
1157		331
1219		331
1239	241	
1277	124	241,395
1286		331
1308	331	
1341	331	

Table V-3 (cont'd)

1381		331
1424	331	

used to determine these relationships was more than three times that shown in Figure V-9. For all but the highest energy peaks we obtained not only the gated coincidence spectrum with background subtraction but also the gated coincidence spectrum without background subtraction as well as the spectra resulting from gating on the high and low backgrounds adjacent to the peaks. The latter spectra were useful in determining whether weak coincidence peaks in the spectra with background subtraction were legitimate or resulted from incomplete background subtraction. From this 2-d experiment we were able to obtain coincidence information on 53 of the 72 γ-transitions assigned to the decay of Pb^{201}.

5.3.5.c. Compton Pair Peaks

In the gated coincidence spectra below 279 keV in energy we noticed a number of "false" coincidence peaks generated by Compton scattering. If we look at the 130-keV gated coincidence spectrum in Figure V-9, we notice a peak at about 203 keV. A γ-ray of 202.7-keV was observed in the singles experiments on Pb^{201}, so it appears that the 202.7 keV γ is in coincidence with the 130-keV γ. However, if one examines the three spectra in Figure V-10 where we have displayed, on an expanded scale, the low and high background spectra as well as the 130-keV gate without background subtraction, we notice that a peak at $\simeq$203 keV (labeled C.P.P. 331) appears in all three spectra but at slightly different positions. They are also somewhat broader than the true coincidence peaks such as the 279- or

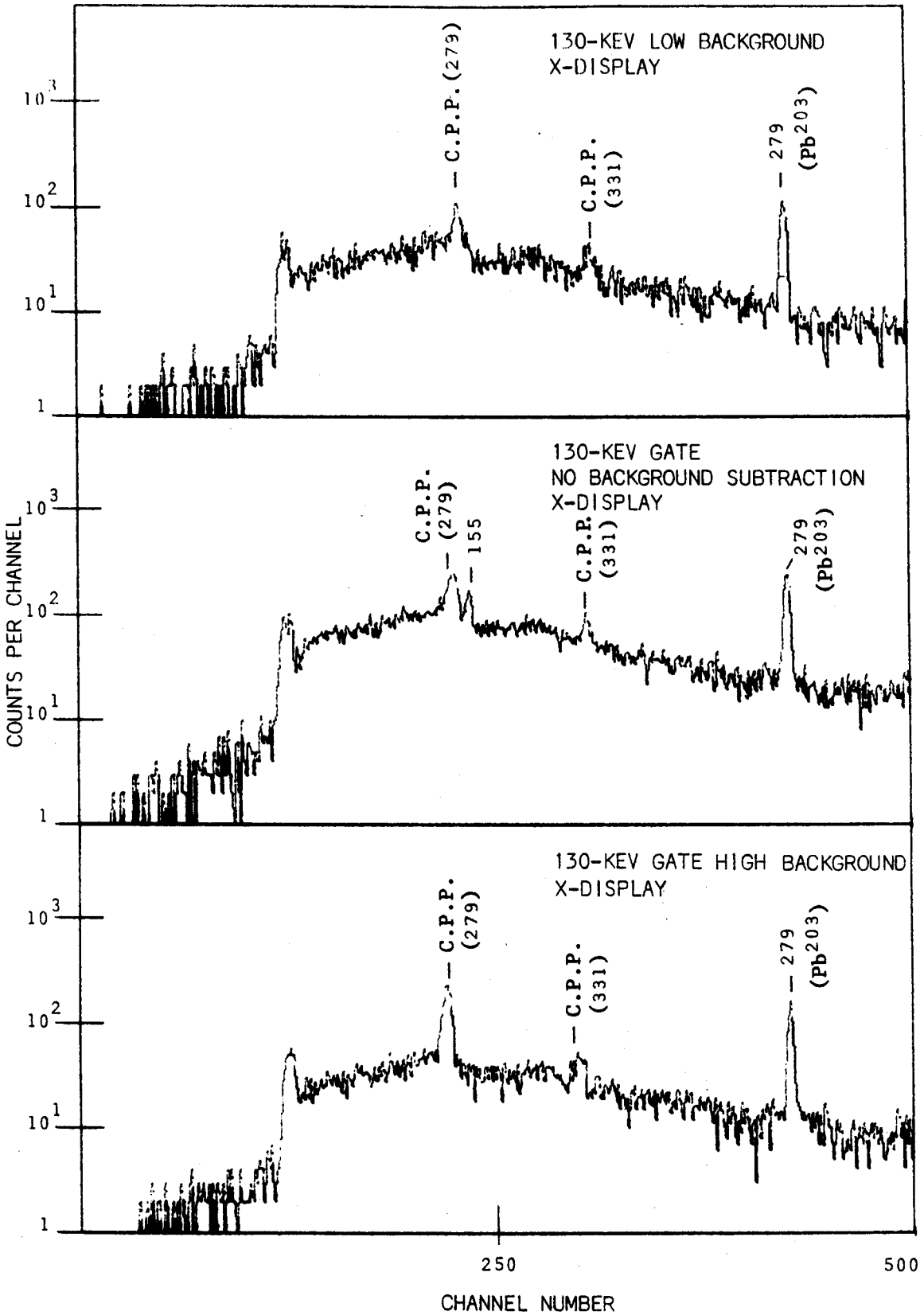

Figure V-10. Low energy portion of the 130-keV gate without background subtraction along with the adjacent low and high energy background gates obtained from the two-dimensional γ-γ coincidence experiment on Pb^{201}. This shows several "false" peaks generated by Compton scattering as well as the 155-keV "true" coincidence peak.

155-keV peaks. These characteristics identify these "false" peaks as Compton pair peaks generated by Compton scattering between the detectors. We can identify the γ-rays giving rise to these by adding the energy of the gate to the energy of the Compton pair peak. A more complete discussion of this phenomenon is given by Giesler in reference [Gi70]. Actually we were surprised to see this phenomenon since we used a 90° geometry and a graded lead absorber between the detectors; however, it is possible that the lead absorber might not have completely shielded the outer edges of the detectors from each other.

Figure V-11 contains another example of this effect. Here we see Compton pair peaks from the three strongest transitions in our sample, the 279-keV γ from Pb^{203} and the 331- and 361-keV γ's from Pb^{201}. As we went to higher energy gates this effect became less pronounced and we did not observe it above the 331-keV gate.

5.3.5.d. The 946-keV Doublet

According to the previous decay scheme, Figure V-1, there is a rather strong γ-transition from the 1277.1-keV level to the 331.1-keV first excited state. This placement was confirmed by Pettersson [Pe61] in electron-gamma coincidence experiments which showed that the 945.8-keV γ-transition was in coincidence with the 331-keV transition but not the 361-keV transition. In our 2-d experiment, however, we noticed in the 946-keV gated coincidence spectrum, Figure V-9, that, in addition to the large 331 coincidence peak, there was also a weak 361 peak.

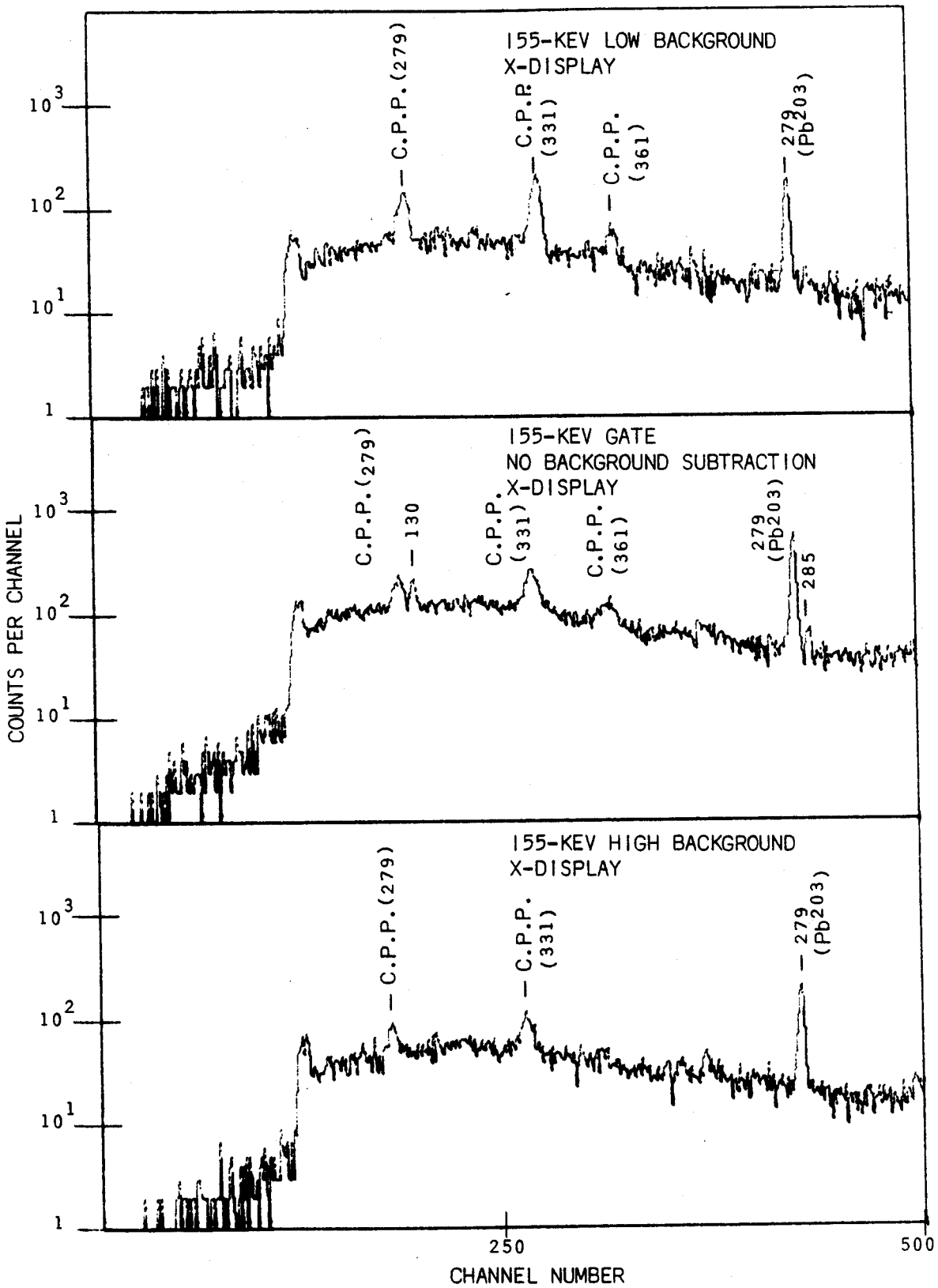

Figure V-11. Low energy portion of the 155-keV gate without background subtraction along with the adjacent low and high energy background gates obtained from the two-dimensional γ-γ coincidence experiment on Pb^{201}. This shows several "false" peaks generated by Compton scattering as well as the 130-keV "true" coincidence peak.

At first this was thought to be due to chance coincidence events, as was the case for the 279-keV peak from Pb^{203}, for the 361-keV peak was the third strongest peak in the singles spectrum. However, we also observed a peak at about 946 keV in the 361- and 692-keV gated spectra. Based on these coincidence results we concluded that the 946-keV peak was probably a doublet with the more intense γ-ray feeding the 331-keV state and the weaker γ-ray feeding the 692-keV state. We have demonstrated the doublet nature of this transition in two ways.

The first experiment consisted of gating on the low, middle, and high energy part of the 946-keV peak. In order to obtain approximately equal statistics for these three spectra, the number of channels used for these gates was chosen to contain the same number of counts after subtracting the background. Therefore, the lower- and higher-energy gates contained more channels than the middle-energy gate but all contained approximately the same number of coincidence events. From the resulting spectra, shown in Figure V-12, it appears that the 361-keV peak becomes more pronounced as we move the gate from the lower to the high energy side of the 946-keV peak. This indicates that the 946-keV peak is indeed a doublet, with the γ-ray feeding the 692-keV level being somewhat higher in energy than the more intense γ-ray feeding the 331-keV level.

We were also able to obtain rough relative intensities for the two γ-transitions from the areas of the 331- and 361-keV peaks appearing in the full 946-keV gated spectrum. After correcting these areas for the difference in detector efficiency we found that $\simeq$4% of

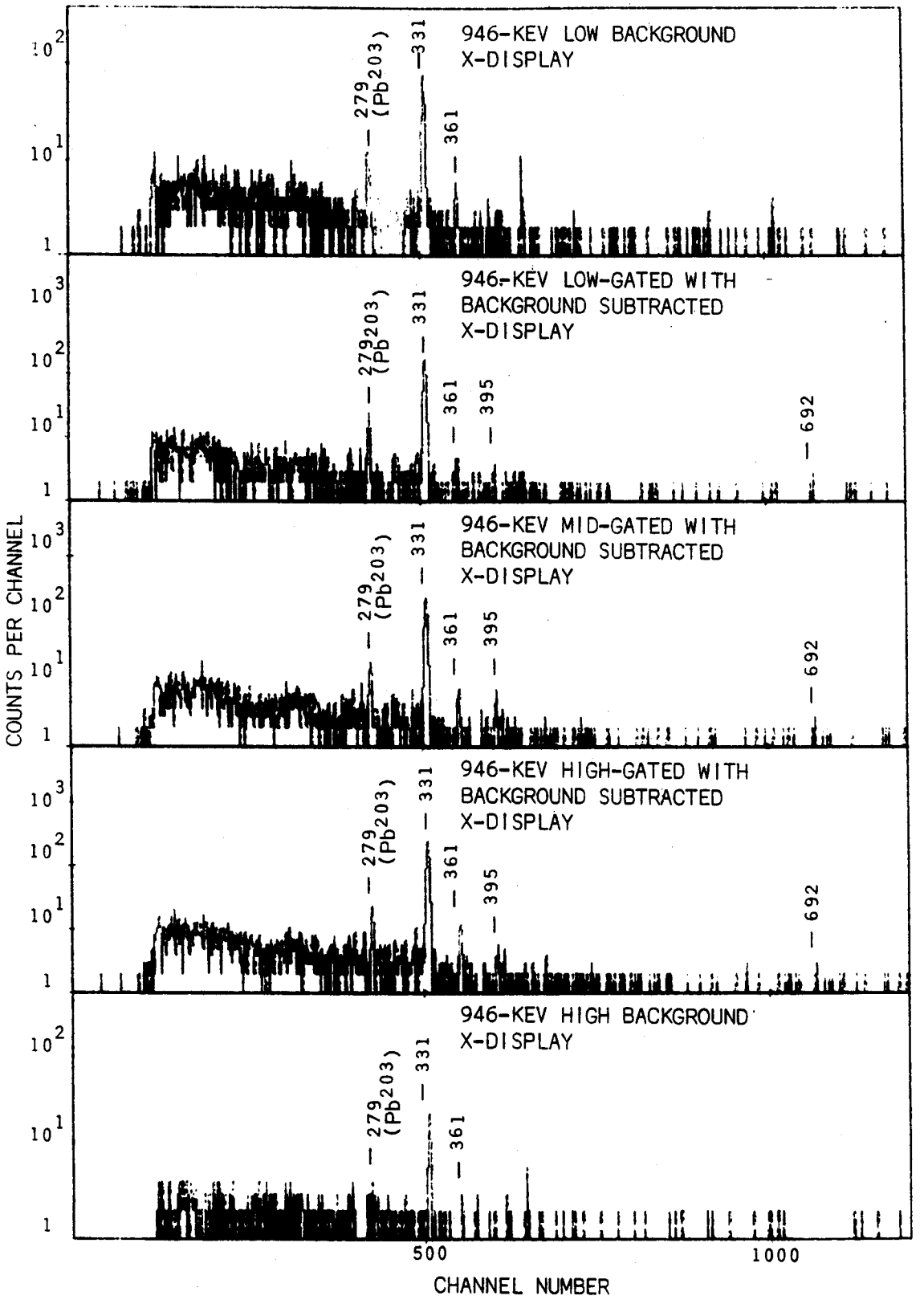

Figure V-12. Results of 2-d γ-γ coincidence experiment used to show that the 946-keV peak is composed of two γ-transitions. Notice that the 361-keV peak gets larger as we scan the 946-keV peak from lower to higher energy.

the 946-keV peak was in coincidence with the 361-keV peak while 96% was in coincidence with the 331-keV peak. However, we still had to make corrections for the fact that the 692-keV level is significantly depopulated by the direct ground state transition and the fact that the 361-keV γ-transition also feeds the 331-keV level. After making these corrections we found that ≈6.2% of the 946-keV peak feeds the 692-keV level while 93.8% directly feeds the 331-keV state. The intensities listed in Table V-2 were then obtained by multiplying the total γ-transition intensity of the 946-keV doublet, 452, by these percentages.

In our next experiment we used the data from the 2-d experiment to obtain the energies of these two transitions in a manner similar to that used in our analysis of the 289.7-keV doublet in Pb^{200} (Section 4.3.2.). According to our decay scheme, Figure V-15, three transitions are in coincidence with only the more intense γ-transition feeding the 331-keV doublet. These are the 124-, 203-, and 395-keV transitions, all of which feed the 1277-keV level. The decay scheme also shows that two transitions, 361- and 692-keV, are in coincidence with only the weaker, high energy component of the doublet. We then separately summed the gated spectra in coincidence with each component of the doublet. The two resulting spectra as well as the integral coincidence spectra were then analyzed by "MOIRAE" [Moir] using the full peak width to determine the centroids. Figure V-13 shows the results of this experiment. The shift in the centroid of the 946-keV peak between

Figure V-13. Results of the 2-d coincidence experiment used to determine the energies of the 945.96- and 946.78-keV doublet. *A*. *Y*-side integral coincidence spectrum used for the gates. The γ-rays which have a 946 in parentheses after the energies were in coincidence with only the lower energy member of the doublet and those γ-rays noted by (947) were in coincidence with only the higher energy . *B*. *X*-side integral coincidence spectrum showing the region near the doublet on an expanded scale. *C*. Sum of gated spectra in coincidence with the 945.96-keV transition. *D*. Sum of gated spectra in coincidence with 946.78-keV transition.

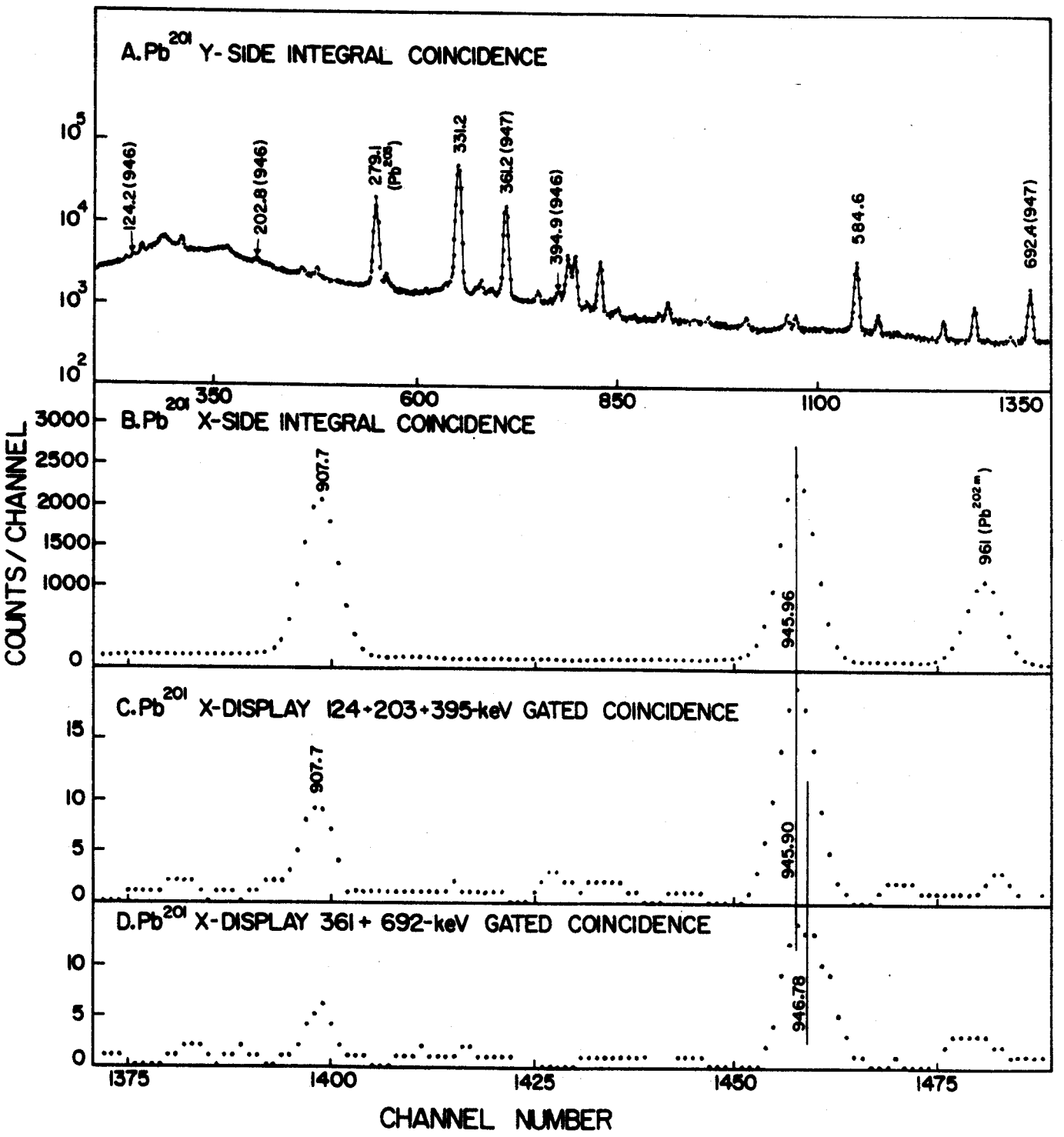
A. Pb201 Y-SIDE INTEGRAL COINCIDENCE
124.2(946)
202.8(946)
279.1 (Pb205)
331.2
361.2(947)
394.9(946)
584.6
692.4(947)
B. Pb201 X-SIDE INTEGRAL COINCIDENCE
907.7
945.96
961 (Pb202m)
C. Pb201 X-DISPLAY 124+203+395-keV GATED COINCIDENCE
907.7
945.90
D. Pb201 X-DISPLAY 361+692-keV GATED COINCIDENCE
946.78
COUNTS/CHANNEL
CHANNEL NUMBER

the two gated spectra was ≈ 1.3±0.5 channels. From the integral coincidence spectrum the gain of the system was found to be 0.64 keV per channel. The centroid shift, therefore, corresponded to a difference of 0.82±0.32 keV between the two components of the doublet. As can be seen in Figure V-13, the centroids of the integral coincidence peak and the lower energy component of the doublet are very close, falling well within the calculated uncertainties of the centroids. Because of this and the fact that the lower energy component is very much stronger than the other, we assumed that the energy determined for the 946-keV doublet in the energy calibration experiment, 945.96-keV, was essentially that of the stronger peak. Based on this assumption, the energy of the higher energy peak was calculated to be 946.78±0.32 keV.

5.3.6. Conversion Coefficients

Until the present study was undertaken, only three conversion coefficients had been determined for γ-transitions in the decay of Pb^{201}. These were the *K*-conversion coefficients for the 331- (α_K=0.113±0.008), 361- (α_K=0.21±0.025), and 585-keV (α_K=0.06±0.01) transitions determined by Pettersson from electron-gamma coincidence data [Pe61]. However, *K*-conversion intensities were known for 25 γ-transitions belonging to the decay of Pb^{201} [Aa64]. Using these *K*-conversion intensities along with our measured photon intensities we were able to determine *K*-conversion coefficients for all 25 of these γ-intensities. In order to normalize the two sets of data we used the measured *K*-conversion coefficient for the 331-keV transition given above as the fiducial point.

Table V-4 contains the transition data for Pb^{201} along with the multipolarity assignments we propose for these transitions based on the theoretical α_K's of Hager and Seltzer. Figure V-14 shows graphically the theoretical α_K's together with the experimental points. The uncertainties associated with these points are based on the uncertainties in both photon and electron intensities as well as the uncertainty in the fiducial point. It is worth noting that out of 21 possible *M*1 transitions only 6 have a significant amount of *E*2 mixing and two of these, the 1070.0 and 1098.5-keV transitions, could be "pure" *E*2's within the calculated uncertainties. The lack of *M*1, *E*2 mixing in this region has already been noted in the decay of Pb^{200} [Section 4.3.3]. It is also gratifying to note that the α_K's determined here for the 361- and 585-keV transitions, 0.22±0.02 and 0.051±0.006 respectively, are in good agreement with those measured by Pettersson and co-workers [Pe61].

Based on the experimental α_K, the 753.4-keV transition would appear to be an *M*2; however, for reasons mentioned later, we have assigned it as an *M*1. As this is a very weak transition, it is quite possible that the measured electron or photon intensities or both are in error.

Table V-4

Transition Data for Pb^{201}

Energy (keV)	Photon intensity	*K*-Conversion intensity[a]	Experimental conversion coefficient	Theoretical conversion coefficients[b] *M*1	*E*2	Assigned multipole order
285.0	10.3 ± 1.0	7.5± 1.5	0.37 ±0.08	0.38	0.072	*M*1
308.9	2.3 ± 0.3	3.0± 0.5	0.67 ±0.15	0.31	0.061	*M*1
331.2	4550 ±250	1000	≡.113 ±0.008	0.255	0.051	*M*1 + *E*2
345.0	18.3 ± 1.0	7.4± 1.5	0.21 ±0.11	0.23	0.047	*M*1
361.3	550 ± 30	240 ±10	0.22 ±0.02	0.201	0.042	*M*1
381.3	12.9 ± 0.7	4.2± 0.7	0.17 ±0.03	0.175	0.037	*M*1
394.9	10.8 ± 0.7	3.6± 1.0	0.17 ±0.05	0.160	0.034	*M*1
406.0	120 ± 6	33 ± 3	0.14 ±0.02	0.148	0.032	*M*1
546.3	16.5 ± 1.0	1.9± 0.2	0.059 ±0.008	0.068	0.017	*M*1
584.6	211 ± 8	21 ± 2	0.051 ±0.006	0.056	0.015	*M*1
597.6	19.0 ± 1.0	0.6± 0.2	0.016 ±0.006	0.053	0.014	*E*2
692.4	254 ± 12	5.0± 0.5	0.010 ±0.001	0.036	0.011	*E*2
708.8	46.2 ± 2	4.0± 0.5	0.044 ±0.007	0.034	0.010	*M*1
753.4	8.75± 0.8	1.5± 0.2	0.087 ±0.016	0.029	0.0085	*M*1
767.3	194 ± 10	9 ± 1	0.024 ±0.003	0.0275	0.0083	*M*1
803.7	90 ± 6	1.3± 0.2	0.0074±0.0016	0.025	0.0076	*E*2
826.3	141 ± 7	2.8± 0.3	0.010 ±0.001	0.023	0.0074	*E*2 + *M*1

Table V-4 (cont'd)

907.7	362 ± 20	10.7 ±1.0	0.015 ±0.002	0.018	0.0062	*M*1
946.0	424 ± 30	12 ±1	0.0145±0.002	0.0165	0.0056	*M*1
1070.0	72 ± 4	0.8 ±0.1	0.0057±0.0010	0.012	0.0045	*E*2 + *M*1 (?)
1098.5	111 ± 6	1.2 ±0.2	0.0055±0.0011	0.011	0.0043	*E*2 + *M*1 (?)
1114.7	9.8 ± 0.6	0.20±0.03	0.010 ±0.002	0.011	0.0042	*M*1
1148.8	47.3 ± 2.5	0.6 ±0.1	0.0065±0.0010	0.010	0.0040	*E*2 + *M*1
1238.8	68 ± 4	0.7 ±0.1	0.0053±0.0009	0.0084	0.0035	*E*2 + *M*1
1308.3	32.6 ± 1.6	0.6 ±0.2	0.0094±0.0040	0.0073	0.0031	*M*1

[a] Ref. [Aa64]

b Ref. [Ha68]

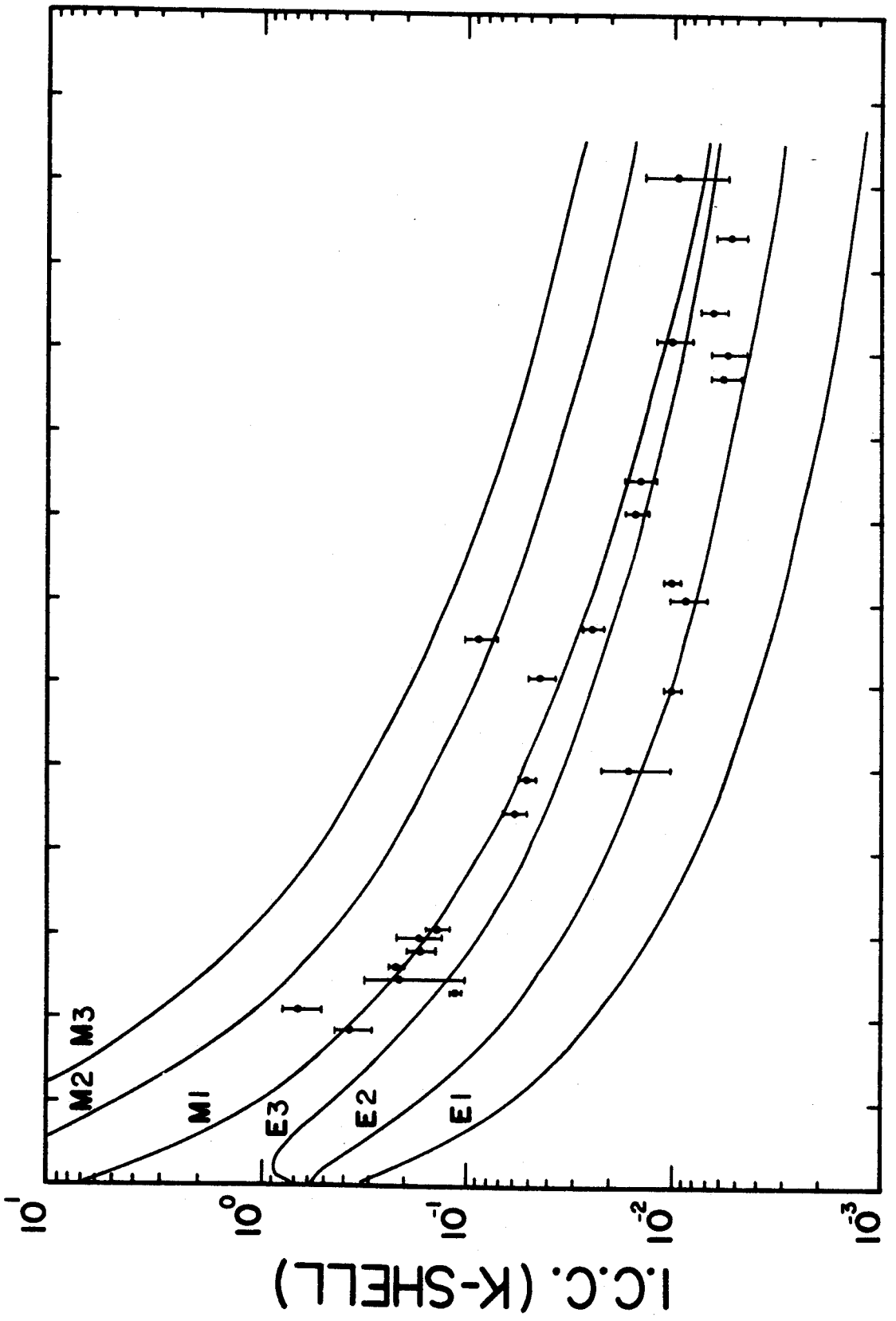

Figure V-14. Experimental and theoretical K-shell conversion coefficients for transitions following the decay of Pb^{201}. The smooth curves were drawn to fit the theoretical values of Hager and Seltzer [Ha68].

5.4. Decay Scheme of Pb^{201}

5.4.1. Level Placements

The level scheme for Pb^{201} deduced from our coincidence studies, energy sums, and relative intensities of the transitions is shown in Figure V-15. Transition and excited-state energies are given in keV, with the adopted energies for the levels being a weighted average based on our confidence in the respective cascade and crossover transitions.

Before we get into the discussion of our reasoning behind the final level placements, we should say a few words about the order in which these will be presented. We have tried to present the discussions in order of increasing level energies; however, the placement of some levels was very much dependent on the establishment of other higher levels. These cases will, therefore, be discussed in the order in which we originally placed them, so as to make the reasoning as straightforward as possible.

5.4.1.a. 331.15-keV Level

As the 331.15-keV transition is by far the most intense γ-transition in the decay of Pb^{201} (its relative intensity in the γ-ray singles spectrum being several times that of all the others added together), we have no choice but to propose an excited state at this energy, in agreement with all previous studies. It also turns out to be the first excited state.

Figure V-15. Decay scheme of Pb^{201}. All energies are given in keV and (total) transition intensities are given in percent of the Pb^{200} disintegrations. The percent ε decay to each state and the log *ft* values for that state are listed to the right of the state.

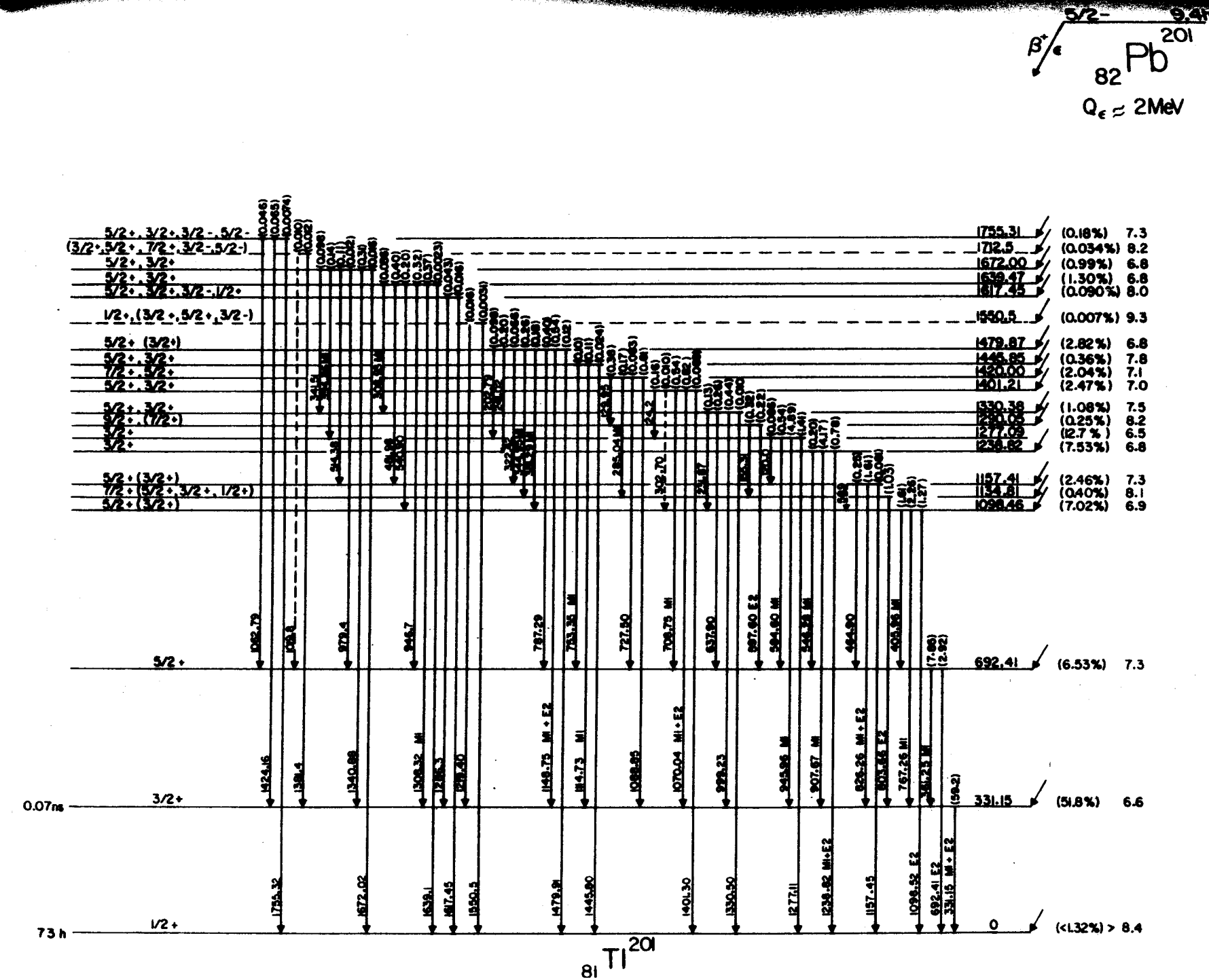
5/2-
9.4h
β+/ε
82 Pb 201
Qε ≈ 2MeV
1755.31 (0.18%) 7.3
1712.5 (0.034%) 8.2
1672.00 (0.99%) 6.8
1639.47 (1.30%) 6.8
1617.45 (0.090%) 8.0
1550.5 (0.007%) 9.3
1479.87 (2.82%) 6.8
1445.85 (0.36%) 7.8
1420.00 (2.04%) 7.1
1401.21 (2.47%) 7.0
1330.36 (1.08%) 7.5
1277.09 (12.7 %) 6.5
1238.82 (7.53%) 6.8
1157.41 (2.46%) 7.3
1134.81 (0.40%) 8.1
1098.46 (7.02%) 6.9
692.41 (6.53%) 7.3
331.15 (51.8%) 6.6
0 (<1.32%) > 8.4
0.07ns
73 h
81 Tl 201

Figure V-15

5.4.1.b. 692.41-keV Level

The second most intense peak in the Pb^{201} γ-ray singles is the 361.25-keV transition. This is also the strongest peak in the 331-keV gated coincidence spectrum. This, coupled with a strong 692.41-keV crossover transition that is somewhat enhanced in the anticoincidence experiment, confirms the previous placement of a level at 692.41 keV.

5.4.1.c. 1098.46-keV Level

The results of the anticoincidence and integral coincidence experiments alone strongly suggest the placement of a level at 1098.46 keV. This placement is also supported by excellent energy sums, the 405.96 + 692.41 = 1098.37 and 767.26 + 331.15 = 1098.41 sums falling within 0.15 keV of the measured 1098.52-keV crossover transition. Finally, the very strong 692-, 361-, and 331-keV peaks in the 405-keV gated coincidence spectrum, along with the absence of the 692- and 361-keV peaks but presence of a 331-keV peak in the 767-keV gated spectrum put any doubts to rest. Again, this placement agrees with the previous decay scheme.

5.4.1.d. 1157.41-keV Level.

The arguments for the placement of this level are substantially the same as those just used above for the 1098-keV level. The 1157-keV γ-transition was shown to be an essentially ε-fed ground-state in the anti- and integral coincidence experiments. There are cascade and crossover transitions to both the 331- and 692-keV levels.

These transitions are substantiated by the 465- and 826-keV gated coincidence spectra. Aasa and co-workers [Aa64] also found evidence for a 58.9-keV transition that fits very nicely between the 1157 and 1098-keV levels. Although we did not observe this transition, we have tentatively included it in the decay scheme.

5.4.1.e. 1238.82- and 1277.09-keV Levels

The observation of a strong 331-keV peak in both the 908- and 945-keV gated coincidence spectra and the strong 331-, 361-, and 692-keV transitions in the 546- and 585-keV gated spectra leads us to propose states at 1238.82 keV and 1277.09 keV. The weak 361- and 692-keV peaks in the 946-keV gated coincidence spectrum did present a problem in placing this transition before we revealed the doublet nature of the 946-keV peak [Section 5.3.5.d.]. The 2-d gated coincidence spectra also show a 120-keV transition feeding the 1157-keV state from the 1277-keV level. The existence of these two levels is also supported by the enhancement of the ground-state transitions in the anticoincidence spectrum and reduction in the integral coincidence spectra. These two levels have also been reported previously.

5.4.1.f. 1330.38-keV Level

Although we observed a 1330-keV γ-ray in the singles and anticoincidence spectra, it appears from the intensities listed in Table V-2 that this peak is not primarily an ε-fed ground-state transition. Of course, this does not mean the 1330-keV peak is not a ground-state transition, just that we were unable to pick this level

out of the anticoincidence experiment. From energy sums we find there are three relationships of the type $E_1+E_L = 1330$ keV where E_L corresponds to the energy of a lower, well-established level and E_1 are the 999-, 638-, and 232-keV transitions. Gating on these three γ's, we find they populate the 331-, 692-, and 1098-keV levels, respectively, substantiating the energy sums and the level at 1330.38 keV. This level is our first new addition to the level scheme and is as firmly based as any of the others already discussed.

5.4.1.g. 1401.21-keV Level

The enhancement of the 1401-keV γ-ray in the anticoincidence spectrum and its great reduction in the integral coincidence spectrum mark this γ-ray as a probable ε-fed ground-state transition. Based on these experiments and the energy sums alone, we would be forced to propose a state at 1401 keV. However, for those who would like all the evidence, we refer you to the gated coincidence spectra, Figure V-9, or Table V-3, where the 2-d results are summarized. These data are all consistent with the placement of a level at 1401.21 keV, depopulated by 1070-, 709-, and 124.2-keV transitions to well-known, lower levels. The very weak 302.70-keV transition was placed between the 1401.21- and 1098.46-keV levels on the basis of its energy alone, as we had no coincidence data for this transition. This level is also consistent with the previous decay scheme.

5.4.1.h. 1445.85-keV Level

The first evidence for the 1445.85-keV level was in the anticoincidence and integral coincidence experiments where it appeared

to be an ε-fed ground-state transition. The 331-keV γ was the only peak in the 1115-keV gated coincidence spectrum and this also suggests a level placement at 1445 keV. The 753-keV gated coincidence spectrum shows the 331- and 361-keV transitions with almost equal intensities. This indicated the placement of the 753-keV γ as feeding the 692-keV state. Because of the weak nature of this 753-keV transition, we did not observe a strong peak at 692 keV in the 753-keV gated spectrum, although a very weak peak at this energy is visible in Figure V-9. Based on the coincidence evidence presented here we are very confident of this placement, even though all the peaks involved are relatively weak. The previous decay scheme [Aa64] did not have a level at 1445 keV but proposed a level at 753 keV fed by the 345-keV transition. This is clearly in opposition to the results we obtained from the 753 gated coincidence spectrum. The 345-keV gated spectrum also failed to produce a peak at 753 keV. We have, therefore, eliminated the 753.2-keV level proposed by Aasa.

5.4.1.i. 1479.87- and 1639.47-keV Levels

The evidence in support of these two levels is quite substantial. Both have been shown to be ε-fed ground-state transitions in the anticoincidence and integral coincidence experiments. Both are supported by numerous cascade transitions to lower, well-known levels, six in the case of the 1479-keV level and five for the 1639-keV level. The placement of these cascade transitions have all been confirmed by the 2-d coincidence data, and we refer the reader to Figures V-9 and

V-15 and Table V-3 for the specific transitions and coincidence results involved in these placements. We should mention here again the doublet nature of the 946-keV peak and that it is the weaker component that populates the 692-keV.

5.4.1.j. 1672.00-keV and 1755.31-keV Levels.

These two levels complete our highest confidence group of levels. Both have ε-fed ground-state transitions as shown by the anticoincidence experiment, both have transitions to the 331- and 692-keV levels which are supported by the 2-d coincidence experiments. In addition, the 514-, 395-, and 341-keV transitions were shown to populate the 1157-, 1277-, and 1330-keV levels, respectively, from the 1672-keV level. Although these two levels have not been reported in any of the previous studies, we are quite confident of their correct placement.

5.4.1.k. 1134.81-, 1290.05-, and 1420.00-keV Levels

Placing these levels was the most frustrating problem in this decay scheme and, as we indicated above, we do not feel as confident of these levels as the ones already discussed. These are three of the four levels where we did not observe a direct ground-state transition. Our first piece of evidence for the 1134.81-keV level came from the 803-keV gated coincidence spectrum shown in Figure V-9. The relative intensities of the peaks in this spectrum indicate that the 803-keV γ directly populated the 331-keV level and the resulting level at 1135 keV was populated directly or indirectly by the 155-, 130-, 285-, and 345-keV transitions. This speculation was supported

by the 345-keV gated coincidence spectrum which contained only two peaks of equal intensity (after correcting for detector efficiency), at 331 and 802 keV. This would indicate that the 345-keV γ-ray depopulates a 1479-keV level,which is quite possible as we have already confirmed a level of this energy.

As we postulated above, the 285-keV transition may directly populate the 1135-keV level. If this were true, we would expect a level at 1420 keV and there is evidence to support such a level. The strong 1089-keV transition was shown to be in coincidence with only the 331-keV transition in our 2-d experiment [Figure V-9]. We also gated on the weak 727-keV γ and observed only 331- and 361-keV peaks of almost equal intensity, indicating the 727-keV γ populated the 692-keV state. These two pieces of evidence strongly support the the placement of a level at 1420.00 keV.

Thus far we have quite confidently placed the 1134.81- and 1420.00-keV states. After placing the 285-keV transition between the 1420- and 1135-keV on the basis of the coincidence data, we noticed that the sum of the 129.95- and 155.31-keV γ-rays is within 0.22 keV of the 285.04-keV transition. If the 130- and 155-keV γ-rays were really cascade transitions from the 1420-keV level to the 1135-keV level, there would have to be an intermediate level at 1265 or 1290 keV. We have already mentioned the fact that the 130- and 155-keV γ's are in coincidence with the 803-keV transition and therefore populated directly or indirectly the 1135-keV level; however, this does not tell us whether or not they are in a cascade thru one intermediate level. In Figures V-10 and V-11 we show the low energy portion of the 130- and 155-keV gated coincidence

spectra. These spectra show that the 130- and 155-keV transitions are indeed in coincidence with each other, although not necessarily in a direct cascade. However, we did observe a 598-keV peak in the 130-keV gated spectrum but not in the 155-keV gated spectrum. Then gating on the 598-keV peak, we observed, in addition to the 130-keV peak, 331-, 361-, and 692-keV γ's in exactly the same intensity ratio as found in the depopulation of the 692-keV level. As these three peaks were by far the strongest in the coincidence spectrum, we are convinced that the 598-keV transition populates the 692-keV level directly, placing a level at 1290 keV. The fact that we did not observe the 155-keV transition in the 598-keV gated spectrum is consistent with the placement of this transition between the 1290- and 1134-keV levels. Based on the evidence presented here we feel certain there is a level at 1290.05 keV, although we do not feel as sure of this placement as the ones discussed earlier.

5.4.1.1. 1550.5-, 1617.45-, and 1712.5-keV Levels.

The evidence for these three levels is somewhat limited and they represent our lowest confidence group. The 1550.5-keV level is supported by the observation of a γ-ray of this energy in the singles spectrum, although we did not observe it in either the anticoincidence or integral coincidence spectra because of its very low intensity. It is also supported by the sum relationship, 1219.40+331.15 = 1550.55, which compares very well with the measured 1550.5-keV γ-ray. The 1219-keV peak is very weak, but we were still able to gate on this in the 2-d experiment. We observed a single peak at 331 keV in the resulting

coincidence spectrum. Therefore, we do have some coincidence information to support this level.

The 1617.45-keV level is supported by a ground-state transition that was shown to be ε-fed in the anticoincidence experiment. We also have the sum relationship 1286.3+331.15 = 1617.45, which is identical to the measured 1617.45-keV ground-state transition. The 1286.3-keV transition is also very weak and the gated coincidence spectrum is Figure V-9 is not very convincing, although it does show a weak peak at 331 keV. From these pieces of evidence we have proposed the 1617.45-keV level.

The 1712.5-keV level is by far the most speculative we have included in our decay scheme. As we did not observe a ground-state transition, our first indication of this level came from the 1381.4-keV gated coincidence spectrum in which we observed only a weak 331-keV peak. The energy sums, 1019.8+692.4 = 1712.2 and 1381.4+331.1 = 1712.5, also suggested the level. Unfortunately, the 1019.8-keV transition was so weak we did not observe it in any of the coincidence spectra.

This concludes our discussion of the level placements; however, we would like to add a few parting words as to the completeness of this level scheme. We have included 64 of the 72 γ-rays observed in our singles experiments in this decay scheme and these account for more than 99.95% of the total transition intensity. The vast amount of coincidence data we obtained from the 2-d γ-γ coincidence experiment is consistent with the decay scheme as shown in Figure V-15

with very few exceptions, and these few were weak coincidence observations which are questionable. The 8 γ-rays left unplaced are all very weak and our assignment of these to Pb^{201} decay is also somewhat questionable.

5.4.2. β^+-feeding

In our singles experiments we observed a very weak peak at 510.7 keV which appeared to be slightly broader than the γ-ray peaks next to it. Considering the energy of the peak and its possible broadening, we have assumed that this peak arises from positron annihilation in the β^+-decay of Pb^{201}. Based on the Q_ε of ≈2 MeV, calculated from the "experimental" masses listed in the table of Myers and Swiatecki [My65], we find that β^+-decay is energetically possible in the decay of Pb^{201}. Using the 511-keV γ and the *K* x-ray intensities listed in Table V-2, we have calculated an upper limit of 0.034% for the total β^+-feeding in the decay of Pb^{201}. From theoretical ratios of $EC(K)/\beta^+$ [Wa59], the calculated Q_ε of ≈2 MeV, our spin and parity assignments, and our ε-feeding intensities, we predicted the β^+-feeding intensities listed in Table V-5. These three levels are the only energetically possible ones for β^+-feeding from the ground-state of Pb^{201}. The predicted β^+-feeding to the ground-state was calculated assuming 1.32% ε-feeding [Section 5.4.3.].

The 511-keV peak was also visible in the integral coincidence spectra of the 2-d γ-γ coincidence experiment and we were able to obtain the 511-keV gated coincidence spectrum shown in Figure V-9.

The only γ-ray that we could definitely observe to be in

Table V-5

β^+-feeding in Pb^{201} Decay

Energy of Level (keV)	Experimental ε-feeding	Theoretical ε_{K/β^+}	Calculated β^+-feeding	Observed β^+-feeding
Ground State	<1.32%	260[a]	0.0046%	
331.15	51.8 %	340[b]	0.12 %	≤0.034%
692.41	6.53%	9000[b]	0.0058%	

[a] This is a first-forbidden unique β-transition.

[b] These are first-forbidden nonunique β-transitions.

coincidence with the 511-keV peak was at 331 keV. Although the 361-keV γ shows up in the 511 gated spectrum in Figure V-9, it was also very strong in the coincidence spectra of the adjacent background, and because of the poor statistics we could not definitely determine whether the 361-keV peak in the 511-keV gated spectrum was legitimate or due to chance and incomplete background subtraction. We also observed the 511-keV peak in the 331-keV gated coincidence spectrum. A very weak 511-keV peak was also visible in the 692-keV gated spectrum while in the 361-keV gated spectrum it was either absent or hidden in the Compton background.

The only previous report of positrons in the decay of Pb^{201} indicated two branches approximately 350 keV apart [Be57]. Nothing was mentioned concerning their relative intensities or which states they populated. Based on the results of our experiments, there appears to be a small amount of β^+-feeding to the 331-keV level and some weak evidence for β^+-feeding to the 692-keV state. As these two states are 361-keV apart, this is at least consistent with the previous observations.

A triple γ-coincidence [511 keV-511 keV-any] experiment [Au67] was performed using the 8×8-in. NaI(Tl) split annulus with the 3.6% Ge(Li) detector in an attempt to substantiate the tentative β^+-feeding results of the 2-d experiment. However, because of the extremely weak nature of the 511-keV peak and the wide energy gates used in the NaI(Tl) detectors, we could not draw any conclusions concerning the β^+-feeding from this experiment.

When more and larger volume Ge(Li) detectors become available, it would be interesting to repeat the triple-coincidence experiment using three of these. This would be even more valuable in connection with a 3-dimensional data-taking system similar to our present 2-dimensional system. One could then perform a background subtraction on the two 511-keV gates, which would be very desirable in this case considering the intensity of the Compton background under the weak 511-keV peak.

5.4.3. Log *ft*'s

The total transition intensities, including internal conversion in the *K*, *L*, and *M* shells, were calculated from our singles intensities and the theoretical conversion coefficients of Hager and Seltzer [Ha68]. We assumed an *M*1 multipolarity for all transitions except those shown to be *E*2 or mixed *M*1 + *E*2 from the measured *K*-conversion coefficients listed in Table V-4. These total transition intensities, in percent of the total Pb^{201} disintegrations, are given in the decay scheme, Figure V-15. From the measured *K* x-ray intensity and *K*-conversion intensities and the calculated *K* fluorescent yield, 0.95, [Fi66] the total ε-feeding intensity to the ground-state was determined to be <1.32%. This upper limit on the feeding to the ground has taken into account the uncertainty in the x-ray intensity listed in Table V-2. If we use the actual x-ray intensity listed in Table V-2, we obtain a net negative feeding to the ground-state, and as this is somewhat unorthodox, we assume the actual ground-state feeding to be somewhere in the range 0% - 1.32%. This corresponds

to a log $ft \leq 8.4$. The total ε-feeding intensities to each state in Tl^{201} were then calculated assuming 1.32% ground-state feeding. These intensities are given in the decay scheme to the right of the energy levels. Log ft values based on these ε-feeding intensities, the 9.4-h half-life of Pb^{201}, and the calculated Q_ε appear at the extreme right of the levels.

5.5. Spin and Parity Assignments

5.5.1. Ground and 331-keV States

The Tl^{201} ground-state has a measured spin of 1/2 from both atomic spectra [Hu61] and atomic beam resonance [Li58,Ma58] experiments. This is consistent with the predicted $s1/2$ proton shell model assignment, giving us a spin and parity ($I\pi$) of 1/2+.

Our upper limit of 1.32% on direct ε population to this state corresponds to a log $ft \geq$ 8.4 which is in agreement with a predicted first-forbidden log $ft \geq 9$ for a 5/2- to 1/2+ transition. However, as this transition would be $\pi s1/2 \rightarrow \nu f5/2$, which makes it ℓ-forbidden as well as spin forbidden, the log ft is probably quite a bit higher than 9.

The 331-keV state was previously assigned $I\pi$=3/2+ by Pettersson and co-workers [Pe61] on the basis of the mixed $M1 + E2$ 331-keV γ-transition and the strong ε population of this state (51.8% of our decay scheme). Our work supports this 3/2+ assignment, as the log ft of 6.6 is in the range expected for a first-forbidden transition.

5.5.2. 692- and 1277-keV States

The 361-keV γ-ray depopulating the 692-keV level was previously assigned a multipolarity of $M1$ based on the measured K-conversion coefficient [Pe61]. Our value for this conversion coefficient also suggests an $M1$ multipolarity. This would allow $I\pi$=1/2+, 3/2+, or 5/2+. However, the angular correlation results of Pettersson and co-workers [Pe61] rule out all but the 5/2+ possibility. This assignment also agrees with the log ft of 7.3 which lies in the range of a first-forbidden transition.

The angular correlation results of Pettersson [Pe61] require a spin of 1/2 or 3/2 for the 1277.99-keV state. These spins are both consistent with the $M1$ multipolarity calculated for the 945.96-keV γ to the 3/2+ 331-keV state which, in addition, suggests a positive parity. The $M1$ multipolarity of the 584.60-keV transition moreover is incompatible with a 1/2+ assignment, which leaves us with the 3/2+ assignment for the 1277-keV state. The log ft of 6.5 also supports this assignment, as a 1/2+ assignment would be first-forbidden unique log $ft \geq 9$.

5.5.3. 1098.46-keV State

The calculated log ft for ε decay to this state was 6.9. This indicates either an allowed or first-forbidden nonunique transition, which could populate 3/2-, 5/2-, and 7/2- or 3/2+, 5/2+, and 7/2+ states in Tl^{201}. From the definite $M1$ assignment for the 405.96-keV γ to the 692-keV state ($I\pi$=5/2+), we can eliminate the negative parity assignments. The $M1$ multipolarity of the 767.26-keV γ to the 331-keV state (3/2) narrows the choice to 3/2+ or 5/2+. The $E2$ multipolarity we have assigned to the 1098-keV ground-state transition is based on the measured α_K listed in Table V-4. This would strongly suggest a 5/2+ assignment for the 1098.46-keV state; however, we cannot positively eliminate the 3/2+ assignment on this basis for the transition could possibly be a mixed $M1 + E2$ with the $E2$ component strongly enhanced. However, as there are very few mixed $M1 + E2$ transitions observed in this decay scheme, and we might not expect such a strong collective enhancement at this energy, we feel the 5/2+ assignment is the better choice. We have indicated this in the

decay scheme by putting the 5/2+ assignment first and the 3/2+ assignment in parenthesis.

5.5.4. 1134.81- and 1290.05-keV States

The log ft values calculated for the 1134.81- and 1290.05-keV states allow the $I\pi$ assignments 3/2+, 5/2+, 7/2+, 1/2+, 9/2+, 3/2-, 7/2-, and possibly even 5/2-. Based on the measured α_K's we have assigned both the 803-keV γ from the 1134-keV state to the 331-keV state and the 597-keV γ from the 1290-keV state to the 692-keV state as $E2$'s. These $E2$ transitions eliminate the negative parity possibilities as well as the 9/2+ possibility for the 1134-keV state. This leaves us with 4 possible assignments for the 1134-keV state and 5 possible assignments for the 1290-keV state.

If we assume the 803- and 597-keV γ's are mixed $M1 + E2$ transitions we obtain the following possibilities, 1/2+, 3/2+, and 5/2+ for the 1134-keV state and 3/2+, 5/2+, and 7/2+ for the 1290-keV state. A 1/2+ assignment for the 1134-keV state is somewhat questionable on the basis of the log ft, since this would be a first-forbidden (unique) transition, log $ft \geq 9$, whereas the measured log ft=8.1. For a 1/2+ assignment we might also expect to see this level populated from the 1277-keV level (3/2+) or see a transition to the ground-state (1/2+). For the 1134-keV state we still have the possible assignments 3/2+ and 5/2+. Although the log ft's are in agreement with these assignments, the question again arises as to why so few γ's populate the 1134-keV level and why there is no γ-transition to the 1098-keV (5/2+), 692-keV (5/2+), or ground (1/2+) states. These same arguments hold for the 1290-keV state, but even more so. Under the

assumption of an $M1$ admixture in the 597-keV γ, we have only the possible $I\pi$'s 3/2+, 5/2+, and 7/2+. The 1290-keV state is populated by only one transition out of all the higher lying states, many of which we will show later have $I\pi$'s of 5/2+ and 3/2+. In addition, this level feeds only the 1134- and 692-keV states. If the $I\pi$ were 3/2+ we might have expected at least some branching to the ground or first-excited states.

Having discussed the possible spins arising from a mixed $M1$ + $E2$ assignment for the 803- and 597-keV γ's let us consider the alternative. If we assume no $M1$ admixture in the 803-keV γ, we have the additional possibility of a 7/2+ assignment for the 1134-keV state. This assignment does raise some questions as to the γ-ray branchings, namely, why is there no transition to the 692- or 1098-keV states, which, being 5/2+ states, could be populated by $M1$ transitions. However, a 7/2+ assignment provides the best explanation for the apparently "pure" $E2$ multipolarity of the 803-keV transition. Assuming no $M1$ admixture in the 597-keV γ gives us the two additional possibilities of 9/2+ and 1/2+ for the 1290-keV state. The 1/2+ state might be expected to populate the 1/2+ ground-state or the 331-keV level (3/2+), while the 9/2+ assignment would not be expected to populate these. In addition, the 9/2+ assignment provides the best explanation for the apparently "pure" $E2$ nature of the 597-keV γ. A 9/2+ assignment would also be consistent with the population of the 1134-keV state if we made a 7/2+ assignment here.

The spin and parity assignments most consistent with the above arguments are 7/2+ for the 1134.81-keV state and 9/2+ for the 1290.05-

keV state. These assignments are also consistent with the theoretical predictions of Alaga and Ialongo (Al67). We will discuss these theoretical calculations in more detail in Chapter 6. However, we can not definitely eliminate the 5/2+, 3/2+, and 1/2+ possibilities for the 1134-keV state or the 7/2+ possibility for the 1290-keV state and these have been placed in parentheses following our preferred assignments in the decay scheme.

5.5.5. 1157.41- and 1479.87-keV States

The log ft's for these two states (7.3 and 6.8) fall within the limits for allowed and first-forbidden transitions. However, we can eliminate any negative parity possibilities on the basis of the $M1 + E2$ multipolarities of the 826.26- and 1148.75-keV γ's. This leaves us with the 3/2+, 5/2+, and 7/2+ possibilities. However, since the 826- and 1149-keV γ's to the 331-keV state (3/2+) have strong $M1$ components, the 7/2+ assignment is not possible, leaving us the 3/2+ and 5/2+ possibilities to choose from. On the basis of the γ-ray branching ratios, a notoriously poor criterion but the only one available, we feel the 5/2+ assignment is the more probably for the 1157.41-keV level, although we would definitely not eliminate the 3/2+ possibility. In the case of the 1479-keV level we again prefer the 5/2+ assignment on the basis of the γ-branching ratios but we also have an $M1$ γ-transition, 345-keV, to the 7/2+ 1134-keV level. If we were more certain on the spin and parity of the 1134-keV state, we could be more definite in our assignment of the 1479-keV state. However, as mentioned in

the last section, this 7/2+ assignment is somewhat shakey. Considering all the evidence we have assigned the 1479.87-keV level as 5/2+ with a 3/2+ second choice.

5.5.6. 1238.82-keV State

Because there are $M1$ transitions to the ground and first two excited states, we were able to assign this state as 3/2+ without much question. The log ft of 6.8 agrees with a 3/2+ assignment, falling within the range of a first-forbidden transition.

5.5.7. 1401.21 and 1445.85-keV States

The log ft's for these two states, 7.0 and 7.8, fall within the range of both allowed and first-forbidden transitions. However, both have $M1$ transitions to the 331- and 692-keV levels, eliminating the possibility of an allowed ε transition to these states. A 7/2+ assignment is also inconsistent with the observed $M1$ transitions to the 331-keV state (3/2+). We now are left with a choice between a 5/2+ and 3/2+ assignment for both states, with only the γ-branching ratios on which to base our decision. In both cases the 331- and 692-keV states are populated more strongly than the ground-state, which would be the case if the ground-state transitions were "pure" single-particle $E2$ transitions. Based on this we might predict a 5/2+ assignment for both states. However, this argument is very weak as collective effects could enter strongly into these states and we have only to examine the γ-branching ratios for the 1238- and 1277-keV γ's to see how erroneous these predictions could be. Nevertheless, we have placed the 5/2+

assignment first in the decay scheme but with the 3/2+ assignment following it having almost equal probability.

5.5.8. 1420.00-keV State

The log ft of 7.1 falls within the range of an allowed or first-forbidden ε transition, and the $M1$ nature of the 285-keV transition to the 1134-keV state rules out the negative parity states. Again we have a first-forbidden ε transition, resulting in the 3/2+, 5/2+, and 7/2+ possibilities. The 285-keV $M1$ transition to the 7/2+ state also narrows the choice to the 7/2+ and 5/2+ possibilities. The 7/2+ assignment would definitely be the better choice based on the γ-branchings observed in this case. The first thing we notice is that the 1420-keV state populates only states with spins of 9/2+, 7/2+, 5/2+ and in one case 3/2+. The fact that there wasn't a trace of the ground-state transition in the singles spectrum would also support the 7/2+ assignment, as this would be an $M3$ transition. Of course, the 7/2+ and 9/2+ assignments were not definite for the 1134- and 1290-keV states but we feel that the internal consistency between the 1134-, 1290-, and 1420-keV states lends support to our spin assignments for all of them.

5.5.9. 1550.5-keV State

The log ft of 9.3 for the 1550.5-keV state is the result of an extremely small ε feeding intensity, 0.007%. While this log ft is still in the range for a first-forbidden transition, it is definitely in the range of a first-forbidden (unique) transition. These give rise to the possible $I\pi$'s 1/2+, 3/2+, 5/2+, 7/2+, and

9/2+. Based on the fact that this state was found to populate only the ground (1/2+) and first-excited (3/2+) states, we can limit the spins to 1/2+, 3/2+, or possibly 5/2+, with the 1/2+ being the most probable. We have also included a possible 3/2- assignment for this level since the log ft is close enough to that for an allowed (ℓ-forbidden) ε transition, that we cannot absolutely rule it out. This assignment would also be consistent with the γ-branchings. Of course, an allowed (ℓ-forbidden) ε transition would also allow 5/2- and 7/2- possibilities, but we have ruled these out on the basis of the γ-branchings.

5.5.10. 1617.45- and 1712.5-keV States

The log ft's for ε decay to the 1617.45- and 1712.5-keV states are 8.0 and 8.2. These could indicate $I\pi$'s of the 1/2+ through 9/2+, 3/2-, 5/2-, and 7/2-. The 1617.5-keV state is depopulated by only a ground state transition and a transition to the 331-keV state. This narrows the most probable assignment to 1/2+, 3/2+, 5/2+, or 3/2-. The 1712.5-keV state is depopulated through the 692- and 331-keV states with almost equal intensities, there being no ground-state transition. The γ-branchings in this case make a 1/2+, 9/2+, or 7/2- assignment unlikely. This leaves us with $I\pi$ = 3/2+, 5/2+, 7/2+, 3/2- and 5/2- as possibilities for the 1712.5-keV state.

5.5.11. 1639.47- and 1672.00-keV State

Both the 1639.47- and 1672.00-keV states have a log ft = 6.8. The resulting $I\pi$ possibilities are 3/2±, 5/2±, and 7/2±. The

negative parity assignments can be eliminated in both states on the basis of $M1$ transitions to lower positive parity states. A 7/2+ assignment for the 1639-keV state is not compatible with the 1308-keV $M1$ γ to the first excited state and we are left with the two possibilities 3/2+ and 5/2+. We can rule out a 7/2+ assignment for the 1672.08-keV level on the basis of the 394-keV $M1$ transition to the 3/2+ 1277.09-keV state. Again we are left with the two possibilities 3/2+ and 5/2+.

5.5.12. 1330.38- and 1755.31-keV States

The calculated log ft's are 7.5 and 7.3 for the 1330- and 1755-keV states respectively. The possible $I\pi$'s for these log ft's are 3/2±, 5/2±, and 7/2±. We have eliminated the positive parity possibilities for the 1330-keV level on the basis of the 308-keV $M1$ transition from the positive parity 1639-keV state. The observation of ground state transitions from both of these two states rules out the 7/2 spins as these would be $E3$ or $M3$ transitions. For the 1330-keV state we are left with the 5/2+ and 3/2+ possibilities, and for the 1755-keV state we are left with the 5/2+, 3/2+, 5/2-, and 3/2- possibilities.

5.5.13. Summary of Spin and Parity Assignments

Of the 20 proposed states in Tl^{201}, we have made unique spin and parity assignments for 5 of these. We have narrowed the assignments of 10 more states to two possibilities and narrowed the possible spin and parity assignments of the remaining 5 levels to four.

As mentioned at the beginning of the chapter, we will postpone

a discussion of the systematics and theoretical calculations of the odd-mass Tl isotopes until the end of Chapter 6.

CHAPTER VI

THE DECAY OF Pb^{199} AND STATES IN ODD-MASS Tl ISOTOPES

6.1. Introduction

This chapter contains the experimental results of our study of the states in Tl^{199} populated by the decay of 90 min Pb^{199}, as well as a discussion of the systematics and shell model assignments of these levels and those of the other odd-mass Tl isotopes.

Pb^{199} was first reported by Neuman and Perlman [Ne50] in 1959 as the daughter of 24 min Bi^{199} (made by proton bombardment of Pb). By measuring the yield of 7-h Tl^{199} obtained at 60 minute intervals from a Pb^{199} source, they determined the half-life of Pb^{199} to be ≈80 min.

The second and most recent study of Pb^{199} decay was made by Andersson and co-workers in the mid 1950's [An55, An57]. They produced Pb^{199} sources by proton bombardment of natural Tl, followed in some cases by mass separation of the resulting Pb activities. Using a β-spectrometer of 0.3%-0.4% resolution, they assigned several conversion electron lines to the decay of Pb^{199} and measured the half-life to be 90±12 min. These electron lines corresponded to γ-ray energies of 352.8, 367.0, and 721.0 keV and the K/L ratios of the 353 and 367-keV transitions indicated they were both of mixed $M1+E2$ multipolarities. The 353- and 367-keV transitions were also shown to be in coincidence in an electron-electron coincidence experiment and based on this, and the observation of the 721-keV

cross-over transition, they proposed two excited states at 367 and 720 keV. (These levels are in agreement with our work.) Assuming a $1/2^+$ ground state, they proposed $I\pi$ assignments for these two excited states of $3/2^+$ and $5/2^+$, respectively, based on multipolarity assignments and the systematics of the other odd-mass Tl isotopes. (The ground state spin of 1/2 was later confirmed in atomic beam resonance [Br57] and atomic spectra [Hu61] experiments.) In addition to the three γ-rays already mentioned, for which a definite assignment was made, they also made tentative assignments to Pb^{199} of several electron lines corresponding to γ-transitions of 267 and 1132 keV (also observed in our study).

Andersson and co-workers [An57] also looked at the β^+ spectrum of a complex mixture of isotopes, including Pb^{199}, and after extensive corrections, obtained a maximum end point energy of 2.8 MeV, which they tentatively assigned to Pb^{199}.

In addition to the levels in Tl^{199} excited by the decay of Pb^{199}, several workers have reported the direct excitation of an isomeric state in Tl^{199}. The first report of a possible isomeric state in Tl^{199} was published in 1957 by Leipunskii and co-workers [Le57]. Using a pulsed beam of 20 MeV protons on HgO and a NaI(Tl) detector, they observed a 370±20-keV γ peak decaying with a half-life of 42±5 msec.

In 1963 Diamond and Stephens [Di63] produced an isomeric state in Tl^{199} by bombarding Au^{197} with 22 MeV α's to induce the reaction $Au^{197}(\alpha,2n)Tl^{199m}$. They measured the electron spectrum

following the decay of Tl^{199m} using a single wedge-gap β-spectrometer and assigned the following five γ-transitions to its decay: 29, 353, 367, 382.1, and 720 keV. They measured the half-lives of these transitions to be 27±4 msec and proposed a level at 749 keV de-excited by the 29- and 382.1-keV transitions to the 720- and 367-keV levels respectively. The *K/L* ratio and half-life indicated an *E*3 multipolarity for the 382-keV transition and an $I\pi$ of $9/2^-$ for the 749-keV level. A γ-γ angular correlation experiment confirmed the possibility of a 9/2 (*E*3) to 3/2 (*M*1+*E*2) to 1/2 spin sequence.

Additional studies of Tl^{199m} were made by Demin *et al.* [De63], Gritsyna and Forster [Gr65], and Conlon [Co67]. The results of these studies generally supported the decay scheme proposed by Diamond and Stephens [Di63]. Demin *et al.* obtained a half-life of 28.9±0.6 msec for the isomeric state, Gritsyna and Forster found a half-life of 26.6±1.4 msec, and Conlon, using a Ge(Li) detector, observed γ-rays of 367.0±0.3 and 382.8±0.3 keV decaying with a half-life of 29.2±2.0 msec.

From the survey of previous studies presented above, it is apparent that very little was known about the decay of Pb^{199} before the present study, especially when one considers the fact that the Pb^{199} decay scheme should be at least as complex as that of Pb^{201} (Chapter V). Indeed, where previously 3 γ-transitions between 3 states in Tl^{199} had been observed in the decay of Pb^{199}, we report here 89 γ-transitions placed between 29 levels.

6.2. Source Preparation

6.2.1. $Hg^{200}(He^3,4n)Pb^{199}$

Our first attempts at producing Pb^{199} consisted of bombarding natural HgO with He^3 beams. We made bombardments at various energies from the coulomb barrier up to 70 MeV in an attempt to optimize the production of Pb^{199}. However because of the large number of stable isotopes of Hg (Table IV-1), we could not obtain a source at any energy that didn't contain large amounts of contaminating activities. Aging the sources, as was done in our preparation of Pb^{200} by a similar reaction, does not help in this case because the half-life of Pb^{199} is much shorter than many of the contaminants and comparable to most of the others.

Therefore, we decided very early in our study of Pb^{199} that the use of separated isotope targets was a necessity. We obtained separated isotope Hg^{200} (99.9%) in the form of HgO from Oak Ridge National Laboratory. After a rough excitation experiment, we found a He^3 beam of ≈35 MeV (70 MeV degraded with 56 mil aluminum) maximized the $(He^3,5n)$ reaction on Hg^{200}. However, this energy is slightly above the calculated threshold of 29 MeV for producing Pb^{198} from the $(He^3,6n)$ reaction and we did observe small amounts of Pb^{198} and its daughter, Tl^{198}, in most of our sources produced at this energy. We also observed Pb^{201}, Pb^{200}, and Pb^{199m} in these sources. The Pb^{200} and Pb^{201} were in very small amounts and did not cause any major problems during the first few half-lives of Pb^{199}. However,

because of their longer half-lives they became more of a problem as the Pb^{199} decayed away. Therefore, we seldom counted a source longer than 5 hours from the time it was made. We did make a very significant amount of Pb^{199m} and it could have been a serious problem; however, only one γ-ray is known to be emitted in its decay to Pb^{199} and its half-life is only 12 minutes. In order to reduce this activity in our spectra, we usually waited about 15 minutes from the end of a bombardment before starting the chemical separation. The separation took an additional 30 minutes and, therefore, by the time the source was ready to count, the Pb^{199m} had decayed by almost four half-lives and was no longer considered a problem.

In the course of this study we found we could obtain Pb^{199} sources of useful intensity by bombarding a barely visible amount of the HgO with a highly focused He^3 beam of several μamps for 15 to 30 minutes. The lead activity was then chemically separated from the Tl and Hg contaminants using a procedure similar to that used in separating Pb from Tl targets (Appendix B), the only change in the procedure being the addition of Tl^{+++} in place of Hg^{++} as the hold-back carrier. Most of the sources used in our study of Pb^{199} were made using this method.

6.2.2. $Tl^{203}(p,5n)Pb^{199}$

The second method used to produce Pb^{199} made use of the reaction $Tl^{203}(p,5n)Pb^{199}$. In our first attempts, we bombarded natural Tl foils with 44-MeV protons. Although 44 MeV is slightly above the

calculated threshold of 41 MeV for the $Tl^{203}(p,6n)Pb^{198}$ reaction, we did not observe any γ-rays from either Pb^{198} or its daughter, Tl^{198}, in these sources. However, the sources made with natural Tl targets (29.5% Tl^{203} 70.5% Tl^{205}) did contain a large amount of 9.4h Pb^{201} produced by the $(p,5n)$ reaction on Tl^{205}. The Pb^{201} was a particularly serious contaminant because of the large number (72) of γ-rays emitted in its decay. Using enriched (70%) Tl^{203} targets, we obtained sources with greatly reduced amounts of Pb^{201}. However, these sources still contained a much higher level of Pb^{201} than those made from the He^3 bombardments of Hg^{200}. In addition these sources also contained Pb^{199m}, Pb^{200}, Pb^{202m}, Pb^{203}, and Pb^{204m}.

These sources were chemically purified before counting using the procedure given in Appendix B. Pb-Tl separations were also performed every 45 minutes to reduce the Tl contaminants that kept growing-in.

6.3. Experimental Results

6.3.1. γ-ray Singles Spectra

Pb^{199} γ-ray energies and intensities were determined using the 2.5% and 3.6% efficient Ge(Li) detectors. The γ-ray singles spectrometer systems used in this study were described in sections 2.1. and 5.3.1. and will not be repeated here.

The energies of the prominent γ-rays were determined by counting the Pb^{199} sources simultaneously with the energy standards listed in Table VI-1. The energies of the weaker Pb^{199} γ-rays were then determined by using the now well determined γ-rays from Pb^{199} as secondary standards.

Figure VI-1 shows a typical γ-ray singles spectrum obtained in 45 minutes with the 2.5% efficient Ge(Li) detector at a resolution of 2.3 keV FWHM for the 1332-keV γ-ray of Co^{60}. The source used to obtain this spectrum was made by the $(He^3,4n)$ reaction on separated Hg^{200} as described in Section 6.2.1. From the many singles runs performed during this study, 117 γ-rays have been found to belong to the decay of Pb^{199}. The energies and intensities of these γ-rays are listed in Table VI-2.

During many of the singles experiments, and also in the anticoincidence experiment (Section 6.3.2.), we recorded a series of spectra, usually at 45 minute intervals, over several half-lives of a given source. (To improve the statistics of the weaker γ-rays, we added spectra obtained with other sources during corresponding 45 minute intervals.) In most of these experiments we performed Pb-Tl separations on the source every 45 minutes to remove the Tl and Hg

Table VI-1

γ-Rays Used as Energy Standards

Nuclide	γ-ray Energy (keV)	Reference
Ir^{192}	205.782 ± 0.014	a
	295.938 ± 0.009	a
	308.429 ± 0.010	a
	316.486 ± 0.010	a
	468.053 ± 0.014	a
	588.557 ± 0.017	a
	604.385 ± 0.017	a
	612.435 ± 0.017	a
Co^{56}	846.78 ± 0.06	Average of b, c, and d
	1037.89 ± 0.07	Average of b, c, and d
	1238.30 ± 0.05	Average of b, c, and d
	1360.25 ± 0.05	Average of b, c, and d
	1771.43 ± 0.05	Average of b, c, and d
	2015.37 ± 0.06	Average of b, c, and d
	2034.93 ± 0.06	Average of b, c, and d
	2598.58 ± 0.06	Average of b, c, and d
	3253.63 ± 0.06	Average of b, c, and d

[a] G. Murray, R. L. Graham, and G. S. Geiger, Nucl. Phys. 63 353 (1965).

[b] R. Gunnink, R. A. Meyer, J. B. Niday, and R. P. Anderson, Nucl. Instr. Methods 65 26 (1968).

[c] M. E. Phelps, D. G. Sarantites, and W. G. Winn, Nucl. Phys. A149 647 (1970).

[d] R. A. Meyer and D. Camp, private communication, Lawrence Radiation Laboratory, Livermore, California (1970).

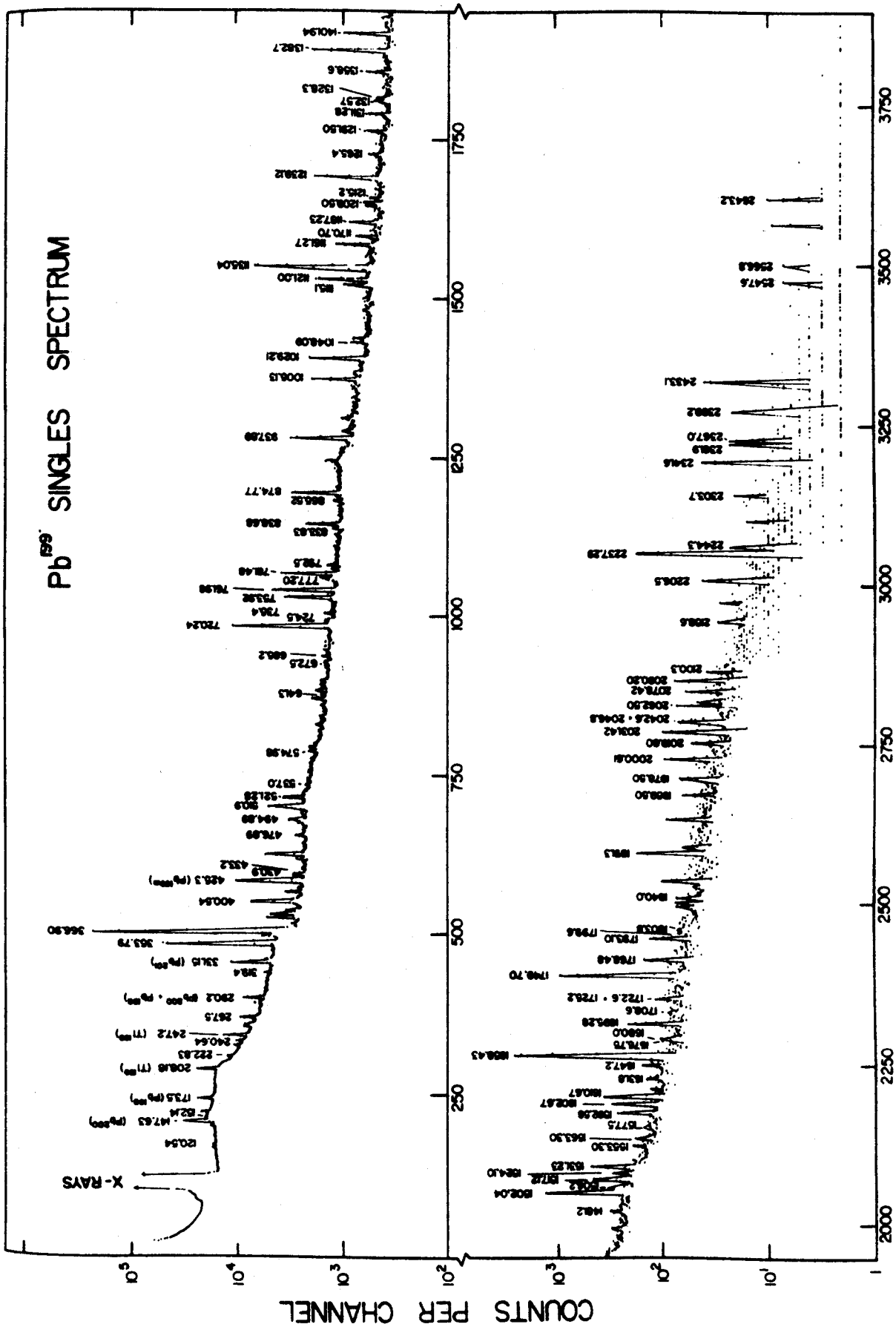

Figure VI-1. A singles γ-ray spectrum of Pb^{199} recorded by a 2.5% efficient Ge(Li) detector during a 45 min period. The Pb^{199} source was prepared by the $(He^3,4n)$ reaction on separated isotope Hg^{2}[illegible]. Because of the large number of γ-rays observed and because of the poor statistics in this spectrum not all of the peaks belonging to the decay of Pb^{199} are labeled.

Table VI-2

Energies and Relative Intensities of γ-rays From the Decay of Pb^{199}

Measured Energies (keV)	Relative Intensities		
	Singles	Anticoincidence	Integral γ-γ Coincidence
K X-rays	1450±150 [a]		
120.54±0.15	1.0±0.3	0.3	---
130.73±0.2	0.5±0.2	---	---
152.14±0.20	1.1±0.4	0.5	---
202.2 ±0.3	0.5±0.2	---	---
222.83±0.10	1.2±0.5	0.3	21
240.8 ±0.2	2.8±0.2	---	64
267.6 ±0.2	6.9±0.4 [a]	3.2	116
312.3 ±0.7	0.5±0.2	---	---
319.2 ±0.4	1.6±0.5	---	---
344.0 ±0.7	0.65±0.25	---	---
353.39±0.06	169 ±8	17	4750
361.4 ±0.6	6.0±2.0 [a]	1.4	199
366.90±0.06	790 ±40 [a]	400	13,000
390.3 ±0.4	3.0±0.5	0.7	85
400.54±0.08	23 ±2	2.3	600
430.9 ±0.3	3.5±0.8	0.3	121
433.2 ±0.3	3.0±0.8	0.4	---
476.9 ±0.2	3.2±0.8	---	131
494.89±0.10	6.6±1.0	---	190
503.15±0.2	1.9±0.6	0.3	---
510.90±0.10	29 ±3	2.0	1400
521.28±0.07	7.5±1.5	0.4	285
537.0 ±0.2	1.2±0.3	---	---
574.98±0.15	1.8±0.3	0.7	---

Table VI-2 (cont'd)

605.8 ±0.6 [a]	0.7±0.4	---	---
641.3 ±0.4	1.1±0.2	---	---
685.2 ±0.2	1.7±0.2	---	64
720.24±0.06	116 ±5	45	1650
724.5 ±0.4	2.0±0.4	---	67
735.4 ±0.3	2.0±0.4	---	67
753.92±0.08	28.4±1.5	4.8	556
761.98±0.07	40.0±2.0	3.2	1060
777.20±0.15	5.4±0.5	0.5	220
781.48±0.07	33.2±2.0	4.6	630
792.5 ±0.4	1.0±0.3	---	---
833.83±0.10	3.3±0.5	0.4	47
838.68±0.10	16.0±1.2	1.0	390
874.77±0.09	29.2±1.5	3.7	564
911.80±0.15	6.6±1.0	1.3	111
937.89±0.08	37.7±2.0	5.1	730
984.4 ±0.5	1.0±0.4	---	---
995.6 ±0.4	2.1±0.4	---	78
1005.13±0.08	24.0±1.2	3.8	470
1029.21±0.09	28.9±1.5	4.9	540
1048.09±0.09	5.2±0.8	---	130
1052.66±0.09	5.0±0.8	---	110
1115.1 ±0.4	11.3±1.0	1.6	240
1121.00±0.7	26.8±1.5	21	185
1135.04±0.08	140 ±7	33	1400
1161.27±0.09	15.4±1.0	1.3	335
1170.70±0.09	5.5±0.5	1.0	106
1177.2 ±0.4	1.2±0.3	---	---
1187.23±0.10	8.3±0.8	1.4	140
1209.60±0.10	4.6±0.3	---	64
1215.2 ±0.3	1.8±0.3	---	---
1239.12±0.10	37.8±1.5	6.5	610

Table VI-2 (cont'd)

1265.4 ±0.3	3.2±0.3	0.69	63
1291.50±0.10	5.5±0.5	2.0	75
1311.28±0.10	7.0±1.0	0.9	131
1325.7 ±0.3	3.3±0.5	---	
1328.3 ±0.3	3.3±0.5	---	87
1358.6 ±0.3	6.2±0.8	1.3	46
1382.71±0.09	51.0±2.0	12.4	494
1401.94±0.10	18.0±1.0	3.8	220
1481.2 ±0.6	2.4±0.4	1.4	28
1502.04±0.08	38.3±1.5	38.1	47
1506.2 ±0.4	3.8±0.4	---	59
1517.12±0.10	8.3±0.6	1.0	200
1524.10±0.15	2.9±0.7	0.7	26
1531.23±0.10	9.2±0.6	2.2	113
1553.3 ±0.3	1.5±0.3	0.4	30
1563.30±0.15	1.4±0.3	---	---
1577.5 ±0.5	1.0±0.2	---	---
1592.58±0.15	4.7±0.5	1.5	34
1602.61±0.9	7.3±0.6	6.6	25
1610.67±0.10	10.2±0.7	2.5	107
1631.8 ±0.3	1.6±0.3	1.6	24
1647.2 ±0.6	2.0±0.4	1.6	29
1658.43±0.09	≡100	≡100	≡100
1695.28±0.10	6.0±0.5	2.3	40
1725.3 ±0.5	1.2±0.4	0.8	---
1749.70±0.10	41.4±2.0	41.9	50
1768.48±0.15	4.0±1.0	2.6	30
1793.10±0.2	4.0±0.7	0.7	27
1840.0 ±0.4	1.4±0.2	0.5	---
1859.3 ±0.3	2.3±0.5	0.8	21
1891.3 ±0.3	7.2±0.5	4.7	---
1898.7 ±0.6	1.5±0.5	1.6	10

Table VI-2 (cont'd)

1930.69±0.20	2.0±0.5	2.0	---
1959.50±0.20	1.2±0.2	1.2	---
1978.5 ±0.3	1.3±0.2	1.5	---
2000.61±0.15	3.3±0.3	0.8	38
2019.60±0.15	1.7±0.3	1.3	---
2031.4 ±0.5	4.2±0.8	4.2	---
2042.6 ±0.3	2.3±0.6	4.4	23
2046.8 ±0.6	2.3±0.6	2.3	---
2062.50±0.20	1.8±0.2	1.7	---
2066.95±0.20	1.2±0.1	---	20
2078.4 ±0.2	1.8±0.2	0.31	20
2090.20±0.20	2.9±0.3	2.8	---
2100.3 ±0.3	0.8±0.2	---	17
2158.6 ±0.3	0.8±0.2	0.33	16
2180.2 ±0.4	0.77±0.2	---	---
2206.5 ±0.3	1.5±0.3	1.8	---
2226.7 ±0.3	0.5±0.3	0.4	---
2237.29±0.10	11.0±0.7	10.8	14
2244.3 ±0.3	0.6±0.2	0.4	---
2303.7 ±0.3	0.9±0.2	1.0	---
2341.6 ±0.3	2.7±0.2	2.9	---
2361.9 ±0.3	1.6±0.3	1.6	---
2367.0 ±0.5	1.5±0.3	1.5	---
2399.2 ±0.3	1.4±0.2	1.4	---
2433.1 ±0.3	2.7±0.2	2.7	---
2547.6 ±0.4	0.5±0.2	0.7	---
2566.8 0.4	0.5±0.2	0.5	---
2643.2 ±0.4	0.6±0.2	0.8	---
2751.9 ±0.7	0.3±0.2	0.3	---

[a]These intensities have been corrected for underlying peaks from the decay of other isotopes.

contaminants that kept growing-in, while in a few experiments we allowed these contaminants to accumulate over several half-lives. From the relative intensities of the γ-rays observed in these various experiments, it was then an easy matter for us to separate γ-rays belonging to Pb^{199} from those belonging to other Pb isotopes as well as Tl and Hg contaminants. As an additional check on our assignment of these 117 γ-rays, we required that the γ-ray singles relative intensities observed in sources made by the $(p,5n)$ reaction on enriched Tl^{203} agree with those observed in sources made by the $(He^3,4n)$ reaction on Hg^{200}.

The uncertainties in the energies listed in Table VI-2 are based on the uncertainties in the energy standards, the heights of the peaks above the underlying Compton background, and the reproducibilities of the calculated energies from the many singles spectra. Uncertainties in the relative γ-intensities are based on their reproducibilities in many spectra and the uncertainties in the experimentally determined efficiency curves for the Ge(Li) detectors.

The *K* x-ray intensity listed in Table VI-2 was obtained from the singles spectra in the same manner as the γ-ray intensities, although in this case we had to correct for the *K* x-ray intensities contributed by the Pb^{200} and Pb^{201} impurities in their ε decay. Pb^{200} and Pb^{201} were the most abundant impurities in most of our sources made by the $(He^3,4n)$ reaction on separated isotope Hg^{200}; although even these were present in rather small amounts as is evident in Figure VI-1.

6.3.2. Anticoincidence Spectra

In order to determine which γ's are primarily ε-fed ground-state transitions, we used the 2.5% detector in an anticoincidence experiment with an 8x8-in. NaI(Tl) split annulus and a 3x3-in NaI(Tl) detector as described in Section 2.2.1. Figure VI-2 shows an anticoincidence spectrum obtained in 8 hours using a coincidence resolving time of 250 nsec. In order to reduce contamination from 7.4 hour Tl^{199}, which was constantly growing-in, a fresh source, free of Tl and Hg was prepared every hour, and a new target was bombarded every four hours. The relative intensities obtained are listed in Table VI-2. In order to compare the anticoincidence with the singles intensities and also the integral coincidence results, we have arbitrarily assigned a relative intensity of 100 to the 1658-keV transition in all three cases. This was chosen because it is a relatively strong transition and an essentially 100% ε-fed ground-state transition (a γ-transition depopulating a level which is primarily fed directly by electron capture with little or no γ-feeding from higher levels). The argument may sound a little circular here, as we did not know the 1658-keV level was primarily ε-fed until after we analyzed the anticoincidence data, however, for the purpose of displaying the final results this met the above requirements.

The results of the anticoincidence experiment indicate a great number of apparent ε-fed ground-state transitions, 33 in all, and these are listed in Table VI-3 as possible states in Tl^{199}.

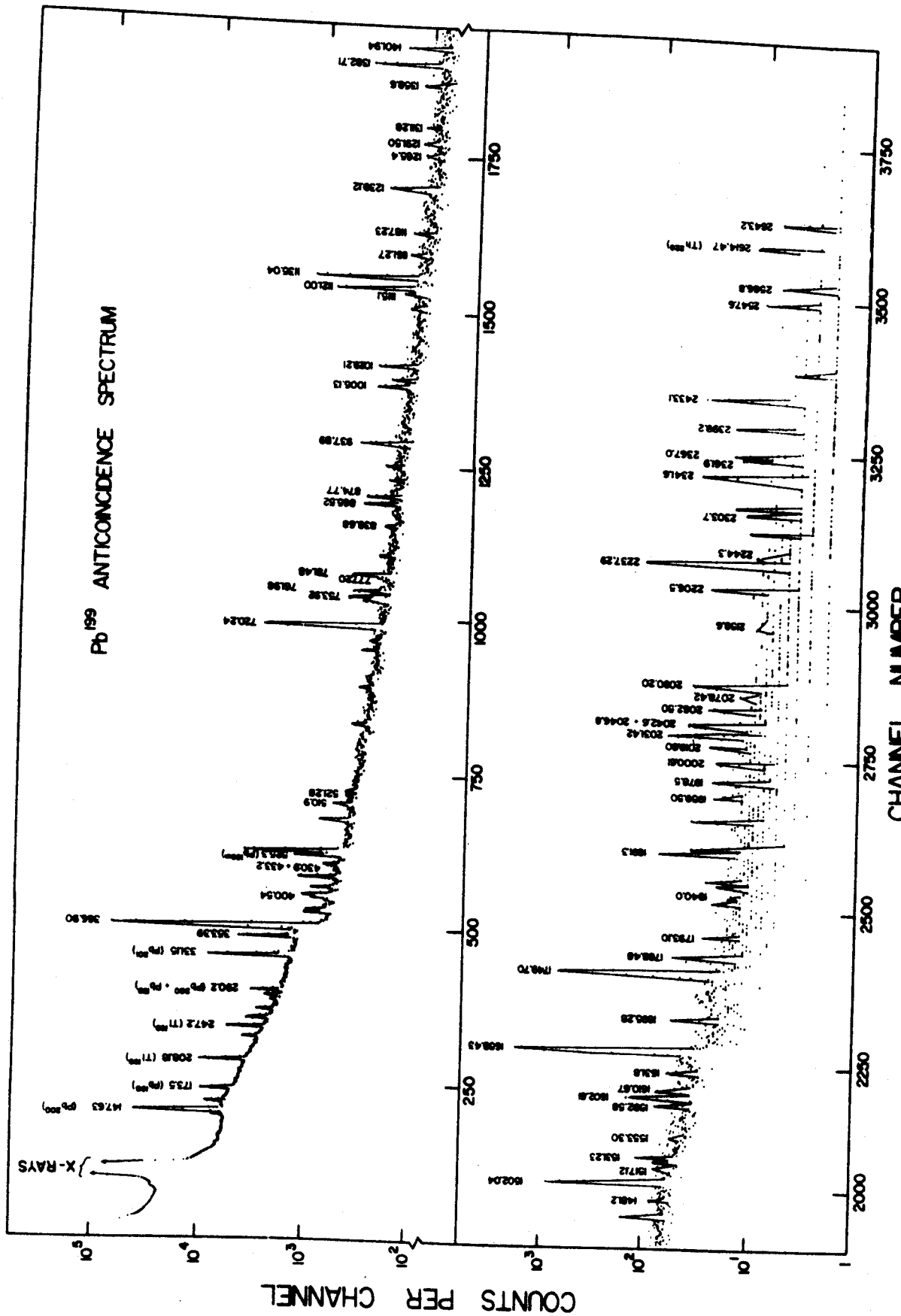

Figure VI-2. Anticoincidence spectrum of Pb^{199} γ-rays obtained with a 2.5% efficient Ge(Li) detector placed inside an 8x8 in. NaI(Tl) annulus with a 3x3 in. NaI(Tl) detector blocking the open end. Only peaks belonging to Pb^{199} decay are labeled except where otherwise noted.

Table VI-3

Possible Levels in Tl^{199} Indicated by Anticoincidence and Integral Coincidence Experiments

E_γ (keV)	E_γ (keV)	E_γ (keV)
1121.00	1959.50	2244.3
1502.04	1978.5	2303.7
1602.61	2019.60	2341.6
1631.8	2031.4	2361.9
1647.2	2042.6	2367.0
1725.3	2046.8	2399.2
1749.70	2062.50	2433.1
1768.48	2090.20	2547.6
1891.3	2206.5	2566.8
1898.7	2226.7	2643.2
1930.69	2237.29	2751.9

6.3.3. Integral Coincidence Spectra

To compliment the anticoincidence experiment and determine which γ-rays are involved in cascades, we wanted to perform an integral coincidence experiment. However, instead of doing an entirely separate experiment using a Ge(Li) detector in coincidence with the 8x8-in. NaI(Tl) annulus, we used the integral coincidence spectrum recorded by the 2.5% detector in the 2-d γ-γ coincidence experiment (Section 6.3.4.) to obtain the intensities listed in Table VI-2. This spectrum is shown in Figure VI-3.

The results of this experiment were entirely consistent with the results of the anticoincidence experiment.

6.3.4. 2-d γ-γ Coincidence Experiment

From the results of the anticoincidence experiment we placed 33 γ-rays as possible ε-fed ground-state transitions; however, we were still left with 84 unplaced γ-rays. The placement of most of these remaining γ-transitions in the Pb^{199} decay scheme was aided greatly by a 2-d γ-γ coincidence experiment of 4096 x 4096 channels, using the 2.5% and 3.6% efficient Ge(Li) detectors. The general experimental setup for this experiment was described in Section 2.3. and will not be repeated here.

During the 24 hours of counting $\simeq$2.2 million coincidence events were recorded. The two integral coincidence spectra obtained from this data are shown in Figure VI-4. The *Y*-side spectrum was recorded by the 3.6% detector and the *X*-side by the 2.5% detector.

Sources for this experiment were made by the He^3 irradiation of separated isotope Hg^{200}, however, in this case no

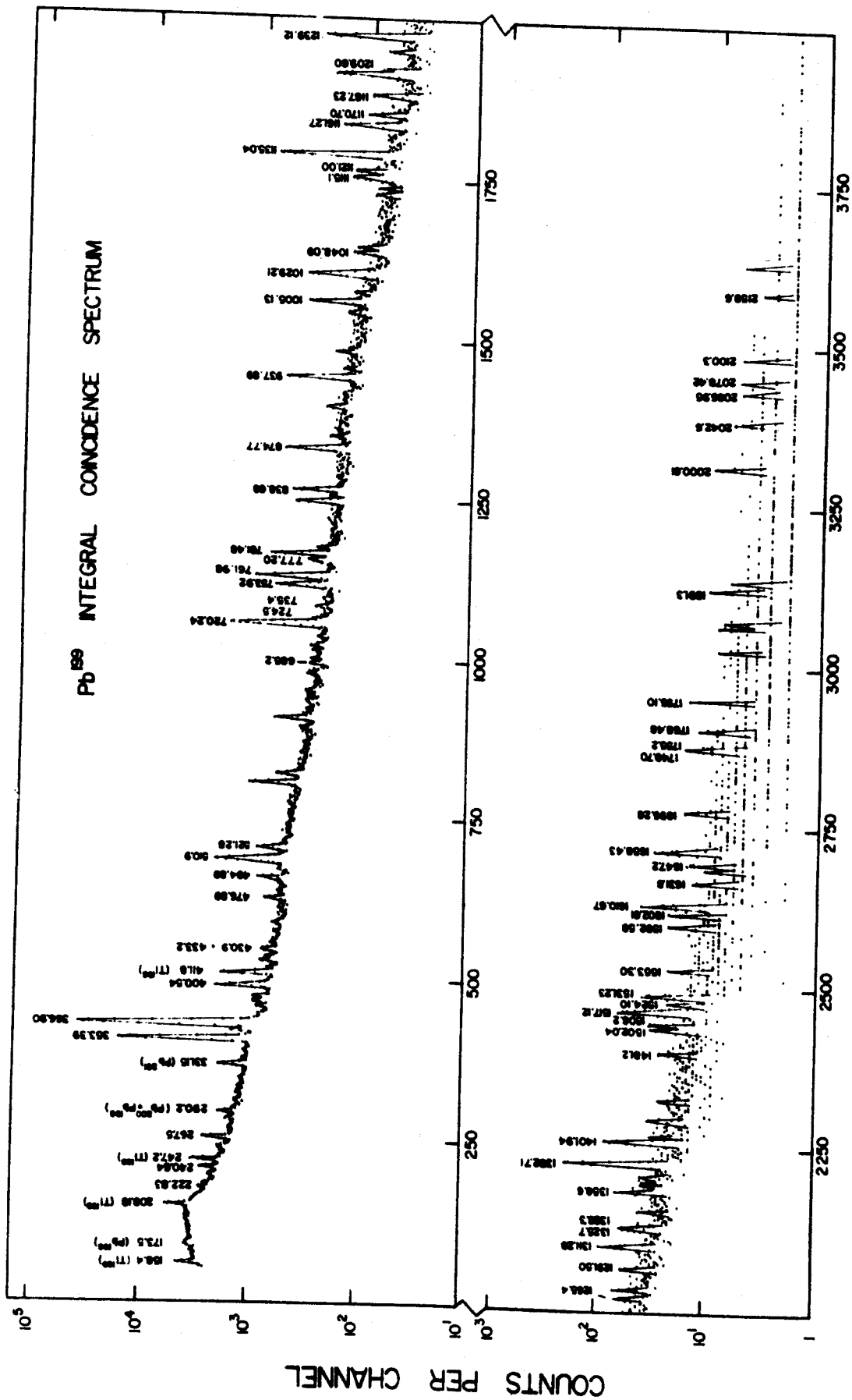

Figure VI-3. Integral coincidence spectrum of Pb^{199} γ-rays obtained by using a 2.5% efficient Ge(Li) detector in coincidence with a 3.6% efficient Ge(Li) detector at 90° to the source. In this case no chemical separation was performed on the Hg^{200} target after the bombardment.

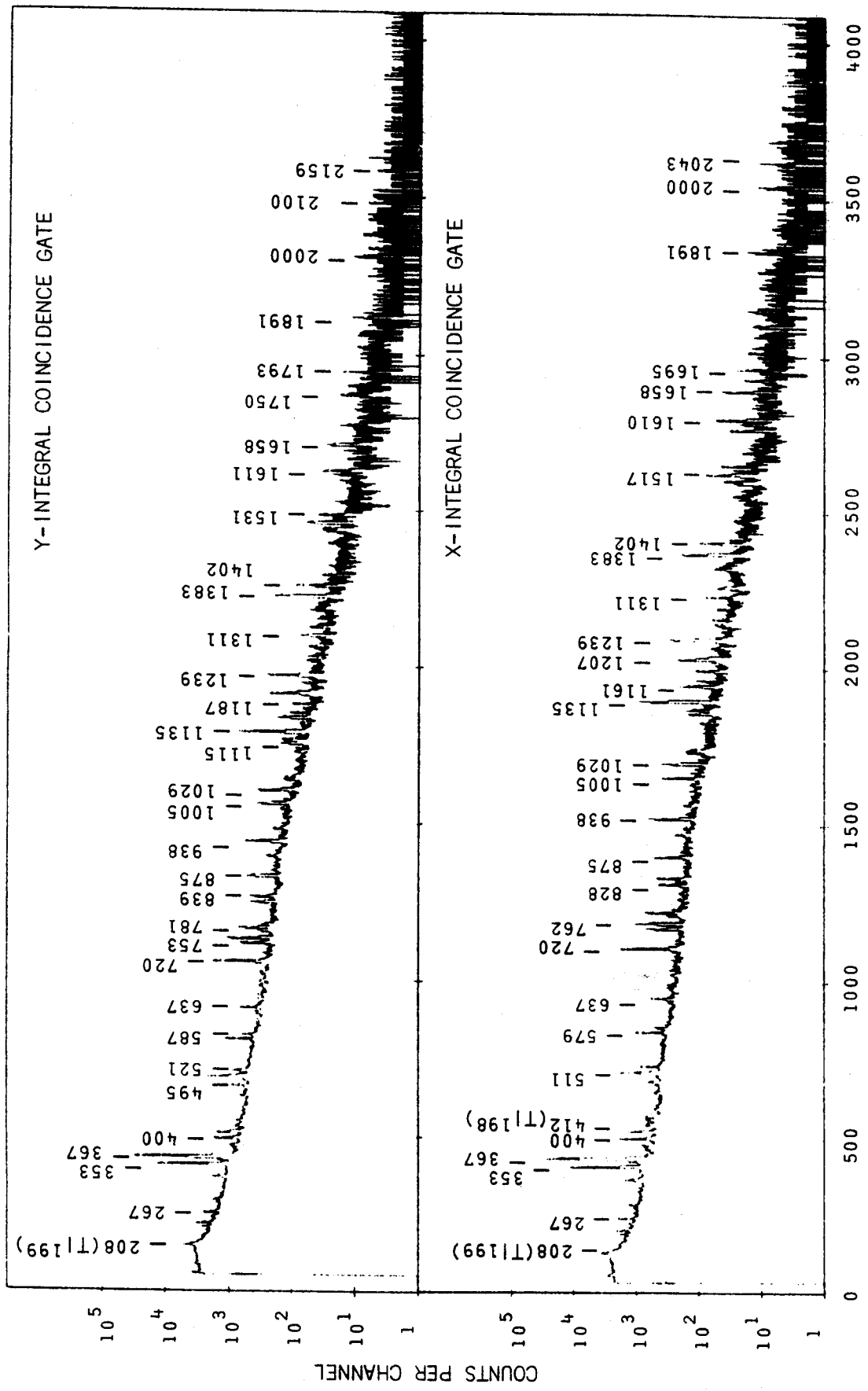

Figure VI-4. Integral coincidence spectra recorded during the two-dimensional γ-γ coincidence experiment on Pb^{199}. The Y-side spectrum was recorded by the 3.6% Ge(Li) detector and the X-side spectrum by the 2.5% Ge(Li) detector.

chemical separation was performed on the targets before counting.

A selection of the gated coincidence spectra obtained from this experiment are shown in Figure VI-5 and a summary of the coincidence relationships obtained is given in Table VI-4. The actual number of gated coincidence spectra used to determine these relationships was more than three times that shown in Figure VI-5. For all but the highest energy peaks we obtained not only the gated coincidence spectrum with background subtraction but also the gated coincidence spectrum without background subtraction as well as the spectra resulting from gating on the high and low backgrounds adjacent to the peaks. The latter spectra were useful in determining whether weak coincidence peaks in the spectra with background subtraction were legitimate or resulted from incomplete background subtraction. From this 2-d experiment we were able to obtain coincidence information on 80 of the 117 γ-transitions assigned to the decay of Pb^{199}.

In both Figure VI-5 and Table VI-4 we have included the results of gating on γ-rays belonging to impurities in the source and have identified these, where possible, in the gated coincidence spectra and in Table VI-4. We included the results of gating on these impurity peaks because they may be of use to someone working on the decay scheme of Tl^{199}, Pb^{198}, and Tl^{198}. Most of the impurity γ-rays could be assigned to one of these three isotopes, based on the coincidence relationships, even though some of them have not been reported in previous studies.

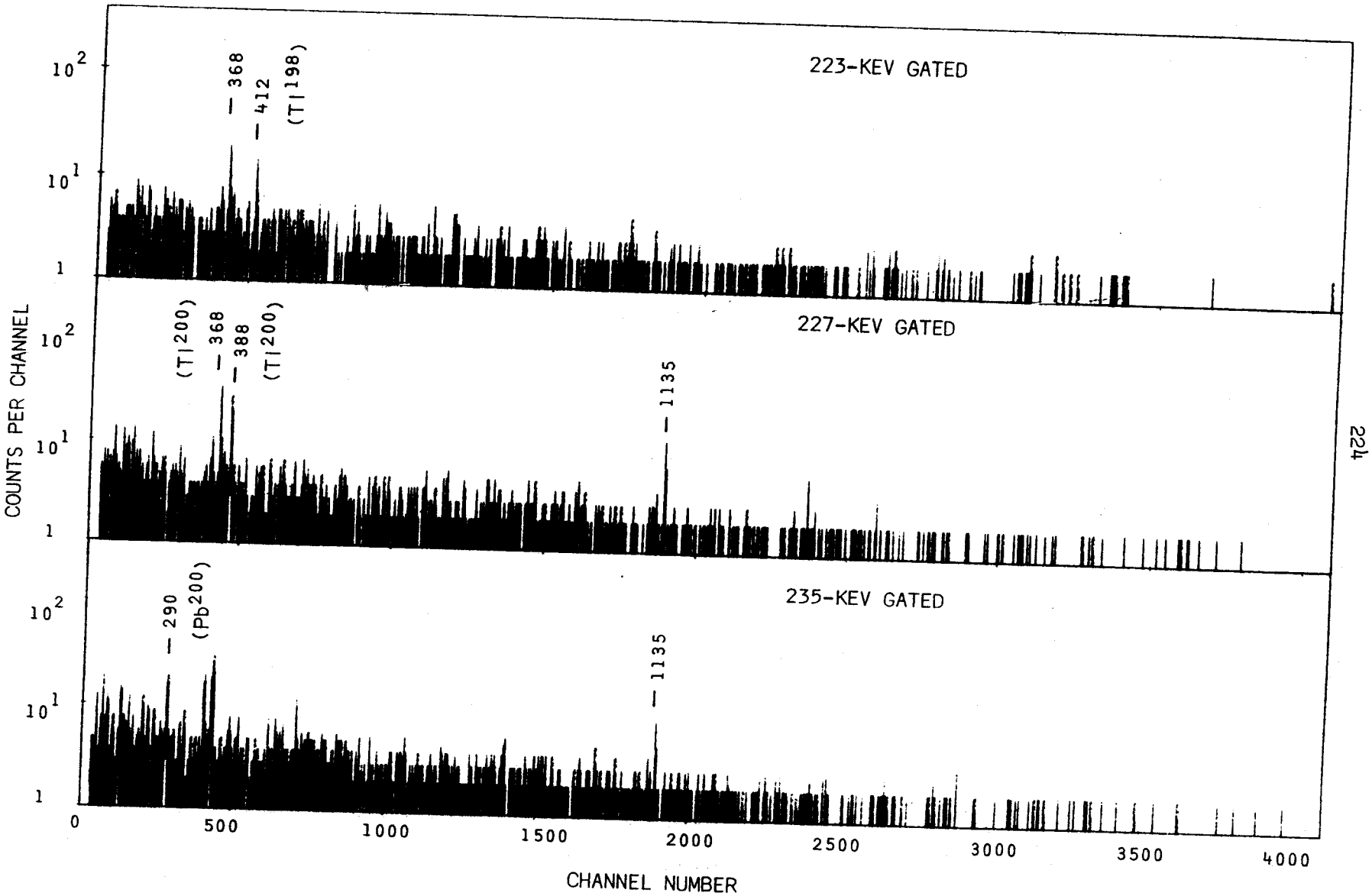

Figure VI-5. A selection of the gated coincidence spectra obtained from the two-dimensional γ-γ coincidence experiment on Pb^{199}. All gated spectra have had the background subtracted except where otherwise specified. All spectra were obtained by gating on the *Y*-side (3.6% detector) and displaying the *X*-side (2.5% detector).

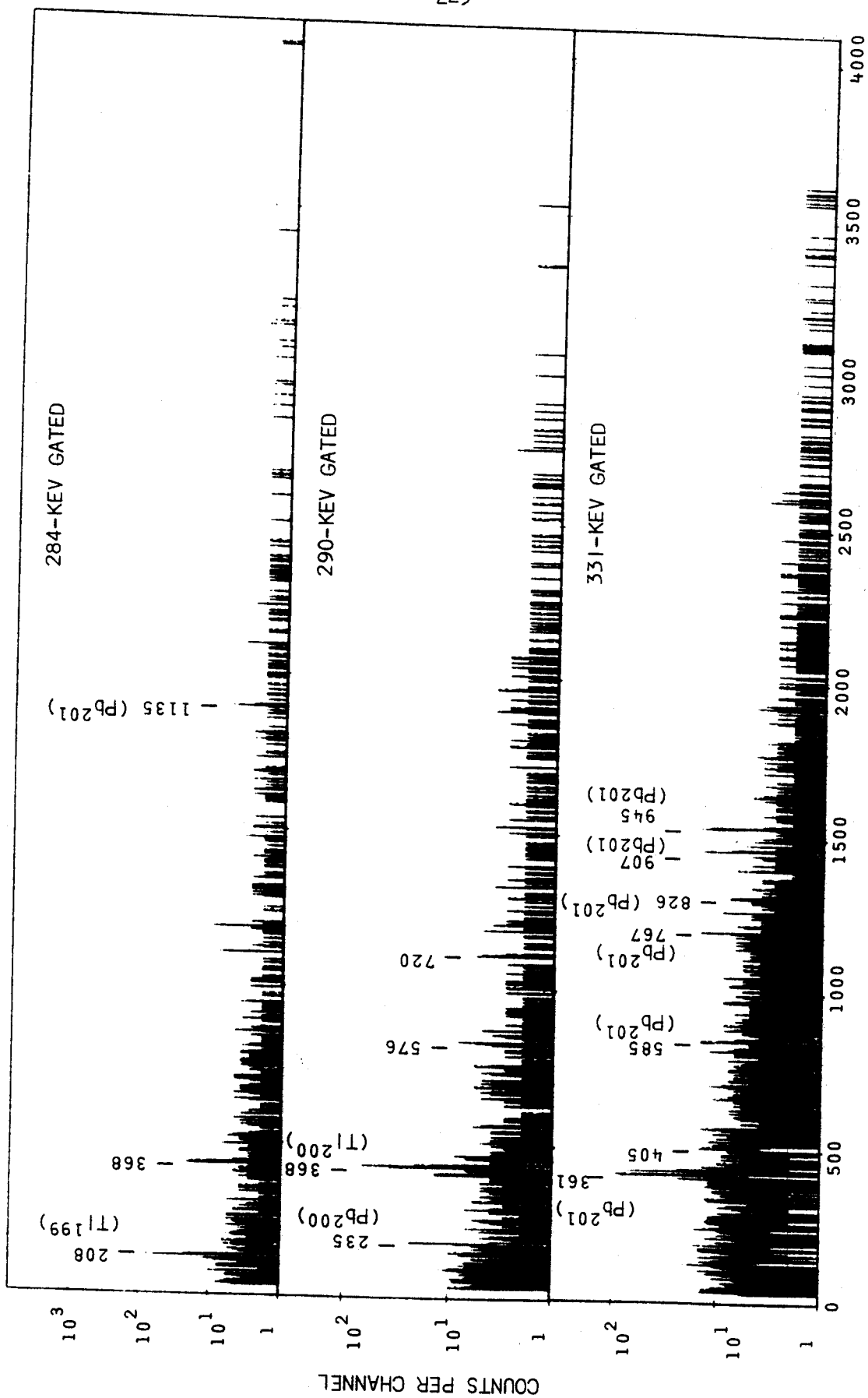

Figure VI-5 (cont'd)

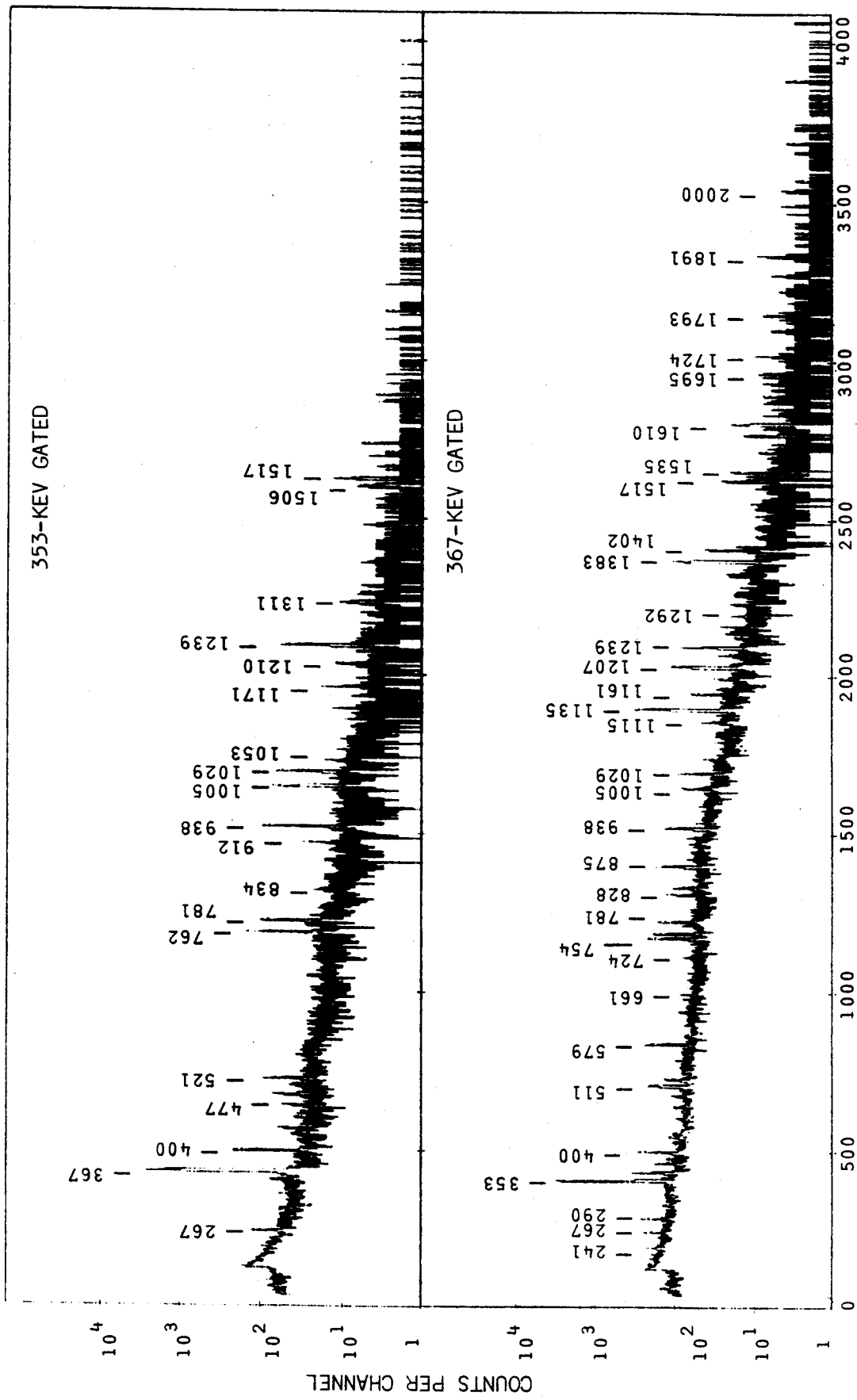

Figure VI-5 (cont'd)

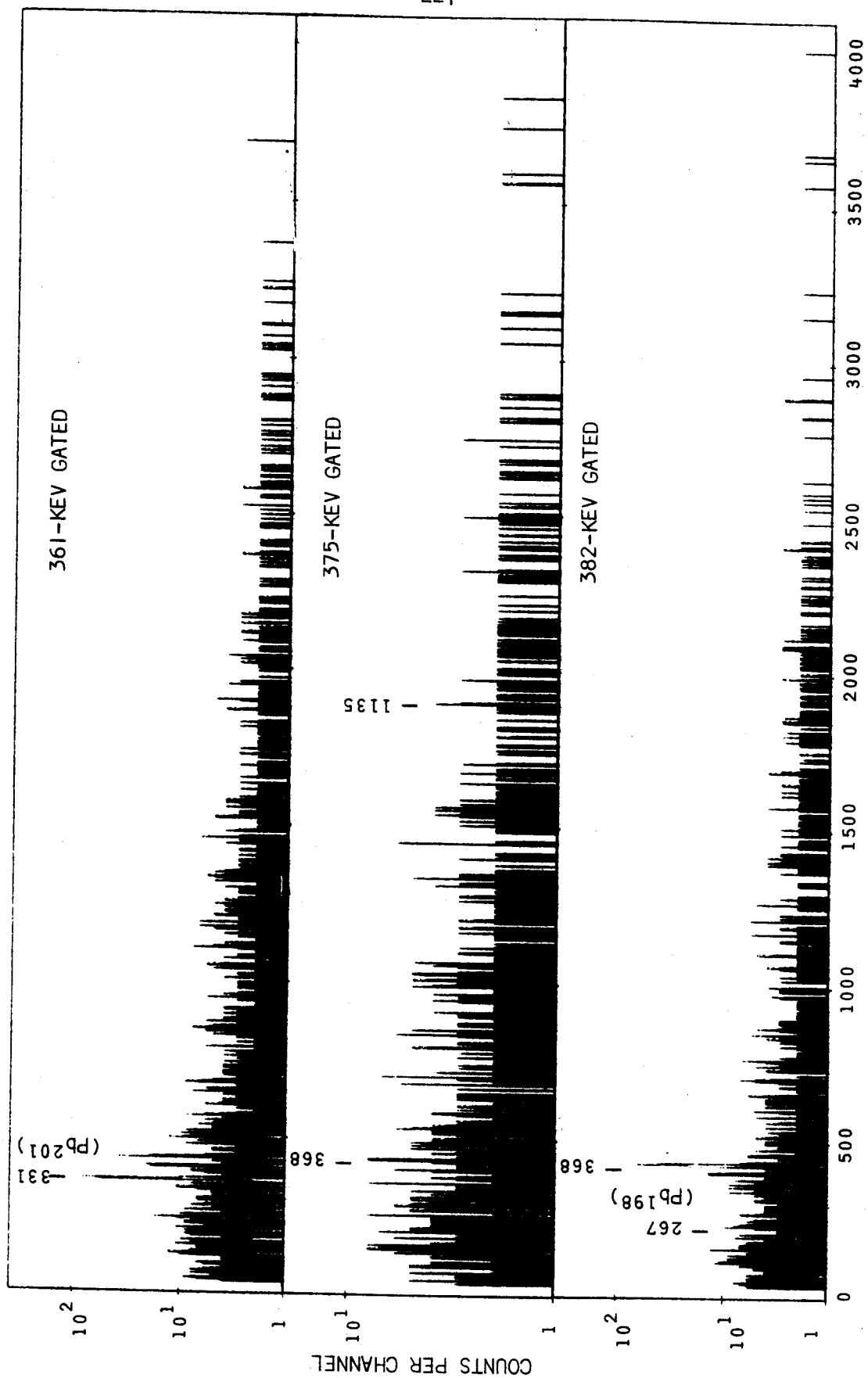

Figure VI-5 (cont'd)

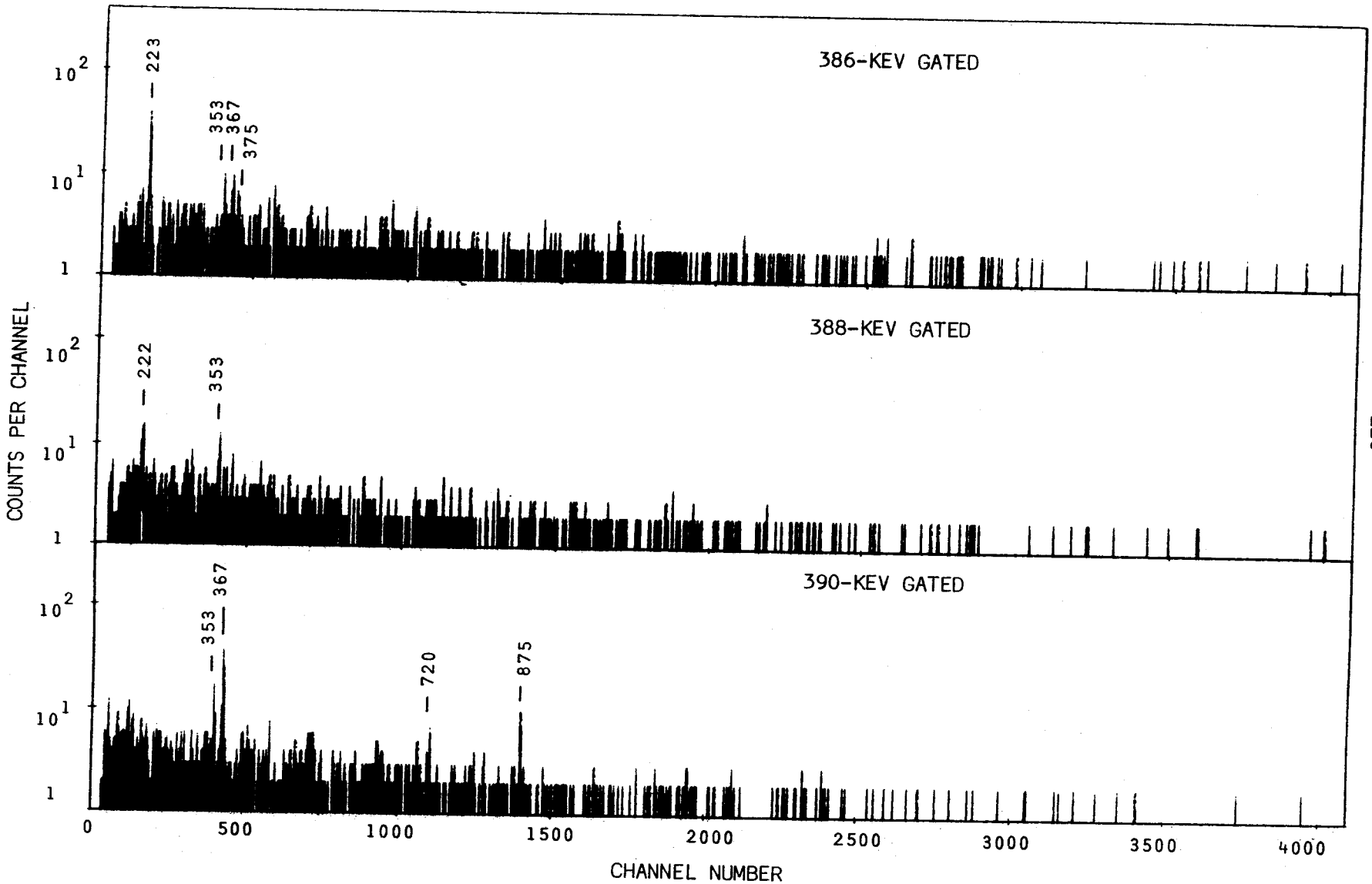

Figure VI-5 (cont'd)

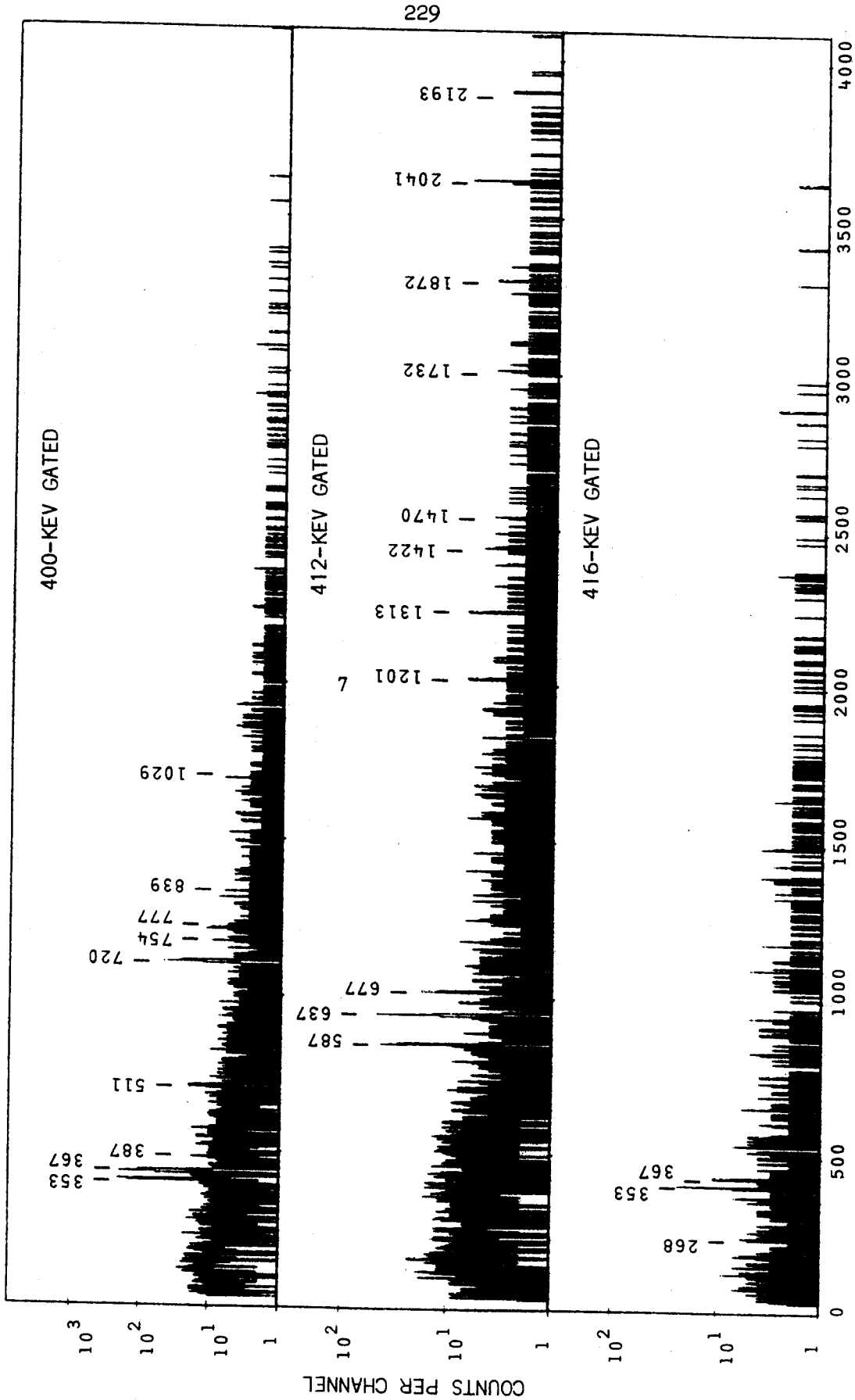

Figure VI-5 (cont'd)

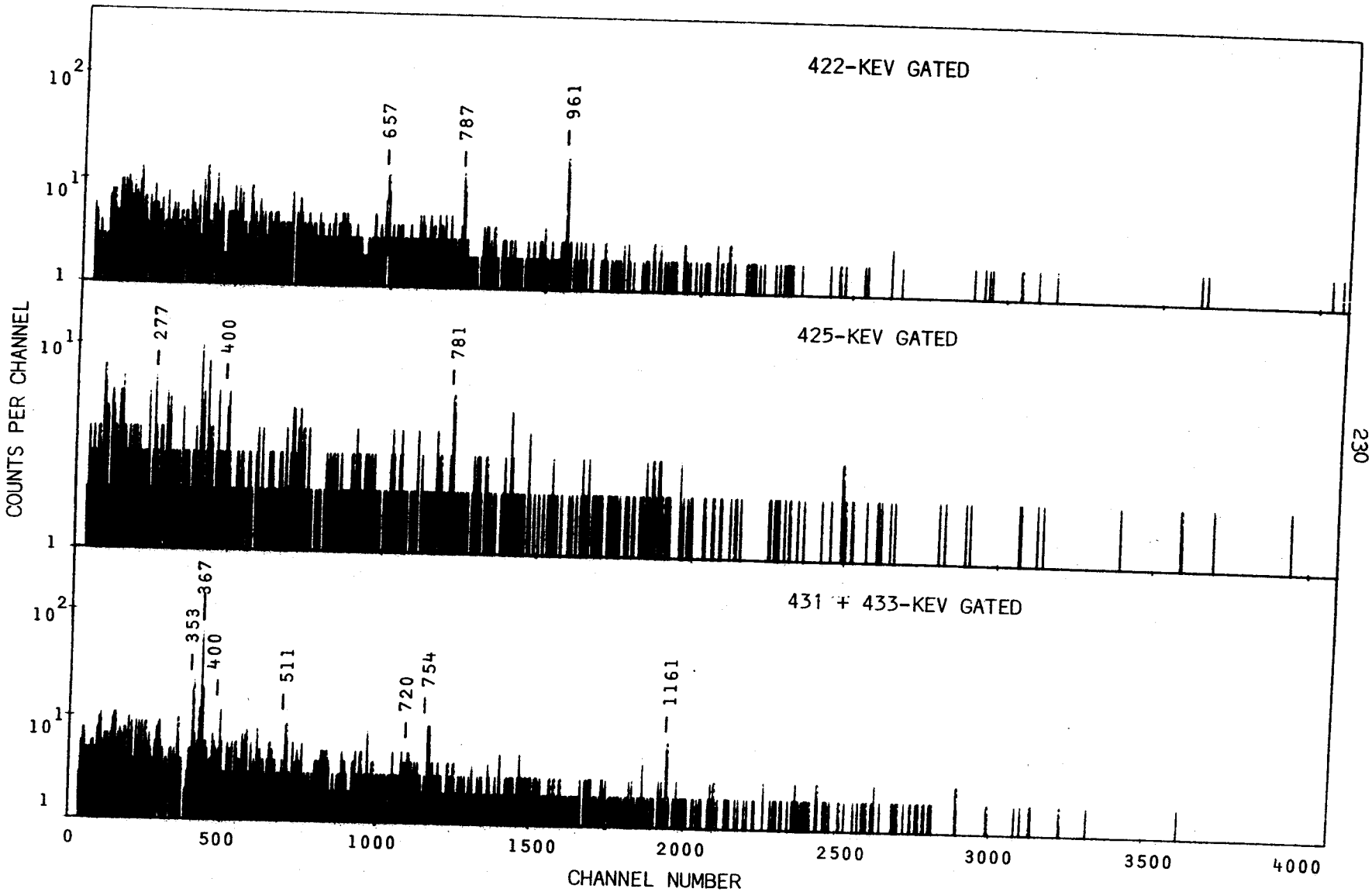

Figure VI-5 (cont'd)

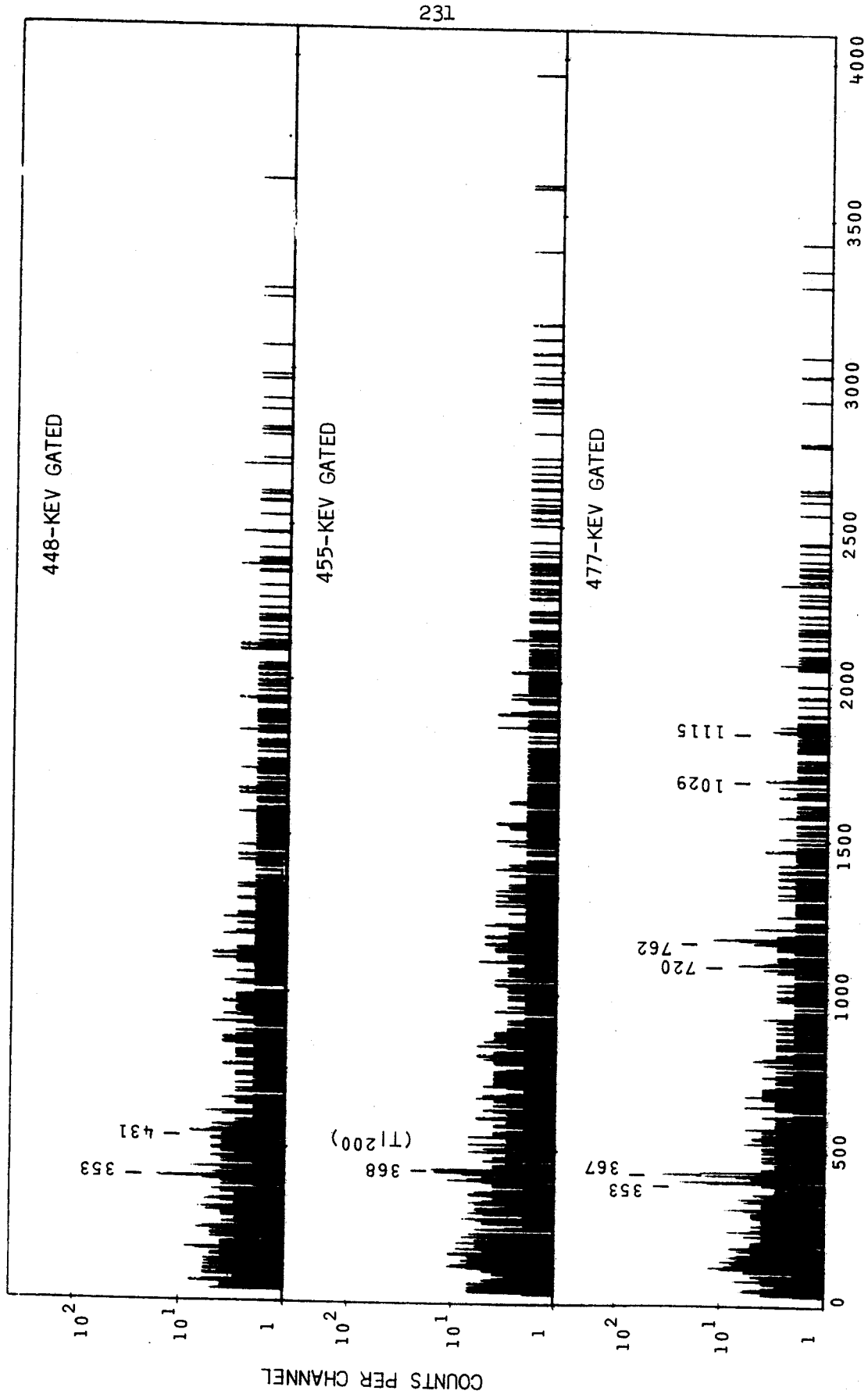

Figure VI-5 (cont'd)

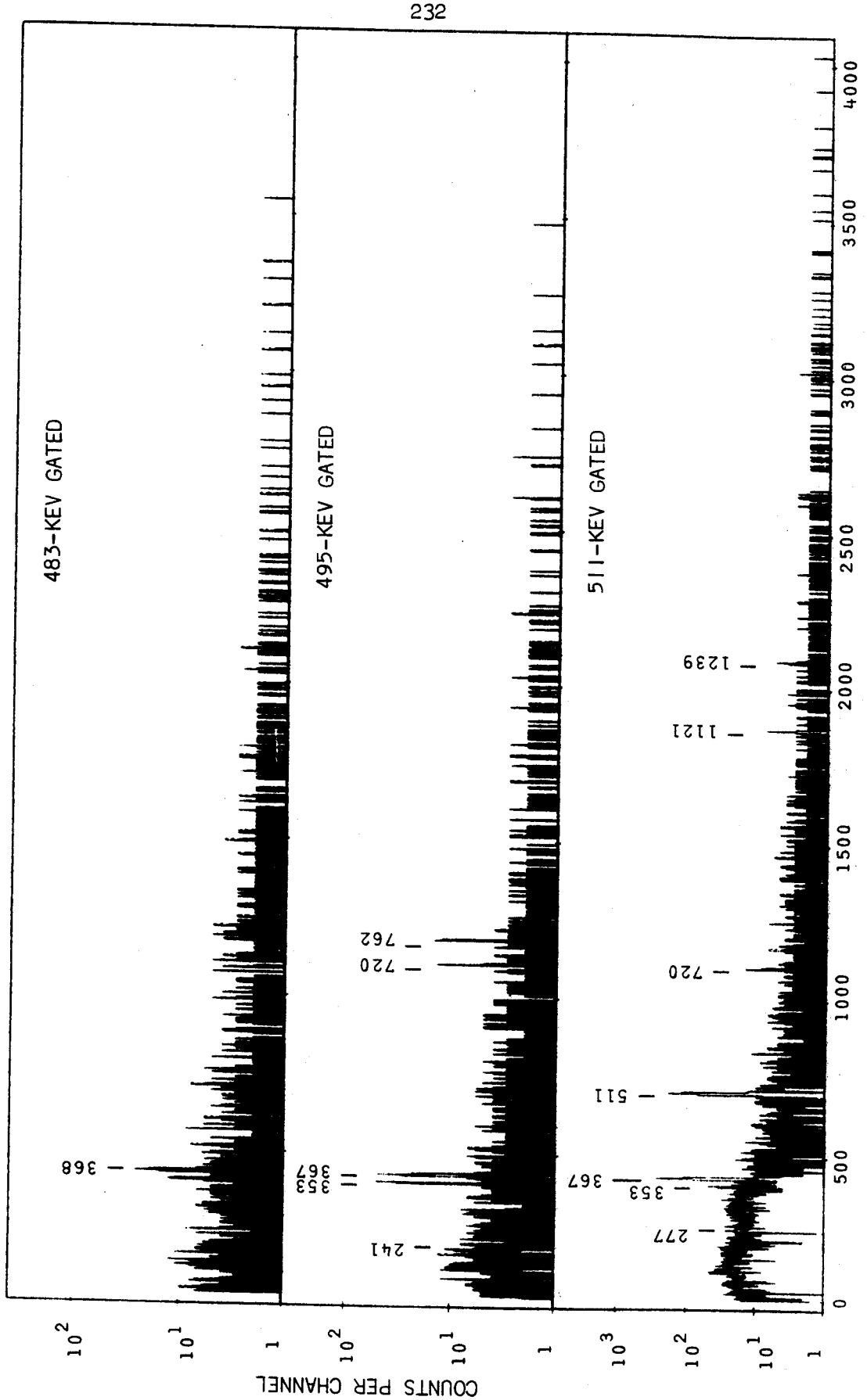

Figure VI-5 (cont'd)

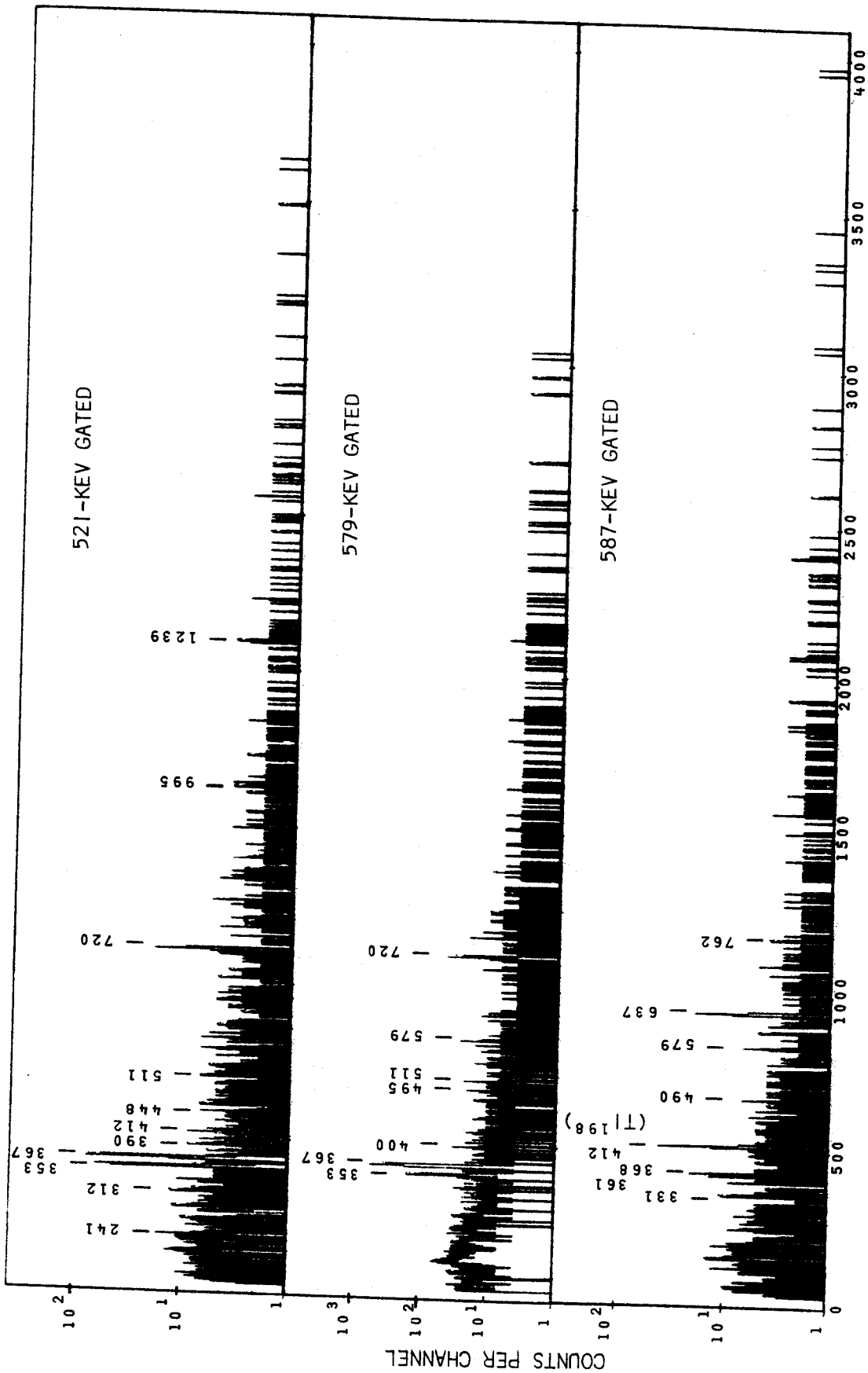

Figure VI-5 (cont'd)

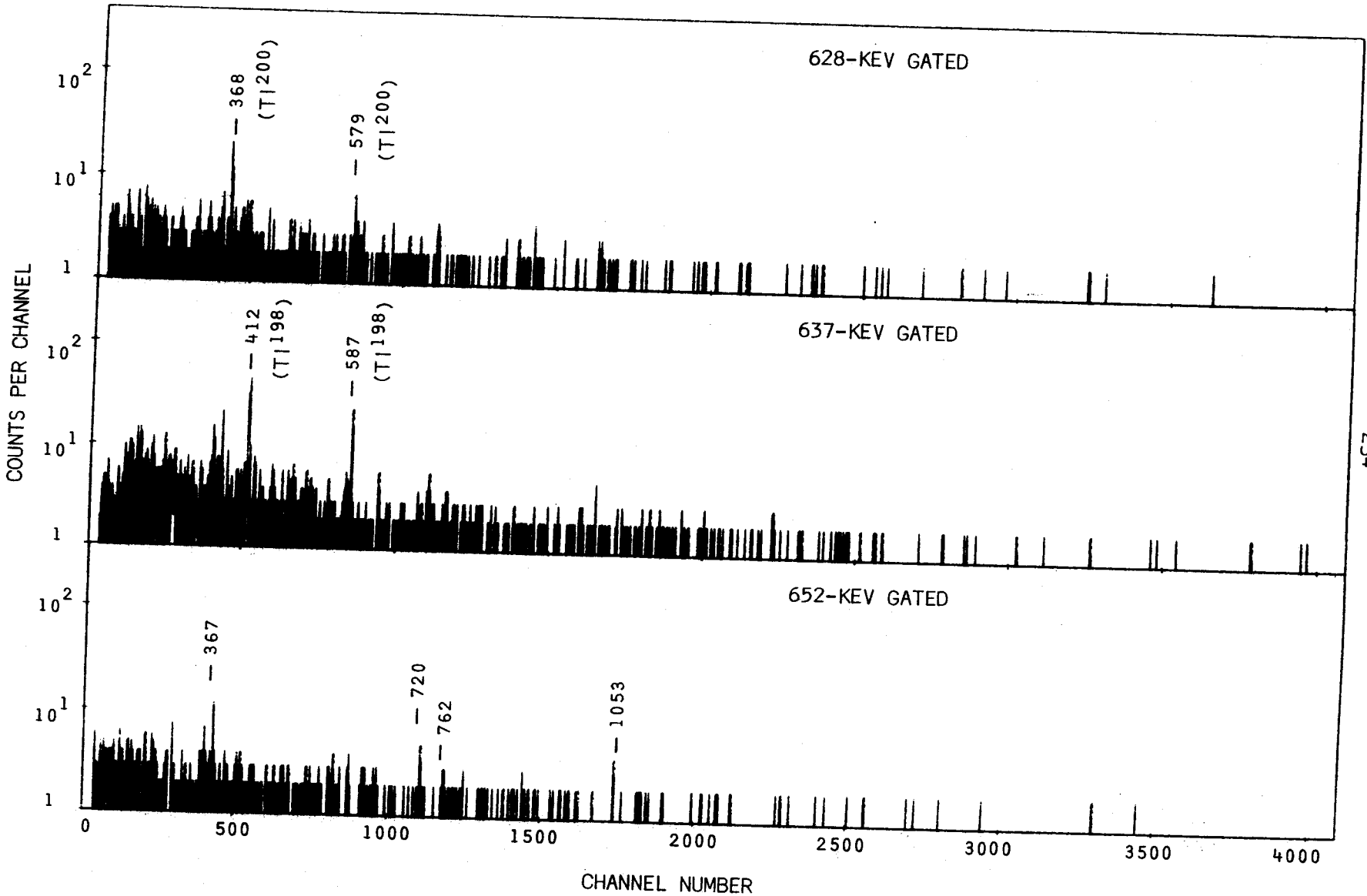

Figure VI-5 (cont'd)

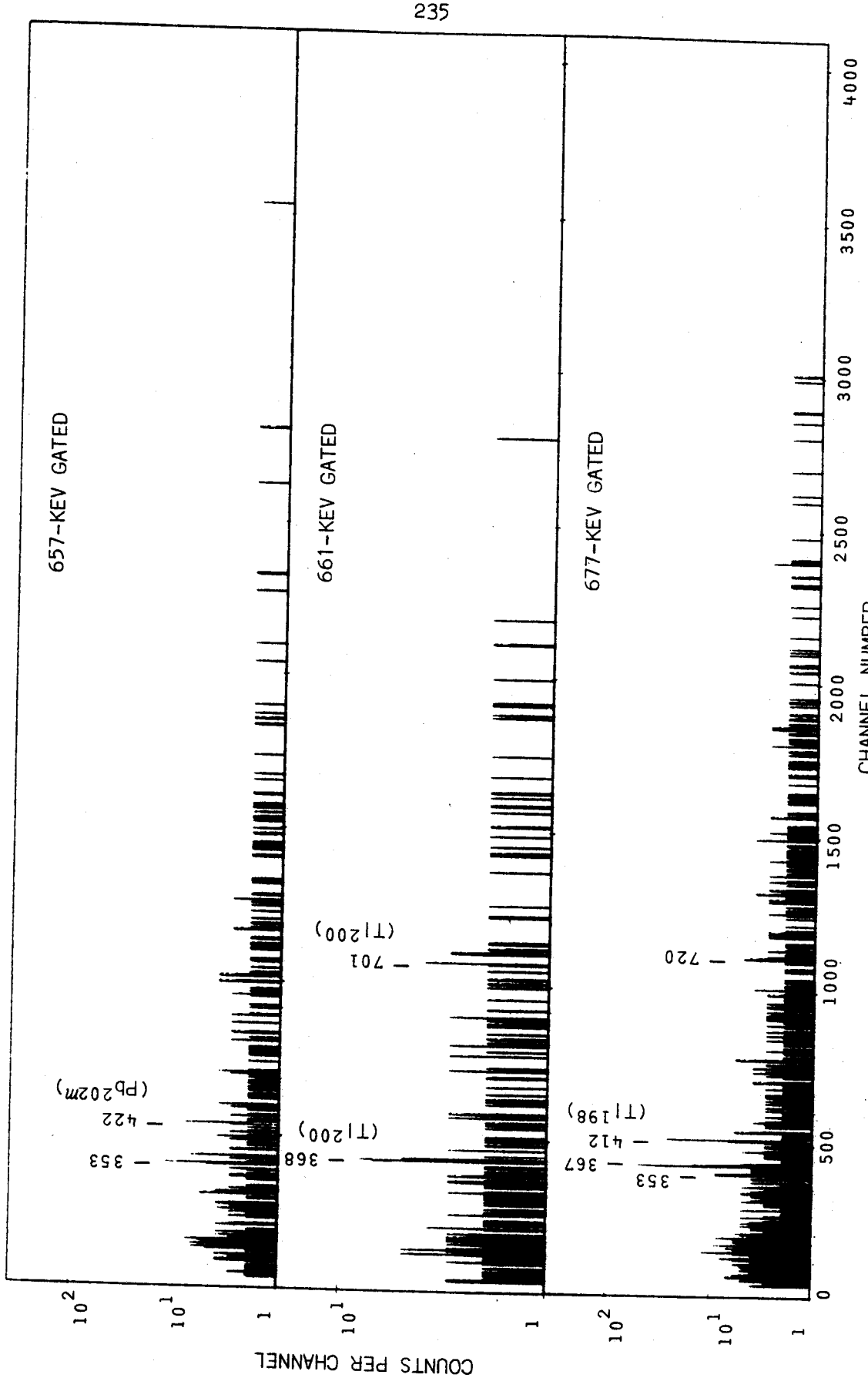

Figure VI-5 (cont'd)

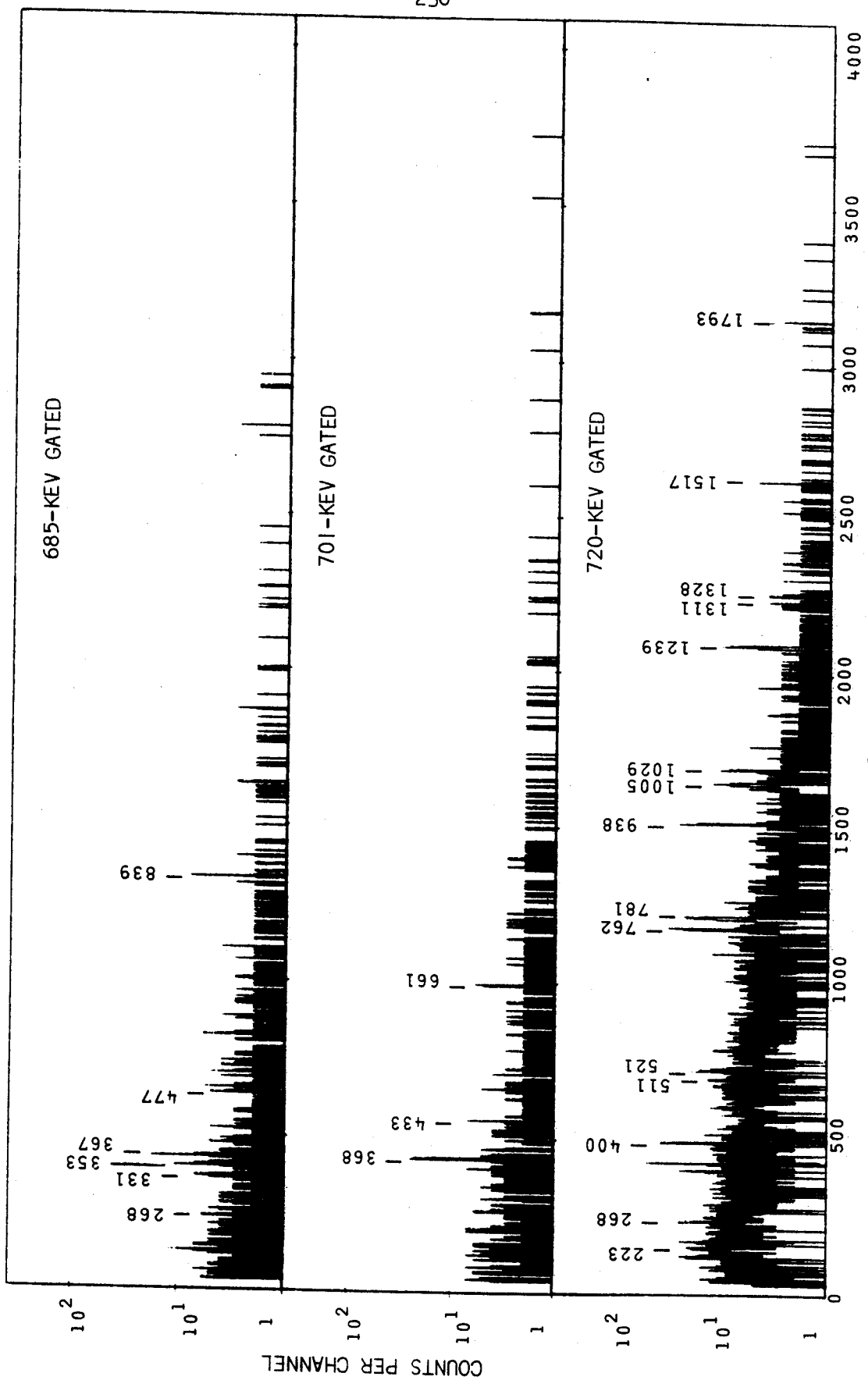

Figure VI-5 (cont'd)

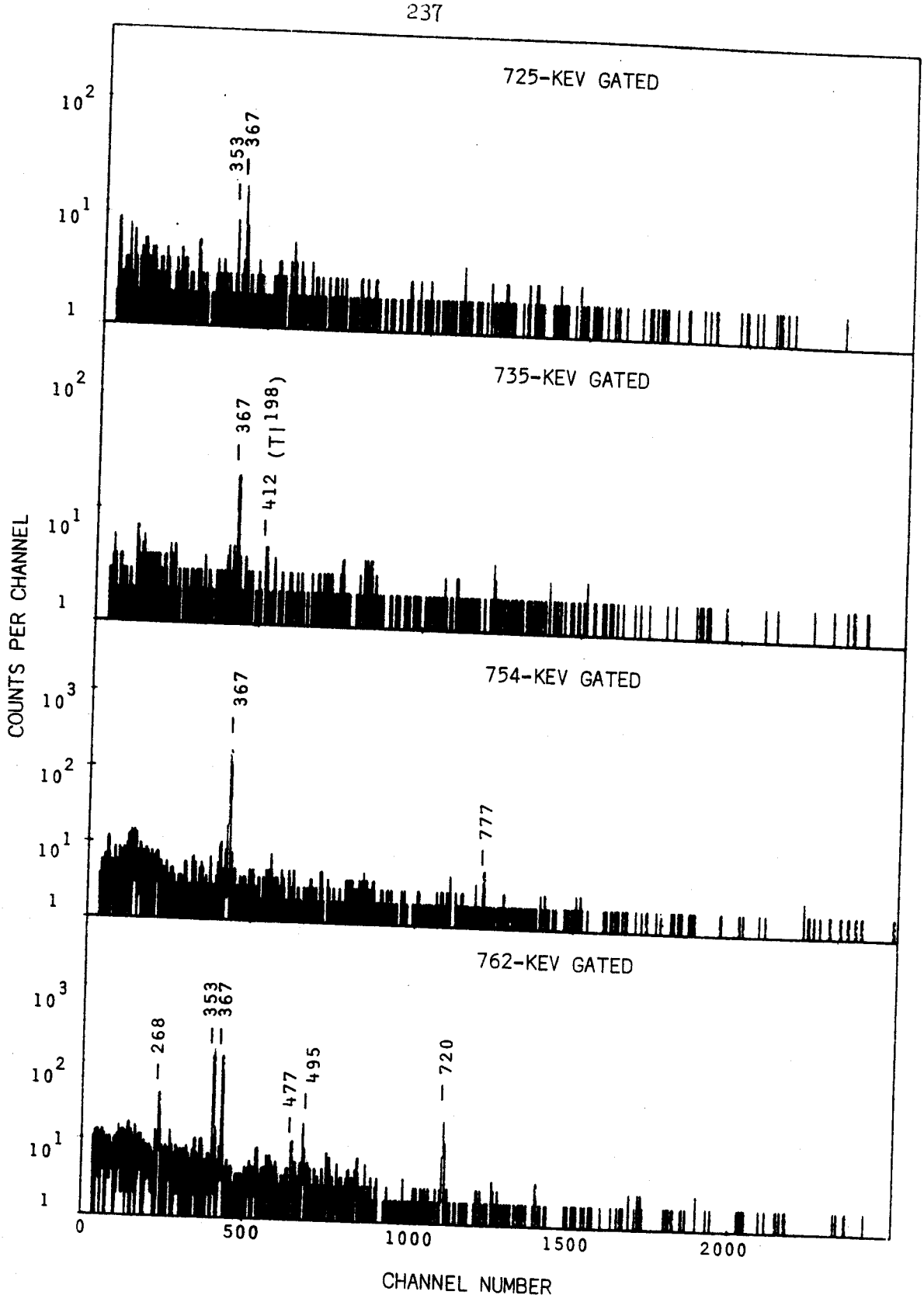

Figure VI-5 (cont'd)

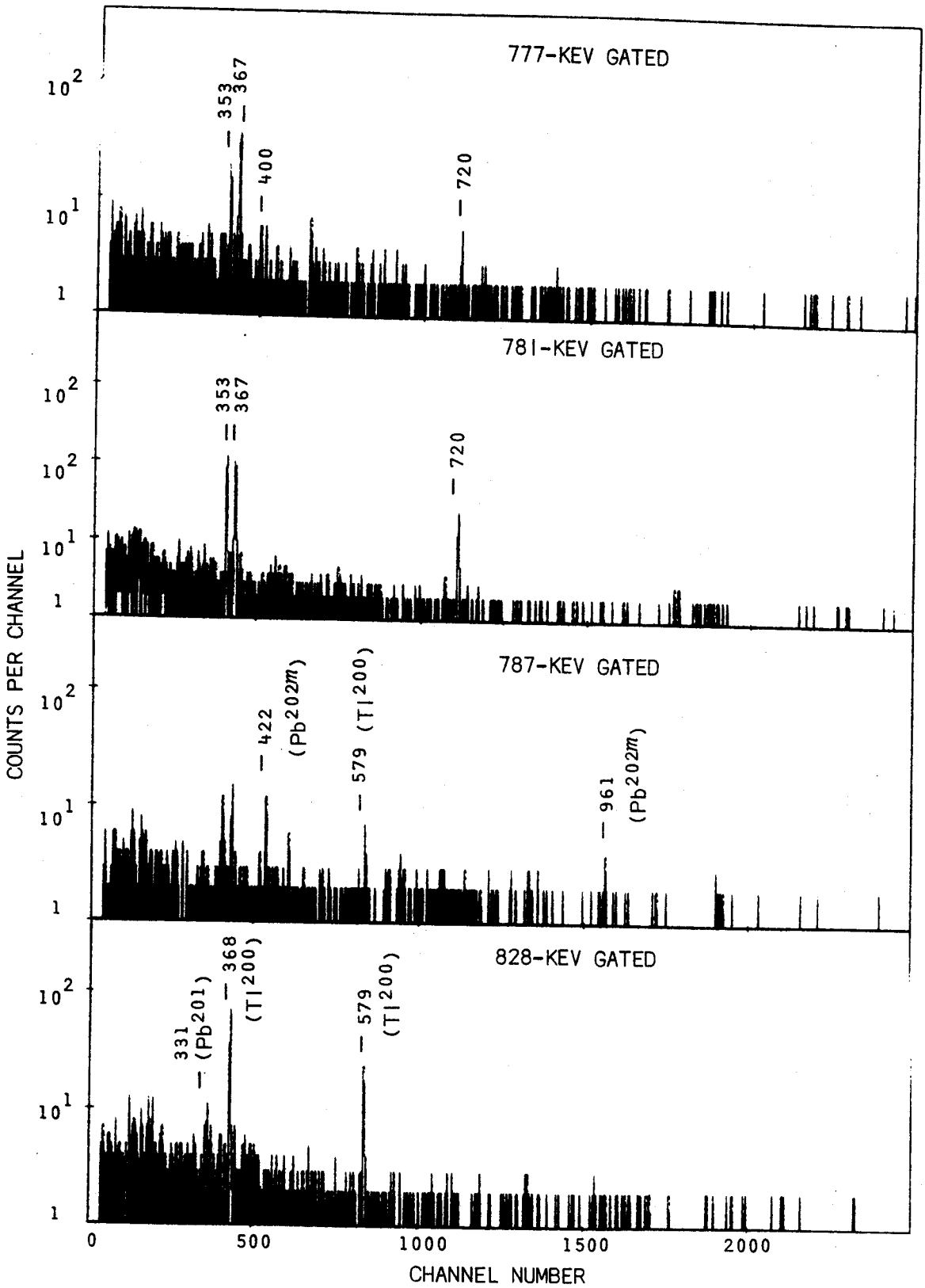

Figure VI-5 (cont'd)

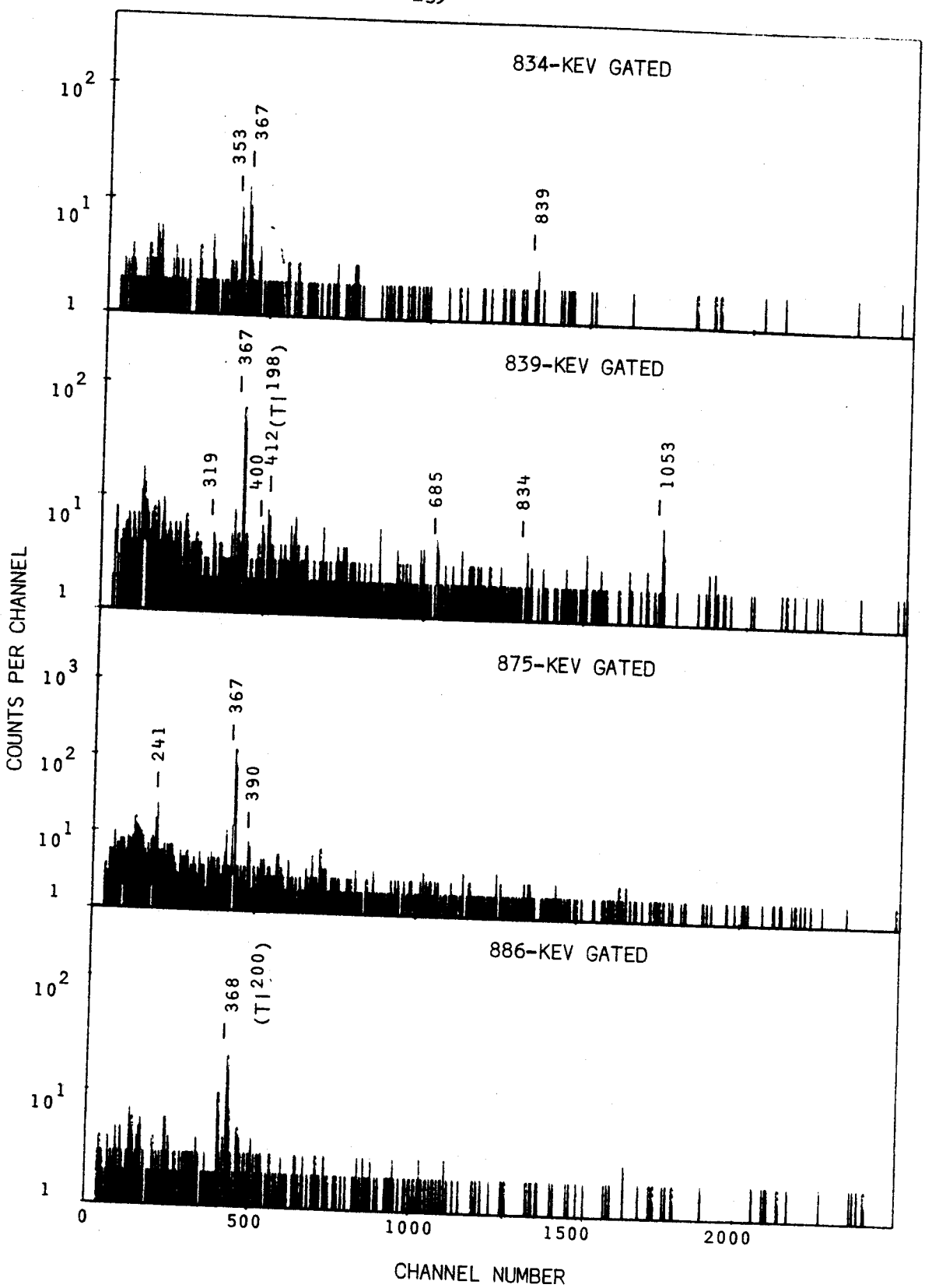

Figure VI-5 (cont'd)

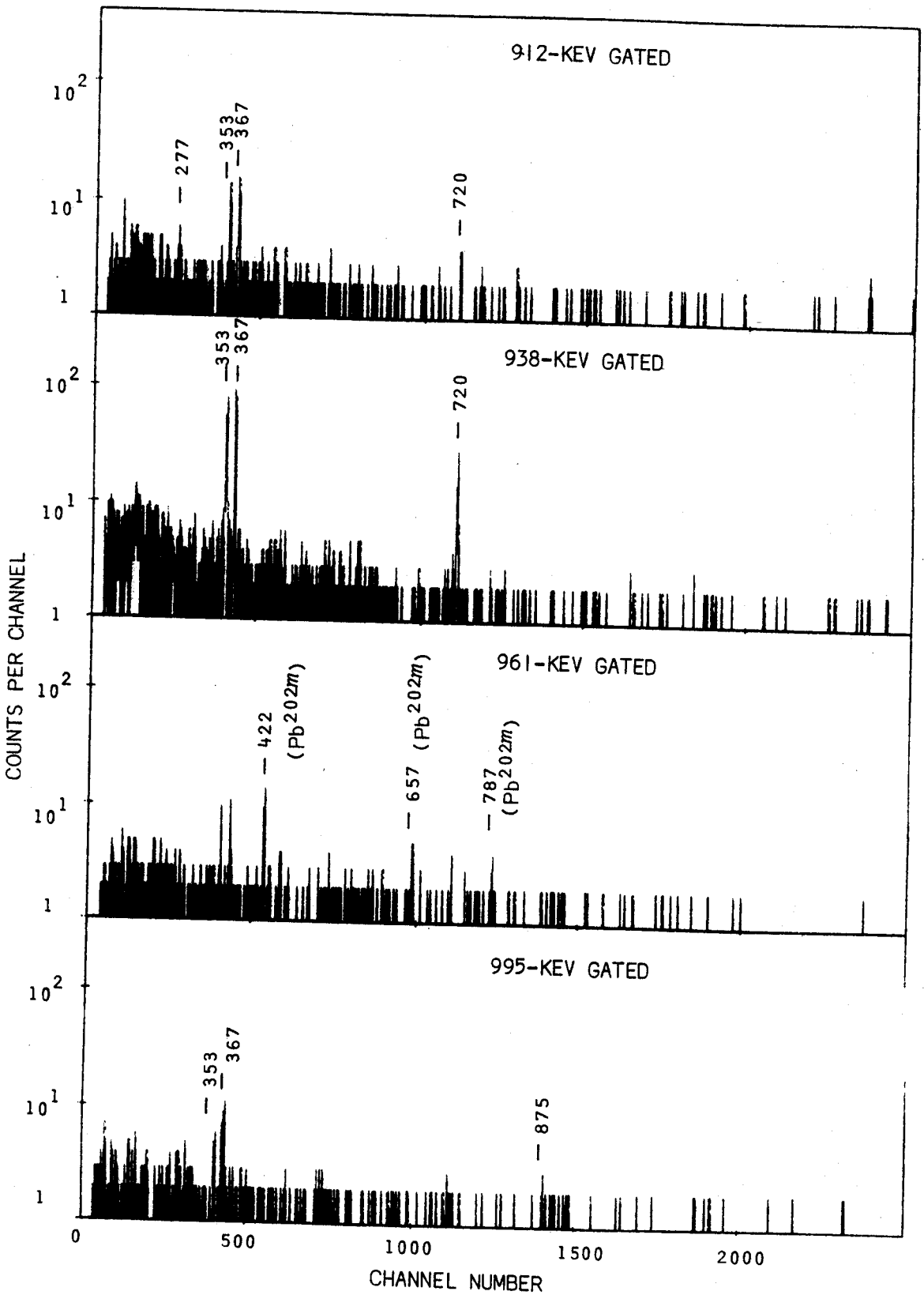

Figure VI-5 (cont'd)

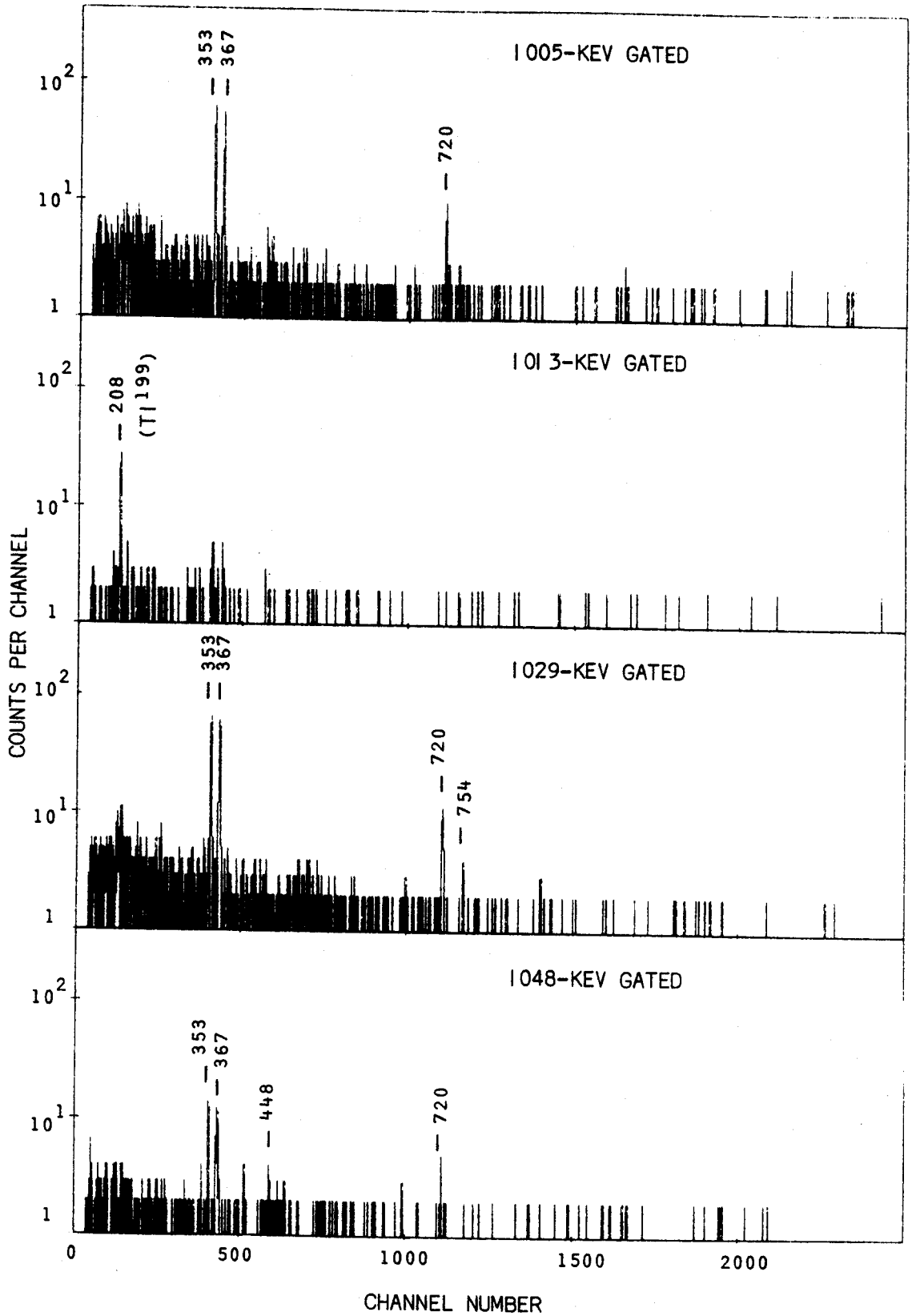

Figure VI-5 (cont'd)

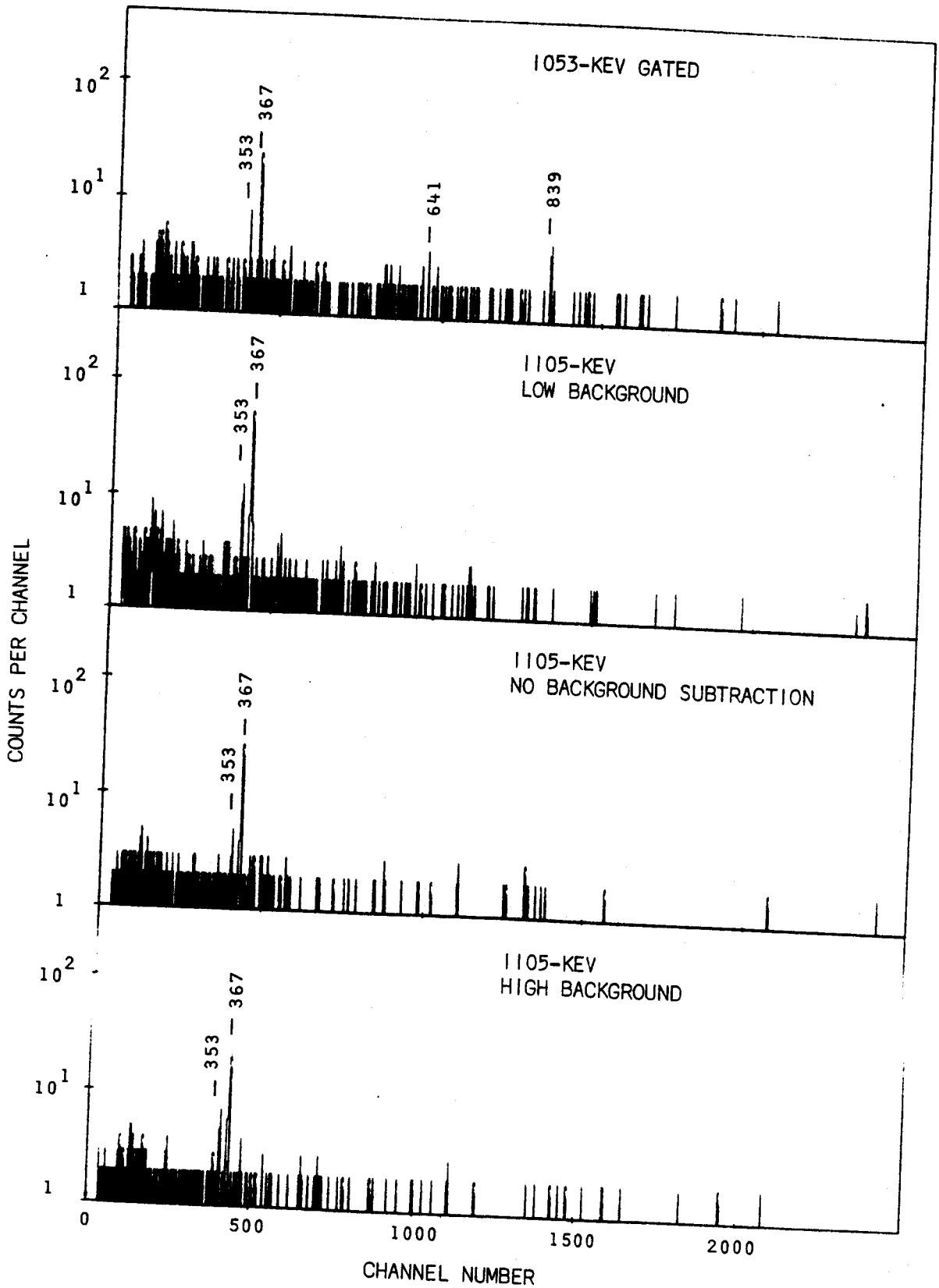

Figure VI-5 (cont'd)

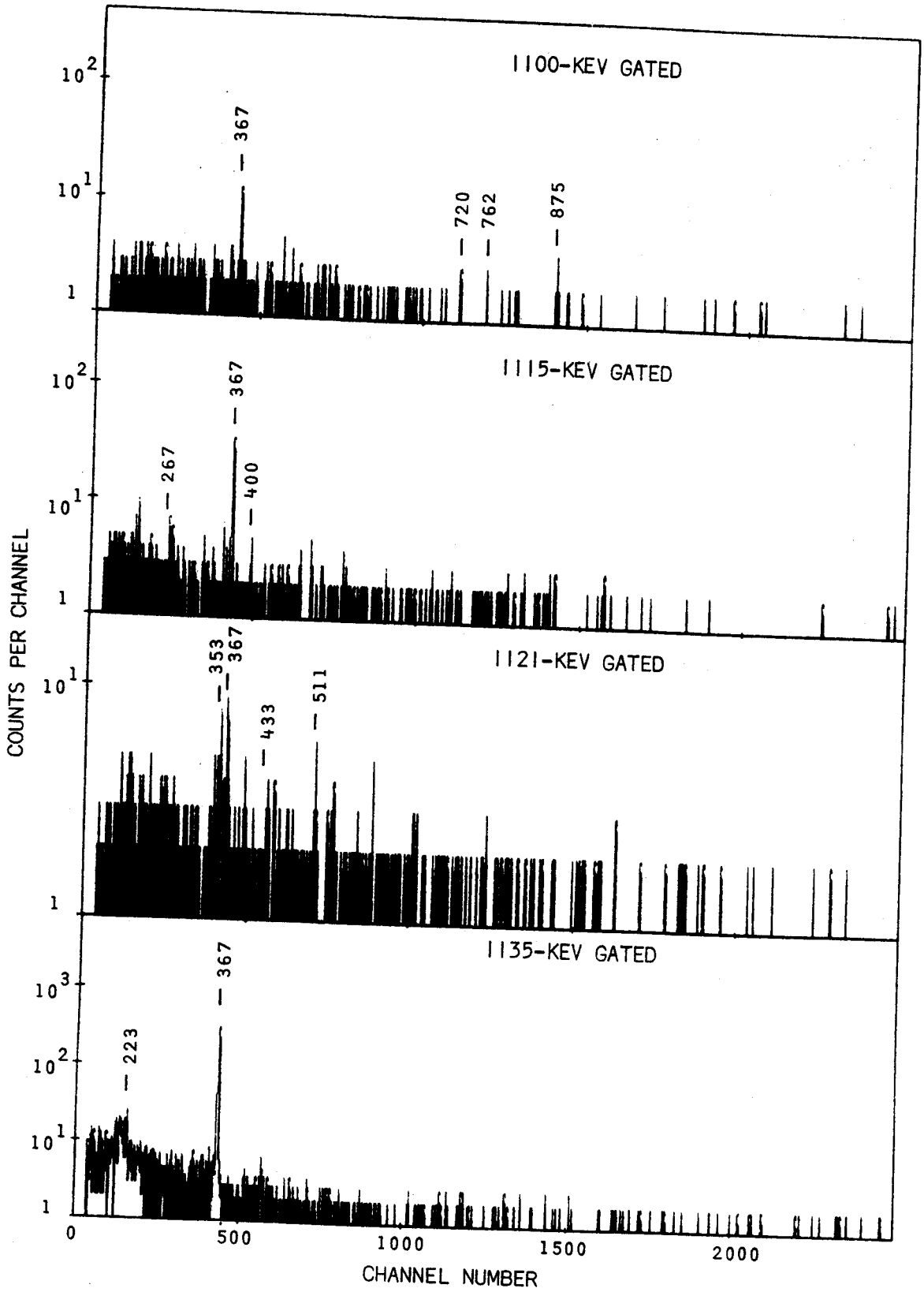

Figure VI-5 (cont'd)

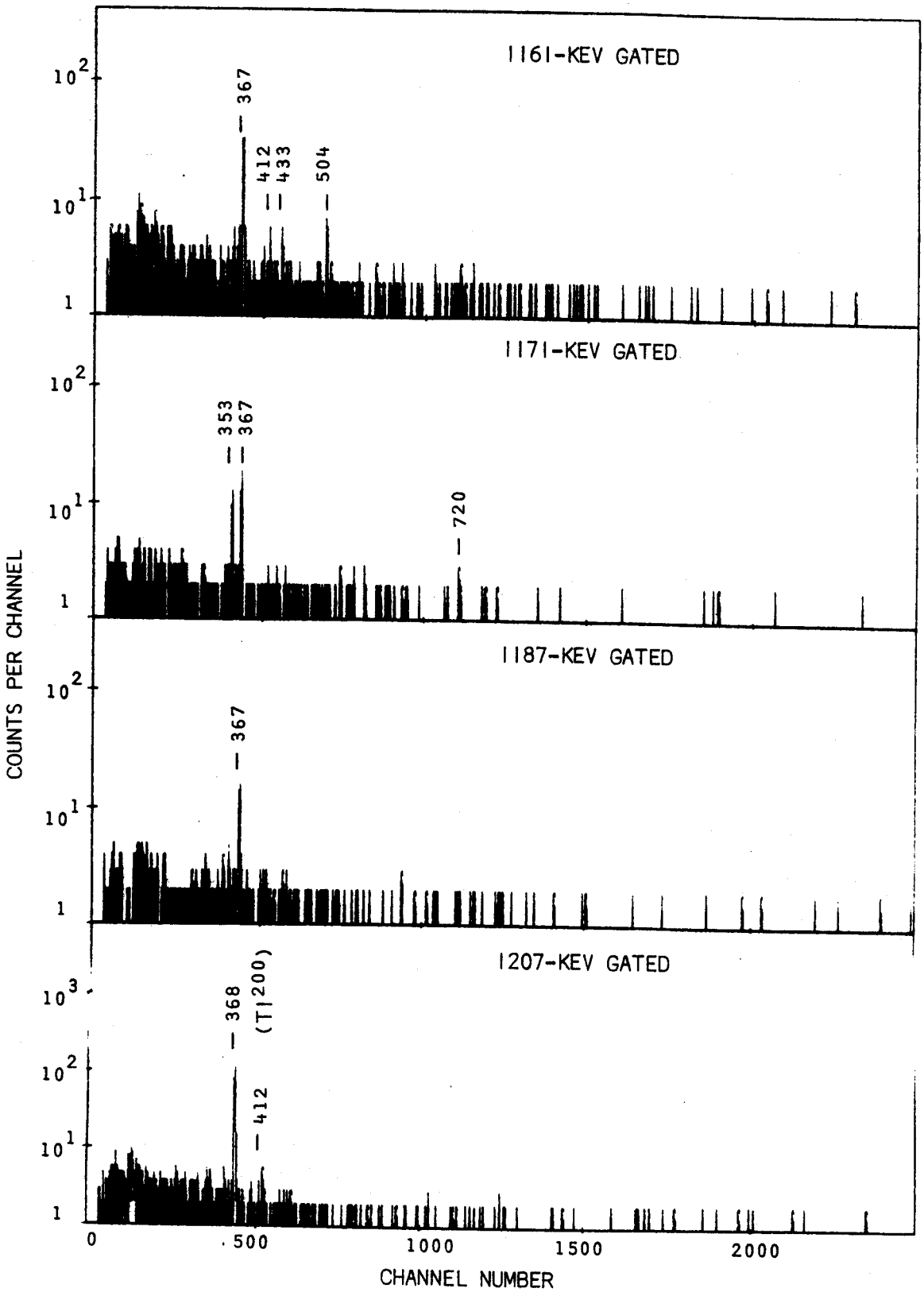

Figure VI-5 (cont'd)

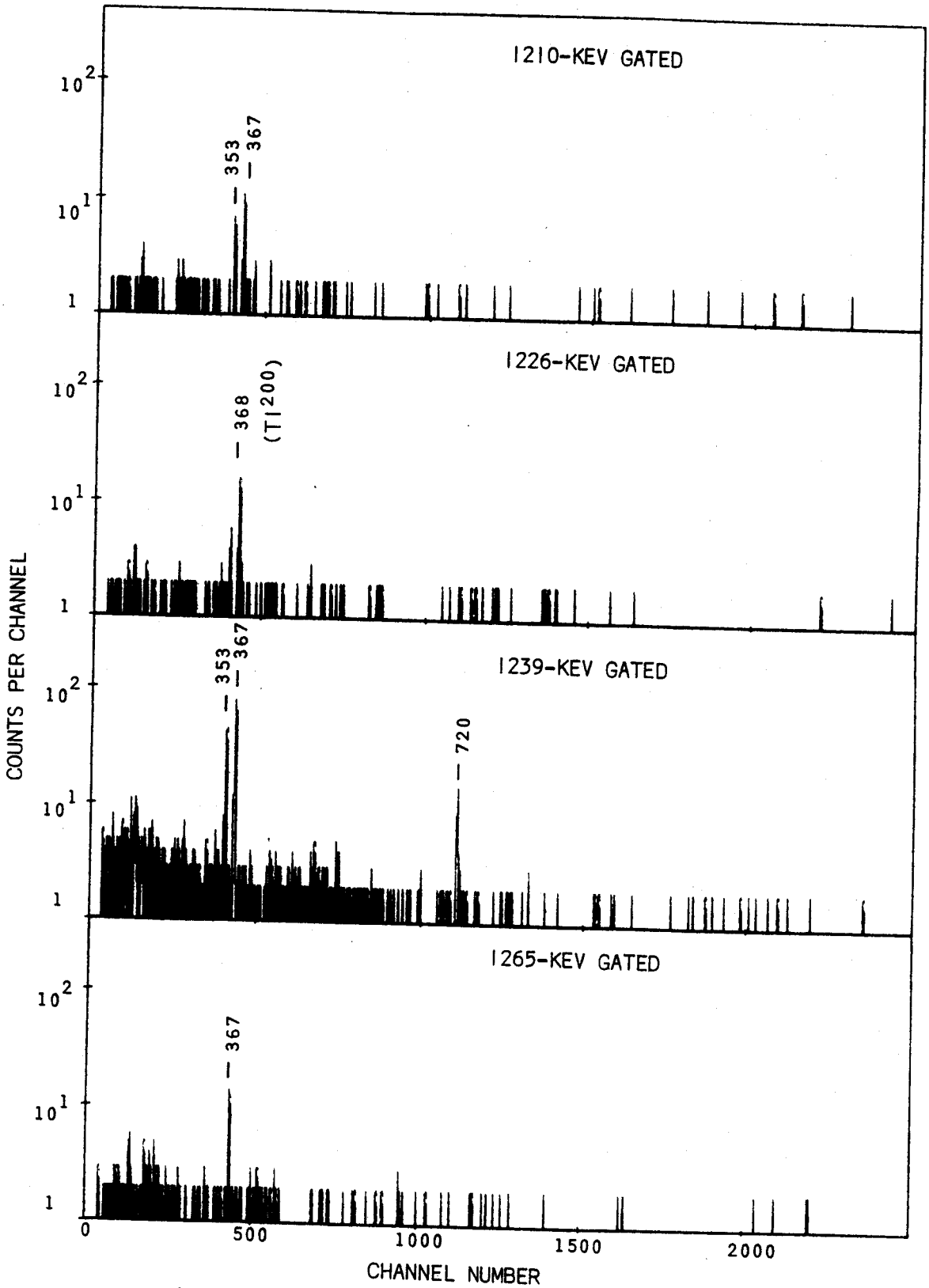

Figure VI-5 (cont'd)

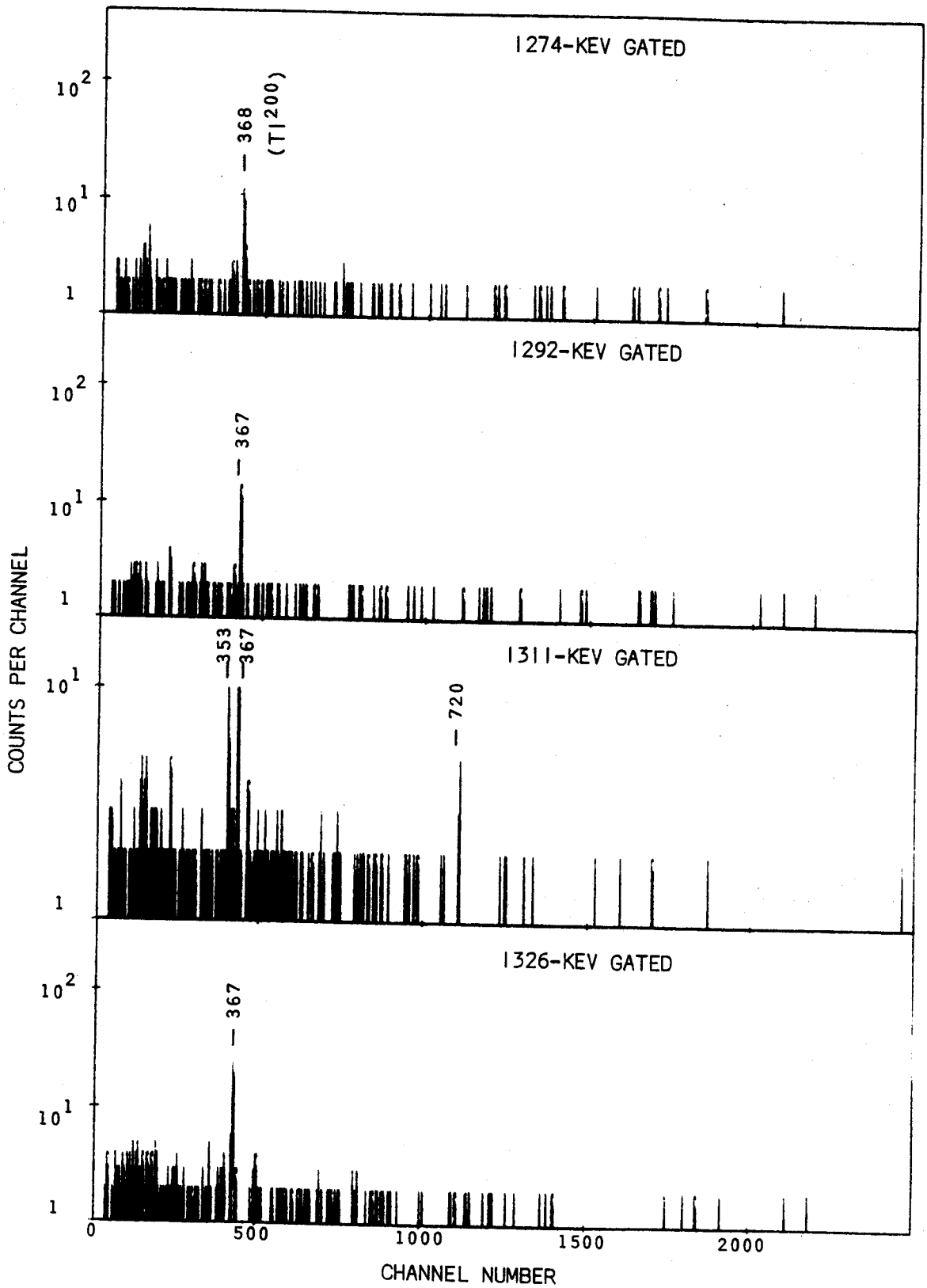

Figure VI-5 (cont'd)

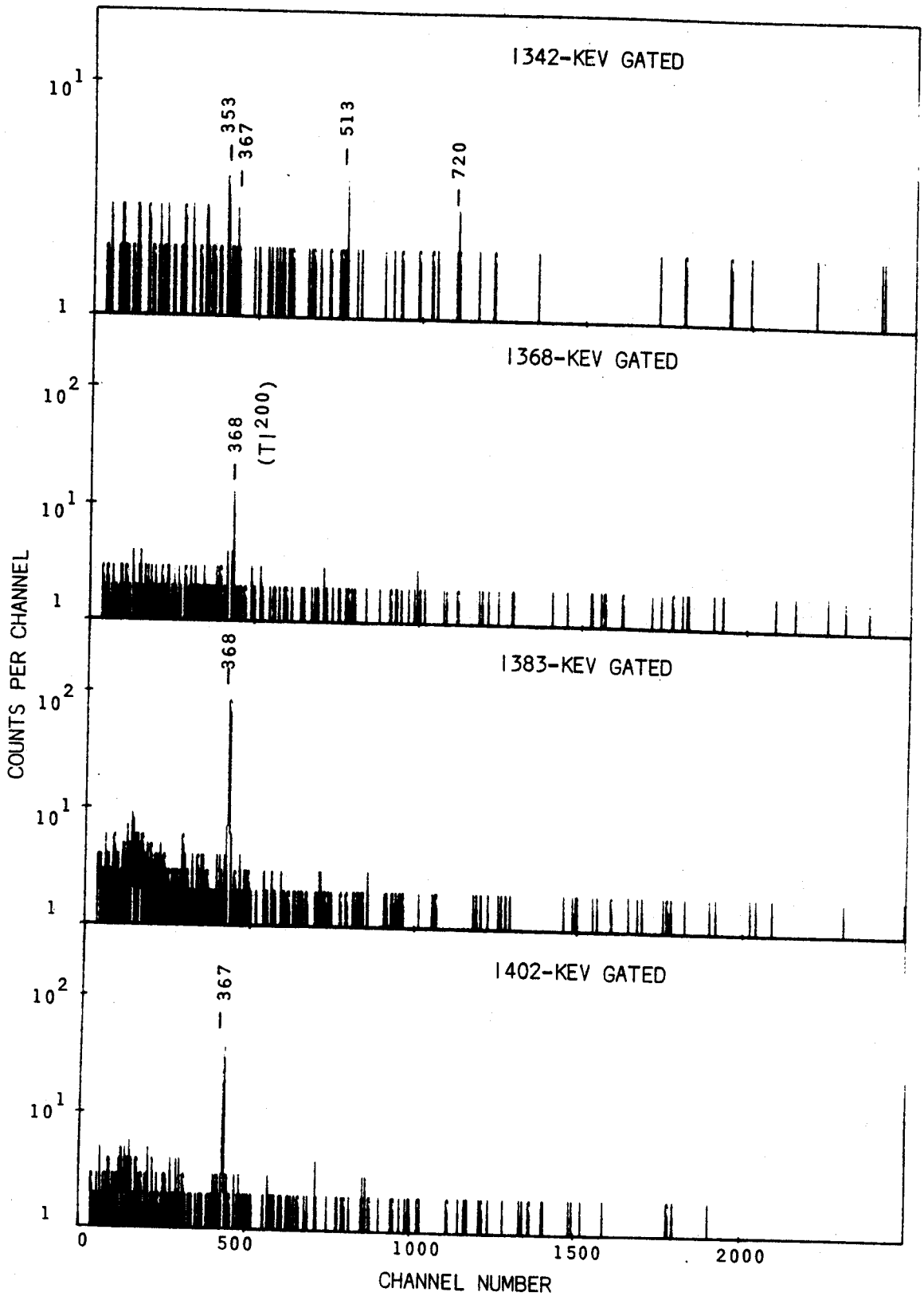

Figure VI-5 (cont'd)

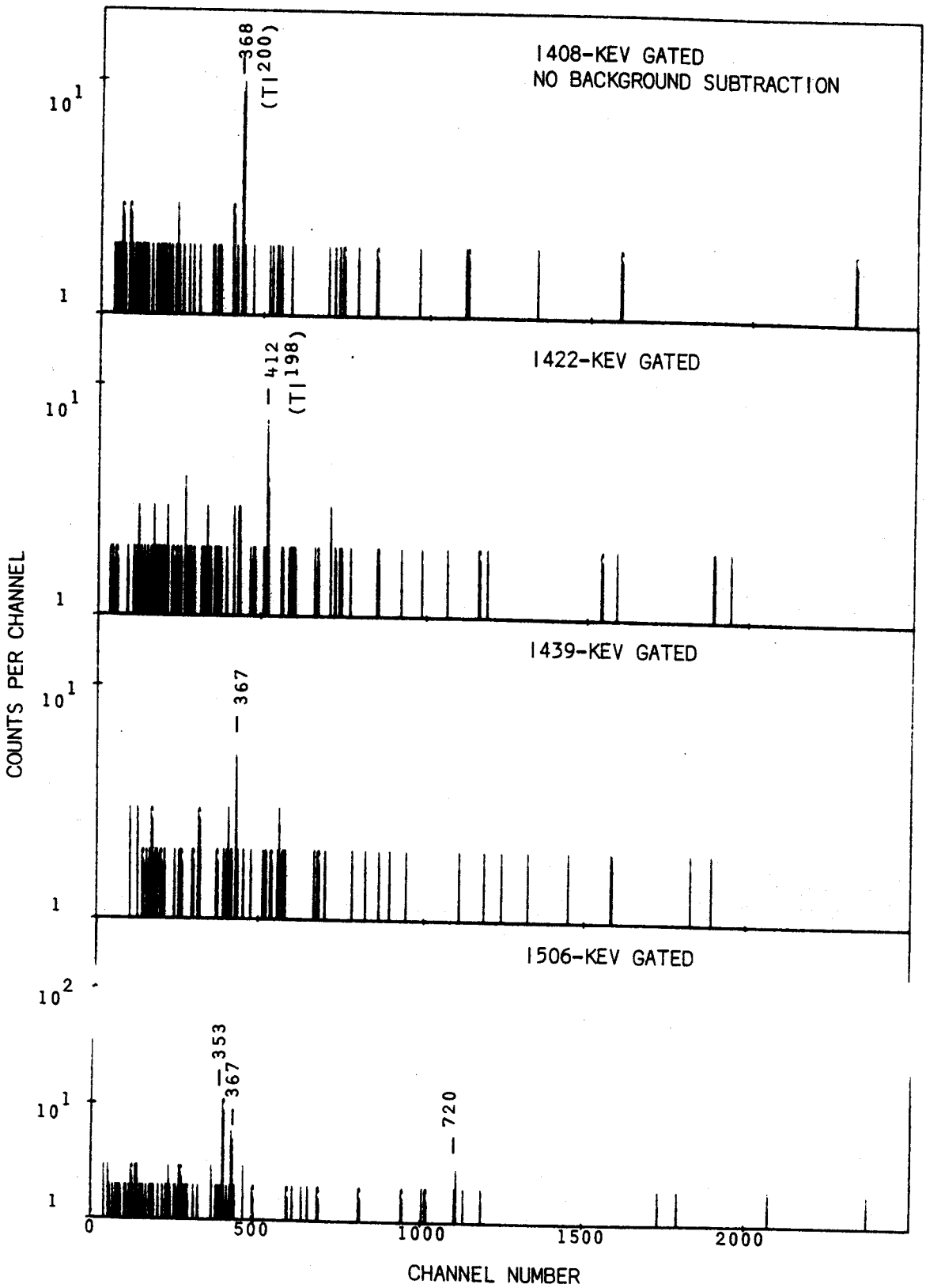

Figure VI-5 (cont'd)

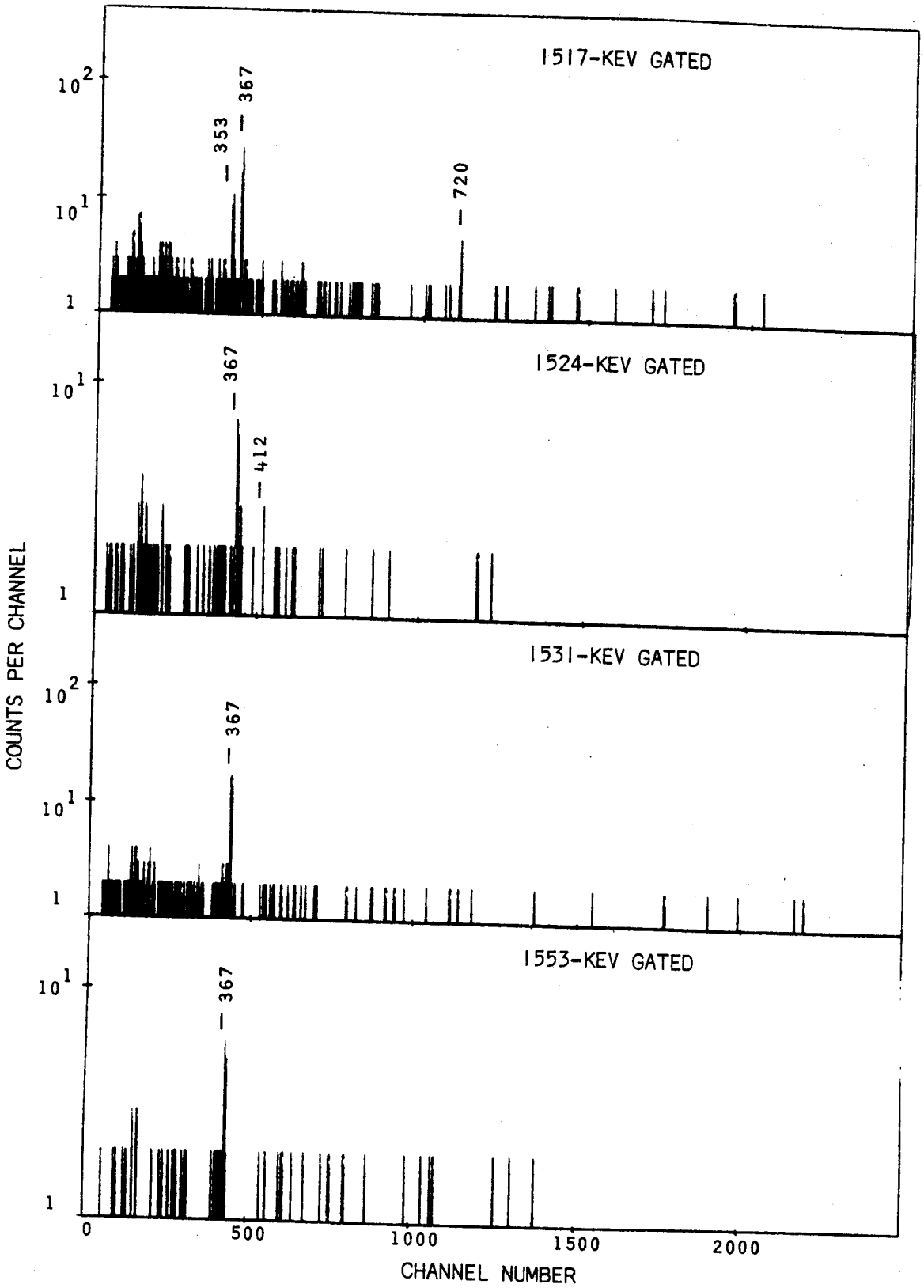

Figure VI-5 (cont'd)

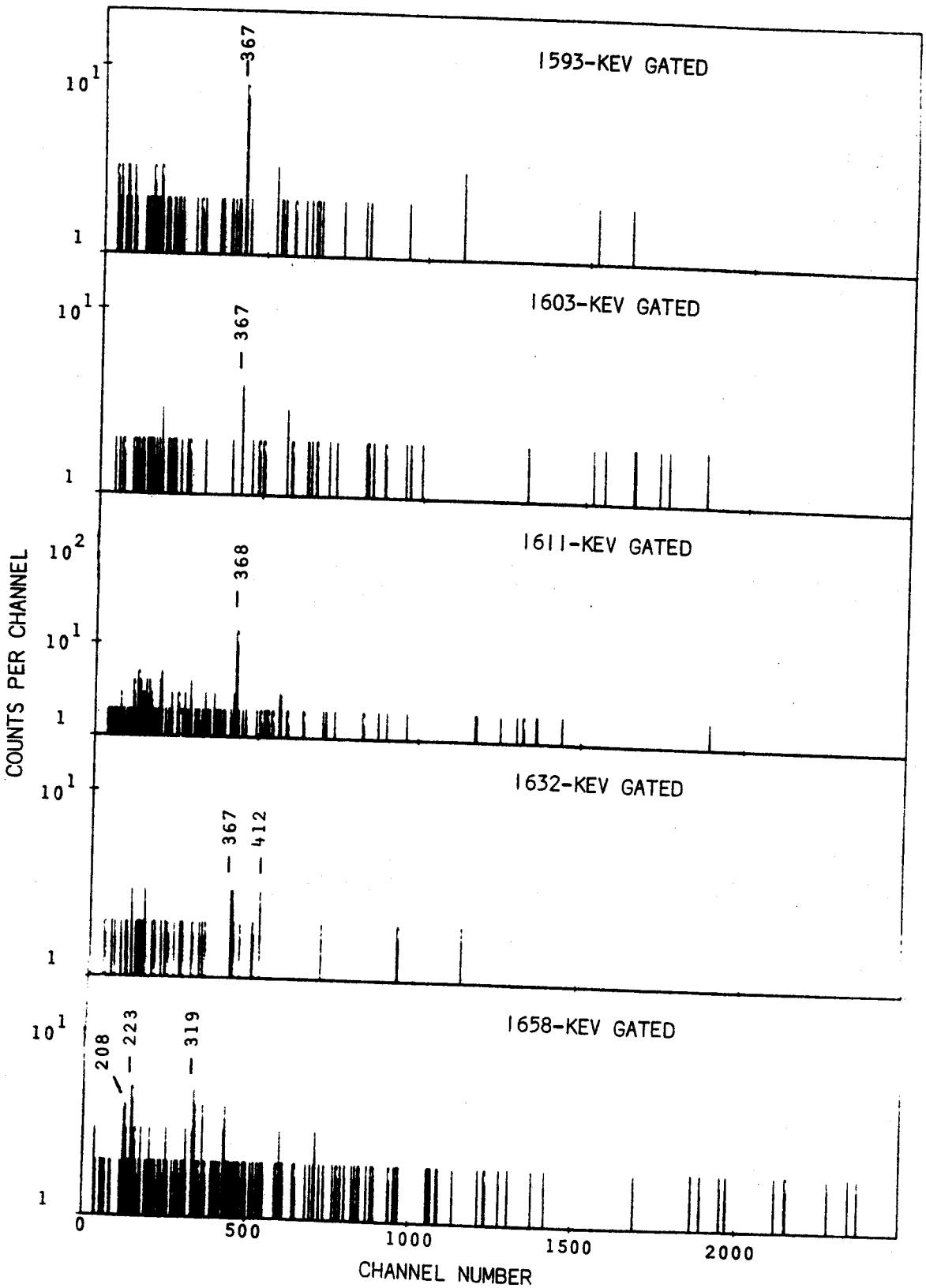

Figure VI-5 (cont'd)

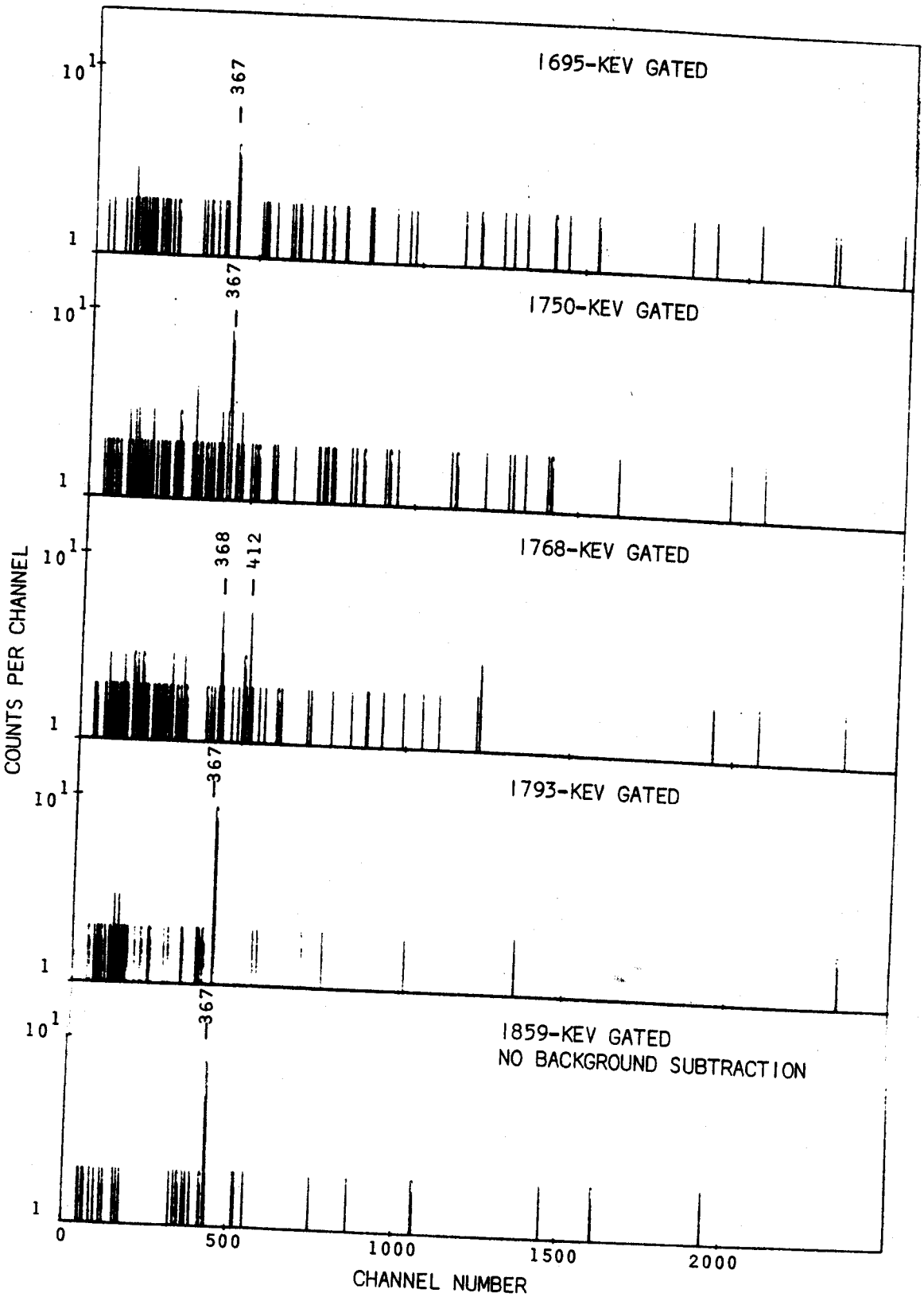

Figure VI (cont'd)

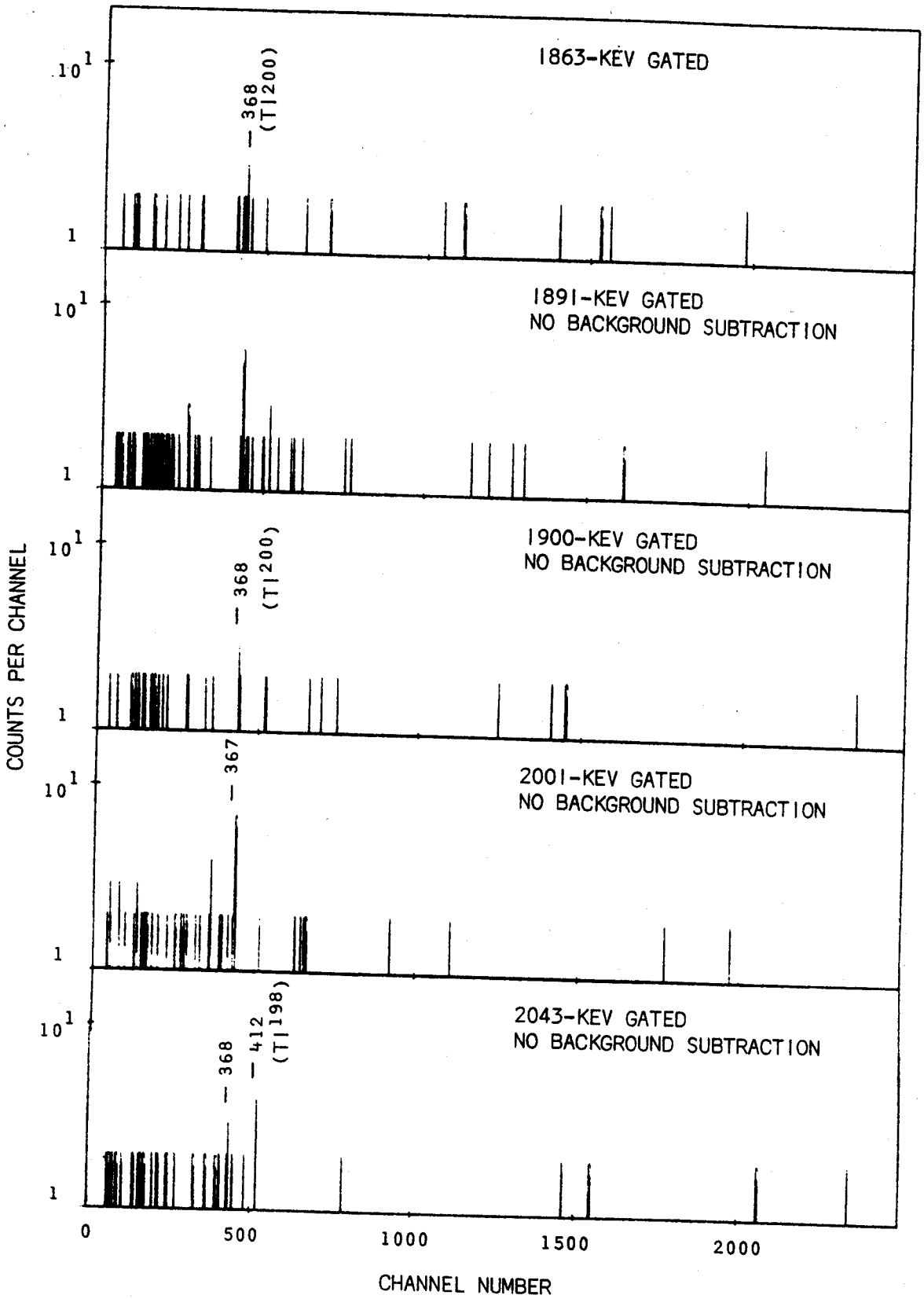

Figure VI-5 (cont'd)

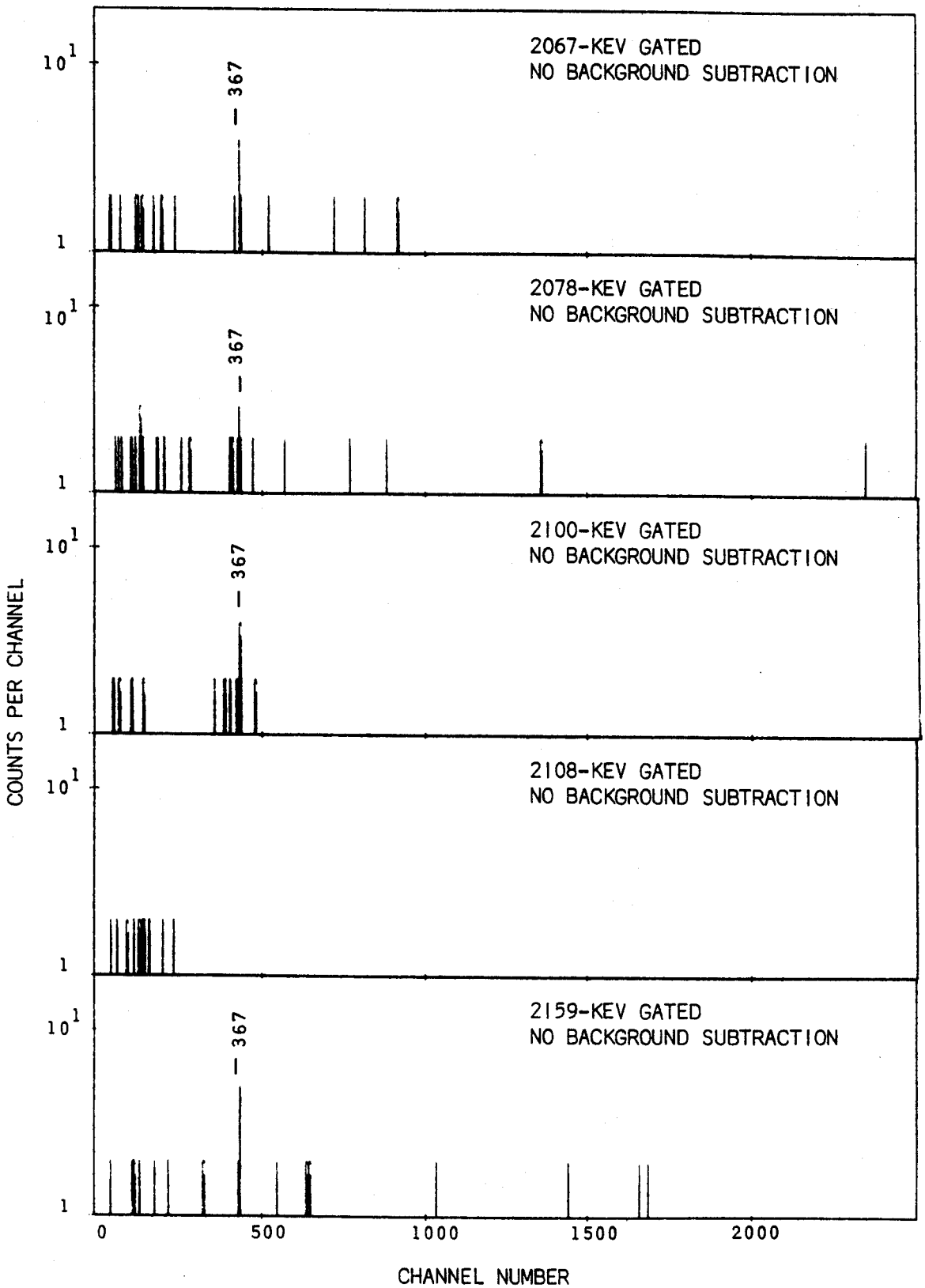

Figure VI-5 (cont'd)

Table VI-4

Results of γ-γ coincidence Study of Pb^{199}

Using 2-dimensional Analysis

Gated energy[a] (keV)	Energies of γ-rays in Coincidence with Gate	
	Strong	Weak
159 (Tl^{199})	248, 284, 300, 334, 375	353, 367
174 (?)	762	320, 353, 367
177 (?)	575	248, 367
208 (Tl^{199})	198, 248, 284, 1013	542
224 (?)	412	367
227 (?)	386	368, 1135
235 (Pb^{200})	290	
241	267, 353, 367, 720, 875	521, 400
248 (Tl^{199})	208	
257 (Pb^{200})	235, 268	396
267 (Pb^{199}+Pb^{200})	257, 353, 367, 762	361
284 (Tl^{199})	208	
290 (Pb^{200}+Pb^{198})	235, 365, 575	
331 (Pb^{201})	361, 405, 585, 767, 907, 946	652
336 (Tl^{198})	412	
344 (Pb^{201}+Pb^{199})		331
353	173, 175, 223, 241, 267 367, 400, 438, 440, 477 495, 511, 521, 762, 777, 834, 912, 938, 1005, 1029, 1053, 1171, 1210, 1239, 1311, 1327, 1506, 1517	361, 688, 690, 1439, 1577, 1647
361 (Pb^{199}+Pb^{201})	267, 331, 585	400, 440, 495, 637, 688
367 (Pb^{199}+Tl^{200})	173, 175, 223, 241, 259, 267, 290, 353, 382, 390, 400, 425, 432, 457, 477, 495, 511, 521, 579, 661,	361, 416, 622, 735, 745, 834, 887, 912, 1647, 1891

Table VI-3 (cont'd)

	685, 725, 754, 762, 776, 781, 828, 839, 875, 922, 938, 947, 976, 1005, 1029, 1053, 1115, 1135, 1161, 1171, 1187, 1207, 1210, 1226, 1239, 1265, 1274, 1292, 1309, 1311, 1327, 1358, 1361, 1383, 1402, 1408, 1480, 1525, 1517, 1531, 1593, 1603, 1610, 1695, 1724, 1793, 1859, 1975, 2001, 2181	
374 (Pb^{204m})	899	579
382 (?)	267, 368	511, 1239
386 (?)	223	376, 637, 899
388 (?)	306	353, 223
390	367, 875	353, 521
400	353, 361, 367, 511, 720, 777	387, 425, 440, 526, 754, 839, 1029
412 (Tl^{198})	587, 637, 677, 1204, 1312	223, 1422, 1444, 1470, 1732, 2042, 2193
416 (?)	268	922, 875
422 (Pb^{202m})	657, 787, 961	
425 (?)		277
431 + 433	754, 1161	295, 912, 353, 367
448 (?)		353
455 (?)		207, 227, 284, 562, 781
477	241, 267, 353, 368,720 762	754, 1029, 1115
482 (?)		208, 268, 412, 720, 762, 353, 368
495	241, 353, 367, 720, 762	449
511	277, 331, 353, 368, 400 412, 511, 720, 754, 1121 1239	267, 320, 521, 961
521	241, 312, 353, 367, 390, 720	412, 448, 511
579	368, 828	

Table VI-3 (cont'd)

587 (Pb^{201}+Tl^{198})	331, 361, 412, 490, 579, 637	762
629 (Tl^{200})	368, 579	
639 (Pb^{199}+Tl^{198})	227, 412, 587	
652 (?)		490, 637, 720, 1005
657 (Pb^{202m})	422	295, 1053
661 (Tl^{200})		
676 (Tl^{198})	412	368
685	839	367
701 (Tl^{200})	661	367, 482
720	267, 390, 400, 521, 762, 781, 938, 1005, 1029 1517	368, 433
725		353, 367, 1171, 1311, 1327
735		353, 367, 292
754	367, 777	367, 412
762	267, 353, 376, 477, 495, 720	361, 433
777	353, 367, 400	286, 422, 579
781	277, 353, 367, 720	482, 320
787 (Pb^{202m})	422, 961	223, 433
828 (Pb^{201}+Tl^{200})	331, 368, 579	579
834		246, 260
839	367, 685, 1053	353, 367
875	241, 367, 390	241, 277, 400
886 (Tl^{200})	368	312
912	353, 367, 720	276
938	353, 367, 720	319, 440
961 (Pb^{202})	422, 787	
1005	353, 367, 720	267, 290
1013 (Tl^{199})	208	
1029	353, 367, 720	388, 440, 754
1048	353, 367, 720	448
1053	367, 839	

Table VI-3 (cont'd)

1100 (?)		367, 438, 875
1115	267, 367	477, 495
1121	511, 433	
1135	223, 367	438
1161	367, 432, 504	
1171	353, 367	
1187	367	344
1207 (Tl^{200})	368	412
1210	353, 367	
1226 (Tl^{200})	368	
1239	353, 367, 720	
1265	367	
1274 (Tl^{200})	368	
1292	367	
1311	353, 367, 720	
1326		367
1328	367	
1358	367	
1368 (Tl^{200})	368	
1383	367	
1402	367	
1422 (Tl^{198})	412	
1481		212
1506	353, 367	
1517	353, 367, 720	
1524	367	
1531	367	
1593	367	
1603 (Pb^{199}+Tl^{200})	368	
1611	367	
1631		412
1658		320, 511

Table VI-3 (cont'd)

1695		367
1750		312
1768	412	
1793	367	
1859	367	
2001	367	
2041 (?)	412	
2067		367
2078		367
2100		367
2159		367

[a] Many of the gates set in analyzing the γ-γ coincidence experiment included γ-rays belonging to isotopes other than Pb^{199} and these are identified in parenthesis following the energy of the gate. In cases where the origin of the gated γ-ray was not known or uncertain, we have used the notation (?) following the gated energy.

6.3.5. Conversion Coefficients and Multipolarity Assignments

Because internal conversion data were available for only three γ-transitions, we were unable to obtain conversion coefficients, and hence multipolarities, as we did in our previous studies of Pb^{200} and Pb^{201}. However, we will discuss here the small amount of data that is available.

Andersson and co-workers [An57] reported conversion electron intensities for only the 353- 367-, and 720-keV transitions. They determined the multipolarities of the 353- and 367-keV transitions to be mixtures of 75% $M1$ + 25% $E2$ and 30% $M1$ + 70% $E2$, respectively, based on the internal conversion K/L and $L_I + L_{II}/L_{III}$ ratios. For the 720-keV transition they obtained only the K-conversion intensity and therefore couldn't determine its multipolarity. However, using this K-conversion intensity and our measured photon intensity, we can obtain the K-conversion coefficient and hence the multipolarity, provided we can normalize the two sets of data. Unfortunately, there are no directly measured conversion coefficients or even a transition of known "pure" multipolarity which we could use, and we had to normalize the two sets of data to the mixed $M1+E2$, 367-keV transition. From their measurement of the electron spectrum of 28 msec Tl^{199m}, Diamond and Stephens [Di63] obtained a multipole mixture of 23% $M1$ + 77% $E2$ for the 367-keV transition, in fair agreement with the results of Andersson and co-workers mentioned above. Using the average multipole mixture of these two studies, 26% $M1$ + 74% $E2$, and the theoretical conversion coefficients of Hager and Seltzer [Ha68],

we obtained a K-conversion coefficient of 0.011 for the 720-keV transition which is in good agreement with the theoretical value of 0.0095 for an $E2$ transition. We also calculated the K-conversion coefficient for the 353-keV transition and obtained a value of 0.144. This corresponds to a multipolarity of 60% $M1$ + 40% $E2$ compared to 75% $M1$ + 25% $E2$ obtained by Andersson [An57] from conversion coefficient ratios.

6.4. Decay Scheme of Pb^{199}

6.4.1. Level Placements

The level scheme for Pb^{199} deduced from our coincidence studies, energy sums, and relative intensities of the transitions is shown in Figure VI-6. Transition and excited-state energies are given in keV, with the adopted energies for the levels being a weighted average based on our confidence in the respective cascade and crossover transitions.

Before we get into the discussion of our reasoning behind the final level placements, we should say a few words about the order in which these will be presented. We have tried to present the discussions in order of increasing level energies; however, the placement of some levels was very much dependent on the establishment of other higher levels. These cases will, therefore, be discussed in the order in which we originally placed them, so as to make the reasoning as straightforward as possible.

6.4.1.a. 366.90-keV Level

The large relative intensity of the 366.90-keV transition along with its coincidence behavior leads us to place a level at 366.90-keV. This placement is in agreement with the previous study of Pb^{199} decay [An57] and all studies of 28 msec Tl^{199m} decay [Di63, De63, Co67]. This also turns out to be the first excited state.

6.4.1.b. 720.26-keV Level

The second most intense peak in the Pb^{199} γ-ray singles

Figure VI-6. Decay scheme of Pb^{199}. All energies are given in keV and (total) transition intensities are given in percent of the Pb^{200} disintegrations. The percent ε decay to each state and the log ft values for that state are listed to the right of the state.

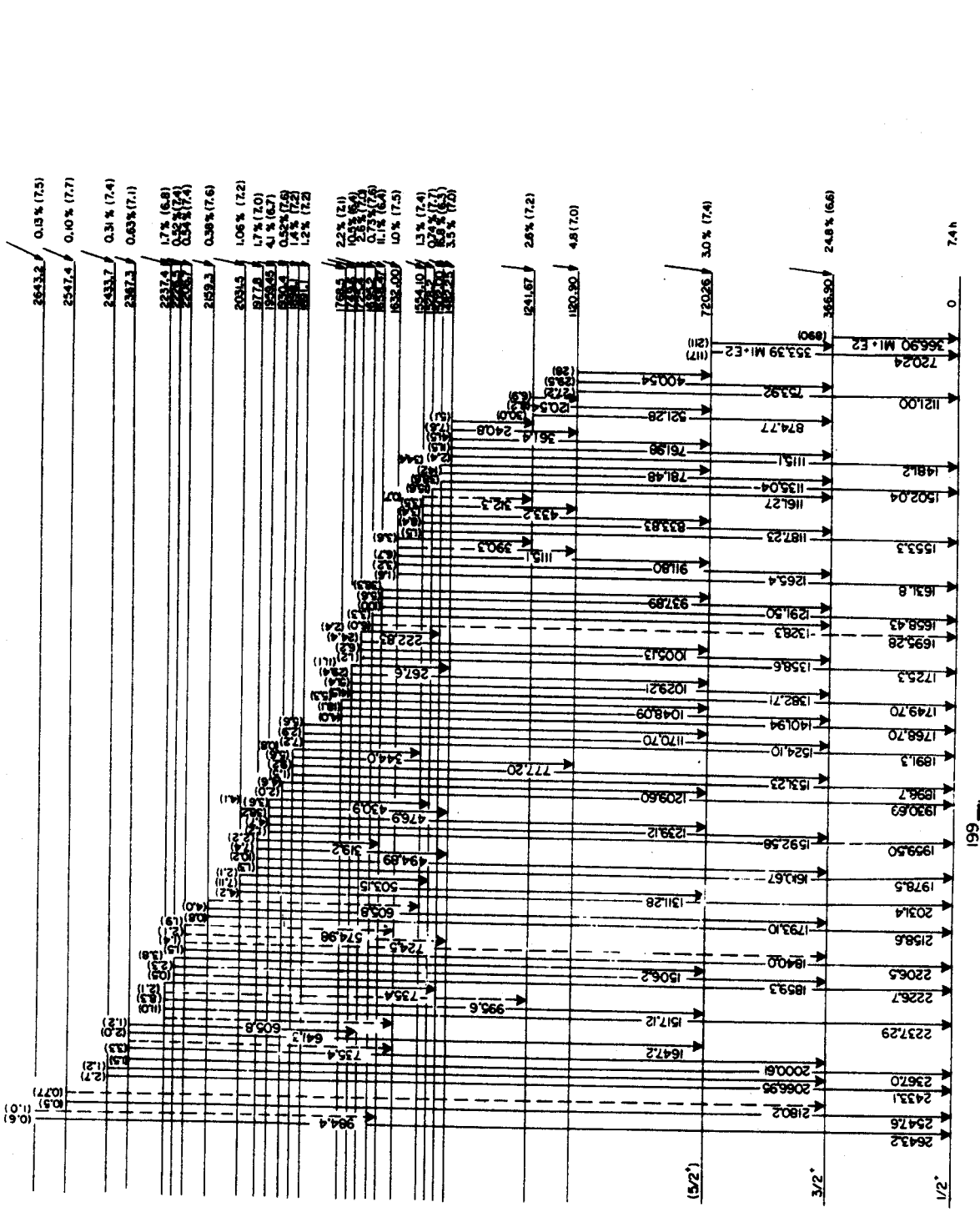
5/2⁻
90 min
β⁺ ε
199 Pb 117
82
Q_ε = 3.2 MeV
199 Tl 118
81
3/2⁺
1/2⁺
7.4 h
366.90 M1 + E2
353.39 M1 + E2
720.24
112.00
148.2
1502.04
155.3.3
1631.8
1658.43
1695.28
1725.3
1749.70
1766.70
1891.3
1898.7
1930.69
1959.50
1978.5
2031.4
2158.6
2206.5
2226.7
2237.29
2364.0
2433.1
2547.6
2643.2

Figure VI-6

spectrum is the 353.39-keV transition. This is also the strongest peak in the 367-keV gated coincidence spectrum. This, coupled with a strong 720.24-keV crossover transition that is somewhat enhanced in the anticoincidence experiment, confirms the previous placement [An57, Di63] of a level at 720.26 keV.

6.4.1.c. 1120.90-keV Level.

The results of the anticoincidence and integral coincidence experiments alone strongly suggest the placement of a level at 1120.90 keV. This placement is also supported by excellent energy sums, the 400.54 + 720.26 = 1120.80 and 753.92 + 366.90 = 1120.82 sums falling within 0.22 keV of the measured 1121.00-keV crossover transition. Finally, the very strong 720-, 353-, and 367-keV peaks in the 400-keV gated coincidence spectrum, along with the absence of the 720- and 353-keV peaks, but presence of a 367-keV peak in the 767-keV gated spectrum put any doubts to rest.

6.4.1.d. 1241.67-keV Level.

The level at 1241.67-keV was placed on the basis of gated coincidence results and energy sums. The 521.28-keV transition was strongly in coincidence with the 353-, 367- and 720-keV transitions while the 875-keV transition was in coincidence with the 367-keV transition but not with either the 353- or 720-keV transitions. The 120.54-keV transition was placed between the 1241.67- and 1120.90-keV levels on the basis of energy sums only, as our coincidence data did not extend below about 160 keV.

6.4.1.e. 1482.25-keV Level

The presence of this state was first suggested by the results of the anticoincidence experiment in which the weak 1481.2-keV transition appeared to be a partially ε-fed ground-state transition. The presence of this state was confirmed by gated coincidence spectra which showed the 241-keV transition in coincidence with the 521- and 865-keV γ's, the 762-keV transition in coincidence with the 720-, 353-, and 376-keV γ's, and the 1115.1-keV transition in strong coincidence with the 367-keV γ. The 361-keV transition was found to be in weak coincidence with the 400-keV transition and based on this and the energy sum, we placed this transition between the 1120.90-keV and 1482.25-keV levels.

6.4.1.f. 1502.00-, 1632.00- and 1658.47-keV Levels

The evidence in support of these three levels is quite conclusive. All three were shown to be ε-fed ground-state transitions in the anticoincidence and integral coincidence experiments and all three are supported by cascade transitions to the 366.90- and 720.26-keV levels. The 1632.00-keV level also feeds the 1241.67-keV level via a 390.3-keV transition. The placement of these cascade transitions have all been confirmed by the 2-d coincidence data. We refer the reader to the decay scheme (Figure VI-6), the gated coincidence spectra (Figure VI-5), and the summary of the 2-d coincidence results (Table VI-4) for the specific transitions and coincidence results involved in these placements.

6.4.1.g. 1725.4-, 1749.6-, 1768.5-, and 1891.1-keV Levels

The evidence for these four levels is essentially of the same nature as that presented for the previous three levels. The 1725.3-, 1749.70-, 1768.48- and 1891.3-keV γ's have been shown to be ε-fed ground-state transitions in the anticoincidence experiment and all four levels are supported by cascade transitions to the first and second excited states. The results of the 2-d coincidence experiment as summarized in Table VI-4 confirm the placement of these cascade transitions.

On the basis of the energy sum alone we would probably place the 222.83-keV transition between the 1725.4- and 1502.00-keV levels. In the 224-keV gated coincidence spectrum, Figure VI-5, we see a strong 412-keV peak and a weak 367-keV peak, indicating a doublet, the more intense and higher energy component belonging to the decay of Tl^{198} and the weaker component belonging to the decay of Pb^{199}. Although the observation of the 367-keV peak in this spectrum does not conflict with our placement of the 223-keV transition, it does not really pin it down either. However, the observation of a strong 223-keV peak in the 353-, 367- and 1135-keV gated coincidence spectra, as well as a weak 223-keV peak in the 781-keV gated spectrum, provides the best evidence for our placement of this transition.

The placement of the 267.6-keV transition between the 1749.6- and 1482.25-keV levels was based on the energy sum, 1482.25 + 267.6 = 1749.8-keV, and the 2-d coincidence results, which leave little doubt as to the certainty of this placement.

6.4.1.h. 1898.1-, 1959.45-, and 1977.8-keV Levels

These three levels have been quite firmly established in our Pb^{199} decay scheme. Again, the behavior of the ground-state transitions from these levels in the anticoincidence and integral coincidence experiments was a primary piece of evidence. Strong cascade transitions from all of these levels to the 366.90-keV level, as well as cascade transitions to the 720.26-keV and 1482.25-keV levels from both the 1949.45- and 1977.8-keV levels, were confirmed by the 2-d coincidence data. The only inconsistency we found between these placements and the coincidence data occurred in the 477-keV gated spectrum. As summarized in Table VI-4, the 477-keV gated coincidence spectrum contained strong 241-, 267-, 353-, 367-, 720-, and 762-keV peaks and weak 754-, 1029-, and 1115-keV peaks, all consistent with our placement except for the strong 267-keV peak and the weak 1029-keV peak. However, as we did not observe a 477-keV peak in the gated spectrum of either the 267- or 1029-keV γ's, we have assumed that these peaks in the 477-keV gated spectrum are spurious (they may arise from incomplete background subtraction). We also have good coincidence data to support the placement of the 777.20-keV transition between the 1898.1- and 1120.90-keV levels. The 319.2-keV transition was placed between the 1977.8- and 1658.47-keV levels on the basis of the energy sum and the observation of a weak 319-keV peak in both the 1658- and 938-keV gated coincidence spectra.

6.4.1.i. 2226.5- and 2367.3-keV Levels

These two levels complete our highest confidence group of

levels. Both have ε-fed ground-state transitions as shown by the anticoincidence experiment, and both have transitions to the 366.90- and 720.26-keV levels which are supported by the 2-d coincidence experiment. In addition to these transitions, the 2367.3-keV level may be depopulated by a 641.3-keV transition to the 1725.4-keV level and a 735.4-keV transition to the level at 1632.00 keV. We have some very weak coincidence evidence for our placement of the 641.3-keV γ in that weak 720- and 1005-keV peaks were observed in the 639-keV gated coincidence spectrum (actually this gate included two γ's, one from Tl^{198} of 637-keV and the weaker 641-keV γ from Pb^{199}). However, we did not observe the 641-keV γ in any of the other gated coincidence spectra including the 720- and 1005-keV gates and we have no explanation as to why it is absent other than poor statistics. The 735.4-keV transition has been placed solely on the basis of the energy difference between the 1632- and 2367.3-keV levels without any supporting coincidence evidence. We have indicated our uncertainty about this placement by using a dotted line for the 735.4-keV transition in the decay scheme, Figure VI-6.

6.4.1.j. 1554.10-keV Level

Although we are including the 1554.10-keV level in our intermediate confidence group of levels, the evidence for this level is so strong that we could probably have included it in our highest confidence group. The strongest piece of evidence for this level is the observation of a single strong 367-keV peak in the 1187-keV gated coincidence spectrum. This coincidence relationship is confirmed

by the fact that the 1187-keV peak appeared in only the 367-keV gated spectrum. Another piece of evidence supporting this level comes from the 834-keV gated spectrum which shows only two weak peaks at 353- and 367-keV, indicating that the 833.83-keV γ feeds the 720.26-keV level. This coincidence relationship is also supported in the 353- and 367-keV gated spectra. Although we observed a 1553.3-keV γ in the singles spectra, we are not positive that this γ is the ground-state transition from the 1554.10-keV level. The most obvious reason for our questioning of this placement is the poor energy agreement of the 1553.3 keV γ with the energy sums 366.90 + 1187.23 = 1554.13 and 720.26 + 833.83 = 1554.09. A second problem with this placement is the behavior of the 1553.3-keV transition in the anticoincidence and integral coincidence experiments. In our decay scheme, the 1554.10-keV level is fed almost entirely by direct ε-decay from Pb^{199}(>90%) with only weak feeding from higher levels in Tl^{199}, and yet from a comparison of the measured intensities of the 1553.3-keV γ in the singles, anticoincidence and integral coincidence experiments, this γ-transition behaves as if it were in relatively strong coincidence with other γ's. However, considering the very weak nature of this transition and the resulting poor statistics obtained in the coincidence experiments we are somewhat skeptical of any conclusions based on these experiments.

The 433.2-keV transition was placed between the 1554.10- and 1120.90-keV levels on the basis of the energy sum 433.2 + 1120.9 = 1554.1 and the observation of a 433-keV peak in the 1121- and 754-

keV gated coincidence spectra. The 312.3-keV transition was placed on the basis of the energy sum 1241.7 + 312.3 = 1554.0 and its presence in the 875- and 521-keV gated spectra.

Considering all the evidence presented for the placement of a state at 1554.10-keV, it seems to us to be quite firmly established.

6.4.1.k. 1930.4- and 2031.5-keV Levels

The evidence we have to support these two levels is typical of that which we required to include a level in our intermediate confidence group. Both levels are depopulated by ε-fed ground-state transitions as shown by the anticoincidence and integral coincidence experiments and both have at least one transition to an established level which is supported by the results of the 2-d coincidence experiment. In this case both the 1930.4- and 2031.5-keV levels feed the 720.26-keV level. The 1209.60-keV transition which depopulates the 1930.4-keV level is observed strongly in the 367- and 353-keV gates but not in the 720-keV gate while the 1311.28-keV transition which depopulates the 2031.5-keV level is observed in all three of these gated spectra. These coincidence relationships are confirmed in the 1210- and 1311-keV gated coincidence spectra. Although the evidence we have presented for our placement of these two levels is fairly conclusive, it is also somewhat limited and we couldn't place these levels in our highest confidence group.

6.4.1.l. 2237.4- and 2433.7-keV Levels

These two states complete our intermediate confidence

group of levels. Again, both levels were shown to have ε-fed ground-state transitions in the anticoincidence experiment.

The second strong piece of evidence for the 2237.4-keV level comes from the 1517-keV gated coincidence spectrum which contains only 353-, 367- and 720-keV peaks. The 353-, 367-, and 720-keV gated spectra support these coincidence relationships and show a strong 1517-keV peak, and in addition, these are the only gates in which the 1517-keV peak was observed. From these coincidence results it is fairly certain the 1517.12-keV transition directly feeds the 720.26-keV level, and the energy sum 1517.12 + 720.26 = 2237.38 is in excellent agreement with the ground-state transition of 2237.29-keV. The remaining three transitions we show depopulating this level were placed solely on the basis of the energy differences between the levels, as we don't have sufficient coincidence information on these transitions to make definite placements. This is especially true for the 605.8- and 735.4-keV transitions which could be placed elsewhere in the decay scheme on the basis of energy sums and, in fact, both transitions appear twice in our decay scheme, Figure VI-6.

In addition to the ε-fed ground-state transition of 2433.1 keV, the 2433.7-keV level is depopulated by only one other transition, the 2066.95-keV transition to the first excited state. This transition is supported by the observation of a 367-keV peak in the 2067-keV gated coincidence spectrum. Although we did not observe a 2067-keV peak in the 367-keV gated spectrum, this could easily have been missed because of the much higher background in the 367-keV gated spectrum.

6.4.1.m. 1528.2- and 1695.2-keV Levels

These are the first of six levels we placed in our lowest confidence group, which means they are based on very limited and sometimes conflicting evidence. However, we still required one piece of solid evidence, such as the observation of an ε-fed ground-state transition, plus at least one weak supporting argument, such as a cascade transition placed solely on energy sums.

The principal piece of evidence for the 1528.2-keV level came from the 1161-keV gated coincidence spectrum which contains strong peaks at 367, 432, and 504 keV. However, the 367-keV peak is by far the most intense, suggesting that the 1161-keV transition directly populates the first excited state giving rise to a state at 1528.2-keV. Although no other transitions were found to depopulate this level, it appears to be fed from the well-established 1959.45- and 2031.5-keV levels via the 430.9- and 503.15-keV transitions.

The 1695.2-keV level is supported mainly by the observation of a single strong peak of 367 keV in the 1328-keV gated coincidence spectrum. This evidence is supplemented by the excellent agreement between the energy sum 366.9 + 1238.3 = 1695.2 and the 1695.28 -ray observed in the singles spectra.

However, there is a conflict between our placement of the 1695.28-keV transition in the decay scheme and the results of the anticoincidence and integral coincidence experiments. As the decay scheme now stands, the 1695.2-keV level is populated only by direct electron capture from Pb^{199}, with no feeding from higher energy levels

in Tl^{199}. This means that the 1695.28-keV transition intensity should be enhanced in the anticoincidence and reduced in the integral coincidence spectra, or in the case of Table VI-2, the intensities listed in the singles, anticoincidence, and integral coincidence columns should be equal within experimental error. Unfortunately this is not the case, and the 1695.28-keV transition behaves as if it were in coincidence with another transition (or transitions) having an energy greater than ≈100 keV (low energy cutoff for the anticoincidence experiment). Although we did observe a 1695-keV transition in the 367-keV gated coincidence spectrum, the 1695-keV gated spectrum contained only a very weak 367-keV peak, in fact the 367-keV peak was just about as strong in the gated spectrum of the background adjacent to the 1695-keV transition. Based on these observations we can't satisfactorily account for the behavior of the 1695.28-keV transition in the anticoincidence and integral coincidence experiments unless it consists of an unresolved doublet. This possibility will be discussed later in Section 6.4.1.p. In our decay scheme, the 1695.28-keV transition is shown as a dotted line to indicate our uncertainty about its placement.

6.4.1.n. 2159.3-keV Level

The 2159.3-keV level is based on evidence quite similar to that presented in support of the 1695.2-keV level. The principal support for this level comes from the observation of a single strong 367-keV transition in the 1793-keV gated coincidence spectrum which is verified by the presence of the 1793-keV transition in only the 367-keV gated spectrum. Additional evidence for this level consists

of a possible ground-state transition and a possible cascade transition to the 1554.10-keV level. The placement of the 605.8-keV transition is uncertain as we have already placed a transition of this same energy between the well-known 2237.4- and 1632.00-keV levels, although neither placement is supported by coincidence results. The 2158.6-keV transition presents us with the same problems we faced in placing the 1695.28-keV transition in the previous section. According to our decay scheme, the 2159.3-keV level is fed entirely by ε-decay. However, in the anticoincidence and integral coincidence experiments, the 2158.6-keV transition does not behave as the other totally ε-fed ground-state transitions, its intensity is reduced in the anticoincidence experiment and enhanced in the integral coincidence experiment. Although we observed a weak 367-keV peak in the 2158-keV gated coincidence spectrum, it was so weak that it could easily have been the result of chance coincidence events and we did not observe the 2158-keV peak in the 367-keV gated spectrum. All things considered, we have serious reservations about the placement of the 2158.6-keV transition in our decay scheme but much less doubt as to the placement of the 2159.3-keV level.

6.4.1.o. 2206.7-, 2547.4-, and 2643.2-keV Levels

All three of these levels were based on the observation of ε-fed ground-state transitions in the anticoincidence experiment and at least one cascade transition to an already established level. Unfortunately these cascade transitions were all too weak to observe in the 2-d coincidence experiment and were placed solely on the basis of energy sums.

For the 2547.4-keV level we were able to find only one possible cascade transition, the 2180.2-keV transition to the first excited level. The 2643.2-keV level was also found to have only one possible cascade transition, the 984.4-keV transition to the 1658.47-keV level. In addition to the 2206.5-keV ground-state transition, we have placed possible cascade transitions from the 2206.7-keV level to the 366.90-, 1482.25-, and 1632.00-keV levels. Again, all of these placements are tentative and were based only on energy sums.

6.4.1.p. Possible Additional Levels

Although we have concluded our discussion of the levels shown in the decay scheme, Figure VI-6, we would like to add a few words here concerning some possible additional levels.

As we mentioned in Section 6.4.1.m., the 1695.28-keV transition may be a doublet with one component being the ground-state transition from the 1695.2-keV level while the second is in coincidence with the 367-keV transition. This would mean a possible state at 2062.18 keV. Such a state is supported by the observation of an ε-fed ground-state transition in the anticoincidence experiment.

In Table VI-3 we have listed 33 possible levels based solely on the anticoincidence and integral coincidence experiments. Of these 33 possible levels, 19 have been supported with some additional evidence and are included in our decay scheme and another, the 2062-keV possibility, is discussed above. Although the remaining 13 possible levels could not be supported by any cascade transitions and were left out of our decay scheme, they still remain good possibilities.

6.4.2. Log *ft*'s

In this section we will explain how we obtained the ε-feeding intensities and corresponding log *ft* values for the levels in Tl^{199} populated from the ε-decay of Pb^{199}. Because the β^+-decay of Pb^{199} is weak compared to ε-decay, we can ignore it in the following calculations without significantly affecting the results. We will discuss the β^+-decay of Pb^{199} in Section 6.4.3.

The total transition intensities, including internal conversion in the *K*, *L*, and *M* shells, were calculated from our singles intensities and the theoretical conversion coefficients of Hager and Seltzer [Ha68]. We assumed *M*1 multipolarities for all transitions except the 720-keV transition which we assumed to be *E*2 and the 353- and 367-keV transitions which were mixed *M*1+*E*2 (See Section 6.3.5. for discussion of these multipolarities). The total relative transition intensities are given in the decay scheme, Figure VI-6.

Using our measured *K* x-ray intensity, the calculated *K*-conversion intensities, and the calculated *K* fluorescent yield of 0.95 [Fi66], the total ε-feeding intensity to the ground-state was found to be ~54%. This corresponds to a log *ft* of 6.4. Such a low log *ft* is in serious conflict with the generally assumed first-forbidden (unique) character of this β transition and leads to the conclusion that the x-ray intensity given in Table VI-2 is too high. The only other possibility is that the ground-state $I\pi$ of Pb^{199} is 3/2- and not 5/2- as is generally believed. (The ground-state spin of Tl^{199} has been measured to be 1/2 in atomic beam [Br57] and atomic

spectra [Hu61] experiments.) However, from the systematics of the Pb isomeric states, the 5/2- ground-state assignment seems fairly well established and it is more likely that the error here is due to our measurement of the x-ray intensity. Considering the systematics of the other odd-mass Tl isotopes and the first-forbidden (unique) nature of the ground-state β transition, we can fairly safely assume that ε-feeding of the ground state is very small, probably <1%. Therefore, for the purpose of calculating the percent ε-feeding to the excited states and their log ft's, we have assumed no ground-state feeding. The resulting ε-feeding intensities and log ft's appear in the decay scheme to the right of the energy levels.

6.4.3. β^+-feeding

In the γ-ray singles spectra we observed a moderately strong peak at 510.9-keV which was definitely broader than the γ-ray peak next to it. Considering the energy of this peak and its obvious broadening, we have assumed that this peak arises from positron annihilation in the β^+-decay of Pb^{199}. This assumption is verified by the results of the 2-d coincidence experiment which shows a strong 511-keV peak in the 511-keV gated coincidence spectrum. Based on the Pb^{199} $Q\varepsilon$ of ≃3.2 MeV, calculated from the experimental masses listed in the table of Myers and Swiatecki [My65], we find that β^+-decay is energetically possible to levels in Tl^{199} up to ≃2180 keV.

From theoretical EC(K)/β^+ ratios [Wa59], the calculated $Q\varepsilon$ of ≃3.2 MeV, our ε-feeding intensities, and theoretical subshell ratios for electron capture [Wa59], we predicted the β^+-feeding

intensities listed in Table VI-5. We also had to make the assumption that all β-transitions to these levels were allowed or first-forbidden nonunique, as the spins of most of the levels are unknown (See Section 6.4.4.). However, based on the log *ft*'s calculated in the preceeding section this is a good assumption. Using the intensity of the 511-keV peak listed in Table VI-2 and the calculated *K* x-ray intensity due to ε-decay assuming no ε-feeding of the ground state, we have calculated an upper limit of 1.4% for the total β^+-feeding in the decay of Pb^{199}.

The 511-keV peak was fairly strong in the integral coincidence spectra of the 2-d γ-γ coincidence experiment and we were able to obtain the 511-keV gated spectrum shown in Figure VI-5. In this spectrum we observed fairly strong coincidences with transitions de-exciting the 1120.90-, 720.26-, and 366.90-keV levels. We also observed a weak 511-keV peak in several gated coincidence spectra of transitions depopulating the 1241.67- and 1658.47-keV levels. However, based on the 511-keV gated coincidence spectrum, it appears that the 366.90-, 720.26-, and 1120.90-keV levels receive the bulk of the β^+-feeding. This conclusion is supported by the theoretically calculated β^+-feeding intensities listed in column four of Table VI-5. From the intensities of the 367-, 353-, 720-, 400-, 754-, and 1121-keV transitions in the 511-keV gated spectrum and the measured upper limit of 1.4% for total β^+-feeding of Tl^{199}, we were able to make a rough calculation of percent β^+-feeding to the 366.90-, 720.26-, and 1120.90-keV levels. These β^+-feeding intensities are listed in column five of Table VI-5. Considering the rough nature of these calculations, the

Table VI-5

β^+-feeding in Pb^{199} Decay

Energy of Level (keV)	Experimental ε-feeding	Theoretical ε_{K/β^+}[a]	Calculated β^+-feeding	Observed β^+-feeding
Ground State	Assumed = 0%	--	--	--
366.90	24.8%	9.3	2.2%	0.94%
720.26	3.0%	18	0.14%	0.18%
1120.90	4.8%	56	0.07%	0.27%
1241.67	2.6%	80	0.03%	--
1482.25	3.5%	250	0.01%	--
1502.00	16.8%	290	0.05%	--
1528.2	0.74%	320	0.002%	--
1554.10	1.3%	390	0.003%	--
1632.00	1.0%	640	0.001%	--
1658.47	11.1%	800	0.01%	--
1695.2 through 2159.3	26.0%	10^3 to 10^6	0.008%	--
			Σ = 2.5%	Σ = 1.4%

[a] Assumed all β-transitions to be either allowed or first-forbidden unique.

agreement between the predicted β^+-feeding and that observed is better than we expected. The worst agreement is between the observed β^+-feeding of 0.27% to the 1120.90-keV level and that predicted by the theoretical calculation, 0.07%. This is somewhat anomalous in that all of the other β^+-feeding intensities we have observed in Pb^{199}, as well as Pb^{201} (Section 5.4.2), decay are either approximately equal to the theoretical predictions or much less. This anomalous intensity could be explained by the existence of a 511.10-keV γ-transition between the 1632.00- and 1120.90-keV levels. In our decay scheme, we show this possible transition as a dotted line. Based on our 2-d coincidence data, we were unable to rule out such a transition. A 511-511-γ triple coincidence experiment using the 8x8 in. NaI(Tl) split annulus would be of great help in resolving this question as well as providing better quantitative data on the β^+-feeding of all the levels in Tl^{199}.

6.5. Spin and Parity Assignments

Before getting into the discussion of the specific spin and parity ($I\pi$) assignments for these levels we would like to make a few quite general statements concerning the criteria used in making these assignments. As we discussed in Section 6.3.5. we have multipolarity assignments for only three γ-transitions, and as these are all connected with the ground and first two excited states, they are only of help in assigning the $I\pi$'s of the 366.90- and 720.26-keV states. Therefore, we discuss the assignments of these two states in a separate section (Section 6.5.2.) following a brief discussion of the ground state (Section 6.5.1.). The $I\pi$'s of the remaining 26 excited states were based entirely on the calculated log ft's, γ-branching ratios, and the systematics of the odd-mass Tl isotopes, particularly Pb^{201}.

The log ft values we calculated for the excited states in Tl^{199} all fell between 6.3 and 7.7 which is well within the range of both allowed (ΔI=0, ±1 $\Delta\pi$ =no) and first-forbidden nonunique (ΔI=0, ±1 $\Delta\pi$ =yes). Although a log ft of 7.7 is somewhat low for a first forbidden unique transition (ΔI=2, $\Delta\pi$=yes), we have somewhat arbitrarily and conservatively included such a possibility for those states where our calculated log ft was $\geq$7.5 and rejected this possibility for log ft's $\leq$7.4. Based on this difference in log ft, we have divided our discussion of the 26 remaining excited states between Section 6.5.3. (log ft's $\leq$7.4) and Section 6.5.4. (log ft's $\geq$7.5).

The γ-branching ratios were generally used only to limit the

transition multipolarities to *M*1, *E*2, *E*1, or *M*1+*E*2. The systematics of the odd-mass Tl isotopes were useful only for the lowest energy levels, although we did use the results of our study of the levels in Tl^{199} in a general way to support our preference for positive parity assignments.

Our $I\pi$ assignments for the levels in Tl^{199} are summarized in Table VI-6. In general, where more than one $I\pi$ assignment was possible for a level, we have listed the preferred assignments first. However, for most of the levels, this means only that the positive parity possibilities are listed before those with negative parity and the ordering of the positive parity possibilities is generally by increasing spin and does not indicate a preference for low spin assignments.

6.5.1. Ground State

The ground-state spin of Tl^{199} has been measured in both atomic spectra [Hu61] and atomic beam resonance [Br57] experiments to be 1/2. This is consistent with the predicted $s_{1/2}$ proton shell model assignment, giving us a spin and parity ($I\pi$) of 1/2+. Based on an $f_{5/2}$ ground state for Pb^{199}, direct ε-population of the Tl^{199} ground state would involve the transition $\simeq \pi s_{1/2} \rightarrow \nu f_{5/2}$, which is l-forbidden as well as spin forbidden and one would expect the log to be quite a bit higher than 9. This supports our assumption made in Section 6.4.2. of ≃0% ε-feeding to the ground state.

Table VI-6

Spin Assignments for Levels in Tl^{199} Populated in Pb^{199} Decay

Level (keV)	$I\pi$	Level (keV)	$I\pi$
0.00	1/2+	[a]1891.1	3/2+, 5/2+, 3/2-
366.90	3/2+	[a]1898.1	3/2+, 5/2+, 3/2-
720.26	5/2+	[b]1930.4	3/2+, 5/2+, 3/2-, 1/2+
[a]1120.90	5/2+, (3/2±)	[a]1959.45	3/2+, 5/2+, 3/2-
[a]1241.67	5/2±, 3/2±, 7/2+	[a]1977.8	3/2+, 5/2+, 3/2-
[a]1482.25	3/2+, 5/2+, 3/2-	[a]2031.5	3/2+, 5/2+, 3/2-
[a]1502.00	3/2+, 5/2+, 3/2-	[b]2159.3	3/2+, 5/2+, 3/2-, 1/2+
[b]1528.2	3/2±, 5/2±, 7/2+, 1/2+	[a]2206.7	3/2+, 5/2+, 3/2-
[a]1554.10	3/2+, 5/2+, 3/2-	[a]2226.5	3/2+, 5/2+, 3/2-
[b]1632.00	3/2+, 5/2+, 3/2-, 1/2+	[a]2237.4	3/2+, 5/2+, 3/2-
[a]1658.47	3/2+, 5/2+, 3/2-	[a]2367.3	3/2+, 5/2+, 3/2-
[b]1695.2	3/2+, 5/2+, 3/2-, 1/2+	[a]2433.7	3/2+, 5/2+, 3/2-
[a]1725.4	3/2+, 5/2+, 3/2-	[b]2547.4	3/2+, 5/2+, 3/2-, 1/2+
[a]1749.6	3/2+, 5/2+, 3/2-	[b]2643.2	3/2+, 5/2+, 3/2-, 1/2+
[a]1768.5	3/2+, 5/2+, 3/2-		

[a] The log ft's for these levels were $\leq$7.4 and first-forbidden unique transitions were not allowed.

[b] The log ft's for these levels were $\geq$7.5 and first-forbidden unique transitions were considered possible.

6.5.2. 366.90- and 720.26-keV States

The 366.90-keV state was previously assigned $I\pi = 3/2+$ by Andersson and co-workers [An57] on the basis of the mixed $M1+E2$ 367-keV γ-transition and the strong ε population of this state (24.8% in our decay scheme). The mixed $M1+E2$ multipolarity of this transition has been substantiated in all succeeding studies. (See Section 6.3.5. for a discussion of the multipolarity assignments.) Our work supports this 3/2+ assignment as the log ft of 6.6 is in the range expected for a first-forbidden β-transition.

The 353.39-keV transition depopulating the 720.26-keV level was also found to be mixed $M1+E2$ multipolarity in the previous studies, and our calculated α_K supports this multipolarity assignment. This would then allow an $I\pi$ assignment of 1/2+, 3/2+, or 5/2+ for the 720.26-keV level. The calculated log ft of 7.4 for ε decay to this state rules out the 1/2+ possibility, as this would then be a first-forbidden unique transition, log $ft \geq 8$. This leaves only the 3/2+ and 5/2+ possibilities. From the measured α_K of 0.011 we were able to assign an $E2$ multipolarity to the 720.24-keV ground-state transition (Section 6.3.5.). While this strongly suggests a 5/2+ assignment here, we can't positively eliminate the 3/2+ assignment on the basis of this multipolarity as the transition could be mixed $M1+E2$ with the $E2$ component strongly enhanced, although we would be surprised to see such a strong collective enhancement in this case. Based on the systematics of the odd-mass Tl isotopes, a 5/2+ assignment is also the best choice for the 720.26-keV state.

6.5.3. Remaining States with Log ft's $\leq$7.4.

The log ft's of the 19 levels to be discussed in this section range from 6.3 to 7.4, all of which are well within the ranges for allowed (ΔI=0, $\pm$1 $\Delta\pi$=no) and first forbidden nonunique (ΔI=0, $\pm$1 $\Delta\pi$=yes) β-transitions and significantly below the log ft's usually found for first forbidden unique (ΔI= $\pm$2 $\Delta\pi$=yes) transitions. (These 19 states are identified in Table VI-6 by a superscript a preceeding the level energy.)

Based on the log ft's alone, we have six possible $I\pi$'s for each of these 19 states, 3/2$\pm$, 5/2$\pm$, or 7/2$\pm$. However, for all but one of these states, which we will discuss below, we were able to eliminate the 5/2-, 7/2+, and 7/2- possibilities on the basis of the γ-branching ratios. In order to avoid repetitious arguments for these states we will discuss a typical example, the 1658.47-keV level, and let the reader go through the arguments for the other similar levels. The 1698.47-keV level is depopulated by three γ-transitions, the 1658.43-keV γ to the ground state ($I\pi$=1/2+), the 1291.50-keV γ to the first excited state ($I\pi$=3/2+), and the 937.89-keV level to the second excited state ($I\pi$=5/2+). Based on this γ-branching from the 1658.47-keV level we can clearly rule out the 7/2+, 7/2-, and 5/2- possibilities, as these assignments would mean $M3$, $E3$, or $M2$ ground-state transitions competing with $M1$, $E2$, or $E1$ cascade transitions. (While a few examples of such competing transitions are known, they are extremely rare.) We are now left with the 3/2+, 5/2+, and 3/2- possibilities and this is as far as we can go with the data presently

available. As we mentioned earlier, we do prefer the two positive parity possibilities based on systematics and we listed the 3/2- possibility last in Table VI-6.

Looking over our decay scheme, Figure VI-6, we note that, with the exception of the 1241.67-keV state, all states with a log ft $\leq$7.4 have transitions to the 1/2+ ground state plus an additional transition to either or both the 3/2+ first-excited or 5/2+ second-excited states. The same γ-branching argument used above can be applied to all of these states giving us the final $I\pi$ possibilities of 3/2+, 5/2+, and 3/2-.

From a comparison of the levels in Tl^{201}, Chapter V, with those reported here for Tl^{199}, we believe the 1120.90-keV level in Tl^{199} corresponds roughly to the 1098.46-keV level in Tl^{201}. (The 1098.46-keV level in Tl^{201} was assigned a preferred spin of 5/2+ with a 3/2+ spin also considered possible.) Based on this similarity, we have tentatively assigned the 1120.90-keV level in Tl^{199} an $I\pi$ of 5/2+. However, we can't definitely rule out the 3/2+ or 3/2- possibilities on this weak argument alone, and so we have listed them in parentheses in Table VI-6 following the preferred 5/2+ assignment.

The 1241.67-keV state has a log ft of 7.2 which allows $I\pi$'s of 3/2±, 5/2±, and 7/2±. However, no ground-state transition was observed in this case, although this state did populate the 366.90-, 720.26- and 1120.90-keV levels. Based on our $I\pi$ assignments for these three levels, Table VI-6, we see that, of the six $I\pi$ possibilities given above, only the 7/2- possibility is inconsistent with the γ-branching

from this level. Therefore, we are left with five possible $I\pi$ assignments for this level, 3/2±, 5/2±, and 7/2+.

6.5.4. States with log ft's ≥7.5.

The log ft's of the remaining 6 levels placed in our decay scheme range from 7.5 to 7.7. (These 6 states are identified in Table VI-6 by a superscript b preceeding the level energy.) While these log ft's are well within the range for allowed (ΔI=0,±1 $\Delta\pi$=no) and first forbidden nonunique (ΔI=0,±1 $\Delta\pi$=yes) β-transitions, they are high enough that we decided to include first forbidden unique (ΔI=2 $\Delta\pi$=yes) transitions as additional possibilities. Therefore, based on the log ft alone, we have 8 possible $I\pi$ assignments for these states, 3/2±, 5/2±, 7/2±, 1/2+, and 9/2+. On the basis of the γ-branchings from the 1632.00-, 1695.2-, and 1930.4-, 2547.4-, and 2643.2-keV levels we can eliminate the 5/2-, 7/2±, and 9/2+ possibilities. This leaves us with the final possible $I\pi$ assignments of 3/2+, 5/2+, 3/2-, and 1/2+ for these 5 levels.

Although we can't definitely eliminate any of these possible assignments we can say that, based on the log ft's, 1/2+ assignments for these states are the most unlikely, and we have indicated this by placing this $I\pi$ possibility last in Table VI-6 for these 5 states.

The log ft of 7.7 for the 1528.2-keV state allows $I\pi$'s of 3/2±, 5/2±, 7/2±, 1/2+, and 9/2+. However, unlike the states discussed above, this level is depopulated by only one transition, the 1161.27-keV transition to the first excited state (3/2+), and based on this observation, we can eliminate only the 7/2- and 9/2+ possibilities.

This leaves us with 6 possible $I\pi$ assignments for this level, 3/2±, 5/2±, 7/2+, and 1/2+. Although the 1528.2-keV level is fed by the 1959.45- and 2031.5-keV levels, this information does not limit the $I\pi$ assignments beyond the choices given above.

This concludes our discussion of the spin and parity assignments. As is evident from Table VI-6, we were unable to assign unambiguous spins or parities for very many levels, and the few states for which we have made a unique assignment were known before the present investigation was undertaken. The lack of measured conversion electron intensities and hence conversion coefficients with which to make multipolarity assignments has severely limited our ability to assign unique spins and parities. A careful measurement of the conversion electron spectrum of Pb^{199} should, therefore, be of highest priority in any future investigation of this decay scheme.

6.6. Theoretical Description of Odd-mass Tl Isotopes

Because our studies of the states in Tl^{199} and Tl^{201} are of an "experimental" nature rather than "theoretical", it is easy for us to become obsessed with the details and results of the experiments leading to a decay scheme and lose sight of the principal reason for obtaining the data, which is to provide a test for present and future nuclear models. Indeed, during the ~2 years we spent in obtaining and analyzing the data, very little time was devoted to the theoretical studies of these isotopes. While we will now attempt to examine the odd-mass Tl isotopes, particularly Tl^{201} and Tl^{199}, in terms of some of the current models, we do not pretend to have the sophistication of a theoretician and will make no attempt to predict a future direction for the theoretical calculations. However, as several calculations have been made of the levels in Tl^{199} and Tl^{201} we do feel that a critical comparison of these with our results will be of some help in future calculations.

6.6.1. Shell Model Description of Odd-mass Tl Isotopes

As we are in the region of the double shell of Z=82 and N=126, it seems quite reasonable to start our description of the levels in the odd-mass Tl isotopes in terms of the single-particle shell model. Figure VI-7 shows the shell model states available in this region. Of all the odd-mass Tl isotopes Tl^{207} should provide the best test for this model as it has a closed neutron shell (N=126) and, like all Tl isotopes, a single proton hole in the Z=82 closed shell. The excited states of Tl^{207} up to 2.0 MeV are shown in Figure VI-8, along with

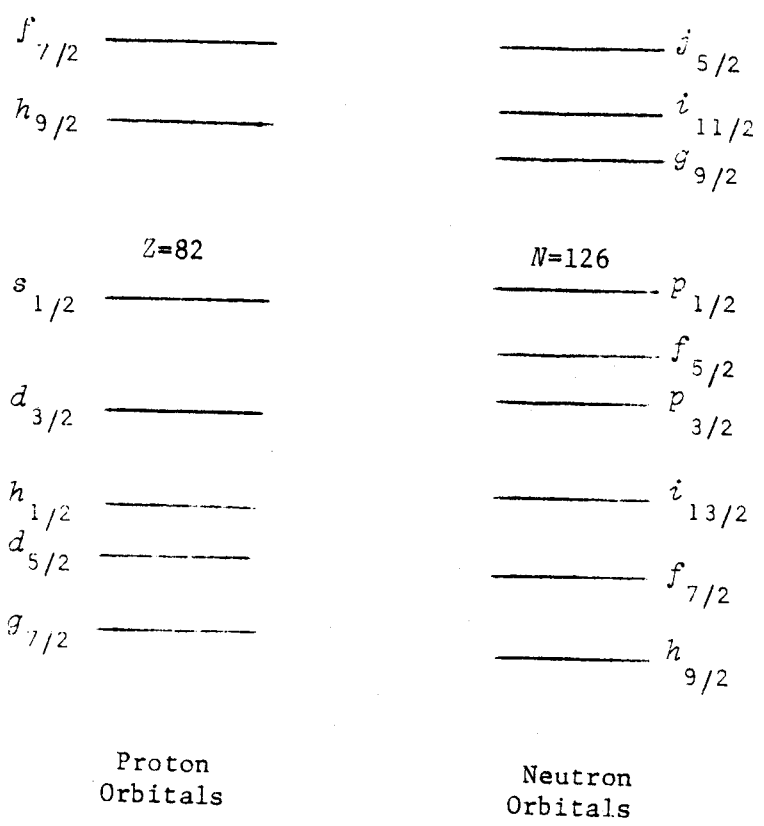

Figure VI-7. Shell-model orbitals near the N=126 closed shell and the Z=82 closed shell. The order of these states may change somewhat as the total number of protons or neutrons change. The order shown here is that observed near the double shell closure at $_{82}Pb^{208}_{126}$.

Figure VI-8. Systematics of states in neutron-deficient odd-mass Tl isotopes below 2.0 MeV. All states populated by radioactive decay and nuclear reactions have been included except for the high spin states in Tl^{199} observed by Newton *et al.* [Ne70] in their study of the reaction $Au^{197}(\alpha,2n\gamma)Tl^{199}$.

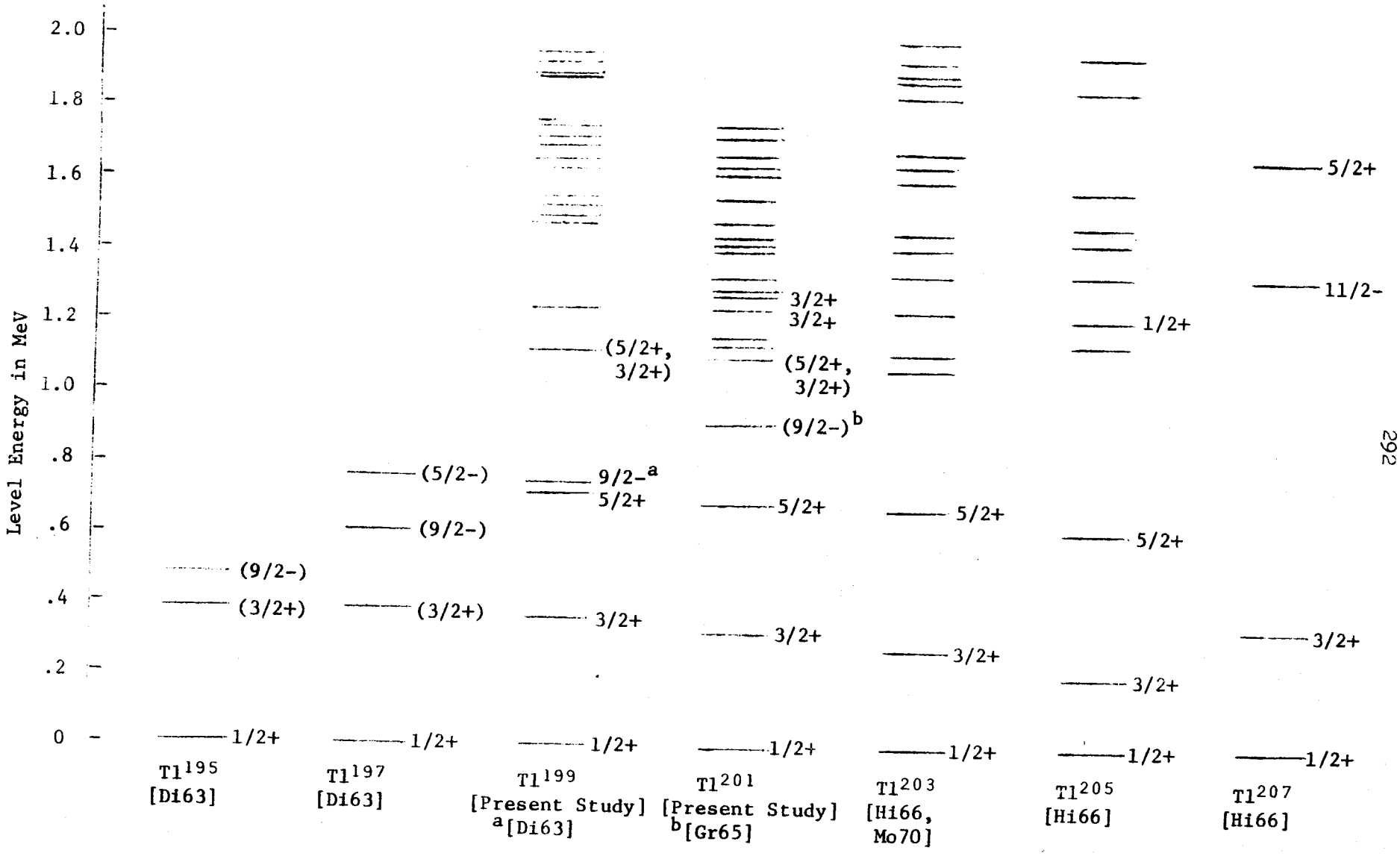
Level Energy in MeV
2.0
1.8
1.6
1.4
1.2
1.0
.8
.6
.4
.2
0
(9/2-)
(3/2+)
1/2+
Tl195
[Di63]
(5/2-)
(9/2-)
(3/2+)
1/2+
Tl197
[Di63]
(5/2+, 3/2+)
9/2-a
5/2+
3/2+
1/2+
Tl199
[Present Study]
a[Di63]
3/2+
3/2+
(5/2+, 3/2+)
(9/2-)b
5/2+
3/2+
1/2+
Tl201
[Present Study]
b[Gr65]
5/2+
3/2+
1/2+
Tl203
[Hi66, Mo70]
1/2+
5/2+
5/2+
3/2+
1/2+
Tl205
[Hi66]
5/2+
11/2-
3/2+
1/2+
Tl207
[Hi66]

Figure VI-8.

selected states of the other neutron-deficient odd-mass Tl isotopes. The presence of a 1/2+ ground state and excited states with $I\pi$'s of 3/2+, 11/2-, 5/2+, and 7/2+ in Tl^{207} are in agreement with predicted shell model states between Z=50 and Z=82, namely the $s_{1/2}$, $d_{3/2}$, $h_{11/2}$, $d_{5/2}$, and $g_{7/2}$. (The $g_{7/2}$ level in Tl^{207} lies at 3.48 MeV and is not shown in Figure VI-8.) Moreover, the electromagnetic properties, beta transition rates and single neutron transfer reaction spectroscopic factors all indicate that these are fairly "pure" single-particle states.

As we go from Tl^{207} to the lower mass Tl isotopes, we are breaking up the N=126 closed shell. However, for the single-particle shell model we assume the even numbers of neutrons are paired-up to give a resultant spin of zero, and, therefore, the ground state spin is predicted to be 1/2+ for all the odd-mass Tl isotopes, and looking at Figure VI-8 we see that this is indeed the case. Based on the $d_{3/2}$ first excited state in Tl^{207}, the single-particle shell model would predict a $d_{3/2}$ first excited state for all the odd-mass Tl isotopes and we see in Figure VI-8 that this prediction also appears to be correct. Based on the similarity in the energies of the $d_{3/2}$ single-particle state in Tl^{207} and the 3/2+ states in the other Tl isotopes, we can probably assume these are also fairly "pure" $d_{3/2}$ states.

The second excited state in Tl^{207} is the $h_{11/2}$ shell model state at 1341 keV and although possible 11/2- states have been observed in some odd-mass Tl isotopes close to this energy [Ne70], a number of

states appear between the $d_{3/2}$ states and ~1300 keV in all these isotopes except, of course, for Tl^{207}. The second excited state for Tl^{205} through Tl^{197} is 5/2+. These 5/2+ states could be explained as being the $d_{5/2}$ shell model state, which is indeed, the next state in Tl^{207}. However, the $d_{5/2}$ state lies at 1674 keV in Tl^{207} and we would be hard pressed to explain the lowering of this state to 615 keV in Tl^{205} where the first 5/2+ state appears. These 5/2+ states have been interpreted in the past as $d_{5/2}$ shell model configurations [An57, Be57, Pe61] and we have also assumed this assignment in our discussion of states in Tl^{200} (Chapter IV). Assuming for the moment that this description is correct, our single-particle model cannot account for the very high density of states we observed in Tl^{201} and Tl^{199} above ~1 MeV and we are forced to abandon this description in favor of a many-particle shell model.

Silverberg [Si61] has made such a shell model calculation on Tl^{205}. He considered the nucleus as three holes moving in a static potential and interacting with each other by some residual force. While this approach could qualitatively describe the behavior of Tl^{205}, quantitatively the results were poor. Nevertheless, these calculations did show that the 5/2+ second excited state has as its principal component $|s_{1/2}[p_{1/2}f_{1/2}]^2;5/2>$ mixed with a significant amount of $|s_{1/2}[p_{1/2}f_{5/2}]^3;5/2>$ and a much smaller mixing of configurations containing the $d_{5/2}$ proton state.

Although we can generalize some of the results obtained by Silverberg to the more neutron-deficient Tl isotopes, the quantitative

calculation of energy levels becomes meaningless, and as these calculations become more complex as one gets further from the closed neutron shell, no significant shell model calculations have been performed below Tl^{205}.

6.6.2. Core-coupling Model

Nuclei within a few nucleons of a double-magic core can usually be described successfully by nucleons moving in a static shell model potential and nuclei very far from closed shells assume a stable equilibrium deformation and the collective modes can be treated as nuclear rotations with energies which are smaller than the single-particle excitations (Collective Model). For nuclei between these two extremes, such as the neutron-deficient Tl isotopes, which are spherical, but where there is evidence of low lying core excited states, we can use variations of the Core-coupling Model. In this model collective effects are treated as vibrations of the spherical core and are coupled more or less strongly to the single-particle states.

In addition to performing three-particle shell model calculations on Tl^{205} as mentioned in Section 6.6.1., Silverberg [Si61] calculated this same nucleus as one proton hole coupled to a vibrating core and concluded that this later calculation provided a satisfactory description of this nucleus with considerably less numerical work. Since this work was published in 1961 several additional studies have been made of the odd-mass Tl isotopes using the intermediate-coupling unified model [Cv66, Al67, Az69] and

two of these included calculated levels for Tl^{201} and Tl^{199} [Cv66, Al67]. These calculations are of particular interest to us as they give us a chance to compare our proposed level scheme with this model.

As a complete description of the unified model exists elsewhere [Zz52], we will restrict ourselves here to a comparison of the assumptions and parameters used in the calculations by Covello and Sartoris [Cv66] and Alaga and Ialongo [Al67] and end with a comparison of the resulting calculated levels with our experimentally determined levels.

In their calculation, Covello and Sartoris [Cv66] considered all the proton-hole orbits within the shell ending at Z=82, namely, $3s_{1/2}$, $2d_{3/2}$, $1h_{11/2}$, $2d_{5/2}$, and $1g_{7/2}$, and included all the core states up to three phonons. Alaga and Ialongo [Al67] however, used only the $3s_{1/2}$, $2d_{3/2}$, $1h_{11/2}$, and $2d_{5/2}$, shell model states but also included vibrator states up to three phonons.

The two parameters which specify the collective motion of the core and its interaction with the motion of the hole are the phonon energy $\hbar\omega$ and the strength of the surface-hole coupling η or α. The phonon energy, $\hbar\omega$, is deduced for each odd-mass Tl isotope from the neighboring even isotope (for Pb^{201} this would be the first 2+ state in Pb^{202} at 960 keV). The coupling constant η or α is treated as a free parameter to be varied within reasonable limits. Although both calculations used the same values for $\hbar\omega$, 960 for Tl^{201} and 1027 for Pb^{199}, the coupling constant which gave the best fit to the existing experimental data was different as one might expect.

Another difference between these calculations has to do with the assumption made concerning the single-hole excitation energies, $\Delta_j = \varepsilon_j - \varepsilon_{1/2}$. Alaga assumed these energies were fixed and equal to the excited single-particle states in Tl^{207}. However, Covello states that these energies can't be taken from the experimental spectrum of Tl^{207} because these experimental energies should be corrected for the interaction with the core, which is also effective in Tl^{207}. Furthermore, the interaction between the odd hole and the core contains a short-range part, which has not been included in the model Hamiltonian. This short-range part of the force would act in first-order perturbation theory as a renormalization of the single-hole energy spectrum, thus producing effective spacings peculiar to each isotope [Si61]. Because of this they considered the quantities Δ_j as adjustable parameters for all levels except the $g_{7/2}$ level which is so high in energy that any changes in its position due to these corrections are irrelevant and they took $\Delta_{7/2}$ from the Tl^{207} $g_{7/2}$ level.

In Figure VI-9 the energy levels calculated by Alaga [Al67] are compared with those calculated by Covello [Cv67] and both of these are compared to the Tl^{201} and Tl^{199} levels found experimentally. We have not included the recent high spin levels in Tl^{199} proposed by Newton and co-workers [Ne70] or the isomeric 9/2- levels found in both nuclei [Di63]. With the exception of those levels mentioned above, the other experimentally known low-lying levels in Tl^{201} and Tl^{199} are reproduced fairly well in both calculations, although they both fail to account for the high density of states above ≈1 MeV. The

Figure VI-9. A comparison of the levels in Tl^{201} and Tl^{199} from our decay scheme with those calculated by [Cv67] and [Al67]. The parities for all the levels are positive except where indicated.

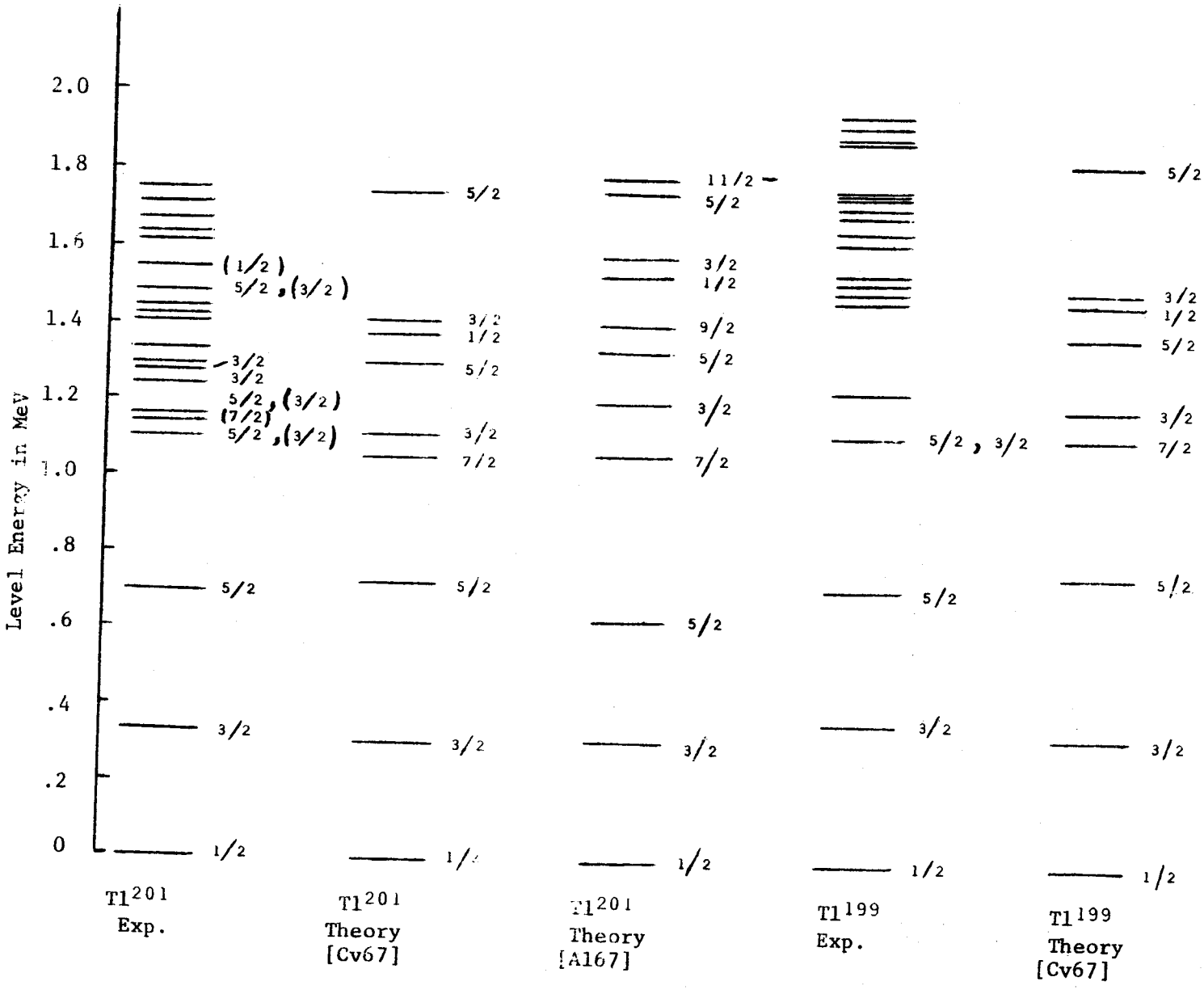
Level Energy in MeV
2.0
1.8
1.6
1.4
1.2
1.0
.8
.6
.4
.2
0
(1/2)
5/2 ,(3/2)
3/2
3/2
5/2 ,(3/2)
(7/2)
5/2 ,(3/2)
5/2
3/2
1/2
Tl201 Exp.
5/2
3/2
1/2
5/2
5/2
3/2
7/2
Tl201 Theory [Cv67]
11/2
5/2
3/2
1/2
9/2
5/2
3/2
7/2
5/2
3/2
1/2
Tl201 Theory [A167]
5/2
5/2 , 3/2
5/2
3/2
1/2
Tl199 Exp.
5/2
3/2
1/2
5/2
3/2
7/2
5/2
3/2
1/2
Tl199 Theory [Cv67]

Figure VI-9

order of the states are similar in both calculations for Tl^{201}, although they vary considerably in energy. Because of the many states observed in our decay schemes, it is difficult to draw a correspondence between the experimental and theoretical levels. This is especially true for Tl^{199}, where most of the $I\pi$ assignments are ambiguous. Because of this we will restrict this discussion largely to the states in Tl^{201}.

As we mentioned before, the agreement between the calculated and measured energies for the 3/2+ and 5/2+ first two excited states are quite reasonable, and we can fairly safely draw a correspondence between them. Both calculations place a 7/2+ level next, 1047 keV according to [Cv67] and 1065 keV according to [Al67] for Tl^{201}, while the next observed level is at 1098 keV. However, this 7/2+ calculated level does lend support to our preferred 7/2+ assignment for the observed level at 1135 keV (see Section 5.5.4.) as the only other level we observed in Tl^{201} that could possibly be 7/2+ were at 1920 and 1712 keV. Of course, it is also possible that this state is not populated in Pb^{201} decay.

The next level predicted by both calculations has $I\pi$=3/2+ and an energy of 1125 keV by [Cv67] and 1200 keV by [Al67]. Although the 1098-keV level has been assigned a preferred $I\pi$ of 5/2+, we couldn't rule out a 3/2+ assignment, so it is possible that this level corresponds to the second 3/2+ state of these calculations. Another possibility for this predicted level is the 1157-keV level, although here too we have assigned a preferred $I\pi$ of 5/2+. Of course the most

likely candidates for the predicted level are the 1238- and 1277-keV levels, which we have assigned an unambiguous $I\pi$ of 3/2+, although they lie quite a bit higher in energy than the calculated level.

The second 5/2+ level predicted by these calculations lies at 1299 keV [Cv67] and 1335 keV [Al67]. The observed 1330-keV state falls nicely between these calculated energies, and indeed, a 5/2+ assignment is one of the two $I\pi$'s considered possible for this state.

At this point the calculations disagree with each other to some extent. The theoretical calculations of Alaga predict a 9/2+ level at 1405 keV, while Covello does not show a 9/2+ level below ~2 MeV. In support of Alaga, we did observe a state at 1290 keV which we assigned a preferred $I\pi$ of 9/2+ (7/2+ also possible). Although we observed no other states in the decay of Pb^{201} which could have $I\pi$= 9/2+, we can't definitely state that the calculated 9/2+ state corresponds to our 1290 keV level as such high spin levels are not very likely to be populated in the decay of Pb^{201} (g.s.$I\pi$=5/2-).

The second calculated 1/2+ state at 1386 keV [Cv67] or 1530 keV [Al67] is also of some interest as we have made a preferred $I\pi$=1/2+ assignment to only one state, 1550 keV. Based on the closeness of this energy to that calculated by [Al67] for the 1/2+ state, we are tempted to suggest a correspondence here. However, as in the case of the 9/2+ state, 1/2+ states are not likely to be populated in the decay of Pb^{201} and we can't rule out the existence of other unobserved 1/2+ states in this region.

Both calculations predict another 3/2+ state <60 kev above

the 1/2+ state, 1412 keV according to [Cv67] and 1583 keV according to [Al67]. We observed three levels between these two calculated energies, 1446-, 1480-, and 1550-keV levels. Of these, the 1445-keV level is considered most likely to have a $I\pi$ = 3/2+, although any correspondence drawn here would be mere speculation.

The calculations predict another 5/2+ state at 1740 keV [Cv67] or 1750 keV [Al67]. Although these energies are very close to the observed level at 1755 keV, we can't expect to base a correspondence between the calculated and observed levels for this state on the basis of the energy alone when such accurate level energy determinations are absent for the other levels above ~1 MeV. This is especially true in this case as there are six levels from 1617 to 1755 keV which could have $I\pi$=5/2+.

Based on the above observations two conclusions are obvious. One is that, without further experimental clarification of the $I\pi$'s of these states, the testing of theoretical calculations becomes somewhat speculative. Based on the vast amount of new experimental data obtained in our studies, it is also obvious that the present models are woefully inadequate to provide a comprehensive description of these nuclei.

BIBLIOGRAPHY

BIBLIOGRAPHY

A

[Aa64] E. Aasa, T. Sundström, O. Bergman, J. Lindskog, and K. Sevier, Arkiv Fysik 27, 133 (1964).

[Al67] G. Alaga and G. Ialongo, Nucl. Phys. A97, 600 (1967).

[An55] G. Andersson, E. Arbman, I. Bergström, and A. H. Wapstra, Phil. Mag. 46, 70 (1955).

[An57] G. Andersson, E. Arbman, and B. Jung, Arkiv Fysik 11, 297 (1957).

[As57] B. Astrom, B. Johannson, and I. Bergström, Arkiv Fysik 12, 205 (1957).

[Au67] R. L. Auble, D. B. Beery, G. Berzins, L. M. Beyer, R. C. Etherton, W. H. Kelly, and Wm. C. McHarris, Nucl. Instr. Methods 51, 61 (1967).

[Az69] N. Azziz and A. Covello, Nucl. Phys. A123, 681 (1969).

B

[Ba70] E. Barnard, N. Coetzee, J. A. M. De Villiers, D. Reitmann, and P. Van Der Merwe, Nucl. Phys. A157, 130 (1970).

[Be55] K. E. Bergkvist, I. Bergström, C. J. Herrlander, S. Hultberg, H. Slätis, E. Sokolowski, A. H. Wapstra, and T. Wiedling, Phil. Mag. 46, 65 (1955).

[Be57] I. Bergström and G. Andersson, Arkiv Fysik 12, 415 (1957).

[Be60] I. Bergström, E. C. O. Bonacalza, A. Jech, M. Perez, and P. Thieberger, Nucl. Instr. Methods 8, 151 (1960).

[Be67] G. J. Berzins, Ph.D. Thesis, Michigan State University, 1967.

[Br57] G. O. Brink, J. C. Hubbs, W. A. Nierenberg, and J. L. Worcester, Phys. Rev. 107, 189 (1957).

[Br60] M. H. Brennan and A. M. Berstein, Phys. Rev. 120, 927 (1970).

[Br64] K. Brandi, R. Engelmann, V. Hepp, E. Kluge, H. Krehbiel, and U. Meyer-Berkhout, Nucl. Phys. 59, 33 (1964).

C

[Co67] T. W. Conlon, Nucl. Phys. A100, 545 (1967).

[Cr70] J. B. Cross, Ph.D. Thesis, Michigan State University, 1970.

[Cv67] A. Covello and G. Sartoris, Nucl. Phys. A93, 481 (1967).

D

[De61] A. de-Shalit and J. D. Walecka, Nucl. Phys. 22, 184 (1961).

[De63] A. G. Demin, Yu. P. Kushakevich, E. A. Makovew, I. M. Rozman, and A. F. Chachakov, Zhur. Eksptl. i Teoret. Fiz. 45, 1344 (1963) - [translation: Soviet Phys. JETP 18, 925 (1964)].

[Di63] R. M. Diamond and F. S. Stephens, Nucl. Phys. 45, 632 (1963).

E

[Ep70] R. E. Eppley, Ph.D. Thesis, Michigan State University, 1970.

[EVENT] EVENT RECOVERY, a FORTRAN program written by D. Bayer and D. B. Beery, Ph.D. Thesis, Michigan State University, 1970 (unpublished).

F

[Fi66] R. W. Fink, R. C. Jopson, H. Mark, and C. D. Swift, Rev. Mod. Phys. 38, 513 (1966).

[Fr56] A. R. Fritsch, University of California Lawrence Radiation Laboratory Report No. UCRL-3452, 1956; A. R. Fritsch and J. M. Hollander, J. Inorg. Nucl. Chem. 6, 165 (1958).

G

[Ge55] T. R. Gerholm, unpublished results quoted in [Be55].

[Ge56] T. R. Gerholm, Arkiv Fysik 11, 55 (1956).

[Gi70] G. C. Giesler, Wm. C. McHarris, R. A. Warner, and W. H. Kelly, Nucl. Instr. Methods, accepted for publication (1970).

[Gr65] V. T. Gritzyna and H. H. Forster, Nucl. Phys. 61, 129 (1965).

[Gr69] C. R. Gruhn, R. R. Todd, C. J. Maggiore, W. H. Kelly, R. E. Doebler, and Wm. C. McHarris, Nucl. Instr. Methods 75, 109 (1969).

H

[Ha68] R. S. Hager and E. C. Seltzer, Nucl. Data A4, 1 (1968).

[He57] C. J. Herrlander and T. R. Gerholm, Nucl. Phys. 3, 161 (1957).

[Hi66] S. Hinds, R. Middleton, J. H. Bjerregaard, O. Hansen, and O. Nathan, Nucl. Phys. 83, 17 (1966).

[Ho46] J. J. Howland, D. H. Templeton, and I. Perlman, University of California declassified report BC 31 (1946).

[Hu61] R. J. Hull and H. H. Stroke, Phys. Rev. 122, 1574 (1961); J. Opt. Soc. Am. 51, 1203 (1961).

[Hy64] E. K. Hyde, I. Perlman, and G. T. Seaborg, The Nuclear Properties of the Heavy Elements, Englewood Cliffs, N. J., Prentice-Hall, 1964.

J

[Je49] O. Haxel, J. H. D. Jensen, and H. E. Suess, Phys. Rev. 75, 1766 (1949).

[Jo59] B. Johannson, T. Alväger, and W. Zuk, Arkiv Fysik 14, 439 (1959).

[Ju59] B. Jung, Nucl. Phys. 10, 440 (1959).

[Ju60] B. Jung and G. Andersson, Nucl. Phys. 15, 108 (1960).

K

[Ki60] L. S. Kisslinger and R. A. Sorensen, Kgl. Danske Videnskab. Selskab, Mat.-Fys. Medd. 32, No. 9 (1960).

[Ko69] K. Kosanke, in Michigan State University Nuclear Chemistry Annual Report for 1969, No. COO-1779-13 (unpublished).

L

[Le57] O. I. Leipunskii, A. M. Morozov, Iu. V. Makarov, and P. A. Iampol'skii, J. Exptl. Theoret. Phys. (U.S.S.R.) 32, 393 (1957).

[Le67] C. M. Lederer, J. M. Hollander, and I. Perlman, Table of Isotopes, 6th Ed., New York, John Wiley & Sons, Inc., 1967.

[Li58] I. Lindgren, C. M. Johansson, and S. Axensten, Phys. Rev. Letters 1, 473 (1958).

[Li60] J. Lindskog, E. Bashandy, and T. R. Gerholm, Nucl. Phys. 16, 175 (1960).

M

[Ma49] M. G. Mayer, Phys. Rev. 75, 1969 (1949).

[Ma54] D. Maeder, A. H. Wapstra, G. J. Nijgh, and L. Th. M. Ornstein, Physica 20, 521 (1954); Phys. Rev. 93, 1433 (1954).

[Ma58] L. L. Marino, Bull. Am. Phys. Soc. Ser. II, 3, 186 (1958).

[Mc57] A. McDonell, R. Stockendal, C. J. Herrlander, and I. Bergstrom, Nucl. Phys. 3, 513 (1957).

[Me70] R. A. Meyer and D. Camp, private communication, Lawrence Radiation Laboratory, Livermore, California (1970).

[Mo53] S. A. Moszkowski, Phys. Rev. 89, 474 (1953).

[Mo70] R. Moreh, A. Nof, and A. Wolf, Phys. Rev. C2, 249 (1970).

[Moir] MOIRAE, a program developed for the Michigan State University Cyclotron Laboratory Sigma-7 computer by R. Au and G. Berzins.

[Mu63] G. Murray, R. L. Graham, and J. S. Geiger, Nucl. Phys. 45, 177 (1963).

[My65] W. D. Myers and W. J. Swiatecki, University of California Lawrence Radiation Laboratory Report No. UCRL-11980, (1965) (unpublished).

N

[Ne50] H. M. Neumann and I. Perlman, Phys. Rev. 78, 191 (1950).

[Ne70] J. O. Newton, S. D. Cirilov, F. S. Stephens, and R. M. Diamond, Nucl. Phys. A148, 593 (1970).

[No50] L. W. Nordheim, Phys. Rev. 78, 294 (1950; Rev. Mod. Phys. 23, 322 (1951).

[No58] T. Novakov, R. Stockendal, M. Schmorak, and B. Johansson, Arkiv Fysik 14, 85 (1958).

O

[Oq59] B. Oquidam and B. Jancovici, Nuovo Cimento 11, 579 (1959).

P

[Pe61] B. G. Pettersson, T. R. Gerholm, Z. Grabowski, and B. Van Nooijen, Nucl. Phys. 24, 196 (1961).

[Ph70] M. E. Phelps, D. G. Sarantites, W. G. Winn, Nucl. Phys. A149, 647 (1970).

[Pr61] L. Perrson and R. Stockendal, Arkiv Fysik 19, 303 (1961).

R

[Ro68] M. E. Rose, Internal conversion coefficients, North-Holland, Amsterdam (1958).

[Ro69] J. T. Routti and S. G. Prussin, Nucl. Instr. Methods 72, 125 (1969).

[Ro70] D. Royer, M. Arditi, L. Bimbot, H. Doubre, N. Frascaria, J. P. Garron, and M. Riou, Nucl. Phys. A158, 516 (1970).

S

[Sa65] M. Sakai, H. Ikegami, T. Yamazaki, and H. Saito, Nucl. Phys. 65, 177 (1965).

[Sh65] W. D. Schmidt-Ott, F. Smend, W. Weirauch, and A. Flammersfeld, Z. Physik 188, 282 (1965).

[Sl65] L. A. Sliv and I. M. Band, in Alpha-, Beta-, and Gamma-ray Spectroscopy, edited by K. Siegbahn, North Holland Publishing Co., Amsterdam (1965).

[St55] R. Stockendal, J. A. McDonnell, M. Schmorak, and I. Bergström, Arkiv Fysik 11, 165 (1955).

[St60] R. Stockendal, Arkiv Fysik 17, 579 (1960); Arkiv Fysik 17, 553 (1960).

[Su50] A. W. Sunyar, D. Alburger, G. Friedlander, M. Goldhaber, and G. Scharff-Goldhaber, Phys. Rev. 79, 181 (1950).

[Sv61] J. Svedberg and B. Jung, Arkiv Fysik 19, 441 (1961).

W

[Wa54] A. H. Wapstra, D. Maeder, G. J. Nijgh, and L. Th. M. Ornstein, Physica 20, 169 (1954).

[Wa59] A. H. Wapstra, G. J. Nijgh, and R. vanLieshout, Nuclear Spectroscopy Tables, North Holland Publishing Co., Amsterdam, 1959.

[Wi62] B. Wirhed and C. J. Herrlander, Arkiv Fysik 23, 355 (1962).

Z

[Ze58] N. Zeldes, Nucl. Phys. 7, 27 (1958).

[Zz52] A. Bohr, Mat. Fys. Medd. Dan. Vid. Selsk. 26, No. 14 (1952); A. Bohr and B. R. Mottelson, *ibid* 27, No. 16 (1953).

APPENDICES

APPENDIX A

Separation of Carrier-Free Bismuth from Lead Cyclotron Targets

1. Dissolve $PbNO_3$ target with minimum amount of 6*N* HNO_3 in a test tube.

2. Concentrate the solution in the test tube by heating in a water bath while directing a stream of air over the solution.

3. Add red-fuming nitric acid to precipitate $PbNO_3$. Centrifuge and draw off the supernatant liquid which contains the Bi fraction.

4. Evaporate the supernatant liquid to dryness as in step 2 and dissolve the Bi residue in a few drops of 6*N* HCl.

5. Load the Bi activity onto a Dowex 1×8 200-mesh anion-exchange column heated with boiling isopropyl alcohol. The Pb fraction can then be removed from the column by elution with 0.1*N* HCl.

6. The column can now be used as a reservoir for obtaining very clean sources of Pb activity from the Bi parents or the Bi activity can be stripped from the column with 1*N* H_2SO_4 to obtain very pure Bi sources.

APPENDIX B

Separation of Lead from Thallium Cyclotron Targets

1. Dissolve Tl target in 6*N* HNO_3, the smallest amount possible. Add 5 mg. Pb^{++} carrier and 5 mg. Hg^{+++} as hold-back carrier.

2. Add small amount of 6*M* H_2SO_4 to precipitate $PbSO_4$. Centrifuge and wash with small amount of Tl^{+++} and Hg^{++} carriers in 2*M* H_2SO_4.

3. Add conc. H_2SO_4 to the $PbSO_4$ precipitate and heat until precipitate dissolves. White fumes of SO_2 should appear just before the precipitate dissolves.

4. Dilute (carefully) the conc. H_2SO_4 solution with 2 volumes of H_2O to which 5 mg. of both Hg^{++} and Tl^{+++} hold-back carriers have been added. $PbSO_4$ again precipitates. Wash ppt. twice with 2*M* H_2SO_4, to which small amounts of Hg^{++} and Tl^{+++} carriers have been added.

5. Steps 3 and 4 may be repeated, depending on the degree of separation desired; however, the Pb activity is usually sufficiently pure without repeating.

APPENDIX C

Separation of Bismuth from Thallium Cyclotron Targets

1. Dissolve the Tl target in the minimum possible amount of 6*N* HNO_3.

2. Evaporate solution to dryness. Add small amount of conc. HCl. Evaporate to dryness again and add about 10 ml of conc. HCl.

3. Recover Tl by several extractions with diethyl ether saturated with conc. HCl.

4. After the final extraction, concentrate the aqueous phase to about 1 ml and place on a Dowex-1 anion-exchange column.

5. The Pb fraction can then be removed from the column by elution with 0.1*N* HCl. The column can now be used as a reservoir for obtaining very clean sources of Pb activity from the Bi parents or the Bi activity can be stripped from the column with 1*N* H_2SO_4 to obtain very pure Bi sources.

APPENDIX D

Separation of Carrier-free Lead from Thallium Cyclotron Targets

1. Dissolve the Tl target in 1*N* HNO_3.

2. Saturate the solution with SO_2 gas to reduce the Tl^{+++} to Tl^{+} and heat the solution to expel excess SO_2.

3. Add 10 mg of Fe^{+++} carrier and make the solution basic with NH_4OH. Centrifuge the $Fe(OH)_3$ precipitate and discard the supernatant solution.

4. Wash the $Fe(OH)_3$ precipitate twice in dilute NH_4OH solution with stirring, centrifuge and discard; wash the solution each time. Dissolve the precipitate in 1*N* HNO_3.

5. Add 5 mg of Tl^{+++} carrier and repeat steps 2-4.

6. Repeat steps 2-4 once more without addition of thallium carrier and dissolve the final $Fe(OH)_3$ precipitate in the minimum amount of 6*N* HCl instead of 1*N* HNO_3.

7. Remove the iron by four extractions with equal volumes of ethyl ether. The final aqueous solution contains the carrier-free lead.